The 11th International Conference on Magnetic Resonance Microscopy
Joint Topic Conference on NMR in Well Logging and Core Analysis

August 14-18, 2011, Beijing, China University of Petroleum

http://icmrm11.cup.edu.cn

ICMRM Background

The objectives of the ICMRM are to communicate recent developments in spatially resolved magnetic resonance methods and their applications. The first ICMRM was held in 1991 in Heidelberg and was originally known as the "Heidelberg Conference". It is the biennial conference of the Division of Spatially Resolved Magnetic Resonance of the AMPERE Society.

Society of Core Analysts (SCA) is a professional organization specialized in core analysis and its wide range applications. There will be a dedicated session on core analysis in unconventional oil and gas.

Committees

International Committees:	Committee of the Division of Spatially Resolved Magnetic Resonance of The AMPERE Society. Society of Core Analysts.
Scientific Advisors:	Bruce Balcom, Bernhard Blumich, Paul Callaghan Eiichi Fukushima
Program Committee:	Henk van As, Peter Basser, Hu Dong, Marc Fleury Derrick Green, Xudong Jing, Mike Johns, Katsumi Kose Hao Lei, Gengying Li, Jun Li, Yi-Qiao Song, Lizhi Xiao
Organization Committee:	Honorary Chair and Advisors: Chaohui Ye (Academician, Chinese Academy of Sciences) Laibin Zhang (President, China University of Petroleum) Shicheng Zhang, Baoping Lu, Shouli Qu, Cancan Zhou Chair: Lizhi Xiao Deputy Chair: Sam Sun, Guo Tao Coordinator: Flora Sun, Tianlin An Logistic and Accommodation Support: Guohe Li Web Support: Qiang Lu Exhibitor Coordinator: Shuangquan Chen Peiqiang Yang, Xudong Sun, Jingen Deng, Ranhong Xie, Zhiqiang Mao
Organizers:	China University of Petroleum China Society of Magnetic Resonance China Chapter, Society of Core Analysts

Organization Committee

Chair: **Lizhi Xiao**

Ph.D. Chinese Academy of Sciences

Professor and Dean
College of Geophysics and Information Engineering
China University of Petroleum, Beijing

Executive Committee Member, SRMR, AMPERE Society
Committee Member, China Society of Magnetic Resonance

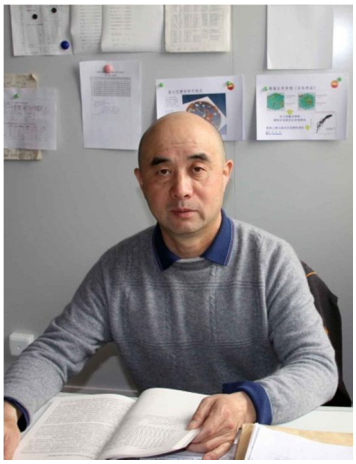

Deputy Chair: **Guo Tao**

Ph.D. Imperial College, London

Post-Doctoral Massachusetts Institute of Technolog

Director China Chapter SCA

Professor China University of Petroleum, Beijing

Deputy Chair: **Zandong (Sam) Sun**

Ph.D. University of Calgary, Canada

More than 20 years with ExxonMobil

Professor China University of Petroleum, Beijing

Coordinator: **Langqiu (Flora) Sun**

Ph.D. University of Toronto, Canada

Research fellow China University of Petroleum, Beijing

Exhibitor Coordinator: **Shuangquan Chen**

Post-Doctoral British Geological Survey, Edinburgh

Ph.D. China University of Petroleum, Beijing

Research fellow China University of Petroleum, Beijing

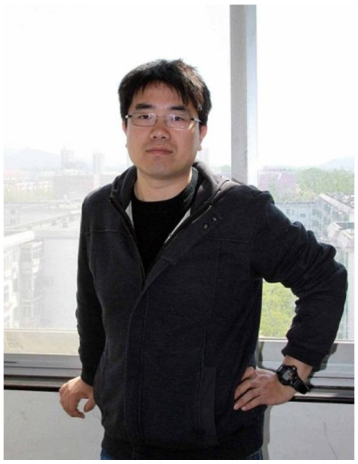

Web Support: **Qiang Lu**

Ph.D. Chinese Academy of Sciences

Associate Professor China University of Ptroleum, Beijing

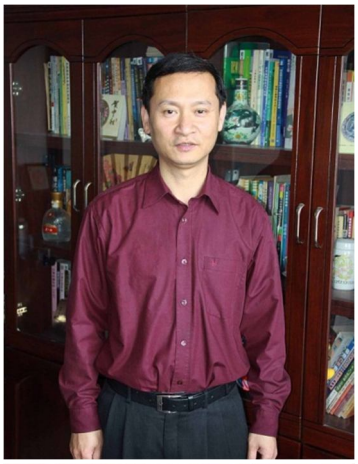

Logistc and Accommodation Support: **Guohe Li**

Ph.D. Beihang University, China

Visiting Scholar National University, Australia

Professor China University of Petroleum, Beijing

Ranhong Xie

Ph.D. China University of Petroleum, Beijing

Visiting Scholar Oakland University, USA

Professor China University of Petroleum, Beijing

Volunteers:

More than 30 volunteers from Graduate Student Union of China University of Petroleum have been trained to serve the Conference.

Division of SRMR

The Division was founded in 1995 during the 3rd meeting on Magnetic Resonance Microscopy. The purpose of the division is to advance the subject of Spatially Resolved Magnetic Resonance by means of the International Conference organized biennially across the world and symposia, summer schools and workshops. The governing organization of the Division consists of the Executive Committee, the Division Committee and the General Membership composed of conference attendees who are automatically members of the AMPERE Society.

Executive Committee Meeting:
The Executive Committee is responsible for the management, administration and finances of the SRMR Division
The following members of the Executive Committee (2009-2013) are asked to attend the Executive Committee Meeting

Chair:	B. Balcom (CAN)
Vice Chair:	M. Johns (UK)
Treasurer:	H. Van As (N)
Secretary General:	J. Seymour (US)
Vice Secretary General:	I. Koptyug (R)
Past-Conference Chair:	S. Codd (US)
Conference Chair:	L. Xiao (C)
Past Chair:	B. Blümich (G)
Advisors:	P. Callaghan (NZ), E. Fukushima (US) A. Haase (G)

The meeting will take place in VIP Room of the Dining Hall on the first floor of Conference Centre during the Monday lunch break. Lunch will be provided.

Division Committee Meeting:
The Division Committee is responsible for carrying out the business of the Division, including the scientific organization of the conference.
The following members of the Division Committee are asked to attend the Division Committee Meeting.

	All above members of the Executive Committee
(2007-2011)	A. Coy (NZ), K. Kose (J), Y. Seo (J)
(2005-2011)	S. Altobelli (US), P. Blümler (G), D. Gross (G), Y.-Y. Lin(US), R. Mair (US), J. Reimer (US), K. Saito(J)
(2009-2011)	M. Britton (UK), M. Hurlimann (US), F. Casanova (G), B. Newling (CAN), P. Basser (US), B. Manz (NZ), M. McCarthy (US), I. Sersa (SLO), L. Ciobanu (FR), A. Sederman (UK), L. Bouchard (US), S. Appelt (G), D. Sakellariou (FR), S. Handa (J)

The meeting will take place in the VIP Room of the Dining Hall on the first floor of Conference Centre during the Tuesday lunch break.

General Meeting:
The General Meeting has the final authority of the Division. All conference attendees are automatically members of the General Meeting and are encouraged to attend.
The General meeting will take place in the same room as the oral presentations on Thursday afternoon following the Prizes session.

Sponsors and Exhibitors

Gold:

Sinopec Group
http://english.sinopec.com/default.shtml

China National Petroleum Corporation
http://www.cnpc.com.cn/en/

China National Offshore Oil Corporation
http://en.cnooc.com.cn/

Shanghai Niumag Corporation Ltd
http://en.niumag.com/index.php

Huanding Energy Services
http://www.huanding.com/en/index.php

China University of Petroleum, Beijing
http://www.cup.edu.cn/internationaloffice/en/

K. C. Wong Education Foundation
Hong Kong

Shell China
http://www.shell.com.cn/home/content/chn-en/

Chevron
http://www.chevron.com/

Magritek Limited
http://www.magritek.com/
ACT Aachen Mobile NMR Solutions
http://www.act-aachen.com/

Silver:

Agilent Technologies
http://www.chem.agilent.com/en-US/Products/Instruments/magneticresonance/pages/default.aspx

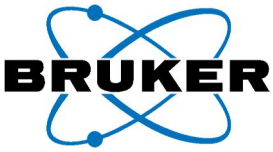

Bruker BioSpin
http://www.bruker-biospin.com/

iRock Technologies
http://irocktech.com/
Xradia
http://www.xradia.com/

Stelar
http://www.stelar.it/
HTS-110
http://www.hts110.co.nz/

Oxford Instruments
http://www.oxinst.com/Pages/home.aspx
Green Imaging Technologies
http://www.greenimaging.com/

University of New Brunswick
http://www.unb.ca/

J S Reseach INC.
http://www.jsresearch.com/

Bronze:

Schlumberger
http://www.slb.com/services/characterization/wireline_open_hole/nmr.aspx

Rapid Biomedical
http://www.rapidbiomed.de/

Tecmag
http://www.tecmag.com/

Exhibitors

Main reasons for exhibiting at ICMRM11

- Meet existing and acquire new customers
- Introduce new products and services
- Demonstrate your technology and equipment
- Monitor the competition
- Expand your network

Event facts	
Date	Aug 14-18, 2011
Location	Beijing, China
Venue	China University of Petroleum Conference Centre
Exhibition space	300m^2 (gross)
Expected exhibitions	50
Exhibition Hours	
Aug 15, 2011	09:00 - 17:30
Aug 16, 2011	09:00 - 17:30
Aug 17, 2011	09:00 - 17:30
Aug 18, 2011	09:00 - 17:30

Welcome to ICMRM 11

Dear colleagues and friends,

On behalf of the organizing committee, I warmly welcome you to participate in the 11th International Conference on Magnetic Resonance Microscopy (ICMRM) and Joint Topic Conference on NMR in Well Logging and Core Analysis.

The 11th ICMRM will follow the fine tradition that has been established starting with the very first ICMRM in Heidelberg in 1991. The conference will be devoted to the latest developments in the methods, equipment, and applications of spatially resolved NMR; it is also designed to enhance scientific communication between industry and academia, and between researchers from countries spanning the globe.

We have invited 25 renowned scientists to give presentations on various aspects of NMR, including Professors Warren S. Warren, Axel Haase, Ben Newling, Paul Glover, Bernhard Blümich, Eiichi Fukushima, and Bruce Balcom. Contributions from colleagues all over the globe have resulted in 50oral presentations as well as 98 posters.

We sincerely appreciate the generous donations from our industry friends and the enthusiastic assistance from the China University of Petroleum (CUP) and other Chinese research institutes. We would also like to thank in advance all the delegates and exhibitors for their interest in presenting their high-quality work. We believe that all our attendees will greatly benefit from this conference.

We, the faculty and graduate students from CUP, have the honour to volunteer in the organization of the 11th ICMRM. CUP specializes in petroleum-related research and education and is one of the best industry-oriented universities in China. NMR is widely used for petroleum and natural gas exploration and recovery in well logging, and in core analysis to measure rock porosity and permeability, or to identify pore fluids. We are delighted to incorporate contributions from the Society of Core Analysts and have created a Joint Topic Conference on NMR in Well Logging and Core Analysis.

This year, ICMRM will for the first time be held in China. In addition to the technical program, we hope you will enjoy your trip to Beijing and China. Chinese civilization has endured and prospered for thousands of years, and Beijing has been the capital for nearly 900 years. It is a city both old and new at same time. Young with inexhaustible energy and an open attitude for new developments, it is already one of the great world cities. We have arranged a wonderful excursion to show you the old and the young faces of Beijing on this special occasion.

To conclude this welcome note, I would like to quote Confucius, a famous Chinese philosopher, “How happy we are to have friends from afar!” We look forward to welcoming you to Beijing this August.

Sincerely yours,

Lizhi Xiao, Ph. D.
Conference Chair, ICMRM 11
Professor and Dean
College of Geophysics and Information Engineering, China University of Petroleum
Executive Committee Member, SRMR, AMPERE Society
Committee Member, China Society of Magnetic Resonance

Venue Map

The conference will be hosted by China University of Petroleum in Changping, a small city that is part of greater Beijing, 50 km north of the city centre.

The address is:
China University of Petroleum, Beijing, 18 Fuxue Road, Changping, Beijing, China
The conference centre is on the north campus of China University of Petroleum.
The meals will be served in the on-site restaurant.
Exhibition and poster space are on the same floor as the conference centre.

Map of the China University of Petroleum (CUP) campus:

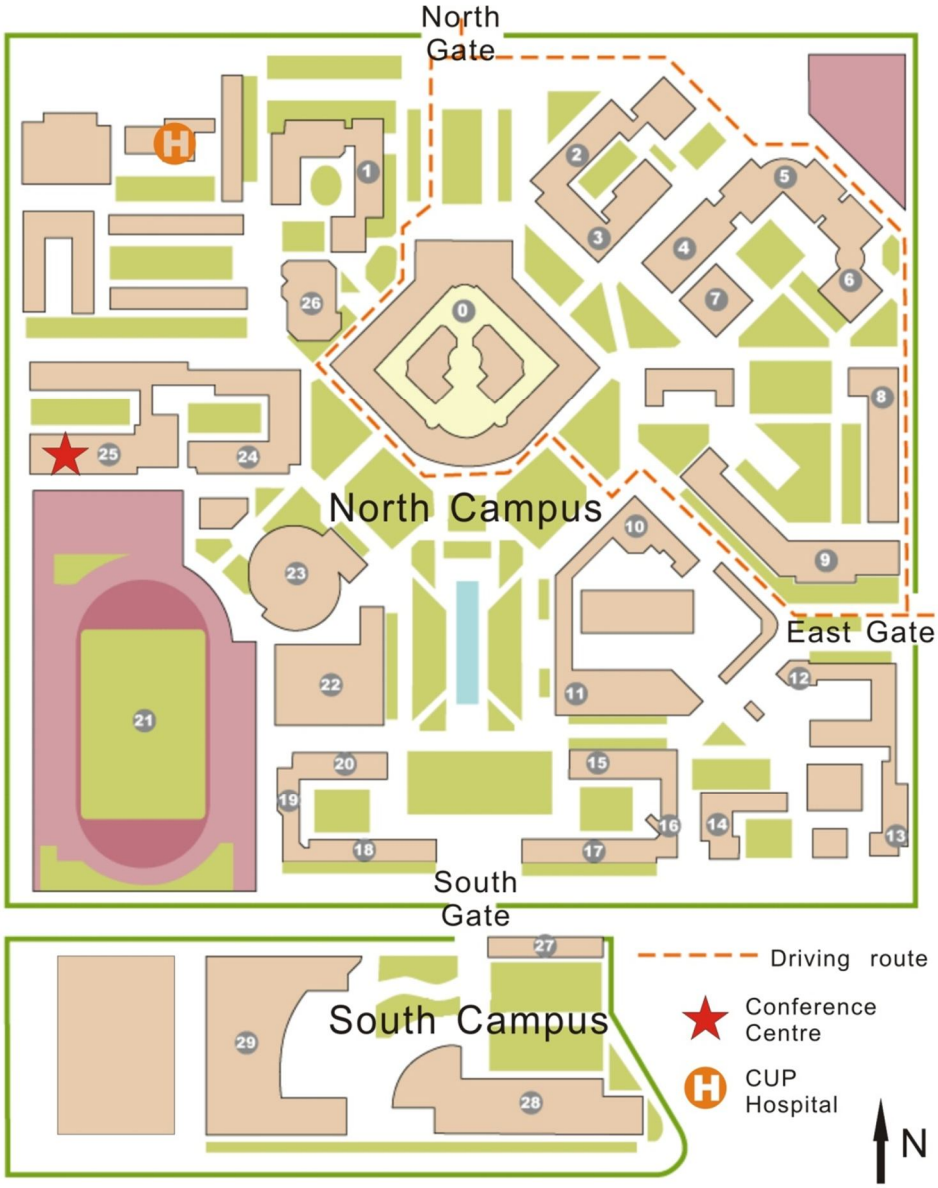

0 Library	4 Classroom Building	8 Laboratory Building	12 Vehicle Centre	24 International Office
1 Fundamental Sc. Building	5 Science Hall	9 Laboratory Building	21 Stadium	27 Convenient store
2 Office Building	6 Multifunctional Building	10 Dining Hall	22 Natatorium	28 Geoscience Building
3 Classroom Building	7 Science Hall	11 Dining Hall	23 Gymnasium	29 Classroom Building

Medical Services

CUP campus
The CUP Hospital is only 2 min walk from the CUP conference centre (see the campus map). The hospital provides medical cares for common sickness. Ask any conference volunteers for help if you need.

Wednesday excursion
A physician from the CUP Hospital will be seated in one of the buses with a first aid package. Call Flora (15901052730) or Tianlin (13426268000) in case you need help.

Call for Ambulance: 120 or **999**
Free phone call but paid ambulance

Map of the Hotels

Two hotels have been reserved for the conference.
One is China University of Petroleum (CUP) Conference Centre Hotel (Location A), which is connected to the Conference Centre by indoor walkways.
The other is Auspicious Hotel (Location B) 500 meters away from the Conference Centre.

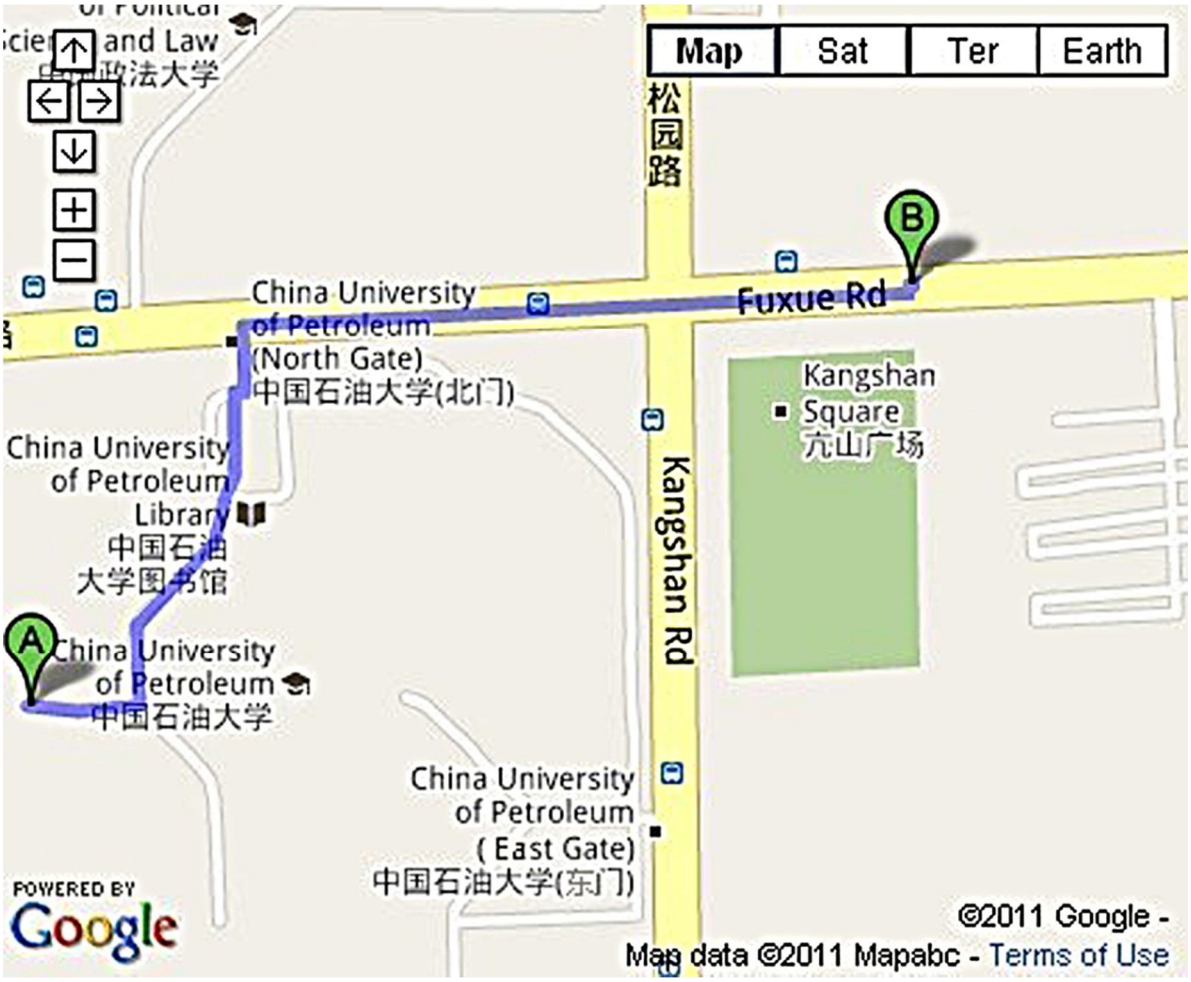

Layout of the Conference Centre

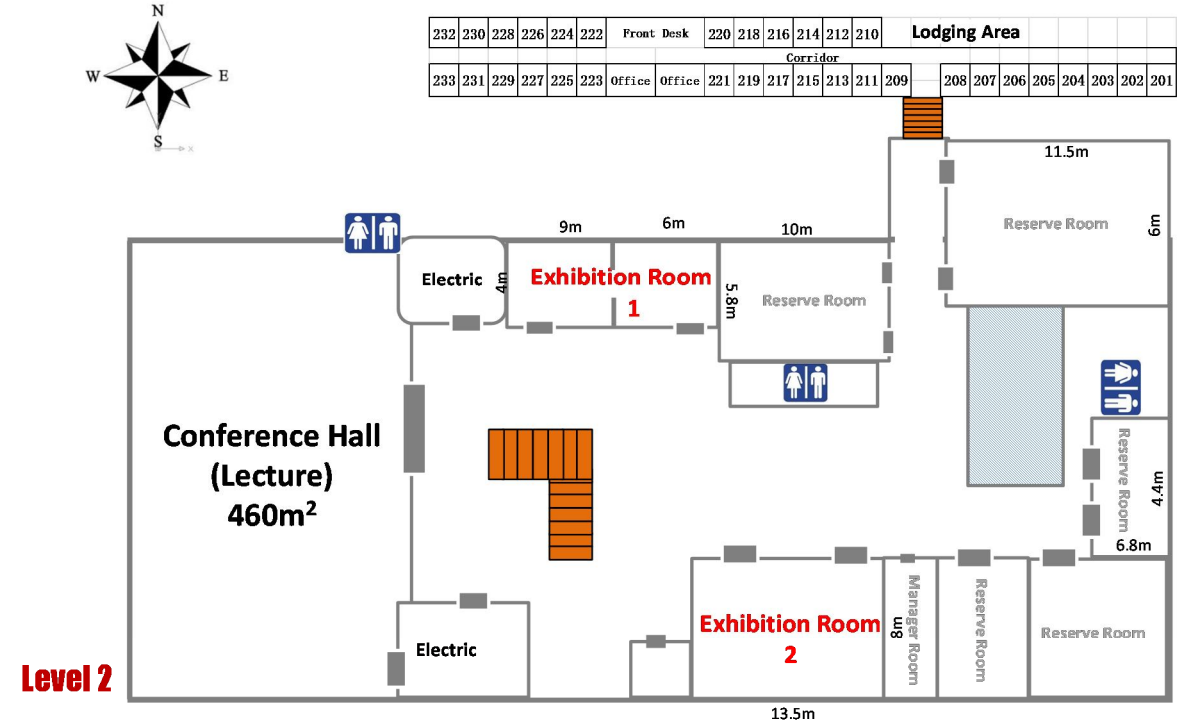

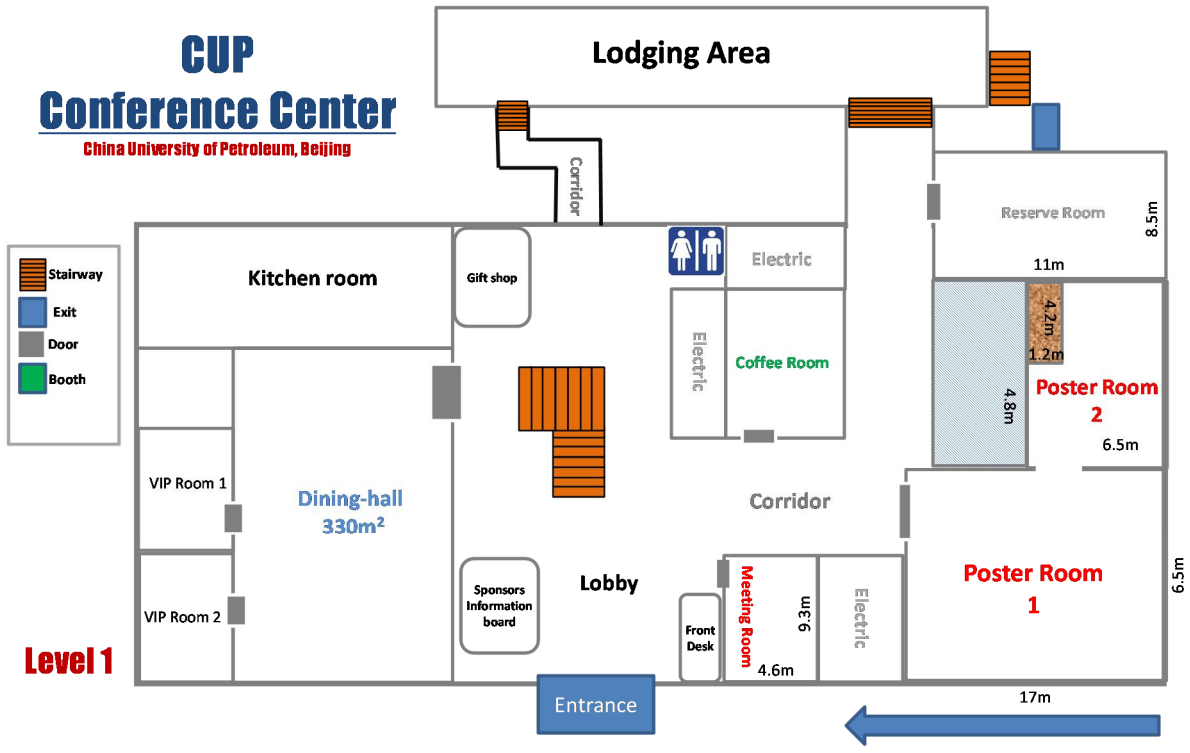

Tennis Court

ICMRM 11: Session Chairs

Session	Date	Time	Chair
Educational	Sunday	10:15-16:00	**Mike Johns**
Plenary 1 (Warren)	Sunday	16:30-17:30	**Bruce Balcom**
Plenary 2 (Haase)	Monday	08:00-08:50	**Lizhi Xiao**
Biological NMR/MRI Session 1	Monday	08:50-10:00	**Paul Glover**
Biological NMR/MRI Session 2	Monday	10:15-12:05	**Peter Basser**
Novel NMR/MRI	Monday	15:45-17:35	**Yi-Qiao Song**
Young Investigators	Tuesday	08:00-10:00	**Sarah Codd**
NMR/MRI Hardware	Tuesday	10:15-12:00	**Bernhard Blumich**
Flow and Diffusion NMR/MRI	Tuesday	15:45-17:30	**Andrew Sederman**
NMR logging and Core Analysis	Wednesday	08:00-10:00	**Petrik Galvosas**
Materials NMR/MRI	Wednesday	10:15-12:00	**Flora Sun**
Mobile NMR/MRI	Thursday	08:00-10:00	**Ben Newling**
Food/Other NMR	Thursday	10:15-12:15	**Siegfried Stapf**
Computational NMR/MRI	Thursday	13:30-15:30	**Joe Seymour**
Core analysis in unconventional oil and gas I	Thursday	08:00-10:00	**Hu Dong**
Core analysis in unconventional oil and gas II	Thursday	10:15-12:20	**Xudong Jing**
Core analysis in unconventional oil and gas III	Thursday	13:30-15:30	**Guo Tao**

Judges for Posters: Mike Johns, Andrew McDowell, Martin Hurlimann
Judges for Young Investigators: Bruce Balcom, Lizhi Xiao, Christoph Arns

ICMRM 11: Schedule

	14-Aug	15-Aug	16-Aug	17-Aug	18-Aug		19-Aug
	Sunday	**Monday**	**Tuesday**	**Wednesday**	**Thursday**		**Friday**
Morning 08:00-10:00	Registration	Plenary Lecture 2 Biomedical NMR Inv01 O1-O2	Young Investigators OY1-OY6	NMR Logging & Core Analysis Inv07-Inv09 O18-O19	Mobile NMR Inv11 O24-O28	Core analysis in unconventional oil and gas Inv15-Inv16 O38-O40	Optional Excursion(Ming Tombs &Great Wall)
Coffee Break							
Morning 10:15-12:00	Educational Session 1 Educational Session 2	Biological NMR Inv02 O3-O6	NMR Hardware Inv04 O11-O14	Materials NMR Inv10 O20-O23	Food / other NMR Inv12 O29-O33	Core analysis in unconventional oil and gas Inv17 O41-O45	
12:00-13:30	Lunch Buffet at Conference Centre						
Afternoon 13:30-15:30	Educational Session 3 Educational Session 4	Poster Session	Factory Tour to Huanding MRIL Poster Session	Wednesday Excursion Event	Computational NMR Inv13-Inv14 O34-O36	Core analysis in unconventional oil and gas Inv18 O46-O50	
Afternoon 15:45-17:30	Educational Session 5 15:10-16:00 Coffee Break 16:00-16:15 President Welcome Speech 16:15-16:25 Plenary Lecture 1	Coffee Break Novel NMR Inv03 O7-O10	Flow NMR Inv05-Inv06 O15-O17		Coffee Break Prize & Conclusion SRMR General meeting 15:45-16:45 Coffee Break 16:45-17:00 VSG Presentation		
Evening 17:30-19:00	Reception (Light meal)	Dinner (Buffet at Conference Centre)		Conference Dinner and show at The Great Hall of People	Dinner (Auspicious Hotel Restaurant)		
19:00-21:00		Stelar User Meeting					

Schedule of the Wednesday Excursion

13:30	Get on buses in front of the CUP Conference Centre. There will be a conference volunteer on each bus to assist you. Bottled water will be provided.
14:40-15:00	Arrive at the east side of Tian'anmen Square, walk through the Square, and go through the entrance of the Forbidden City. We will hire professional tour guides from the Service Centre of the Forbidden City to walk with you. You may also walk by yourself if you prefer. Please note that the following services are optional at your own cost: (1) rental for audio guide; (2) admission to Treasure Gallery or the Hall of Clocks; (3) personal tour guide; (4) other personal expense such as food.
15:00-17:00	A two-hour walking tour from the south/front gate of the Forbidden City towards the north/back gate. For more information of the Forbidden City, please check **http://www.dpm.org.cn**.
17:10	Gather at the north gate of the Forbidden City. Buses will be there waiting for you.
17:10-17:50	Take the buses to the Great Hall of the People, go through the security check, and be seated for the Conference Dinner.
18:00-20:30	The Conference Dinner, performance and entertainment
20:45	Get on buses outside the Great Hall of the People and head to the Olympic Park.
21:30-22:00	Sightseeing outside the National Stadium (the Bird Nest) and the National Aquatics Centre (the Water Cube). You cannot get into either the Stadium or the Aquatics Centre because they are closed at night.
22:10	Get on buses and head back to your hotels.
23:00	Arrive at your hotels.

VERY IMPORTANT

- Please get on the buses ON TIME!! Otherwise, it will be your own responsibility to get to the next stop on this schedule.
- For emergency, call conference coordinators: Flora, 15901052730; Tianlin, 13426268000.

RECOMMENDATIONS

- The weather can be very hot. Sun block, sun glasses, a hat, and a fan are strongly recommended. Remember to take a bottle of WATER with you from your bus before the walking tour.
- Dressing code: SEMI-FORMAL as there will be a fancy dinner. Ties are not necessary. Do wear COMFORTABLE shoes for the walking tour.
- We encourage our delegates to communicate with colleagues outside their everyday communities. Please take the same bus with people who are not familiar to you, walk with them and help each other in the walking tour.

Forbidden City

Great Hall of the People

National Theatre at night

National Stadium (right in the photo) and National Aquatics Centre (left in the photo) at night

Ming Dynasty Tombs

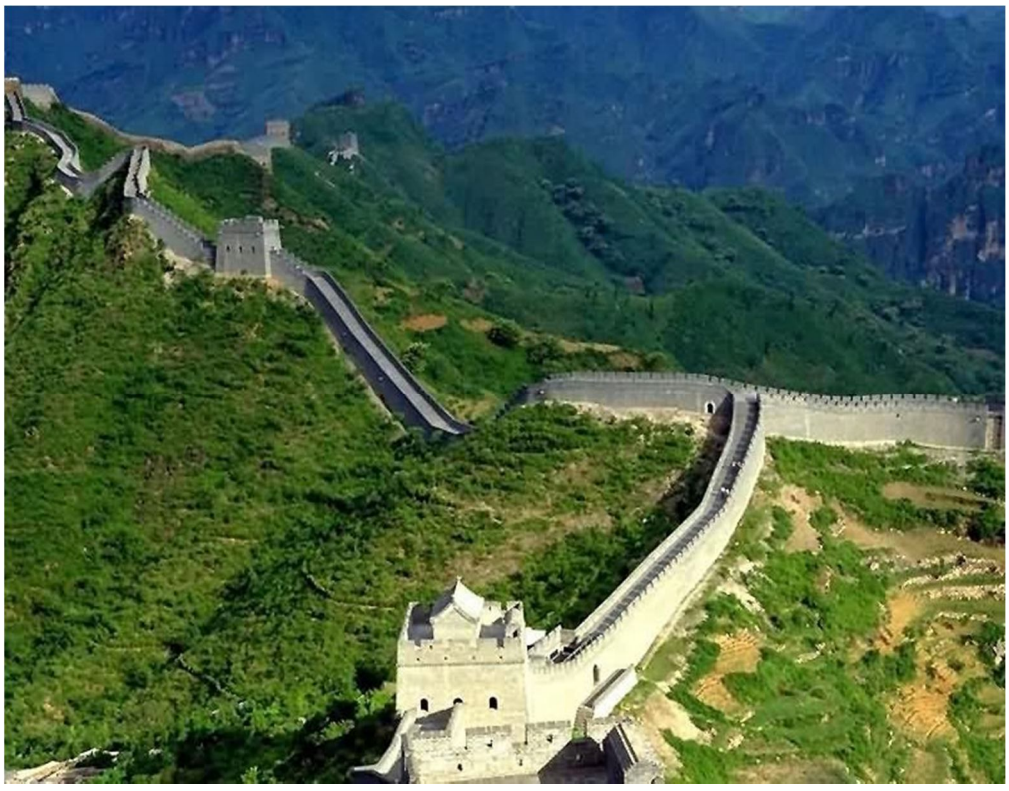

Great Wall

Internet

Internet is available both in the CUP Conference Centre Hotel and Auspicious Hotel. Instructions should be found in your hotel rooms. For additional assistance please ask the hotel front desk. Internet or Wi-Fi is unavailable in the CUP Conference Centre.

Transportation

We do not recommend our attendees to take subway to Changping because there is no direct connection between the subway station and the CUP campus or either of the hotels.

How to get to your hotel from Beijing Capital International Airport

The easiest way (recommended for first-time visitors):
If your flight will land on August 13, you may take the bus arranged by the ICMRM11 organization committee. You can purchase a ticket for the bus when you are registering for this conference.
The bus schedule will be on our website.

By taxi:
Follow the signs of TAXI in the airport and take a taxi. The distance to either hotel is about 45 km. The estimated cost is about 180 RMB in the daytime or 250 RMB at night (11pm to 5am), plus 2 RMB of fuel fee and 20 RMB of toll for the highways (not applicable if your taxi avoids highways); no gratuity.
Please note:

- ✧ DO follow the TAXI signs in the airport. Do not get on any car that is not in the taxi-waiting area.
- ✧ You need RMB cash for taxi.

If you will go to the conference from another part of Beijing

It will be your own responsibility to travel to the conference site if you will not go to the conference directly from the airport. Taxi is recommended.
You may check http://www.tour-beijing.com/taxi/ for taxi information.

Call for help

Phone numbers of the conference coordinators:
Flora Sun: 15901052730
Tianlin An: 13426268000

A member of the local organization committee will be living in Rooms 124 and 125 in the CUP Conference Centre Hotel.

Presentation and Competition Instructions

Instructions for Oral Presentations:

The duration of individual talks are listed in the program. Please time your talk to allow approximately 5 minutes of questions and discussion.

The chair of a session will remind the speakers about time usage. A **yellow card** will be flashed when there is only **5 min** left and a ***red card*** will be displayed when only ***2 min*** remains.

All speakers are required to use the conference computer for presentations. The operating system used is Windows 7 Professional (English version). Microsoft Office 2007, AdobeReader, QuickTime are installed for presentations. File formats **pdf**, **ppt** and **pptx** are acceptable.

Please contact the conference coordinator Tianlin **ONE DAY** before your presentation and upload your documents to the conference computer during session breaks. We strongly suggest you reserve more time to test your presentation with Tianlin after uploading.

Instructions for Poster Presenter

Posters may stay up during the entire conference, from 08:00am on Sunday until 15:30pm on Thursday.

A poster should be one paper with the size of **84 cm** wide and **119 cm** tall. Adhesive tapes will be provided to attach your posters to the boards.

Volunteers will be there helping you to put up the posters during 08:00am to 17:30pm on Sunday and Monday.

Poster Session 1: 13:30-15:30 on Monday, August15

Poster Session 2: 13:30-15:30 on Tuesday, August16

Young Investigator Competition

Please attach a yellow label provided by the local committee to identify your poster as eligible for this competition. You must attend your poster during the poster session.

Winner	Daniel Holland University of Cambridge Bayesian Techniques in Magnetic Resonance
Runners Up	Qingxia Gong Germany Breaking the sensitivity limit of low-field NMR by using para-hydrogen induced polarization
	Antoine Vallatos University of Birmingham Magnetic Resonance Velocimetry in a Vortex Flow Reactor

Poster Competition
All posters are eligible for the poster competition.

Winner	Nadia Amor RWTH Aachen University Continuously Dissolved Hyperpolarized ^{129}Xe for Analysis and Biomedical Applications of Hollow Fibers
Runners Up	Johannes Fuchs University of Würzburg Spectroscopic imaging of metabolite dynamics in plant seeds using Interleaved Variable Density (IVD) acquisition

Image Beauty Competition

For the third year, there will be an Image Beauty Competition. This competition was started by Yang Xia. Some of the top entries from last time are posted here:

http://www.icmrm10.montana.edu/Images.htm

2011 Winner: Nian Wang

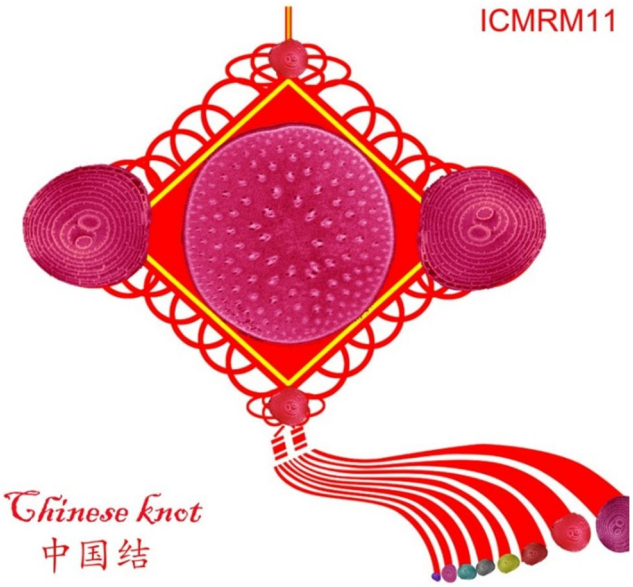

Previous good works

NMR Book Prizes

Copies of the following books are being donated by the authors to the ICMRM 11 conference for distribution as student prizes. Hard copies of the books will be on display throughout the conference.

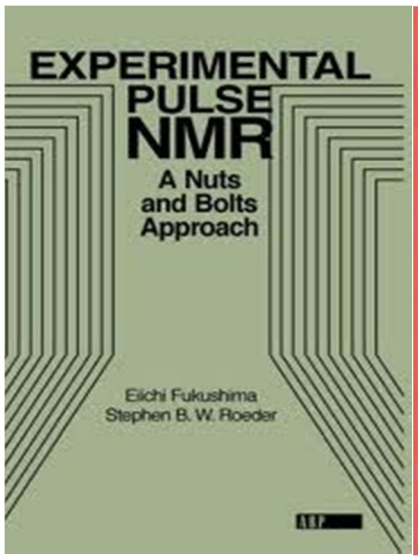

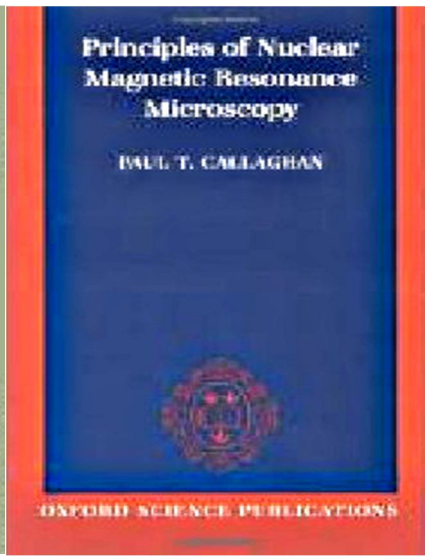

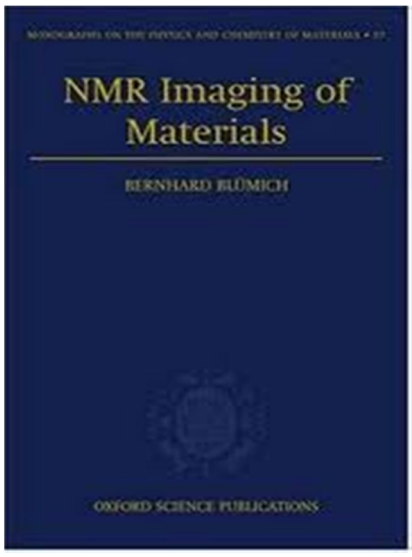

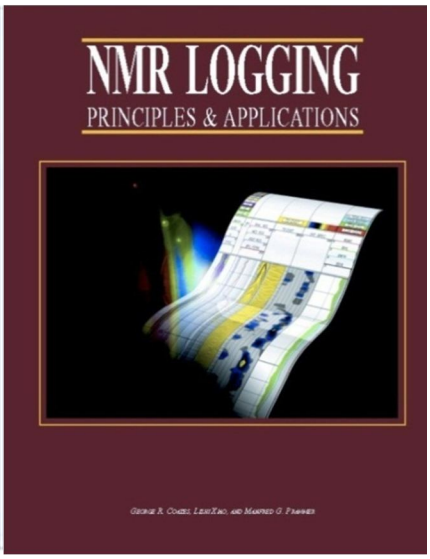

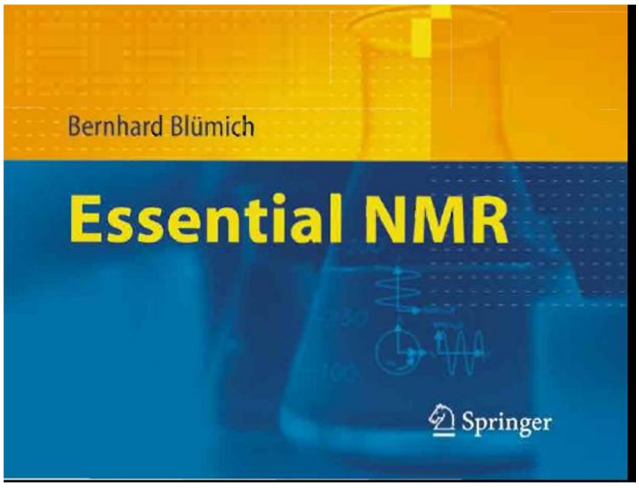

PROGRAM

Sunday 14th August

	Session Chair: Mike Johns	**Educational10:15-16:00**		
ID	**Speaker**	**Topic**	**Duration**	**Time**
Edu1	Ben Newling	Introduction to NMR/MRI	50 minutes	10:15
Edu2	Paul Glover	MRI Hardware	50 minutes	11:05
Edu3	Bernhard Blumich	Mobile MRI/NMR	50 minutes	13:30
Edu4	Eiichi Fukushima	Flow/Diffusion Measurement with MRI/NMR	50 minutes	14:20
Edu5	Bruce Balcom	MRI of Porous Media	50 minutes	15:10

Plenary Presentation 1

	Session Chair: Bruce Balcom	**Plenary/ Opening Speech16:30-17:30**		
ID	**Speaker**	**Topic**	**Duration**	**Time**
Plen1	Warren S. Warren	Re-examining 1950s spin physics to improve modern magnetic resonance microscopy and imaging	60 minutes	16:30

Monday 15th August

Plenary Presentation 2

	Session Chair: Lizhi Xiao	**Plenary/Educational 08:00-08:50**		
ID	**Speaker**	**Topic**	**Duration**	**Time**
Plen2	Axel Haase	Worried about the poor sensitivity of NMR? New technologies promise a bright future for biomedical imaging	50 minutes	08:00

	Session Chair: Paul Glover		**Biomedical NMR/MRI 08:50-10:00**		
ID	**Speaker**	**Authors**	**Topic**	**Duration**	**Time**
Inv01	Michal Komlosh		Tissue Microstructure Revealed Using Double Pulsed Field Gradient Filtered MRI	30 minutes	08:50
O1	Yang Xia	Yang Xia Nian Wang Jihyun Lee Farid Badar	T1 in Articular Cartilage is Strain-Dependent – A μMRI Study	20 minutes	09:20
O2	Ileana Jelescu	I.O. Jelescu R. Nargeot B. Djemaï D. LeBihan L. Ciobanu	Manganese enhanced MRI highlighting neuronal pathways of the buccal ganglion in Aplysiacalifornica	20 minutes	09:40

	Session Chair: Peter Basser		Biological NMR/MRI 10:15-12:05		
ID	**Speaker**	**Authors**	**Topic**	**Duration**	**Time**
Inv02	Gil Navon	Yoni Hertzberg Gil Navon	Magnetic resonance acoustic radiation force imaging	30 minutes	10:15
O3	Yi-Qiao Song	D. Mintzopoulos J. L. Ackerman Y-Q. Song	DDIF: A novel contrast for MRI of trabecular bone	20 minutes	10:45
O4	Patrick Vogel	P. Vogela, M. A. Rückert, P. Klauer W. H. Kullmann P. M. Jakob V. C. Behr	Frequency mixed Traveling Wave for 2D Magnetic Particle Imaging	20 minutes	11:05
O5	Jim Pope	J.M. Pope, B.A. Moffat, C.E. Jones S. Kasthurirangan E. Markwell D.A. Atchison	Non-invasive measurements of water transport and optical properties in the human eye	20 minutes	11:25
O6	Siegfried Stapf	E. Rössler A. Mollova C. Mattea S. Stapf	Low-field depth- and orientation-dependent relaxation imaging of bovine articular cartilage	20 minutes	11:45

	Session Chair: Yi-Qiao Song		Novel NMR/MRI 15:45-17:35		
ID	**Speaker**	**Authors**	**Topic**	**Duration**	**Time**
Inv03	Vikram Bajaj		Applications of Remotely Detected NMR and MRI at the Microscale	30 minutes	15:45
O7	Christine Schmaus	Christine Schmaus Dan J. Holland Andy J. Sederman Andrew Blake Lynn F. Gladden	Compressed sensing SPI for gas velocity imaging in porous media	20 minutes	16:15
O8	Igor V. Koptyug	I.V. Koptyug A.A. Lysova I.V. Skovpin D.A. Barskiy K.V. Kovtunov V.V. Zhivonitko	Multinuclear and hypersensitive MRM in heterogeneous catalysis	20 minutes	16:35
O9	R. Soltani	Rafik Soltani Lizhi Xiao	Independent Component Analysis (ICA) Applied to Adaptive Signal Processing for Multichannel Surface-NMR Instruments	20 minutes	16:55
O10	Boqin Sun	Boqin Sun Bob Carlson Marcus O. Wigand	Laplace Inversion for obtaining relaxation-chemical shift correlation in high-resolution solid state NMR	20 minutes	17:15

Tuesday 16th August

	Session Chair: Sarah Codd		**Young Investigators 08:00-10:00**		
ID	**Speaker**	**Authors**	**Topic**	**Duration**	**Time**
OY1	Joana Diekmann	Joana Diekmann Kristl L. Adams Gregory L. Klunder Carla Vogt Andrew F. McDowell	Miniaturized Capillary Electrophoresis-Microcoil NMR device for 1H and 19F Spectroscopy	20 minutes	08:00
OY2	Antoine Vallatos	Antoine Vallatos Melanie M. Britton	Magnetic Resonance Velocimetry in a Vortex Flow Reactor	20 minutes	08:20
OY3	Cedric Hugon	Cedric Hugon Guy Aubert Dimitris Sakellariou	Rotating permanent magnets: Towards MAS NMR/MRI on a static sample	20 minutes	08:40
OY4	Qingxia Gong	Qingxia Gong Stephan Appelt Bernhard Blümich	Breaking the sensitivity limit of low-field NMR by using para-hydrogen induced polarization	20 minutes	09:00
OY5	Daniel Holland	D.J. Holland A. Blake J.G. Ross A.J. Sederman L.F. Gladden	Bayesian Techniques in Magnetic Resonance	20 minutes	09:20
OY6	Ravinath Kausik	Ravinath Kausik Lukasz Zielinski Martin Hurlimann	Novel multidimensional rotating frame based techniques for probing low frequency dynamics	20 minutes	09:40

	Session Chair: Bernhard Blumich		**NMR/MRI Hardware 10:15-12:00**		
ID	**Speaker**	**Authors**	**Topic**	**Duration**	**Time**
Inv04	Nan Sun	Nan Sun Donhee Ham	Handheld CMOS NMR systems and their biosensing applications	30 minutes	10:15
O11	Bruce J. Balcom	Hui Han Matthew Ouellette Bryce MacMillan Frederic Goora Karun Adusumilli Rodney MacGregor Derrick Green Bruce J. Balcom	High Pressure Magnetic Resonance Imaging with Metallic Vessels	20 minutes	10:45
O12	Petrik Galvosas	Marcel Gratz Stefan Hertel Markus Wehring Mario Großmann Stefan Schlayer Frank Stallmach Petrik Galvosas	Advanced Methods for NMR Diffusometry	20 minutes	11:05

O13	Alan Wong	Alan Wong Pedro M. Aguiar Roxane Andurand Dimitris Sakellariou	Rotating Microcoils for High-Resolution Magnetic Resonance Microscopy	20 minutes	11:25
O14	Soumyajit Mandal	Soumyajit Mandal Yi-Qiao Song	Amplitude-modulated CPMG refocusing pulses	15 minutes	11:45

	Session Chair: Andrew Sederman		**Flow and Diffusion NMR/MRI 15:45-17:30**		
ID	**Speaker**	**Authors**	**Topic**	**Duration**	**Time**
Inv05	Daniel Topgaard	S. Lasic I. Aslund O. Soderman D. Topgaard	Finite gradient pulse lengths in PGSE NMR: homogeneous length scale and intracellular diffusion	30 minutes	15:45
Inv06	Joon Cho	J. Paulsen S.H. Han, G. Zhu Y.K Song, G. Cho Y-Q. Song, H. Cho	CS-accelerated NMR and MRI	30 minutes	16:15
O15	Tyler Brosten	Tyler R. Brosten Robert, S. Maier Sarah, L. Codd Joe, D. Seymour	PGSE NMR measurement of permeability by the short-time effective diffusion coefficient	15 minutes	16:45
O16	Konstantin Romanenko	Konstantin Romanenko Bruce Balcom	Permeability mapping in naturally heterogeneous sandstone cores by magnetization prepared centric-scan SPRITE	15 minutes	17:00
O17	Dan Benjamini	D. Benjamini J. Elsner M. Zilberman U. Nevo	Characterization of porous bioresorbable films in physiological conditions by Angular Double-PFG	15 minutes	17:15

Wednesday 17th August

	Session Chair: Petrik Galvosas		**NMR Logging and Core Analysis 08:00-10:00**		
ID	**Speaker**	**Authors**	**Topic**	**Duration**	**Time**
Inv07	Christoph Arns	Tariq Al Ghamdi Ji-Youn Arns Christoph H. Arns	Relative permeability estimation from NMR responses: a numerical study using X-ray micro-tomography	30 minutes	08:00
Inv08	Lizhi Xiao		Progress in NMR Well Logging and Core Analysis in China	30 minutes	08:30
Inv09	Lukasz Zielinski		Correlations between restricted diffusion and T2 surface relaxation as a probe of porous media	30 minutes	09:00
O18	Ruina Xu	Shu Luo Peixue Jiang Ruina Xu Jin Ma	Water saturation measurement and visualization research on supercritical two-phase flow in sandstone using MRI under CO2 storage conditions	15 minutes	09:30
O19	Jeffrey Paulsen	Jeffrey L Paulsen Yonggang Wang Huiguang Zhu	Nanoparticle Transport Monitored by MRI	15 minutes	09:45

	Session Chair: Flora Sun		**Materials NMR/MRI 10:15-12:05**		
ID	**Speaker**	**Authors**	**Topic**	**Duration**	**Time**
Inv10	Joe Seymour	Joseph D. Seymour Sarah L. Codd Einar O. Fridjonsson Erik M. Rassi	MR measurement of non-equilibrium thermodynamics: Microfluidic colloid suspension and critical phase transition flows	30 minutes	10:15
O20	Ben Newling	Alex Adair Igor Mastikhin Ben Newling	Fast Flow Velocity Mapping of Hydrodynamic Cavitation	20 minutes	10:45
O21	Ulrich Scheler	Ute Böhme, Ludmilla Loose, Ulrich Scheler	Polymers in shear flow at low and high field	15 minutes	11:05
O22	Yang Yu	Sun Zhenping, Yu Yang, Pangmin, Yang Peiqiang, Hu Jingli	Early-age cement paste microstructure evolution: a ^{1}H low-field NMR study	15 minutes	11:20
O23	Jennifer R. Brown	Jennifer R. Brown Timothy I. Brox Sarah J. Vogt Joseph, D. Seymour Mark L. Skidmore Sarah L. Codd	Magnetic Resonance Microscopy Studies of Polycrystalline Ice	15 minutes	11:35
O24	Sergey Dvinskikh	V. Dvinskikh I. Furó M. Henriksson	NMR imaging studies of wood moisture interaction	15 minutes	11:50

Thursday 18th August

	Session Chair: Ben Newling		**Mobile NMR/MRI 08:00-10:00**		
ID	**Speaker**	**Authors**	**Topic**	**Duration**	**Time**
Inv11	Carel Windt		Portable NMR for the plant sciences: from tree trunk to cereal grain	30 minutes	08:00
O25	Andrew F. McDowell	Andrew F. McDowell	Sensitivity in Small-scale Spectroscopy	20 minutes	08:30
O26	Ulrich Scheler	Ute Böhme Ulrich Scheler	Polymers under uniaxial stress	20 minutes	08:50
O27	Sushanta Ghoshal	Sushanta Ghoshal Carlos Mattea Paul Denner Siegfried Stapf	A comparative study on the film formation of bio- and synthetic polymers using single-sided NMR	20 minutes	09:10
O28	Daiki Tamada	Daiki Tamada Yasuhiko Terada Katsumi Kose	Stream function method for a bi-planar single channel shim coil	15 minutes	09:30
O29	Steffen Lother	Steffen Lother Uvo Hölscher Toni Drießle Peter Weberb Peter Jakob Florian Fidler	Optimized Adiabatic and Nonadiabatic Field-Cycling Control Circuit for Prepolarized Earth Field NMR	15 minutes	09:45

	Session Chair: Siegfried Stapf		**Food NMR/MRI 10:15-12:15**		
ID	**Speaker**	**Authors**	**Topic**	**Duration**	**Time**
Inv12	Francois Mariette	F. Mariette S. Le Feuteun	PFG-NMR: a versatile tool for microstructure investigation of dairy protein gels	30 minutes	10:15
O30	Adrian Voda	A. Voda, F. Vergeldt G. van Dalen A. Duijster R. van der Sman L. van Vliet H. Van As J. van Duynhoven	Microstructure and rehydration behaviour of freeze-dried fruits and vegetables	20 minutes	10:45
O31	Takeshi Kimura	Takeshi Kimura Yuto Geya Katsumi Kose Tomoyuki Haishi Hiroshi Gemma Yoshihiko Sekozawa	Development of an electrically mobile and remotely operable MRI systemfor outdoor tree measurements	20 minutes	11:05
O32	Volker C. Behr	Volker C. Behr Simone C. Müller Dieter Mahsberg	3D Micro-Imaging Study of the Metamorphosis of the Caterpillar and Pupa of the Large Cabbage White Butterfly at 17.6T	20 minutes	11:25

O33	Frédéric G. Goora	Frédéric G. Goora Hui Han Bruce G. Colpitts Bruce J. Balcom	Simulation of Magnetic Field Gradient Waveforms in Metallic Vessels	15 minutes	11:45
O34	Igor Serša	Igor Serša Jernej Vidmar Franci Bajd Nina Bizjak Eduard Kralj Aleš Blinc	MR Microscopy in Prognosis of Thrombolysis Outcome	15minutes	12:00

	Session Chair: Joe Seymour		**Computational NMR/MRI 13:30-15:30**		
ID	**Speaker**	**Authors**	**Topic**	**Duration**	**Time**
Inv13	Jun Li			30 minutes	13:30
Inv14	Andrew Sederman	A. J. Sederman A. B. Tayler D. J. Holland L. F. Gladden	Quantitative velocimetry of transient flowing systems	30 minutes	14:00
O35	Liang Xiao	Liang Xiao Zhi-qiang Mao Yan Jin	Estimation of Irreducible Water Saturation (Swirr) from NMR Log without Requiring T2cutoff in Tight Gas Sands	20 minutes	14:30
O36	Nadia Amor	Nadia Amor Julia Kowalski Federico Casanova Marcus Greferath Bernhard Blümich	Advanced Investigation of Low-Power NMR by Frank Excitation	20 minutes	14:50
O37	Mark Hunter	Mark Hunter Paul Callaghan	Nonlocal dispersion tensor measurements: Mass transport and medium structure	20 minutes	15:10

Thursday 18th August

Parallel Sessions to the ICMRM11

	Session Chair: Hu Dong		**Core analysis in unconventional oil and gas Sessions08:00-10:00**		
ID	**Speaker**	**Authors**	**Topic**	**Duration**	**Time**
Inv15	Xudong Jing		Recent advances in core analysis	30 minutes	08:00
Inv16	Derrick Green		An Overview of NMR Core Analysis Techniques	20 minutes	08:30
O38	Fahad Shamim	Fahad Shamim Martin Bencsik Mike Newton Robert Morris	NMR measurements of dynamic clogging of porous systems applied to constructed wetlands monitoring	20 minutes	09:00
O39	Osama A. El Mahdy	O.A. El Mahdy G.M. Hamada	Sands with NMR Logging data	20 minutes	09:20
O40	Ranhong Xie	Ranhong Xie Lizhi Xiao Jiajun Liu	Time Domain Analysis Numerical Simulation and Influence Factors of NMR Logging	20 minutes	09:40

	Session Chair: Xudong Jing		**Core analysis in unconventional oil and gas Sessions10:15-12:20**		
ID	**Speaker**		**Topic**	**Duration**	**Time**
Inv17	Marc Fleury		Low field NMR for characterizing nanoporous systems	30 minutes	10:15
O41	Xin Li	Xin Li Lizhi Xiao	Nuclear Magnetic Resonance Logging While Drilling Tool: Concept and Design	20 minutes	10:45
O42	Xiangmin Zhang	Xiangmin Zhang Scott Campell Albert Hebing Mike Burns	Characterization of microporosity in reservoir rocks by Nuclear magnetic resonance (NMR) spectroscopy	20 minutes	11:05
O43	Yuqin Chen	Yuqin Chen	Applications of NMR Logging in A Clastic Reservoir of Low Porosity and Low Permeability	20 minutes	11:25
O44	Hu Dong	Jeff Gelb, Hu Dong Martin Blundt Allen Gu Tiffany Fong Luke Hunter S H Lau Wenbing Yun	Digital Core Analysis in 3D: Non-Destructive Imaging and Multi-length Scale Flow Modeling	20 minutes	11:45
O45	Yihua Zhu		Determining Klinkenberg Permeability of Tight Gas Reservoir by Lattice Boltzmann	15 minutes	12:05

	Session Chair: Guo Tao		Core analysis in unconventional oil and gas Sessions13:30-15:30		
ID	**Speaker**	**Authors**	**Topic**	**Duration**	**Time**
Inv18	Yingli Zhang	Qing Cai Yingli Zhang Pei-Qiang Yang	Application of 2D NMR Techniques in core analysis	30minutes	13:30
O46	Wenzheng Yue	Wenzheng Yue Guo Tao Xiyuan Chai Bing Xie Hui Zhou	Digital Core Approach to The Effects of Clay on The Electrical Properties of Saturated Rocks Using Lattice Gas Automation	20 minutes	14:00
O47	Yuechao Zhao	Yuechao Zhao YongchenSong Yu Liu, Min Hao Ningjun Zhu Tongli Wang	Visualisation of Supercritical CO2 Miscible Displacement in Porous Media Using MRI	15 minutes	14:20
O48	Junxiao Li	Junxiao Li Guo Tao	Lattice Boltzmann Simulations on the Flow Mechanisms of Micro-Fractures in Low Permeability Gas Reservoirs	15 minutes	14:35
O49	Wenbing Yun	Jeff Gelb Allen Gu Tiffany Fong Luke Hunter S H Lau Wenbing Yun	Non-destructive 3D Pore Modeling using X-ray Computed Microtomography and Nanotomography	20 minutes	14:50
O50	Shawn Zhang	Shawn Zhang Murray Gingras	A virtual material studio to study rock petrophysical properties	20 minutes	15:10

Paul Callaghan's Speech at Conference Banquet

I am so delighted to speak here in The Great Hall of the People at this extraordinary conference. The Magnetic Resonance Microscopy conference is quite unique in the sense that nobody wants to miss it. We know how much we enjoy not only the science, but the great companionship of fine colleagues.

The history of magnetic resonance is a long one. I would like to think it began in 1897 when a young New Zealander called Ernest Rutherford arrived at Cambridge University. Back in New Zealand he had worked on Hertzian waves for his Master's degree at Canterbury University. But his Cambridge PhD supervisor, J J Thompson, suggested he try to discover what Marie Curie's radiation was. Rutherford found that is was comprised of alpha particles. And in 1910, he used the alpha particle to discover the atomic nucleus. But Ernest Rutherford could not possibly have believed what could come out of that discovery. Thirty five years later, in 1945, we had the discovery of the magnetic resonance, and in 1950, the spin echo. I remember 40 years later, when I was in France at the 1989 ISMAR conference in Morzine, John Waugh saying, "NMR is dead, but there may be some twitches left in the corpse". How wrong he was. Here we are, 20 years later, and magnetic resonance is in great heart.

We see so often that technology that creates science, more often than the other way around. The discovery of radio waves and radio communication created magnetic resonance. The development of computing created magnetic resonance imaging while super conductors gave us biomedical NMR. Now developments in cell phone technology and rare earth magnets have enabled portable NMR. What nanotechnology will bring we can only imagine.

Our community is in great heart. It spans across physics, chemistry, food science, geophysics, medicine and chemical engineering, to name but a few areas. And if any one conference represents all those branches of science so well, this one does. There is something remarkable about NMR people because we think broadly. We live in the world of many diverse areas of science and technology, more so than people in any other area of science that I can think of.

To the younger scientists of this community, I would like to make a suggestion. You are in a field where you understand how science and technology benefits humanity. But there is something more that science calls from us. Carl Sagan once said, "Science is our candle in the dark". It is what has enabled humanity to struggle out of a dark world indeed. And we have values in science. Those values are called upon by the world with its enormous problems and by the countries from which we come.

The values of science include: an evidence base for decisions; peer review has a way of life; expressing complex ideas, simply and clearly; what numbers mean and what they do not mean; that nature is rational but is not benign; that knowledge is never to be feared; that common sense should not be trusted because science is a means of discovering knowledge that defies common sense.

We are contrarians at heart in science. We have a point of view to express in the world outside our laboratory walls that is needed by our countries, needed by our communities and needed by business. I encourage you, the younger members of this audience, to think of science as a form of leadership that you can offer.

I want to thank this extraordinary community, which I have so much enjoyed being part of and I want to particularly thank Professor Lizhi Xiao for his excellent organization of this conference. To be speaking in this place that I have known about for so many years my life, is a great honour.

I would like to finish with a salutation in the language of my country:

"Kia ora tatou,
e nga tangata whenua me nga manuhiri, haere mai, haere mai, haere mai.
Kia kaha, ake, ake, ake"

("Thank you to you all, to the local people and to the visitors, thrice greetings. May you have strength forever")

In the Banquet Hall of the Great Hall of The People, Beijing, China

17 August 2011

Plenary Lectures

Plen1

Re-examining 1950s spin physics to improve modern magnetic resonance microscopy and imaging

Warren S. Warren,

Department of Chemistry/Duke Box 90346, Duke University, Durham NC 27708 USA

NMR is by far the most powerful form of spectroscopy to the practicing chemist, and MRI has become a very powerful clinical imaging modality, but the known limitations of MRI are rather fundamental. The Boltzmann distribution implies that the net fractional magnetization is small at room temperature, so in most MRI studies, the signal arises mostly from water. Contrast then arises primarily from parameters that can be traced back to spin physics explorations of the 1940s and 1950s (the local bulk magnetization M_o, the relaxation parameters T1, T2 and T2*, and local values of diffusion, sometimes in different directions), which often only have very indirect correlation with important properties such as metabolism or high resolution morpology. Existing contrast agents have limited specificity; targeted contrast agents are being developed by multiple groups, but they usually need to be present in high concentration to affect the signal.

This talk will focus on our re-examination of a variety of effects which were assumed to be well characterized decades ago, but which in fact were not completely understood; the consequences of this re-evaluation is prediction and demonstration of new sources of contrast. For example, magnetic dipole-dipole interactions in liquids and soft materials were shown over the last few decades to provide new ways to image temperature, remove inhomogeneity, and measure subvoxel image structure[1]; but these results relied on the even earlier theoretical treatment of dipolar interactions in solids, such as the secular approximation[2]. We have recently found subtle flaws in those treatments, which predict new pulse sequences and may be very important for short-T2 images as well. As another example, we have adapted a recent result from the quantum computing literature[3], and found that equal spacing between multiple echo pulses (the traditional CPMG sequence) often does not provide the optimum signal in imaging applications[4]. Finally, we have shown[5] that pairs of equivalent spins permit storage of polarization in molecular states with extremely long values of T1 and T2, which is very useful for hyperpolarized imaging. We will discuss recently developed methods to store and extract population from these states, with or without chemical transformation.

References:

1. See for example G. Galiana, R. T. Branca, E. R. Jenista, and W. S. Warren, Science 322 (2008) 421; W. S. Warren, S.Ahn, R. R. Rizi, J. Hopkins, J. S. Leigh, M. Mescher, W. Richter, M. Garwood, and K. Ugurbil, Science 281 (1998) 247
2. A. Abragam, Principles of Nuclear Magnetism (Oxford University Press, London, 1961) chapter 3; G. Deville, M. Bernier, and J. M. Delrieux, Phys. Rev. B 19 (1979) 5666
3. G. S. Uhrig, Phys. Rev. Lett. 98 (2007), 100504
4. E. R. Jenista, A. M. Stokes, R. T. Branca, and W. S. Warren, J. Chem. Phys. **131**(2009), 204510
5. W. S. Warren, E. Jenista, R. T. Branca, and X. Chen, Science 323 (2009), 1711

Plen2

Worried about the poor sensitivity of NMR? New technologies promise a bright future for biomedical imaging

Axel. Haase

Technical University Munich, Institute for Medical Engineering

The low energy of nuclear magnetic resonance transition provides no side effects in biomedical applications but results in a fundamentally low signal-to-noise ratio. The poor sensitivity of NMR becomes even worse when high spatial or time resolution is required. In addition, NMR gives access to biochemical information, but for the in vivo measurement of crucial metabolites having low concentration, the signal cannot reach the detection threshold.

A few technological advances in magnetic resonance promise a dramatically increased sensitivity and therefore the hope for new areas of applications in life sciences. The following advances will be discussed in the lecture: (i) higher magnetic field strength, (ii) cold NMR coils, (iii) phased-array coils and parallel NMR imaging, (iv) hyperpolarization of selected metabolites. In all cases where NMR has still fundamental barriers, other imaging modalities might help. Recently combined multimodal imaging systems have been developed (e.g. MRI-PET) with excellent new possibilities. First results will be shown in the lecture.

Educational

Edu1

An Introduction to MRI

Ben Newling

UNB MRI Centre, Department of Physics, University of New Brunswick,
Fredericton, Canada.

Magnetic resonance imaging (MRI) has been around since 1973, when Paul Lauterbur [1] and Peter Mansfield [2] independently realised that doing a magnetic resonance (MR) measurement in a magnetic field gradient is something rather special (Fig. 1).

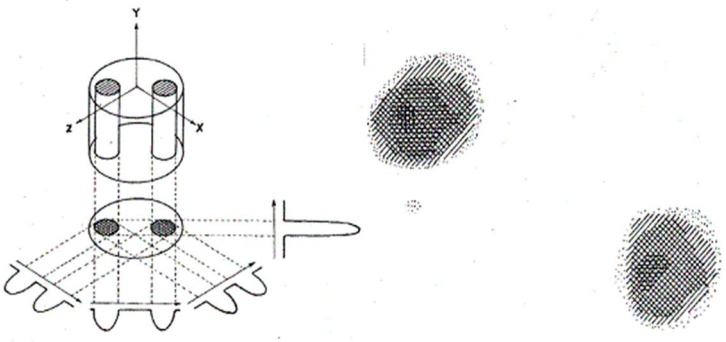

Fig. 1: This is Paul Lauterbur's figure from Nature (1973) [1]. The image to the right shows two tubes of water. Lauterbur named the technique *zeugmatography*, which is a catchy title, but has not survived. Reprinted by permission from Macmillan Publishers Ltd: Nature, 242, 190, copyright 1973.

In this introduction, we will talk about all that one needs to make an MRI experiment work. We will consider the reasons why some materials are MR-active and touch on some of the factors that determine their MR behaviours (including signal lifetimes). We will discuss some common MR techniques and how they operate. The discussion will include spin and gradient echoes, frequency and phase encoding, the definition and usefulness of *k*-space. We will touch on the basics of signal processing.

As with any scientific specialisation, MRI has developed its own jargon (Fig. 2, caption) and is infamous for its extensive use of acronyms. Our introduction will equip the audience with the essential tools to navigate their way through other conference presentations and through the MRI literature.

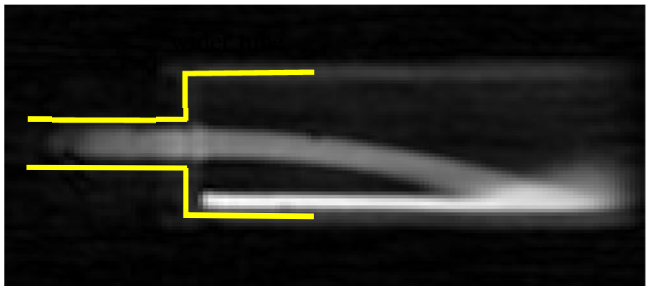

Fig. 2: A purely **phase encoded** MR image of **doped** water ($\mathbf{T_1}$ = 2 ms) flowing from a narrow tube into a wider one. The *k*-**space** data were acquired using a **centric raster** and **zero-filled** to 128 x 128 points before **Fourier transformation**. MRI/signal processing jargon is indicated in **bold face** and will be explained.

Edu2

NMR Hardware

Paul Glover[a],

[a]Sir Peter Mansfield Magnetic Resonance Centre, University of Nottingham, UK

This educational session lecture introduces the elements of the generic MR system hardware required to obtain images or spectra. The design criteria and function of the magnets, gradients, radiofrequency spectrometer and RF coils are examined. Examples of each, how they are designed and optimized is given (with examples) in the lecture. As far as possible examples related to the topics covered by ICMRM 11 will be given.

Magnets

It is most usual for high field, homogeneity and stability magnets to be based on superconductive technology with axially symmetric coil windings. These magnets deliver the highest performance but require cryogenic cooling and are generally not portable (a 7T whole body system is 35 tons). In microscopy and materials applications the desirable parameters may be compromised in order to give portability, light weight or to fit with other constraints. These magnetic fields are then generated by a combination of electromagnet, permanent magnets and other magnetic materials. Magnetic fields may be optimized to give the best homo-geneity or gradient at a particular sweet-spot (which could be outside the magnet itself).

Gradients

In order to spatially resolve the NMR signal then electromagnets are employed to give a (usually) linear profile in B_z with all three (or fewer) spatial axes. Gradient design techniques based on target field and boundary element methods are discussed. Examples of conventional cylindrical gradient design are shown. These design methods can be further exploited to give gradient designs on non-cylindrical geometries or arbitrary former shapes. Gradient design methods can be used to design both shim and pure electromagnet based field profiles.

RF Systems: Spectrometer

The radiofrequency (RF) spectrometer is the central control component for the NMR system and provides system master clock and timings of gradient and RF pulses. The phase and timing stability in a high resolution system is critical and should exceed the magnet in its performance. This level of performance can be achieved if certain design specifications and criteria are followed. The modern spectrometer system is predominantly digital, with analogue components only making up the final parts nearest to the RF coils (i.e. power amplifiers, low-noise pre-amplifiers and transmit-receive switching et el). For example, in the most recent Ingenia body systems from Philips the entire acquisition system is placed on the receive coil itself within the magnet.

RF Systems: Coils

After the main field strength, it is the quality and ability of the coil to faithfully pick up the NMR signal from the sample which defines the overall quality of our information. Signals and noise in an NMR experiment is discussed and the importance of optimum noise matching is introduced. Examples of coils which satisfy a range of demands in various geometries are discussed. The role of finite element RF simulation in coil design is demonstrated.

Edu3

Mobile NMR

Bernhard. Bluemich

Institute fuer Technische und Makromolekulare Chemie, RWTH Aachen University

Mobile NMR started in the well logging industry. Early on, NMR devices were developed to be deployed inside the borehole to characterize the fluids of the well downhole [1]. The successful NMR well-logging devices measure distributions of relaxation and diffusion parameters in the stray field of permanent magnets [2,3]. The same principle is followed with the much smaller NMR-MOUSE [4], which has a higher field, a stronger gradient, and a smaller sensitive volume. It is used for nondestructive materials testing of large objects such as rubber tires, polymer pipes, and objects of art [5]. Today, the NMR force microscope is the smallest stray-field NMR device [6]. While the sensitive volume of stray-field NMR devices can be shaped with proper magnet design [7], the sensitivity can significantly be improved only by enlarging the sensitive volume and the field strength, a strategy which returns mobile NMR to the roots of NMR spectroscopy and imaging with closed magnets. In fact, a variety of desktop MRI magnets has been pioneered by Kose [8], and the first miniature spectroscopy magnet has been developed by McDowell [9]. Today miniature NMR gadgets are targeted for specific detection of biomarkers [10], and the first desktop NMR spectrometers for chemical analysis by high-resolution NMR appear on the market [11,12]. The advances in mobile NMR are expected to benefit from the progress in developing widely applicable and miniaturized hyperpolarization methodologies, alternative detection schemes, microfluidic components for sample preparation and handling, the use of high-TC superconducting magnets, and the development of user-friendly apps for different types of information-driven measurements by untrained NMR consumers.

References:

1. R.J.S. Brown, R. Chandler, J.A. Jackson, R.L. Kleinberg, M.N. Miller, Z. Paltiel, M.G. Prammer, The history of NMR well logging, Concepts Magn. Reson. 13 (2001) 340–411.
2. L.J. Burnett, J.A. Jackson, Remote (inside-out) NMR. II. Sensitivity of NMR detection for external samples, J. Magn. Reson. 41 (1980) 406–410.
3. G.R. Coates, L. Xiao, M.G. Prammer, NMR Logging Principles and Applications, Halliburton Energy Services, Houston, 1999.
4. G. Eidmann, R. Savelsberg, P. Bluemler, B. Bluemich, The NMR MOUSE: a mobile universal surface explorer, J. Magn. Reson. A122 (1996) 104–109.
5. B. Bluemich, F. Casanova, J. Perlo, Mobile single-sided NMR, Progess Nucl. Magn. Reson. Spectrosc. 52 (2008) 197–269.
6. K.W. Eberhardt, C.L. Degen, A. Hunkeler, B.H. Meier, One- and Two-Dimensional NMR Spectroscopy with a Magnetic-Resonance Force Microscope, Angew. Chem. Int. Ed. 47 (2008) 8961 – 8963.
7. F. Casanova, J. Perlo, B. Bluemich, eds., Single-Sided NMR, Springer, Berlin, 2011.
8. K. Kose, T. Haishi, S. Handa, Applications of Permanent-Magnet Compact MRI Systems, in: S.D. Codd, J.D. Seymour, eds, Magnetic Resonance Microscopy: Spatially Resolved NMR Techniques and Applications, Wiley-VCH, Weinheim, 2009, pp 365-379.
9. L.O. Sillerud, A.F. McDowell, N.L. Adolphi, R.E. Serda, D.P. Adams, M.J. Vasile, T.M. Alam, ^{1}H NMR detection of superparamagnetic nanoparticles at 1 T using a microcoil and novel tuning circuit, J. Magn. Reson. 181 (2006) 181–190.
10. J.B. Haun, C.M. Castro, R. Wang, V.M. Peterson, B.S. Marinelli, H. Lee, R. Weissleder, Micro-NMR for Rapid Molecular Analysis of Human Tumor Samples, Sci Transl Med 3

Edu4

Flow and Diffusion Measurement with MR

Eiichi. Fukushima[a]

[a]ABQMR

Nuclear magnetic resonance (NMR) non-invasively accesses many parameters in contrast with other commonly used measurement methods, whether they are non-invasive or not. These parameters can be divided roughly into three classes of information: chemical, physical, and spatial. Chemical includes NMR spectroscopy, the workhorse in analytical chemistry and in structural biochemistry but, to date, there has been relatively little overlap between this class and this conference. Physical information accessible with NMR includes molecular structure, phase transition, diffusion, and flow. Both chemical and physical information can be combined with spatial information to produce maps of such information. In addition, flow and diffusion, by their nature, involve spatial information. Such spatially resolved information is the main emphasis of this meeting. In this lecture, I shall review NMR flow and diffusion measurements.

What is needed for such measurements is the presence of a known gradient of the static magnetic field strength in which the experiments are conducted. When a nuclear spin moves in the field gradient, its precession rate changes and this can be detected to yield the displacement of the spin in the time required to do the experiment – times measured in milliseconds. The dependence of such displacements as a function of measurement time results in identification of the nature of sample motion, i. e., whether it is flow or diffusion. We will start with basic principles and go on to examples with emphasis on gaining physical background knowledge that may aid in understanding flow and diffusion presentations during this meeting. Some references to this subject are listed below. The last three are based on previous ICMRM conferences, specifically in 1991, 1997, and 2009.

References:

1. P. T. Callaghan, Principles of Nuclear Magnetic Resonance, (Clarendon Press, Oxford, 1991).
2. E. Fukushima, Nuclear magnetic resonance as a tool to study flow, Annu. Rev. Fluid Mech. 31 (1999) 95.
3. Magnetic Resonance Microscopy: Methods and Applications in Materials Science, Agriculture, and Biomedicine, edited by B. Blümich and W. Kuhn, VCH Publishers, New York, 1992.
4. Spatially Resolved Magnetic Resonance: Methods, Materials, Medicine, Biology, Rheology, Geology, Ecology, Hardware, edited by P. Blümler, B. Blümich, R. Botto, and E. Fukushima, Wiley-VCH, New York, 1998.
5. Magnetic Resonance Microscopy: Spatially Resolved NMR Techniques and Applications, edited by S. L. Codd and J. D. Seymour, Wiley-VCH Publishers, New York, 2009.

Edu5

Magnetic Resonance Imaging of Fluids in Porous Media

Bruce Balcom

UNB MRI Centre, Department of Physics, University of New Brunswick,
Fredericton, Canada.

Magnetic Resonance Imaging (MRI) is acknowledged to the most flexible and powerful diagnostic imaging modality available to clinical medicine. The rich MR contrast available is remarkably well suited to revealing detailed functional and anatomical information, all non-invasively. Magnetic resonance has long history of application to the study of fluids in porous media, most especially in the areas of core analysis and down hole logging in the petroleum industry.

Porous media is a very broad category of material. For the purposes of this lecture we will restrict our consideration of porous materials to those with an inorganic framework, porosities of at least several percent, and a well developed pore structure with a pore space nominally occupied by water or oil. Prototypical materials would include petroleum reservoir cores and concrete materials.

In this lecture we will outline the basics of spatial encoding and contrast in order to combine the noninvasive spatial resolution of clinical MRI with the information on fluid content, fluid type, fluid environment and fluid dynamics of interest to those who undertake bulk MR core analysis measurements.

Special attention will be paid to the importance, and consequence, of the pore size distribution in realistic porous media, and the relaxation time distributions which result. The important effect of microscopic pores and magnetic susceptibility mismatch of the pore fluid and the inorganic framework will be emphasized.

The lecture will illustrate these ideas through a survey of relevant work by different international laboratories over the last twenty years.

Invited Talks

Inv1

Tissue Microstructure Revealed Using Double Pulsed Field Gradient Filtered MRI

M.E. Komlosh[1,5], E. Ozarslan[1,5], M.J. Lizak[2], I. Horkayne-Szakaly[3], E.J. Rushing[3], R.Z. Freidlin[4] and P.J. Basser[1]

[1]STBB, PPITS, NICHD, NIH; [2]NMRF, NINDS, NIH, [3]Neuropathology and Ophthalmic Pathology, AFIP, [4]CIT, NIH; [5]CNRM, USUHS;

Introduction: Living biological issue, and particularly human tissues and organs are optically turbid. Diffusion MRI methods enable us to learn about tissue microstructure and perform *in situ* and *in vivo* histology. Double Pulsed Field Gradient (d-PFG) NMR multiple scattering techniques[1] in which two diffusion-sensitizing gradients blocks are applied sequentially, can be combined with MRI[2] to glean tissue microstructural information, such as average cell size, shape, and microscopic anisotropy. The diameter of myelinated axons is a crucial neurophysiological parameter that correlates with nerve conduction velocity. In the spine, axons are somatotopically organized into distinct anatomical regions performing specific functions and characterized by different diameters and diameter distributions. The purpose of this study is to evaluate the use of d-PFG MRI[2] to measure and map mean pore or cell diameters within different regions of spinal cord white matter.

Materials and Methods: Formalin-fixed pig spinal cord was rehydrated and put in a 10mm Shigemi tube (Shigemi Inc.) with spinal cord white matter aligned with the z-axis of a 14T vertical-bore Bruker AVANCE III system. The d-PFG NMR parameters were: δ =3.15ms, Δ=60ms, and G was between 0 and 664 mT/m^{-1}; and MRI parameters: TR/TE=3500/6.54 ms, FOV=11mm, matrix size=128x128, and slice thickness=4mm. A recently introduced theoretical framework[3], predicting the MR signal attenuation due to restricted diffusion within a pack of cylinders, was fitted to the data, taking into account a possible free water compartment[4]. A pixel-by-pixel analysis was applied to create a fiber diameter map within the white matter region of the spinal cord. K-means segmentation was performed. For histological studies a portion of the formalin-fixed spinal cord was transferred to 3% glutaraldehyde, post-fixed in osmium tetroxide, and embedded in plastic[5,6]. 1μm-thick tissue sections were stained with toluidine blue. Areas of interest were determined and selected for evaluation on a Zeiss 109 transmission electron microscope.

Results and Discussion: The calculated fiber diameters are in the range expected for such specimen. The clusters produced from the experiment show well-defined regions that generally follow the known anatomy of pig spinal cord white matter. These assignments were verified by histology.

Conclusion: d-PFG filtered MRI is a powerful tool not only for mapping axon diameter, but potentially for other microstructural features of tissues not measurable by other MRI methods.

References:

1. P.P. Mitra, Phys. Rev. B 51 (1995) 15074.
2. M. E. Komlosh, E. Özarslan, M. J. Lizak, F. Horkay, V. Schram, N. Shemesh, Y. Cohen, P. J. Basser J. Magn. Reson. 208 (2011) 128.
3. E. Özarslan, N. Shemesh, P. J. Basser, J. Chem. Phys. 130 (2009) 104702.
4. N. Shemesh, E. Özarslan, A. Bar-Shir, P. J. Basser, Y. Cohen, *J. Magn. Reson*. 200 (2009) 214.
5. H. Finck, Cytol. 7 (1960) 27.
6. J. Freeman, B. Spurlock, Cell. Biol. 13 (1962) 437.

Inv2

Magnetic resonance acoustic radiation force imaging

Yoni Hertzberg, Gil Navon

[a]School of Physics, Tel-Aviv University, Israel,

[b]School of Chemistry, Tel-Aviv University, Israel.

Magnetic resonance guided ultrasonic therapy is a promising minimally invasive technology for constantly growing variety of clinical applications. However the delivery of focused ultrasound energy to the targeted point with optimal intensity is not always achieved, especially in transcranial applications, where the acoustic waves are shifted and distorted mainly by the skull. Magnetic resonance acoustic radiation force imaging (MR-ARFI) is a recently developed technique [1], which utilizes MRI to measure the displacement caused by the ultrasound radiation force. The focused ultrasound (FUS) pulse induces micron-scale static displacement, which is encoded to the MR phase signal by gradients.

We have shown how that aberration caused by the skull can be corrected using the MR-ARFI technique, leading to near optimal focus and more reliable and safer brain FUS treatments [2].

The temporal behavior on the displacement caused by the radiation force can be utilized for the assessment of the elastic properties of the tissue:

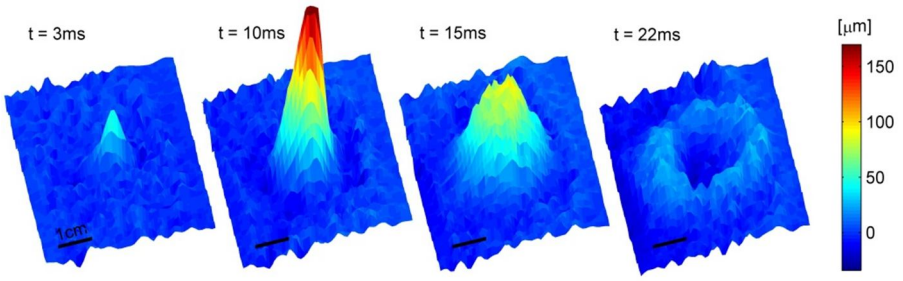

Figure 1. Displacement maps of tissue-mimicking phantom due to a 10ms FUS pulse acquired with 1ms temporal resolution. The phantom starts moving at the beginning of the pulse (3ms) and reaches maximal displacement of 0.15mm near the end of the pulse (10ms). The phantom is moving back to its steady state location after the FUS pulse ended by a shear wave that propagates to the radial direction of the FUS beam (15 and 22ms). The MR-ARFI images were acquired on GE 1.5T scanner using single shot gradient-echo EPI sequenced that was modified to support the ARFI gradients and synchronization with the FUS pulse. Insightec FUS planar phased array transducer, with central frequency of 550kHz, was used to make the ultrasound pulse.

Development of accurate tissue elasticity measurement using MR-ARFI sequences can improve small tumors detection and classification (benign, malignant) using clinical MRI system equipped with FUS. The early detection of small tumors, e.g. cancer breast tumors, is critical for the success of the clinical treatment. The small wavelength (~0.5mm) of the ultrasound waves in tissue in combination with high-resolution MRI provides the most accurate (up to 10^{-8}m displacement resolution and spatial resolution of few tens of microns) elasticity measurement tool for noninvasive detection of small tumors *in vivo*.

References:

1. N. McDannold and S.E. Maier, Med. Phys. 35, 3748-58 (2008).
2. Hertzberg Y, Volovick A, Zur Y, Medan Y and Navon G., Med. Phys. 37 2943–51 (2010);

Inv3

Applications of Remotely Detected NMR and MRI at the Microscale

Vikram Bajaj

Department of Chemistry, University of California, Berkeley

MRI can elucidate the interior structure of an optically opaque object in unparalleled detail but is ultimately limited by the need to enclose the object within a detection coil; imaging of microscopic features within macroscopic objects occurs with low sensitivity because these features occupy only a small fraction of the detector's volume. Here, we overcome this limitation using remotely detected MRI: images of fluids flowing in an object are encoded into the phase and intensity of their NMR signals and decoded by a single volume-matched detector after they flow out of the sample. Using remote detection and compressive sampling, we have obtained microscopic (up to 10 μm) images of flow and velocity distributions in microfluidic devices, packed bead microreactors, polymer monolith chromatography columns, and other structures. Remote detection also separates the polarization, encoding, and detection steps of an NMR experiment, permitting each to be independently optimized. This additional flexibility allows NMR to be integrated with a wide variety of devices, including microfluidic analytical systems and optical detectors of NMR.

Inv4

Handheld CMOS NMR Systems and Their Biosensing Applications

Nan Sun[a], *Donhee Ham*[b],

[a]Department of Electrical and Computer Engineering, University of Texas at Austin, USA
[b]School of Engineering and Applied Sciences, Harvard University, USA

In this talk, we will present our recent work on the development of miniature nuclear magnetic resonance (NMR) systems [1], [2]. The conventional approach for the design of an NMR system is to use a large magnet to boost the NMR signal strength, but this leads a bulky and heavy NMR instrumentation. To substantially reduce the system size, we chose to use very small magnets and designed highly-sensitive radio-frequency (RF) transceivers to cope with the significant signal reduction caused by small magnets. In addition, we integrated transceivers onto CMOS integrated circuit (IC) chips to further reduce the system size and cost. The smallest NMR system that we built weighs only 0.1 kg and can be held at the palm of the hand. It is 1200 times lighter, 1200 times smaller, and yet 150 times more spin-mass sensitive than a state-of-the-art commercial benchtop NMR system.

We used our miniature NMR systems to detect biomolecules by performing an NMR-based biomolecular sensing scheme, whose underpinning physics is that the presence of target biomolecules alters the proton spin dynamics [3]. We detected various types of biological objects, such as cancer marker proteins and cancer cells. Our miniature systems suggest a new way to perform general-purpose biomolecular sensing for disease screening and medical diagnostic in a low-cost, handheld platform. Besides being used for biosensing, our systems can also be used for other applications, including petroleum exploration, material analysis, high-precision magnetometry, and quantum computing.

References:

1. N. Sun, Y. Liu, H. Lee, R. Weissleder, and D. Ham, IEEE J. Solid-State Circuits, 44 (2009) 1629.
2. N. Sun, T.-J. Yoon, H. Lee, W. Andress, R. Weissleder, and D. Ham, IEEE J. Solid-State Circuits, 46 (2011) 342.
3. J. M. Perez, L. Josephson, T. O'Loughlin, D. Hoegeman, and R. Weissleder, Nature Biotechnology, 20 (2002) 816.

Inv5

Finite gradient pulse lengths in PGSE NMR: homogeneous length scale and intracellular diffusion

S. Lasic[a,b], I. Aslund[a], O. Soderman[a], D. Topgaard[a]

[a]Physical Chemistry, Lund University, Sweden, [b]Colloidal Resource AB, Lund, Sweden

The analysis of PGSE NMR data for fluids confined in porous media is greatly simplified by the short gradient pulse (SGP) approximation,[1] stating that the molecular displacements occurring during the gradient pulses of duration δ are much smaller than any structural length scales of the material and the displacements taking place in the time period between the pulses. The displacement probability, mean-square displacement, pore size, and inter-pore distance can be extracted from signal-vs-wave vector q data acquired in the SGP limit. Because of hardware limitations, the PGSE experiment is often performed under conditions in which the SGP approximation is not valid, thus leading to systematic errors of the estimated parameters.[2]

Here we show how the δ-dependence of data recorded at non-SGP conditions can be analyzed to yield information on microscopic diffusion processes and sample microgeometry. More specifically, we estimate the local diffusivity D_0 of water in the intracellular space of yeast cells (see Fig 1) and the homogeneous length scale λ_{hom}, i.e. the minimum length scale at which a microheterogeneous material appears homogeneous, of lyotropic lamellar phases.

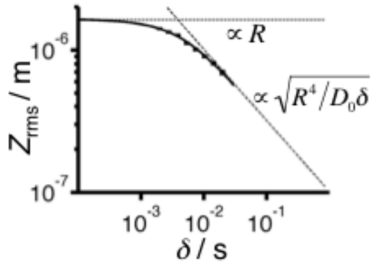

Fig. 1: Estimation of the intracellular diffusivity D_0 by varying the gradient pulse length δ in the PGSE experiment. The figure shows the apparent root-mean-square displacement Z_{rms} (evaluated from the initial decay of signal-vs-q data) vs. δ for intracellular water in a yeast cell suspension. Z_{rms} is proportional to cell radius R at short δ, and to $(R^4/D_0\delta)^{1/2}$ at long δ.[3] A model fit (solid line) to the experimental data (bars with measurement uncertainty given by the height) yields D_0 and R.

For a homogeneous material, the effect of finite δ is taken into account by defining an effective diffusion time $t_d = \Delta - \delta/3$, where Δ is the time between the leading edges of the gradient pulses. For water in a microheterogeneous material, signal-vs-q data recorded with different δ at constant t_d can be separated into two regimes: one at low q where the signal is unaffected by varying δ and one at high q where an increase of δ results in higher signal. An analysis based on Mitra's center-of-mass propagator[4] shows that the high-q dependence on δ corresponds to material heterogeneity a length scale smaller than a threshold value λ_{hom}, the homogenous length scale.[5] The protocol for determining λ_{hom} is especially well suited for structurally disordered materials for which diffusion diffraction peaks cannot be observed.[6]

References:
(1) Callaghan, P. T. *Principles of Nuclear Magnetic Resonance Microscopy*; Clarendon Press: Oxford, 1991.
(2) Linse, P.; Söderman, O. *J. Magn. Reson. A* **1995**, *116*, 77.
(3) Åslund, I.; Topgaard, D. *J. Magn. Reson.* **2009**, *201*, 250.
(4) Mitra, P. P.; Halperin, B. I. *J. Magn. Reson. A* **1995**, *113*, 94.
(5) Åslund, I.; Cabaleiro-Lago, C.; Söderman, O.; Topgaard, D. *J. Phys. Chem. B* **2008**, *112*, 2782.
(6) Åslund, I.; Medronho, B.; Topgaard, D.; Söderman, O.; Schmidt, C. *J. Magn. Reson.* **2011**, *209*, 291.

Inv6

CS-accelerated NMR and MRI

J.Paulsen[a], S.H. Han[b], G. Zhu[c] , Y.K Song[d], G.Cho[d,] Y-Q.Song[a] and H.Cho[b]

[a] Schlumberger Doll Research Center, Cambridge, MA, [b]School of Nano-Bio Science and Chemical Engineering, UNIST, Ulsan, Korea, [c]Bruker Biospin, Billerica, MA, USA, [d]Korea Basic Science Institute, Ochang, Korea.

We present compressed sensing (CS) [1] acceleration of (1) 3D NMR diffusion propagator measurement and (2) *in-vivo* Dynamic Contrast Enhanced (DCE)-MRI.

Multidimensional diffusion propagator measurements are necessary to fully probe the anisotropy of the microstructure from the diffusion propagator, but they greatly increase the sampling requirements for full reconstruction and hence experiment time. In general, CS is an effective reconstruction technique to enable accelerated acquisition for sparse data. We demonstrate that we can greatly reduce the sampling many times with minimal effect on the reconstruction of the diffusion propagator with the example of anisotropic diffusion. CS-assisted 3D propagator measurement is shown in Fig.1

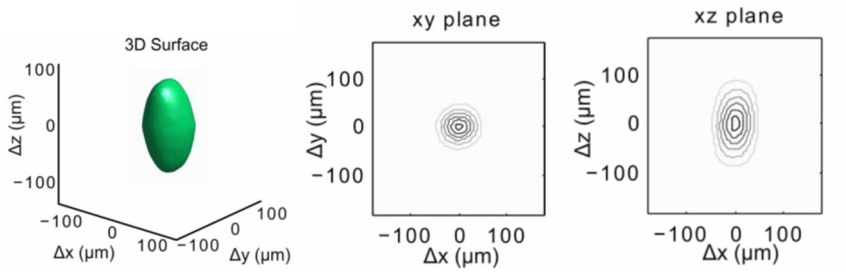

Fig. 1 CS-assisted (x32 subsampled) 3D propagator measurement of an asparagus sample. 2D projection of contour plot is also shown for two different planes. Diffusion anisotropy along stalk axis (*z*) is apparent.

DCE-MRI [2] provides critical information regarding tumor perfusion/permeability by the time resolved measurement of signal increase due to the injection of a T_1 contrast agent. Both high temporal and spatial resolution are required to achieve high fidelity diagnosis of tumor perfusion, but the dynamic nature of the DCE experiment limits simultaneous enhancement of temporal and spatial resolution with conventional methods. The reduction of phase encoding steps possible with CS reconstruction in this case achieved an effective enhancement of temporal resolution, by a factor of 8 at the same spatial resolution, for the *in-vivo* animal tumor models and results are shown in Fig.2.

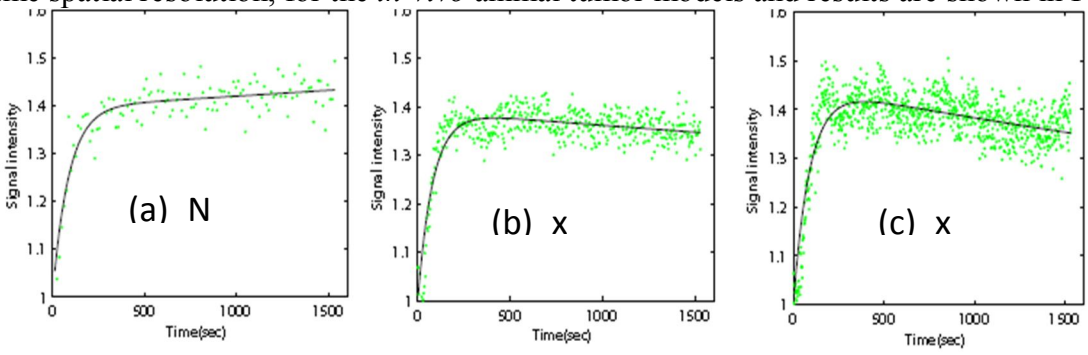

Fig. 2 Time activity curves of DCE-MRI with (a) no CS acceleration, (b) x4 CS acceleration and (c) x8 CS acceleration, respectively. Enhancement in temporal resolution is apparent with CS reconstruction.

References:

1. Lustig M,Donoho D and Pauly JM, Magn Reson Med. 2007 Dec;58(6):1182.
2. Hoffmann U, Brix G, Knopp MV, Hess T and Lorenz WJ, Magn Reson Med 1995 33, 506.

Inv7

Relative permeability estimation from NMR responses: a numerical study using X-ray micro-tomography

T. AlGhamdi[a], J.-Y. Arns[a], C.H. Arns[a],

[a]School of Petroleum Engineering, The University of New South Wales, Sydney, Australia

NMR relaxation measurements are routinely used in the petroleum industry to estimate permeability and to partition the pore space to estimate irreducible water saturation. The shape of the relaxation time distribution, and thus the partitioning of the pore space, is affected by pore-coupling in the presence of heterogeneity, internal gradient effects, and signal to noise ratio. However, given an anchoring of the relaxation time distribution, the logarithmic average of the NMR T_2 distribution is a relatively robust measure and for rocks where a correlation between pore and throat size exist, a reliable estimate of permeability can often be made. In this work we consider NMR correlations with permeability for partially saturated reservoir rocks.

Recent advances in imaging technology, computational facilities, and simulation techniques allow the derivation of multiple petrophysical properties using high resolution tomographic images. We use tomographic images of Bentheimer sandstone and a ferroan dolomite at a voxel size below 3µm with a field of view of 2048^3 voxel to numerically derive measures of permeability, electrical conductivity, and NMR relaxation response (2MHz low field, simulated including susceptibility contrast as in [1]) at partial saturation for the case of drainage by a non-wetting fluid. Correlations between NMR response and relative permeability using the ratios of effective permeability at 100% and partial saturation following the SDR model ([2]) are surprisingly strong (Fig. 1). In particular, a reasonable correlation between lattice Boltzmann derived and NMR estimated relative permeability emerges also for a ferroan carbonate, which was modeled with a low surface relaxivity. This suggests that internal fields help in establishing a surface related/weighted relaxation mechanism for the non-wetting fluid.

While numerically it is easy to partition the fluid phases and thus consider the separate NMR T_2 responses as used here, this is experimentally challenging. Based on careful numerical simulation of T_2-D maps [1] we discuss approaches to fluid partitioning.

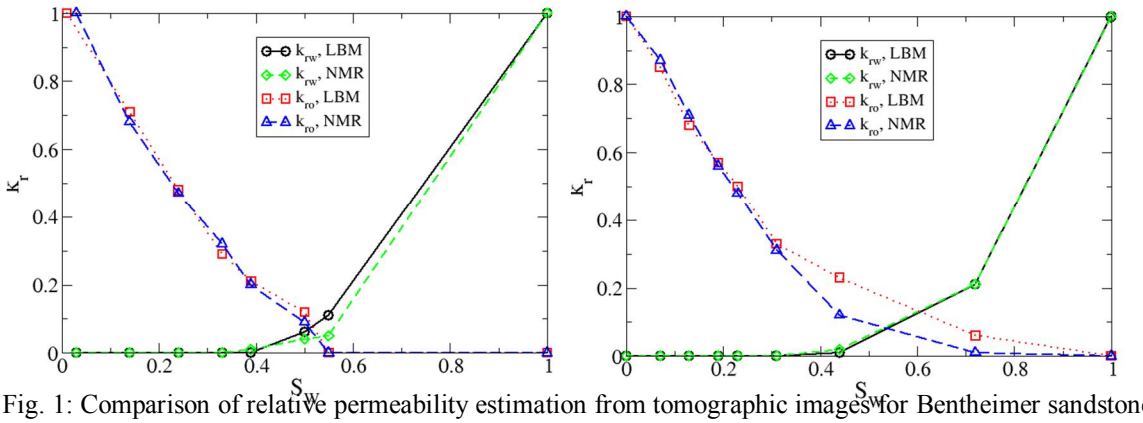

Fig. 1: Comparison of relative permeability estimation from tomographic images for Bentheimer sandstone (left) and a ferroan dolomite (right).

References:

1. C.H. Arns, T. AlGhamdi, and J.Y.Arns, New J. Phys. 13 (2011) 015004.
2. W.E. Kenyon, P.I. Day, C. Straley, G. Gublin, and C. Morris, SPE Formation Evaluation (1986) 622-636.

Inv8

Progress in NMR Well Logging and Core Analysis in China

Lizhi Xiao

China University of Petroleum, Beijing 102249, China

NMR Logging has become an important tool for well logging and core analysis, and is widely used in conventional oil and gas prospecting and development, and has shown big potential in unconventional oil and gas prospecting. China scholars started NMR investigation in well logging in early 1980's, but attracted wide attention followed by Jasper Jackson's visiting in 1996 and run the first and successful NMR logging in June of that year. So far, we have more than fifty NMR logging tools in services, more than ten NMR core analysis laboratories in operation, and several research groups in study. I am going to introduce most of the progress in NMR logging and core analysis in China in this presentation, these include: 1, fundamentals of applications to China complex oil and gas reservoirs; 2, some aspects in tool designs for wire line, LWD and down hole Lab; 3, some aspects in theoretical development, enhancement of SNR, enhancement of vertical resolution, multi-dimensional and pore-scale simulation of NMR response in porous media.

Inv9

Correlations between restricted diffusion and T2 surface relaxation as a probe of porous media

Lukasz Zielinski, Benjamin Chapman, Agnes Haber, and Martin D. Hürlimann,

Schlumberger-Doll Research, One Hampshire Street, Cambridge, MA 02139

The time-dependent diffusion coefficient, $D(t) = \frac{\langle r^2(t) \rangle}{6t}$, where $\langle r^2(t) \rangle$ is the mean-squared displacement of the diffusing molecules, has long been used as a means to characterize porous media[1]. The length scales that can be effectively probed with this technique are limited by the diffusivity of the pore-filling fluid as well as by its relaxation times. For heterogeneous porous media, therefore, such as carbonate rock where structures can vary in size over several orders of magnitude, another technique has been successfully employed that measures the two-dimensional correlations between the diffusion and relaxation (D-T2) properties of the confined fluid[2].

Here we explore how the marriage of these two techniques permits the monitoring of the amount of restriction in different regions of the pore space, based on their associated relaxation times. This has led to a host of new applications, from improved separation of different fluids inside the porous medium, to derivation of rock matrix grain-size distributions and grain wetting properties, to estimation of the permeability of the formation. As an example, in Fig.1 we show how the explicit form of D(T2) correlation which we derived for a simple fluid inside a confining porous medium (curved black dashed line in panel (a)) can be used to obtain a grain size distribution for that medium (panel (b)). This as well as the other applications will be discussed.

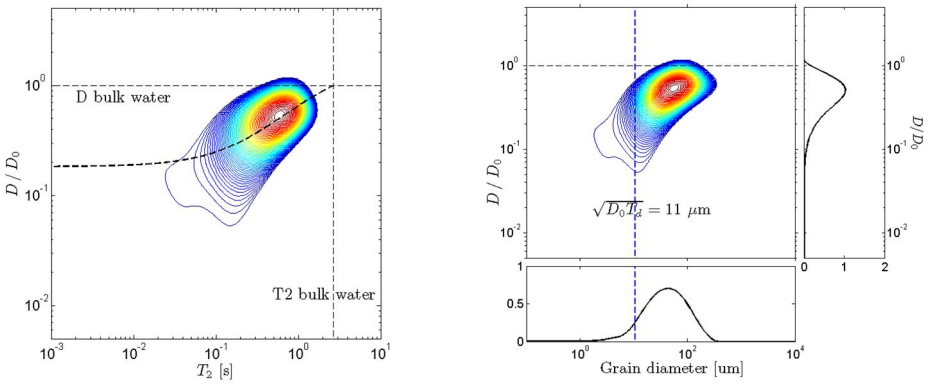

Fig. 1: (a) D-T2 map for a water-saturated carbonate rock core. Black curved line indicates the analytic D-T2 correlation used to obtain the grain size distribution in (b).

References:
1. P. P. Mitra, P. N. Sen, L. M. Schwartz, *Phys. Rev. B*, 47 (1993) 8565.
2. M. D. Hürlimann, *et al.,* Petrophysics 50 (2009) 116.

Inv10

MR measurement of non-equilibrium thermodynamics: Microfluidic colloid suspension and critical phase transition flows

A. Joseph D. Seymour[a], *B. Sarah L. Codd*[b], *C. Einar O. Fridjonsson*[a,*] *and D. Erik M. Rassi*[b]

[a]Department of Chemical and Biological Engineering, [b]Department of Mechanical and Industrial Engineering, [*]Current address: Department of Chemical Engineering and Biotechnology, University of Cambridge

The dynamics of colloid suspensions have become a template system for the study of non-equilibrium thermodynamic phenomena, such as glass transitions, and testing of non-equilibrium statistical mechanics models of fluids. The microscale dynamics of 1 μm radius colloid particles in shear flow in a 125 μm radius capillary measured by PGSE NMR are directly compared to generalized Langevin equation[1] and continuous time random walk[2] models of particle transport in shear flows. The long displacement length, low-*q*, time dependent colloid particle dynamics in the microfluidic flow characterize both the colloid transport and the microstructural rearrangements related to the complex fluid rheology of the suspension. The concept of microrheology[3] by NMR (μ-Rheo-NMR) is discussed in the context of the measured data and established Rheo-NMR[4] methods.

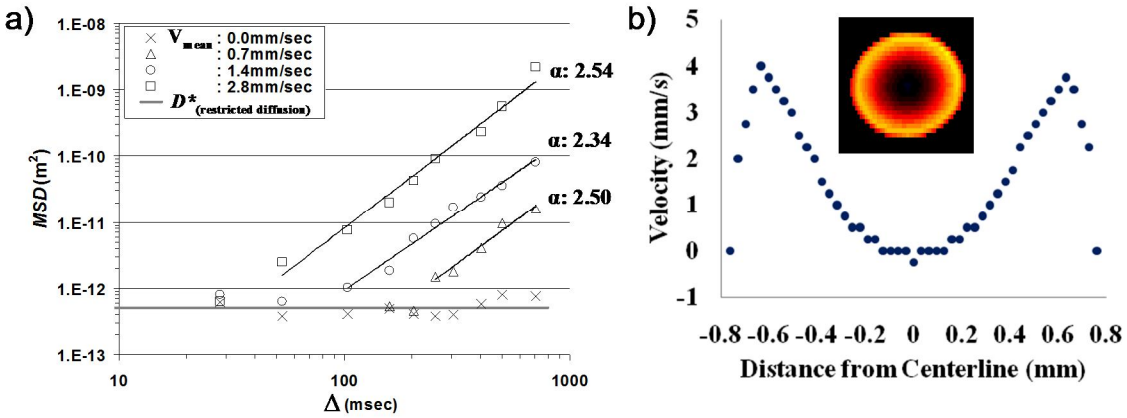

Fig. 1: a)Effective diffusion coefficient of colloid particles (D^*) measured at flow rates from 0.0 to 0.5mL/hr using velocity compensated PGSE experiments. After onset of irreversibility data is fit with $MSD(\Delta) = 2D^*\Delta^{\alpha}$ to obtain the anomalous time dependent collective dynamics scaling. b) Velocity distribution for C_2F_6 in capillary shear flow at the critical point 29 bar and 20.5 °C.

The flow of supercritical fluids are of significant interest in geophysical carbon sequestration, green chemistry and the modeling of critical phase transition dynamics. The displacement length and time scale dependent dynamics for C_2F_6 flow in a capillary and in porous media are analyzed from the gas phase (10 bar) to the supercritical fluid phase (75 bar). Of particular interest are the dynamics in these flows at the critical pressure and temperature, where small fluctuations in pressure result in large fluctuations in density. The data is discussed in terms of nonlinear Langevin models (Model H) for coupled order parameter and momentum evolution.[5]

References:
1. M.G. McPhie *et al*., Physica A 299 (2001) 412.
2. R. Metzler and J. Klafter, Phys. Reports 339 (2000) 1.
3. T.G. Mason and D.A. Weitz, Phys. Rev. Lett. 74 (1995) 1250.
4. P. T. Callaghan, Rep. Prog. Phys., 62 (1999) 599.
5. A. Onuki and K. Kawasaki, Supp. Prog. Theor. Phys., 64 (1978) 436.

Inv11

Portable NMR for the plant sciences: from tree trunk to cereal grain

Carel W. Windt[a], *Peter Blümler*[b]

[a]Forschungszentrum Jülich, IBG-2: Plant Sciences; [b]Universität Mainz, Institut für Physik

Plant breeding was revolutionized by the introduction of genetics. However, the genetic makeup of a plant is only half the story: the expression of the genetic code is modulated strongly by environmental factors. To assess how new genotypes perform under varying conditions, traditional methods (harvest, measure, dry, weigh) are destructive and slow. They require many samples, even for a single point in a time series, whereas typically only a few plants of a genotype exist. To address this issue NMR methods are needed that allow plants to be measured repeatedly or continuously.

The most important indicators of plant performance are parameters such as water content, sap flow, wood deposition, or sugar and starch accumulation. Low field NMR methods to measure these parameters, such as relaxometry, velocimetry or basic imaging, have been well established. However, despite its attractiveness so far only few botanical studies have used portable NMR methods in a field situation, let alone applied it routinely. The trouble is that, although the NMR methods for such studies are available, suitable hardware for the largest part is not.

Some of the largest hardware challenges pertain to the practical issues. For plants we choose to use homogeneous permanent magnets, yet they should provide open access from at least one side. An issue that conflicts with having open systems is shielding; when working in an industrial- or greenhouse environment RF noise is a major concern. To optimize SNR we use close-fitting solenoid RF coils, but we also need to change plants quickly without damaging them. Perhaps the most important problem in the field is temperature. It may change rapidly and will not only affect the plant, but also the magnet and the spectrometer.

In this contribution we present a number of approaches to address these challenges. We tested a number of magnet concepts and explored their suitability for use in simple, sensor-like NMR setups suitable for use in the field. To emulate sensor-like applications that could be run on even the simplest of spectrometers we used basic relaxometric methods to estimate water- and solid content. Such measurements could be done in a highly automated fashion, either leaving the spectrometer to run autonomously for days or control it remotely, and were found to produce data of surprisingly high information content on subjects ranging from the filling of a single rice grain to the daily growth of the trunk of an oak tree.

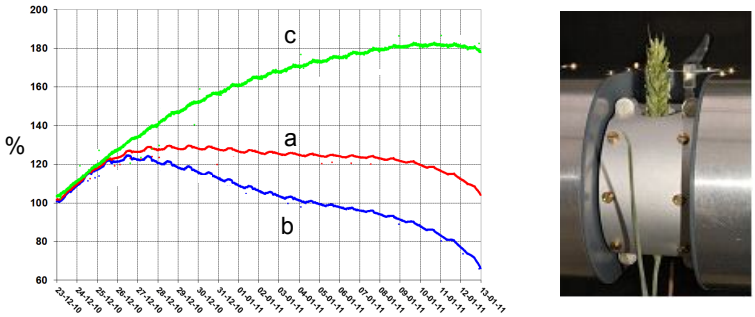

Fig. 1: Growth and starch filling of a wheat ear, monitored during 3 weeks of development. Shown are the relative changes in total proton density (a), liquid water (b) and solids (c).

Inv12

PFG-NMR: a versatile tool for microstructure investigation of dairy protein gels

F. Mariette[a,b], *and S. Le Feuteun*[c,d]

[a]Cemagref, UR TERE, 17 avenue de Cucillé, CS 64427 35044 Rennes, France

[b]Université Européenne de Bretagne, Rennes, France

[c]INRA, UMR782, F-78850 Thiverval Grignon, France.

[d]AgroParisTech, UMR782, F-78850 Thiverval Grignon, France.

In the present study, we illustrate the potentiality of the PFG-NMR technique to investigate structural changes in dairy casein gels. Casein is the main milk protein component. It exists in milk as a suspension of large spherical particles called casein micelles. These colloidal particles can be destabilized in different ways, by addition of rennet, by slow acidification, or by combinations of both. Various parameters influence the dynamics of the coagulation process. Depending on these conditions, the gel microstructure and its rheological properties, which are very important attributes of the product, can therefore be very different. To improve our understanding of the microstructure, different PFG-NMR approaches have been carrying out. The diffusion coefficient of poly(ethylene glycol) (PEG) polymers with varying molecular weights, used as probe, were compared in casein gels obtained with different coagulation processes [1,2]. A time-resolved PFG-NMR method to investigate how and when probe diffusion rates vary during the coagulation process of dairy protein was also implemented [2,3]. The last example will we focus on the study of the self-diffusion of non-aggregated casein molecules used as probe and compared with PEG [4].

References:

1.S. Le Feunteun and F. Mariette. J. Agric. Food Chem. 55 (2007) 10764.
2.S. Le Feunteun, and F. Mariette. Macromolecules 41,6 (2008) 2079
3.S. Le Feunteun, and F. Mariette. Macromolecules 41,6 (2008) 2071.
4.S. Le Feunteun, M. Ouethrani and F. Mariette. Food Hydrocolloids (2011) submitted

Inv13

TBA

Jun Li

Tsinghua University, China

Inv14

Quantitative velocimetry of transient flowing systems

A. J. Sederman, A. B. Tayler, D. J. Holland, L. F. Gladden

Department of Chemical Engineering and Biotechnology, University of Cambridge, Cambridge CB2 3RA

Magnetic resonance imaging (MRI) is well established as a tool for the measurement of quantitative velocity fields. For application to transient systems, however, it is important that images are acquired within the timescales of the changes in the flow. For the most highly unsteady systems, this means images must be acquired in only a few tens of milliseconds. Several approaches to this problem have been developed [1,2], and each have their own advantages and limitations. In the present contribution, the application of echo planar imaging (EPI) towards flowing systems is explored. Previous micro-imaging work has focused on the rectilinear k-space sampling scheme of blipped-EPI, including our earlier developments with GERVAIS [1]. Alternative echo-planar k-space sampling schemes can offer advantages over blipped-EPI, including improved temporal resolution, and better robustness to flow artefacts. In particular, spiral imaging has significantly lower sensitivity to flow when compared with blipped-EPI as the basis for a flow imaging technique. The extent of flow artefacts in spiral imaging is quantified, and the technique is then applied to some transient flow systems, including unsteady single phase flow in a pipe up to a Reynolds number of 12,000, and flow about a rising single bubble. In these results it is demonstrated that the manner in which consecutive images are sampled can allow the flow field to be imaged in either the Eulerian or Lagrangian frames of reference. Lastly, the acceleration of velocity encoded spiral imaging using compressed sensing is demonstrated, which permits both the spatial and temporal resolution of the technique to be significantly enhanced. Under this improvement 64 pixel × 64 pixel images were acquired at a rate of 188 frames per second.

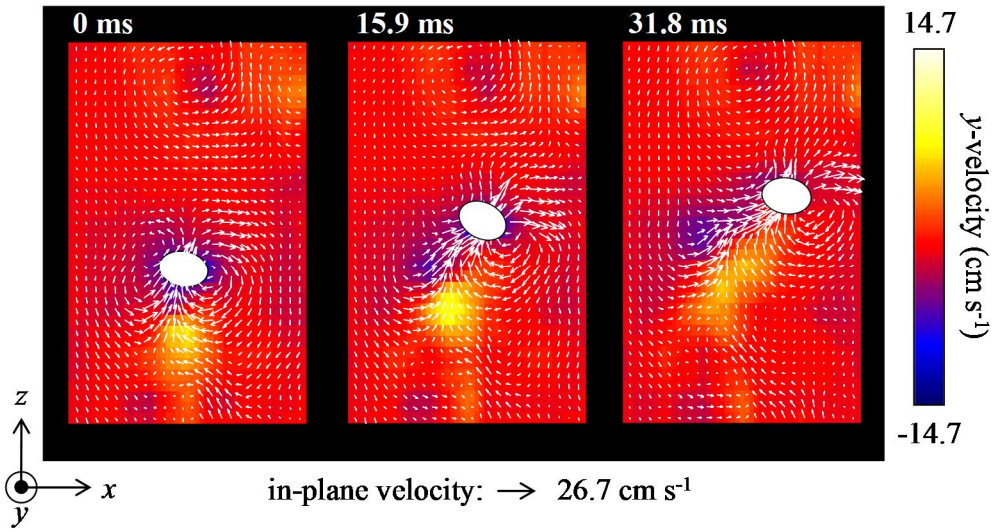

Fig. 1: Three component velocity maps acquired about a rising single bubble. These images are acquired at a rate of 63 fps. The field of view is 20 mm ×30 mm, and the spatial resolution 390 mm × 586mm.

References:

1. A.J. Sederman, M.D. Mantle, C. Buckley and L.F. Gladden, J. Magn. Reson. 166 (2004) 182-189.
2. Amar, A. Blumich, B. and Casanova, F. ChemPhysChem 11 (2010), 2630-2638.

Inv15

Recent Advances in Core Analysis

Xudong Jing

Shell China

This presentation will give a overview of recent advances and current challenges in special core analysis applied to the exploration and production of hydrocarbon resources. It will highlight developments in both measurement and interpretational techniques to help understand petrophysical and multiphase flow properties in reservoir rock and fluid systems including carbonates and unconventional oil & gas developments. Examples of new and emerging technologies in special core analysis (inc the use of NMR and micro-CT techniques) will be discussed.

Inv16

An Overview Of NMR Core Analysis Techniques

D. P. Green
Green Imaging Technologies, Inc., Fredericton, NB, Canada

Nuclear magnetic resonance (NMR) has a long history in the oil industry (almost as long as NMR itself) [1]. A large amount of effort has gone into getting useful petro physical data from both down hole NMR logging tools and laboratory measurements. This presentation will focus on the latter.

The main use of NMR is primarily to define the fluid properties in the pore network. The most basic (and still most used), is to differentiate between clay bound fluid, capillary bound fluid and free or mobile fluid. The NMR signal intensity is directly related to the amount of hydrogen (i.e. saturation) in the sample and more importantly the signal lifetimes depend on the environment of the hydrogen. For example, water in a small pore will have a shorter lifetime then those in larger pores.

With the advancements of new techniques (or the application of older techniques to rocks), we are able to gather a wealth of knowledge about the fluids and the pore network of the rock. NMR can be used to measure the apparent or restricted diffusion of the fluid in the pore network which yields information about the fluid and the tortuosity of the pore network[3]. The NMR relaxation rates are affected by the wettabilty of the rock and thus NMR is a good indicator of wettability[4]. NMR can also be used to investigate the diffusional coupling between different size pore networks common in carbonate rocks[6].

The fluids within the rock can be localized so that saturation images (in 1 or more dimensions) can be obtained. This is useful in producing a porosity image but is even more powerful when combined with external perturbations such as a flow cell or centrifuge. For example, combining 1D saturation profiles with a centrifuge allow for capillary pressure determination[5].

This presentation will focus on providing an overview of basic NMR techniques and will showcase the power of NMR to derive advance rock properties.

References:

1. R. L. Kleinberg, An Introduction to the History Of NMR Well Logging, Concepts in Magnetic Resonance, 13 (2001) 340.
2. G.R. Coates, L. Xiao, and M.G. Prammer, NMR Logging. Principles and Applications, Halliburton Energy Services, Houston (1999).
3. L. L. Latour, R. L. Kleinberg, P. P. Mitra, and C. H. Sotak, Pore-Size Distributions and Tortuosity in Heterogeneous Porous Media, Journal of Magnetic Resonance Series A, 112 (1995) 83.
4. M. Fleury and F. Deflandre, Quantitative Evaluation of Porous Media Wettability using NMR Relaxometry, Magnetic Resonance Imaging, 21 (2003) 385.
5. Q. Chen and B. J. Balcom, Measurement of rock-core Capillary Pressure Curves using a Signal-Speed Centrifuge and One-Dimensional Magnetic Resonance Imaging, Journal of Chemical Physics, 122 (2005) 214
6. M. Fleury, Characterization of Pore to Pore Diffusive Exchange using NMR T2-Store-T2 2D experiments, SCA-21 2009.

Inv17

Low field NMR for characterizing nanoporous systems

Marc Fleury

IFP Energies nouvelles, Petrophysics Dpt,, 1 avenue de Bois-Préau, 92852 Rueil-Malmaison, France

Nuclear Magnetic Resonance (NMR) relaxation techniques are able to detect very small pore sizes, down to nano-meter length scales. Indeed, for water saturated systems, water molecules carrying the nuclear spins explore and interact with the surface at a length scale given by the nuclear interaction between the "solid and liquid" spins. The measured relaxation time is then a measure of the volume to surface ratio of the compartment in the porous media. Taking usual values of the solid-liquid interaction strength, one can easily measure V/S ratio around 1 nm corresponding to relaxation time of about 1 ms or less, well above the resolution of common low field NMR instruments (0.1 ms). We used this technique to characterize nanoporous systems such as coal, clays, catalysis supports. In such systems, there is a potential confusion with protons that are part of the crystallographic lattice (in clays) or the organic matter (in coal). Hence the question of the proton mobility is an important issue and the definition of porosity itself can be become difficult below the nano-meter scale. The diffusive coupling is also a possible important difficulty for identifying the different porosity compartment. We will present several NMR ways of identifying the contribution of the different types of protons, such as deuterium exchange, T_1-T_2 and T_2-store-T_2 maps, solid protons sequences. Finally, we will show some practical applications for characterizing caprocks, shale gas, coal, and catalysis supports, in conjunction with standard petrophysical methods.

Inv18

Application of 2D NMR Techniques in core analysis

Q Cai[a], *B. Y.L. Zhang*[a], *P. Q. Yang*[a]

[a] NIUMAG ELECTRONIC TECHNOLOGY CO., LTD

Abstract

This review paper introduces 2DNMR pulse trains frequently used in core analysis and their applications, as well as relevant relaxation mechanisms. 2D NMR technique content of D-T2 sequence, T1-T2 sequence and 2D NMI technology which can be used to measure the property parameters of formation fluid and the physics parameters directly, such as diffusion coefficient, relaxation time, oil saturation, porosity, permeability and so on. The 2D NMR map can also be used to distinguish between oil, gas and water.

Introduction

Crude oil, water and gas from core are rich in hydrogen nuclei; one-dimensional NMR technique is to measure the T2 relaxation time. Most of time the oil and water T2 relaxation time will be overlap, it's difficult to distinguish, restricted the NMR technology in core analysis.

In recent years, 2D NMR technology have developed rapidly.2D NMR testing give two dimensional information at once experiment, it give more information. This method opens a new area of core analysis. Using the two parameter (transverse relaxation time T2, longitudinal relaxation time T1, fluid diffusion coefficient D), it can distinguish between oil, gas and water easily.

Methods and Principles

1. D-T2 Sequence

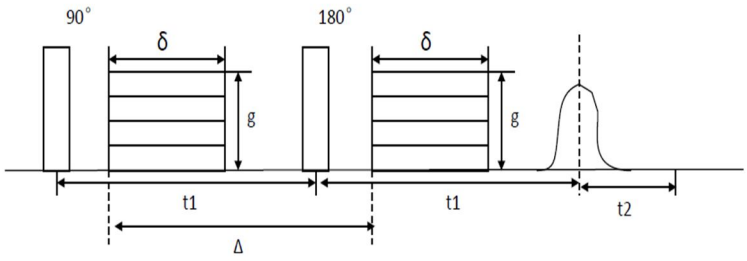

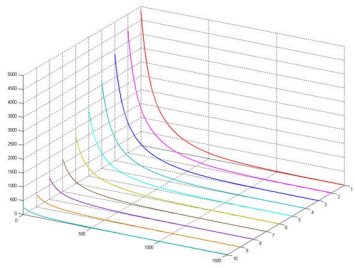

Fig.1 D-T2 Sequence

Fig.2 D-T2 Sequence Sampling

example

The sampling signal M (t) of D-T2 sequence is

$$M(t) = M(0)\exp(-\gamma^2 G^2 \delta^2 (\Delta - \frac{\delta}{3})D)\exp(-\frac{t}{T_2})$$

D-T2 sequence which is the CPMG sequence by adding two changes gradients. According to two-dimensional inversion, we can get T2 relaxation time and diffusion coefficient at the same time. D-T2 sequence can distinguish between oil, water and gas easily. At room temperature, water diffusion coefficient D is 2.5E-9m^2/s, the oil diffusion coefficient is a distribution between 10E-8 m^2/s to10E-11 m^2/s, the gas is 1E-7 m^2/s.

2. T1-T2 Sequence

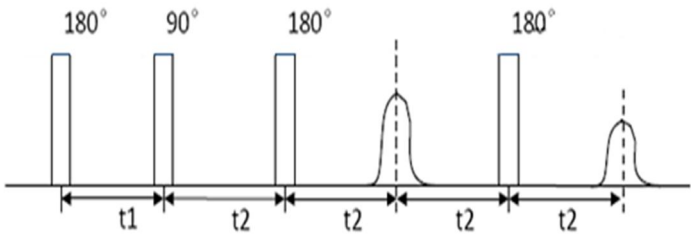

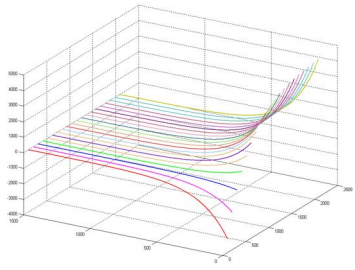

Fig.3 T1-T2 Sequence example

Fig.4 T1-T2 Sequence Sampling

The sampling signal Mis of T1-T2 sequence is

$$Mis = \sum_{j=1}^{m}\sum_{r=1}^{p} f_{ir}\left(1 - 2 * \exp\left(-\frac{T_{w,s}}{T_{ir}}\right)\right)\exp\left(-\frac{t_i}{T_{2j}}\right) + \varepsilon_{is}$$

T1-T2 sequence which is the CPMG sequence by adding 180 degree pulse before. Use the changes of interval time t1 from 180 degree pulse to90 degree pulse as shown in fig.3 to achieve another dimension of the T1 relaxation.

T1-T2 sequence testing has particular advantage in gas identification. Studies have shown that even if the sampled signal to noise ratio of 20, but also a good distinction between bound water, movable water and gas.

3. Imaging Sequence

MRI technology is not used to describe the core itself, but rather describe the cores of the fluid. The technology let intuitive understanding the location and size of fluid come true. Advantages is non-destructive and accurate; disadvantage is when the field is high the image will be distortion. So that, imaging by low-field is intuitive and accurate.

Results and Analysis

1. D-T2 Sequence

Simulated the core sample which content oil, water and gas. Gas saturation is 10%; oil saturation is 40%, water saturation is 50%. Gas diffusion coefficient is 1.5E-7 m^2/s, oil diffusion coefficient is 1.0E-11 m^2/s, and water (bound water) diffusion coefficient is 2.5E-9 m^2/s. T2 relaxation time of gas, oil and water is 40ms，200ms, 20ms, the sampling signal to noise ratio (SNR) is 30.

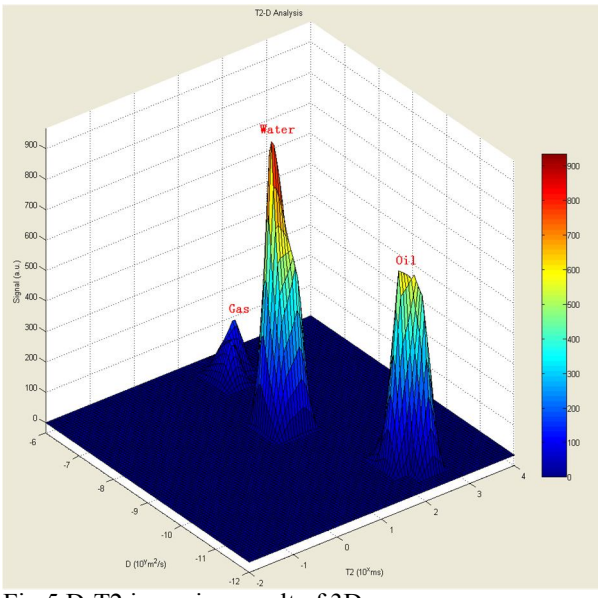

Fig.5 D-T2 inversion result of 3D

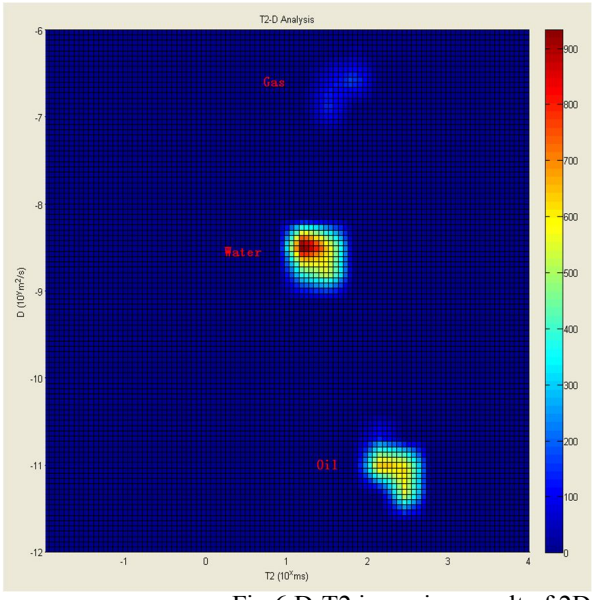

Fig.6 D-T2 inversion result of 2D

As shown in fig.5 and fig.6, we can distinguish between oil, water and gas easily using the different diffusion coefficients. Only one DT2 experiment can get all components ratio and relaxation time.

2. T1-T2 Sequence

Simulated the core sample which content oil, water and gas. Gas saturation is 10%; oil saturation is 40%, water saturation is 50%. T2 relaxation time of gas, oil and water is 40ms，200ms, 20ms; T1 relaxation time of gas, oil and water is 3000ms，400ms, 40ms; SNR is 30.

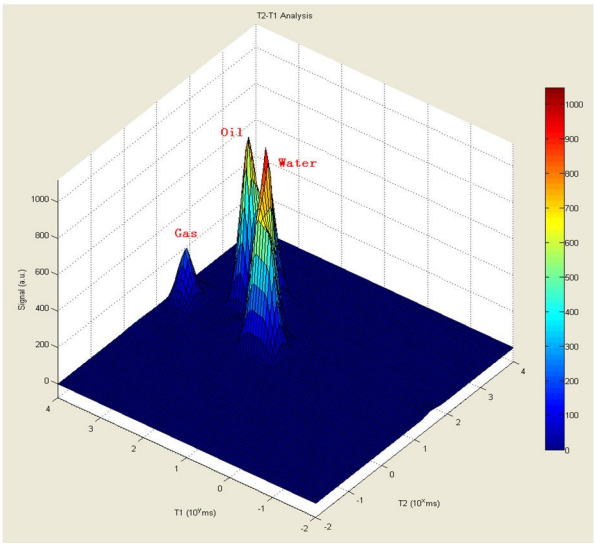

Fig.7 T1-T2 inversion result of 3D

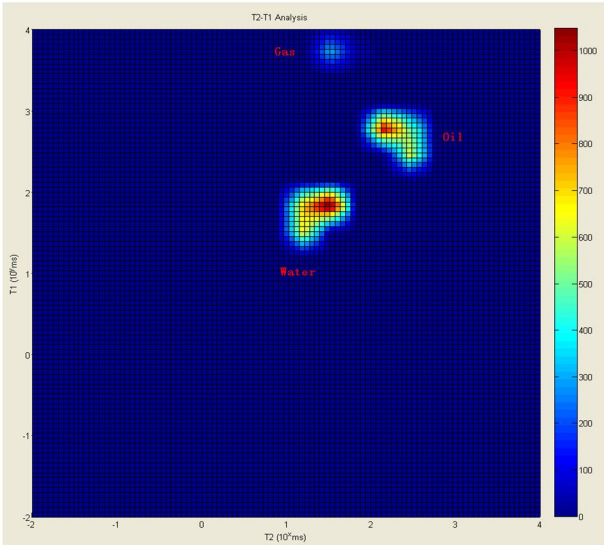

Fig.8 T1-T2 inversion result of 2D

As shown in fig.7and fig.8, the longest T1 relaxation time is gas, and we can distinguish oil and water from T2 relaxation time.

3. Imaging Sequence

Experimental samples: two full-diameter shell rock core; using multi-spin echo sequence, the parameter is TW=0.5s, TE=5ms, similar to T2 weighted images. The imaging thickness is same as sample thickness, phase encoding steps is 128.

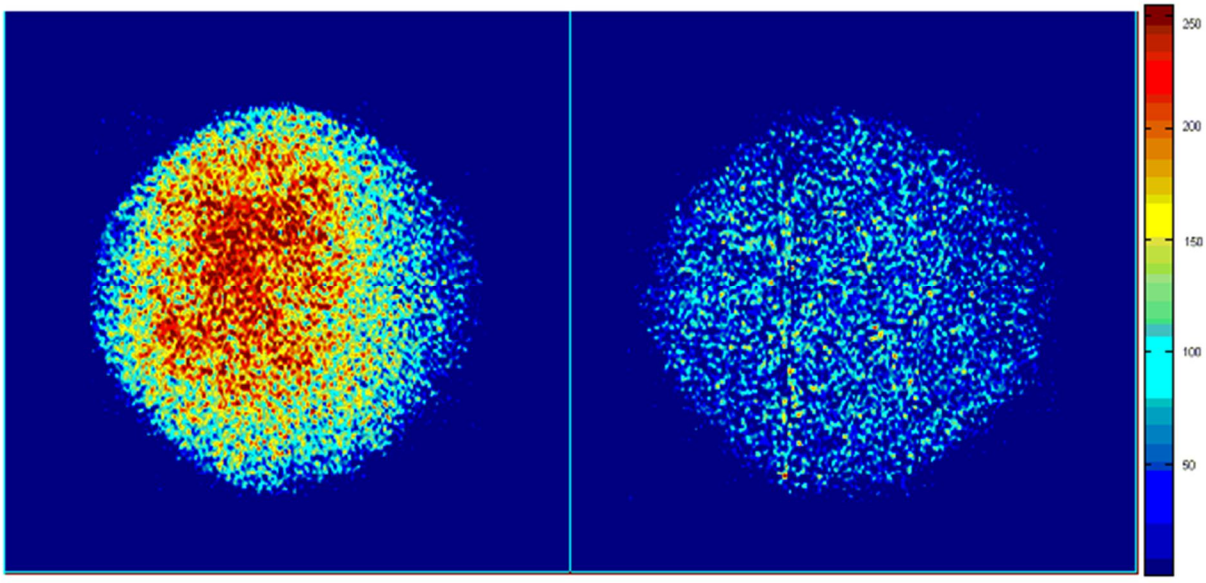

Fig.9 Imaging of No.1 core sample

Fig.10 Imaging of No.2 core sample

As shown in fig.9 and fig.10, the bright circular image area is the sample; the blue surrounding area is background. The color is brighter, the fluid content is more. The colorful area is focus on the left center of No.1 sample, it shows that this area has more water and oil content and the porosity is larger. No.2 sample did not have high lighting area, it shows that this core may have internal cracks; at left side has a vertical distribution cracks and other position has a similar texture, this texture may be cracks or may be the framework among pores.

Inv18

Conclusion

1. Low-field 2D NMR technology can quickly and easily distinguish between the rock samples in the oil, water and gas. The method is more intuitive and visualize.
2. When the SNR is 30, DT2 sequence can distinguish between the oil, bound water and gas, and also can calculate the proportion of each component, T2 relaxation time and other rock physical parameters.
3. When the SNR is 30, T1T2 sequence can distinguish between the oil, bound water and gas, and also can calculate the proportion of each component, T1 and T2 relaxation time.
4. 2D NMI techniques can observe the porosity of core sample intuitive and visualize.

References

1. R.H. Xie L.Z. Xiao, .W. Lu. (T2, T1) Two-Dimensional NMR method for fluid typing, Well Logging Technology. 3(2009), 26.
2. Z. B. Gu, W .Liu, T.Q. Sun. Application of 2D NMR Techniques in Petroleum Logging ,Chinese Journal of Magnetic Resonance. 26(2009), 560.

Oral Presentations

O1

T1 in Articular Cartilage is Strain-Dependent – A µMRI Study

Yang Xia, Nian Wang, Jihyun Lee, Farid Badar
Department of Physics and Center for Biomedical Research,
Oakland University, Rochester, MI 48309, USA (**xia@oakland.edu**)

NMR imaging (MRI) has been used extensively to study the degradation of articular cartilage (1,2), which is a hallmark of osteoarthritis and related joint diseases. Since cartilage is a thin layer of tissue with a number of complex depth-dependent properties, high resolution is critically important in any imaging project (3). Since cartilage is a load-bearing tissue, studying the load-induced tissue deformation provides a unique way to examine the tissue matrix and property (4). This study concerns any strain-dependency in the T1 profiles in the absence and presence of Gd ions in cartilage. We hypothesized that the T1 profiles in cartilage would be depth-dependently sensitive to external strains.

Materials and Methods: Quantitative T1 experiments were carried out on mature canine humeral cartilage before/after the tissue was immersed in a 1mM solution of $Gd(DTPA)^{2-}$ contrast agent (Magnevist) *and* when the tissue was being compressed (up to ~ 48% strains). A Bruker AVANCE II 7T/9cm system was used in this investigation. The slice thickness was 0.8mm; the spatial resolution across the cartilage depth was 17.6µm.

Results: The T1 profile in native tissue (without the presence of gadolinium ions) was strongly strain-dependent, which is also depth-dependent (Left). At the modest strains (e.g., 14% strain), T1 reduced by up to 68% in the most surface portion of the tissue. Further compression (e.g., 45% strain) reduced T1 mostly in the middle-deep portions of the tissue. For the Gd-immersed tissue (Right), both modest and heavy compressions (up to 48% strain) increased T1 slightly but significantly, although the overall shapes of the T1 profiles remained approximately the same regardless of the amount of strains.

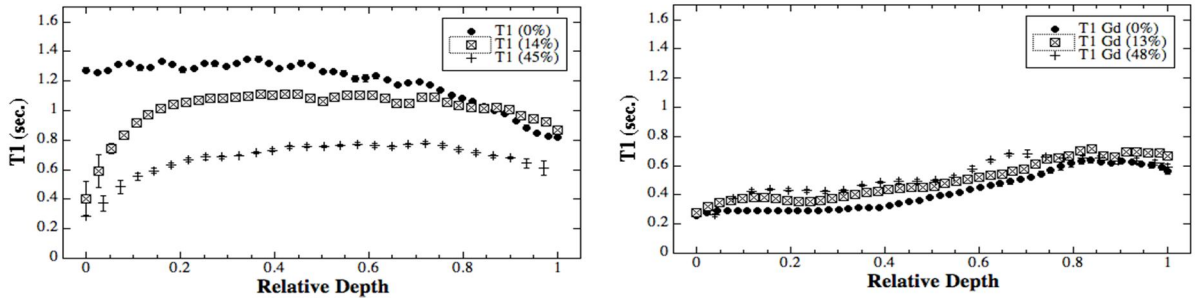

Discussions and Conclusions: This is the first µMRI finding that the T1 profiles in articular cartilage are strain-dependent. The complex relationships between the T1 profiles and the mechanical strains were a direct consequence of the depth-dependent proteoglycan concentration in the tissue, which determined the tissue's mechanical properties (5). This finding has potential implications in the use of Gd contrast agent in clinical MRI (the dGEMRIC procedure (6)), when the loading or loading history of the patients is considered.

ACKNOWLEDGEMENT: Y Xia is grateful for the R01 Grants from the National Institutes of Health (AR045172 and AR052353) and an instrument endorsement from R and J Bennett.

References

1. H. Alhadlaq, et al, **Ann Rheum Dis** 2004; 63: 709-717.
2. Y. Xia, **Magn Reson Med** 1998; 39: 941-949.
3. Y. Xia, **Osteoarthritis Cartilage** 2007; 15: 363-365.
4. H. Alhadlaq & Y. Xia, **Osteoarthritis Cartilage** 2004; 12: 887-894.
5. S. Chen, et al. **Osteoarthritis Cartilage** 2001; 9: 561-569.
6. A. Bashir, et al, **Magn Reson Med** 1996; 36: 665-673.

O2

Manganese enhanced MRI highlighting neuronal pathways of the buccal ganglion in *Aplysia californica*

I.O. Jelescu[a], *R. Nargeot*[b], *B. Djemai*[a], *D. Le Bihan*[a] *and L. Ciobanu*[a]
[a]NeuroSpin, CEA Saclay, [b]Université Bordeaux 1, CNRS UMR 5287

Aplysia californica is a widespread model for the study of the nervous system with MR microscopy[1-3]. Its main advantages are large cell sizes and cell tolerance to non-ideal conditions. In this study, we focus on the perspectives of studying neuronal response within a network of identified neurons using manganese enhanced magnetic resonance imaging (MEMRI).

Materials and methods: The *Aplysia* was anesthetized by injection of an $MgCl_2$ solution (360 mM). The bilateral buccal ganglia were resected and placed in artificial sea water (ASW). Each of the two nerves 2 (n.2, Fig. 1) was isolated by a vaseline wall and dipped in a solution of $MnCl_2$ at 640 mM for the right nerve and at 10 mM for the left. After approximately 4 hrs at 4°C all nerves were cut and the ganglia inserted into a 1.5 mm diameter glass capillary filled with ASW. MR imaging was performed in a 17.2 T horizontal magnet (Bruker BioSpin) using a home-built microcoil as RF transceiver. Imaging consisted of a 3D FLASH (TE = 2 ms / TR = 150 ms / 25µm isotropic / 3 hrs) for T_1 contrast and of a 3D RARE (TE_{Eff} = 18.4 ms / TR = 3 s / 25µm isotropic / 4 hrs) for T_2 contrast.

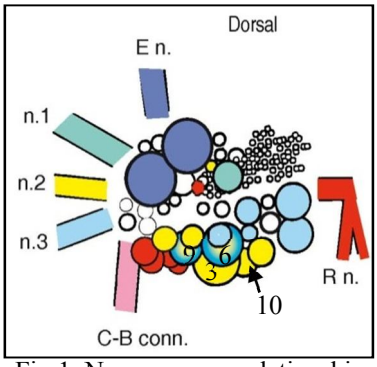

Fig 1. Nerve-neuron relationships in the buccal ganglion

Results and discussion: Representative images are shown in Figure 2. The path of Mn migration from the right side is clear given the high concentration used. Neurons B3, B6, B9 and B10 connected to the nerves 2 display Mn uptake (hyperintense in the T_1 weighted image).

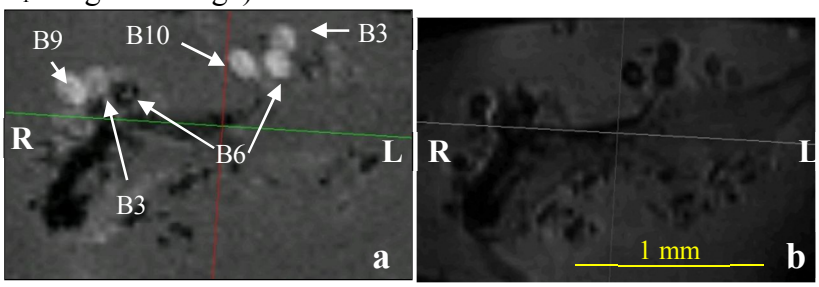

Fig. 2: T_1- (a) and T_2- (b) weighted images of the buccal ganglia (25µm isotropic).

We have demonstrated that the MEMRI technique can be used for tracking neuronal pathways in isolated ganglia of *Aplysia californica,* a well-known model for the study of the nervous system. The results confirm the known axonal projection of identified motor neurons in the peripheral nerves of the buccal ganglion. Future experiments will focus on measuring changes in Mn concentration inside targeted neurons following specific stimulations such as the addition of neuroactive substances as well as measuring axonal transport rates.

References:

1. J.S. Schoeniger, N. Aiken, E. Hsu and S.J. Blackband, J Magn Reson Series B 103 (1994) 261-273.
2. E.W. Hsu, N. R. Aiken and S.J. Blackband, Am J Physiol. 271 (1996) C1895-1900.
3. S.C. Grant, D.L. Buckley, S. Gibbs, A.G. Webb and S.J. Blackband, Magn Reson Med 46 (2001) 1107-1112.

O3

DDIF: A novel contrast for MRI of trabecular bone

D. Mintzopoulos[a], J. L. Ackerman[a], and Y-Q. Song[a,b],

[a]Martinos Center, Department of Radiology, Massachusetts General Hospital, Charlestown, MA, USA
[b]Schlumberger-Doll Research, Cambridge, MA, USA

INTRODUCTION: Bone fragility fracture is a serious and costly public health issue [1]. There is strong interest in non-invasive, clinically applicable MRI methods to characterize trabecular bone structure in vivo [2, 3]. We employed the DDIF method (Decay due to Diffusion in the Internal Field), to study (ex vivo) intact animal trabecular bone specimens of varying trabecular structure and porosity, containing marrow and blood, close to in vivo physiological conditions. DDIF has been studied for marrow-free trabecular bone [4, 5]. However, the reduction of water diffusion and T1 in marrow compared to bulk water may reduce the DDIF contrast. We examined the feasibility of DDIF is in realistic bone specimens, in view of in vivo application to humans.

MATERIALS AND METHODS: Fresh animal bone specimens were acquired locally. Samples were maintained at body temperature during MRI scanning at 4.7 T.

RESULTS:

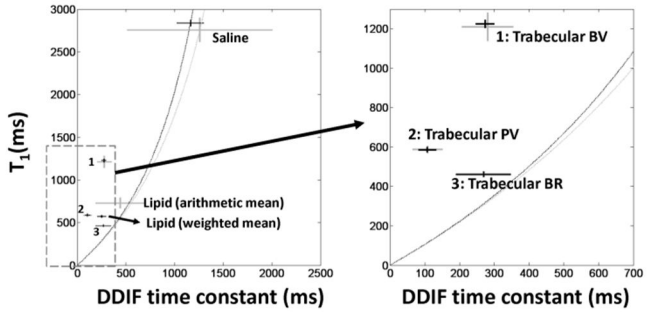

Fig. 1: Comparison of the **measured DDIF time constant and T_1 for several bone samples.** Sample Groups: trabecular bovine vertebra (BV, #1), trabecular porcine vertebra (PV, #2), and trabecular bovine rib (BR, #3) ***Right,*** magnification of boxed area (only trabecular group averages shown). Arithmetic averages in lighter gray; weighted averages in black. The data of BV and PV show significantly DDIF effect ($R_{DDIF} > 1/T_1$). The boundary line separating the region with significant DDIF effect from the unphysical region to the right, is referenced to the saline data. Lipids do not exhibit significant DDIF effect and lie very close to the boundary.

Our data indicate that DDIF imaging is possible in spite of the reduction of T_1 and diffusion coefficient in bone marrow, and suggest that the application of DDIF *in vivo* is possible for improving bone characterization. Work is underway to further test the DDIF methodology in *in vivo* experiments.

References:
1 Rousculp MD, Long SR, Wang S, *et al*. Value Health 2007; 10(2): 144-52
2 Carballido-Gamio J, Majumdar S. Curr Osteoporos Rep 2006; 4(2): 64-70
3 Wehrli FW. J Magn Reson Imaging 2007; 25(2): 390-409
4 Sigmund EE, Cho H, Chen P, *et al.* Magn Reson Med 2008; 59(1): 28-39
5 Sigmund EE, Cho H, Song YQ. NMR Biomed 2009; 22(4): 436-48

O4

Frequency mixed Traveling Wave for 2D Magnetic Particle Imaging

P. Vogel[a,b], M. A. Rückert[a,b], P. Klauer[a,b], W. H. Kullmann[a], P. M. Jakob[b,c], V. C. Behr[b]

[a]Electrical Engineering, University of Applied Sciences Würzburg-Schweinfurt, Schweinfurt
[b]Department of Experimental Physics 5 (Biophysics), University of Würzburg
[c]Research Center for Magnetic Resonance Bavaria e.V (MRB), University of Würzburg

Magnetic **P**article **I**maging is based on the nonlinear response of ferro- and super-paramagnetic particles to magnetic fields [1]. For imaging, a field free region (FFR) of a strong gradient in the order of 1-5 T/m is moved through the sample. A new gradient design allows performing dynamic imaging in a linear sampling scheme by using a traveling wave [3]. We present an extension for doing 2D imaging using a traveling wave in combination with frequency mixing [2]. This approach provides a large field of view (FoV) in one direction (here: z-axis) with the possibility of 2D encoding in a second direction.

The linear gradient system contains 16 consecutive coils (full length: 144 mm) for generating two FFRs (gradient strength: z-axis: 3.5 T/m, x and y-axis: 1.75 T/m, 1.6 kW). They travel in z-direction by applying a sinusoidal current (f_1=1 kHz) with an increasing phase shift to adjacent coils. The coils for frequency mixing are oriented orthogonally to the gradient array direction (Fig. 1A). Their field strength (10-15 mT at f_2=24 kHz, 200 W) is sufficient to move the traveling FFRs about 6 mm out of the symmetry axis (z-axis). The coils were driven using regular audio amplifiers (TSA4-700, t.amp).

In preliminary tests the simulation results of the point spread function (PSF) were confirmed. In addition, the spatial resolution in the z direction was determined to be less than 2 mm. Figure 1E shows the 2D reconstruction corresponding to the data in figure 1D.

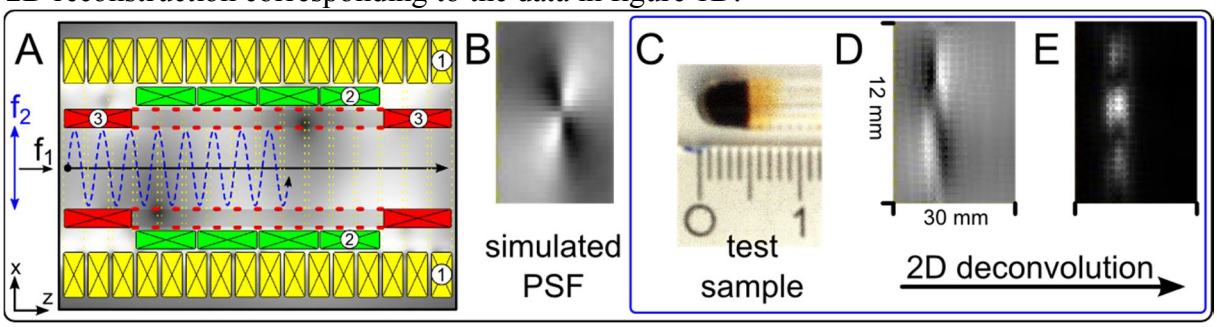

Fig. 1: **A**: Scanner design: yellow (1): linear gradient array, green (2): receiving coil, red (3): new frequency mixing coil. The two FFRs (dark regions) travel now along blue dashed path. **B**: Simulated signal from a delta like sample. **C**: Sample (Resovist ®, Bayer-Schering). **D**: Raw signal. **E**: Deconvoluted signal.

The traveling wave approach provides the possibility to increase the FoV along the symmetry axis without increasing the acquisition time, while keeping the specific absorption rate constant. The frequency mixing increases the SNR by reducing the fractional bandwidth and shifting the signal to a higher frequency. This allows determining the sample position in z-direction with an accuracy of 1.6 mm. Finally, this design inherently provides an additional encoding direction (x-axis).

References:

1. B. Gleich, J. Weizenecker: Tomographic imaging using the nonlinear response of magnetic particles. Nature 435, 1214-121, 2005
2. H. J. Krause et. al.: Magnetic particle detection by frequency mixing for immunoassay applications. JMMM 311, 436-444, 2007
3. P. Klauer et. al.: Magnetic particle imaging: linear gradient array for imaging with a traveling wave. ISMRM 2011 Abstract, 5440

O5

Non-invasive measurements of water transport and optical properties in the human eye

J.M. Pope, B.A. Moffat, C.E. Jones, S. Kasthurirangan, E. Markwell and D.A. Atchison

Institute of Health and Biomedical Innovation, Queensland University of Technology
GPO Box 2434 Brisbane, Australia 4001

We have employed NMR micro-imaging to study properties of the human eye that are not readily measurable by standard techniques of optometry. The lens of the eye has no vasculature, so transport of nutrients and waste products into and out of the lens, which is important for maintaining lens health and preventing development of cataract, relies primarily on passive diffusion. We have measured water transport in the human eye lens in vitro using both isotope (D_2O) substitution and diffusion tensor imaging (DTI). The results showed that a barrier to diffusion develops around the lens nucleus with age[1], which may contribute to the onset of senile cataract.

Unlike a conventional glass or plastic lens, where refraction of light takes place only at the surfaces, the human eye lens exhibits a refractive index distribution, so that refraction occurs continuously through the lens. Until now it was not possible to measure the refractive index distribution non-invasively by optical methods, without making assumptions about the form of the distribution. We have developed an MRI technique that allows us to map the refractive index distribution of human eye lenses both in vitro[2] and in vivo[3] and to investigate changes with age and state of accommodation. The results have provided new insights into the aging of the lens and the origins of presbyopia - the loss of the ability to focus on near objects (i.e. to 'accommodate') with age.

We have also shown that NMR micro-imaging of the human eye can provide useful biometric data[4] of value in developing new methods for restoring accommodation and the treatment of refractive errors such as myopia (short sightedness). Conventional optical methods such as slit lamp photography and phakometry are unable to fully characterise changes in lens shape and equatorial radius with age and state of accommodation due to their inability to image behind the iris. Accurate measurements of lens thickness and the axial length of the eye (important in myopia) are also subject to uncertainties arising from incomplete knowledge of the refractive index distribution. Even ultrasound methods for measuring eye dimensions are subject to uncertainties in the (age related) speed of sound in the lens.

References:

1. Moffat BA, Pope JM. Anisotropic water transport in the human eye lens studied by diffusion tensor NMR micro-imaging. Exp. Eye Res. 74, 677-687 (2002).
2. Jones CE, Atchison DA, Meder R, Pope JM. Refractive index distribution and optical properties of the isolated human lens measured using magnetic resonance imaging (MRI). Vision Res. 45, 2352-2366 (2005).
3. Kasthurirangan S, Markwell EL, Atchison DA, Pope JM. In-vivo study of changes in refractive index distribution of the human crystalline lens with age and accommodation. Investigative Ophthalmology and Visual Science 49, 2531-2540 (2008).
4. Kasthurirangan S, Markwell EL, Atchison DA, Pope JM. MRI study of the changes in crystalline lens shape with accommodation and aging in humans. J. Vision (in press).

O6

Low-field depth- and orientation-dependent relaxation imaging of bovine articular cartilage

E.Rössler, A. Mollova, C. Mattea, S. Stapf

Dept. of Technical Physics II, TU Ilmenau, Germany

The layered structure of mammal articular cartilage is reflected by a pronounced depth dependence of T_2, which is a consequence of different degrees of order of the collagen fibers but also of a gradient of water and glycosaminoglycane concentration, respectively [1,2]. The orientational order results in an angular dependence of T_2 that becomes less pronounced at greater distance from the joint surface. T_1 at conventional laboratory fields does show little variation in comparison.

In this study, the dependence of relaxation times in bovine articular cartilage is investigated at a low magnetic field strength of 0.27 T using a portable scanner. While a systematic variation of T_2 is found (see Fig. 1) that is in agreement to similar mammalian cartilage observed at high fields [1], T_1 also shows a strong depth dependence that correlates with the separation of the tissue into three distinct zones. This pronounced effect is explained by the increased T_1 contrast commonly found towards smaller magnetic field strengths, a consequence of slow and anisotropic molecular reorientations that dominate the relaxation dispersion at small Larmor frequencies. Despite T_1 being identified as a suitable indicator for the collagen properties across the cartilage layer, a variation with orientation during rotation about an axis normal to the surface analyzed at high field [3] yet remains doubtful for T_1 at low field, but is clearly observed for T_2.

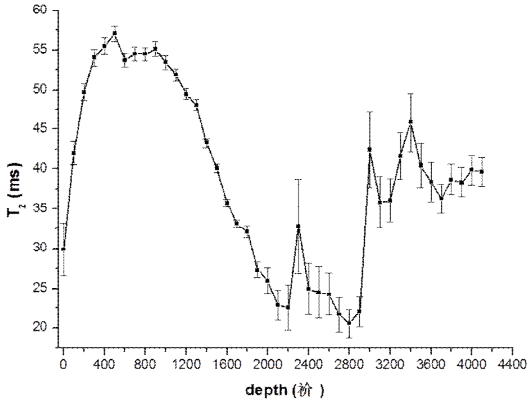

Fig. 1: T_2 as a function of depth for a bovine stifle joint; from left to right, cartilage, calcified zone, and subchondral zone can clearly be identified.

The same experiments has been repeated after saturating the samples in a 0.8 mM aqueous Gd-$(DTPA)^{2-}$ solution that reduces T_1 of water protons. The different degrees of T_1 change serve for an estimation of the local water and GAG concentrations, respectively, and provide a simple tool for a routine assessment of damaged tissue as is found for a number of degenerative diseases.

References:

1. Y. Xia, Relaxation anisotropy in cartilage by NMR microscopy (MRI) at 14- m resolution, Magn. Reson. Med. 39 (1996) 941
2. Y. Xia, S.K. Zheng, A. Bidthanapally, Depth-dependent profiles of glycosaminoglycans in articular cartilage by MRI and histochemistry, J. Magn. Reson. Imag. 28 (2008) 151
3. S. Zheng, Y. Xia, The collagen fibril structure in the superficial zone of articular cartilage by MRI, Osteoarthritis Cartilage 17 (2009) 1519

O7

Compressed sensing SPI for gas velocity imaging in porous media

Christine Schmaus[1], *Dan J. Holland*[1], *Andy J. Sederman*[1], *Andrew Blake*[2], *Lynn F. Gladden*[1]

[1]Department of Chemical Engineering and Biotechnology, University of Cambridge, UK,
[2]Microsoft Research Cambridge, UK

Being able to predict the flow of gas and liquid within a porous medium is a generic problem across many areas of physics and engineering. Magnetic Resonance Imaging (MRI) can play an important role in gaining direct insight into these problems, as well as guiding the development of, and validating, computational fluids dynamics codes used to predict such flow fields. To use MRI in this application, we need to be able to image the gas and liquid velocity at the same spatial resolution, to avoid mis-registration at the gas-liquid interface, and to acquire both velocity images at similar signal-to-noise ratios without need for excessively long image acquisition times. The challenge in achieving this is that the gas phase has a nuclear spin density typically 3 orders of magnitude smaller than the liquid phase. In this paper we demonstrate the application of Compressed Sensing (CS) used in combination with Single Point Imaging (SPI) to image both the liquid and gas velocities in trickle beds. Trickle beds are packings of solid particles contained within a cylindrical column through which gas and liquid flow co-currently downwards. These systems are used throughout the petrochemical industry for hydrogenation reactions; under these circumstances, the packing elements are catalyst particles used to promote the particular catalytic conversion of interest.

Figure 1 shows the results obtained using this CS MRI approach. CS is a novel technique for data sampling and image reconstruction which allows the reduction of acquisition times by sampling fewer data points. Images acquired under violation of the Nyquist criterion can be reconstructed to high quality by nonlinear optimization. Combining CS with SPI allows us to under-sample the data in two dimensions, thereby reducing the number of sampling points and therefore the acquisition time by 80% relative to the same signal-to-noise acquired by full k-space sampling. Figure 1a shows that the gas-liquid interface is clearly identified. From these data the gas-liquid velocities across an interface can be extracted, typical data are plotted in Figure 1b. Such results and many others will be discussed, and their use in computational modeling will be summarized.

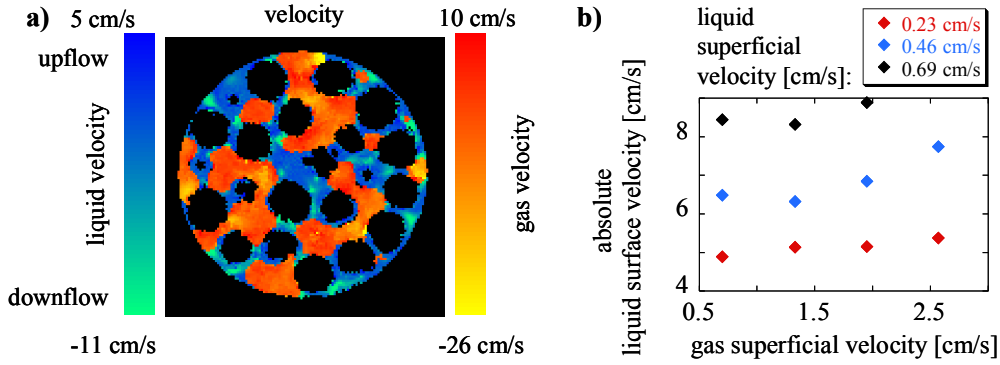

Fig. 1: a) Velocity map of liquid (water) and gas (SF_6) flowing through a column packed with spherical particles. The superficial velocities of water and SF_6 were 0.46 cm/s and 0.70 cm/s, respectively, through a packed bed of 5mm glass beads. In-plane spatial resolution is 236 µm × 236 µm. b) Plot of the absolute liquid velocities at the gas-liquid interface as a function of overall gas superficial velocity, for different overall liquid superficial velocities.

O8

Multinuclear and hypersensitive MRM in heterogeneous catalysis

I.V. Koptyug, A.A. Lysova, I.V. Skovpin, D.A. Barskiy, K.V. Kovtunov, V.V. Zhivonitko

International Tomography Center SB RAS, 3A Institutskaya St., Novosibirsk 630090, Russia

In many heterogeneous catalytic processes, heat transport is an important factor which, if not properly controlled, can lead to the formation of hot spots in the catalyst bed, degradation of reaction conversion and selectivity, reactor runaway and even explosion. The development of non-invasive thermometry techniques for the studies of operating reactors is necessary to advance our understanding of heat transport processes in the catalyst bed and is essential for the development of efficient and environmentally safe industrial reactors and processes. NMR and MRI techniques are known to be able to evaluate local temperatures of liquids. However, for a multiphase gas-liquid-solid reactor the available techniques based on the liquid phase NMR signal detection are not applicable since the local liquid content in the catalyst pores varies with space and time. We have demonstrated earlier that the direct ^{27}Al MRI of industrial alumina-supported catalysts (e.g., Pd/Al_2O_3) is a potential way toward the spatially resolved thermometry of an operating packed bed catalytic reactor. Recently, we were able to implement this approach and to obtain 2D temperature maps of the catalyst directly in the course of an exothermic catalytic reaction. The images obtained clearly demonstrate the temperature changes with the variation of the reactant feed and also the existing temperature gradients within the catalyst at a constant feed.

One of the obstacles in developing novel applications of MRM in porous media is its fairly low sensitivity even if ^{1}H signal detection is used. A number of hyperpolarization techniques are currently being developed that can enhance the NMR signal by 4-5 orders of magnitude even at intermediate (3-7 T) magnetic fields, and even more in low and ultra-low magnetic field applications that are currently gaining popularity. Parahydrogen-induced polarization (PHIP) is the only hyperpolarization technique of relevance to catalysis as PHIP effects are observed in hydrogenation reactions when parahydrogen is involved. We have shown that PHIP can be generated not only in homogeneous hydrogenation reactions but also in heterogeneous catalytic processes catalyzed by a broad range of different heterogeneous catalysts. Thus, the development of the novel hypersensitive NMR/MRI techniques for heterogeneous catalysis becomes possible. Also, this approach can provide hyperpolarized gases and catalyst-free hyperpolarized liquids for a wide range of novel applications of NMR and MRI in, e.g., materials science, chemical engineering and in vivo biomedical research. Applications of this hypersensitive approach to the studies of gas flow in microfluidic chips and of the hydrogenation reaction in a packed bed microreactor will be demonstrated.

This work was supported by the following grants: RAS 5.1.1, RFBR 11-03-00248-a and 11-03-93995-CSIC-a, SB RAS integration grants 9, 67 and 88, NSh-7643.2010.3, FASI 02.740.11.0262 and MK-1284.2010.3.

References:

1. I.V. Koptyug, A.V. Khomichev, A.A. Lysova, R.Z. Sagdeev, JACS 130 (2008) 10452.
2. A.A. Lysova and I.V. Koptyug, Chem. Soc. Rev. 39 (2010) 4585.
3. K.V. Kovtunov, I.E. Beck, V.I. Bukhtiyarov, I.V. Koptyug, Angew. Chem. Int. Ed. 47 (2008) 1492.
4. V.-V. Telkki, V.V. Zhivonitko, S. Ahola, K.V. Kovtunov, J. Jokisaari, I.V. Koptyug, Angew. Chem. Int. Ed. 49 (2010) 8363.
5. L.-S. Bouchard, S.R. Burt, M.S. Anwar, K.V. Kovtunov, I.V. Koptyug, A. Pines, Science 319 (2008) 442.

O9

Independent Component Analysis (ICA) Applied to Adaptive Signal Processing for Multichannel Surface-NMR Instruments

Rafik. Soltani, L. Xiao,

China University of Petroleum, Beijing 102249, China
State Key Laboratory of Petroleum Resource and Prospecting
Key Laboratory of Earth Prospecting and Information Technology, Beijing

The surface-NMR has become known as an advanced NMR electronics technology, with increasing capabilities for non-invasive, direct and rapid near-surface hydrogeophysical exploration. Two novel multichannel surface-NMR instruments have been emerged very recently: GMR [1], and Numis-Poly [2]. Fig. 1 shows a field survey at the Nauen site in Germany, which was carried out with the GMR instrument in September 2008. Adaptive and robust signal processing is central for multichannel surface-NMR technology. This helps for the detection of the very-weak and very-noisy groundwater NMR signals, whose amplitudes are typically in nano-Volts. We propose a new adaptive signal processing algorithm for multichannel surface-NMR instruments, using independent component analysis (ICA), (Fig. 2). This algorithm performs statistical independence, as maximum as possible, between the canceler output signal $\varepsilon(t)$ and its reference input signal $n(t)$. Such an algorithm can be viewed as an extension, from statistical decorrelation to statistical independence, which is much stronger, of the actual processing software of the GMR instrument; thereby practically more robust. We demonstrate the performance of the proposed adaptive algorithm using field measurements of the GMR instrument. This new development is part of our ongoing R&D project on multichannel surface-NMR electronics technology [3, 4, 5].

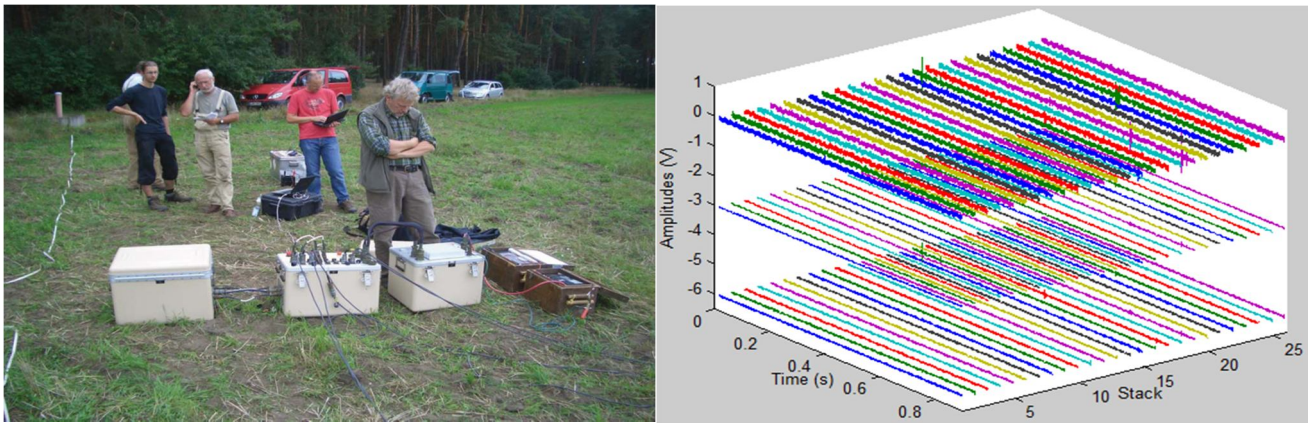

Fig. 1: Left, a picture of field survey at the Nauen site in Germany, carried out with the GMR instrument, September 2008. Right, a 3-channel dataset of 26 stacks, recorded by one primary receiver (top) and two reference receivers.

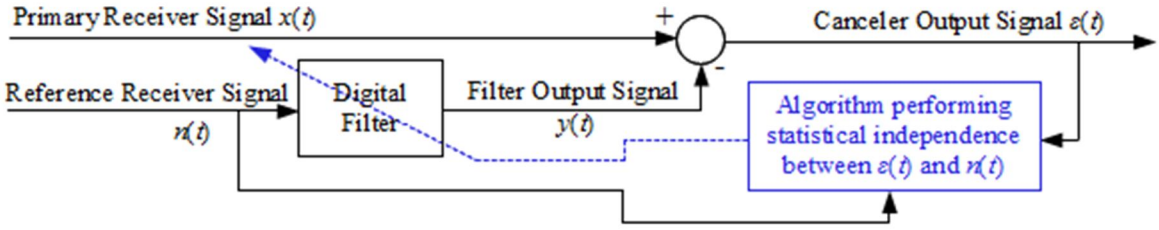

Fig. 2: ICA-based adaptive signal processing algorithm for multichannel surface-NMR instruments.

References:

1. D. O. Walsh, J. App. Geophys. 66 (2008) 140.
2. IRIS-Instruments Website: http://www.iris-instruments.com/index.html.
3. R. Soltani and L. Xiao, MRS'2009, Grenoble, France, October 20-23, 2009.
4. R. Soltani and L. Xiao, IEEExplore, Digital Object Identifier: 10.1109/IIT.2009.5413750.
5. R. Soltani and L. Xiao, HOS Applied to Surface-NMR, ICMRM'11, Beijing, China, 2011.

O10

Laplace Inversion for obtaining relaxation-chemical shift correlation in high-resolution solid state NMR

Boqin Sun, Bob Carlson, and Marcus O. Wigand

Chevron Energy Technology Company

Kerogen is the most abundant organic matter that is dispersed in the earth's formation and is the source of fossil fuels such as oil and gas. Large amounts of kerogen exist in the form of oil shale which is not favorable for extraction. The largest accumulation of oil shale is located in the Piceance Basin, Colorado. The so called 'Green River oil shale' was deposited in a lacustrine environment and contains type-1 kerogen as an organic resource. Even though the depositional environment is known there are details of the molecular structure of type-1 kerogen which still have to be identified. We used ^{13}C and ^{15}N high resolution solid state NMR spectroscopy as one of the primary methods to elucidate the structure of kerogen through measurements of chemical shift, spin-lattice relaxation time, variable contact time, and dipolar dephasing rates. Using single or double exponential fitting methods, one can extract structural information from the variation of peak intensity with mixing times used in CP/MAS or dipolar dephasing experiments. Here we introduce a new data processing method that uses a Laplace inversion algorithm to process a set of CP/MAS NMR data with different mixing times to generate 2D NMR spectrum that gives a chemical shift in one dimension and relaxation time in the second dimension. The relaxation-chemical shift 2DNMR can be used to determine ^{13}C (or ^{15}N) chemical shift, proton spin-lattice relaxation time, cross polarization time, and dipolar dephasing time constant as well as their distributions for mixture samples such as oil shale. It also improves the accuracy of deriving structural parameters of macromolecules using both ^{13}C or ^{15}N chemical shift and relaxation cutoffs.

OY1

Miniaturized Capillary Electrophoresis-Microcoil NMR device for ^{1}H and ^{19}F Spectroscopy

J. Diekmann[1], K. L. Adams[2], G. L. Klunder[2], C. Vogt[1], A. F. McDowell[3]

[1]Leibniz University Hannover, Faculty of Natural Sciences, Institute of Inorganic Chemistry, Department of Analytical Chemistry, Callinstraße 1, 30167 Hanover, Germany
[2]Lawrence Livermore National Laboratory, 7000 East Ave., Livermore, CA 94550, USA
[3]ABQMR, Inc., 2301 Yale Boulevard SE, Suite C-2, Albuquerque, NM 87106, USA

Capillary electrophoresis (CE) coupled to portable microcoil nuclear magnetic resonance spectroscopy (microNMR) provides several advantages for applications in analytical chemistry, pharmaceutical industries, as well as academia, and allows further development towards nanoliter sample volume analysis, reduced cost and minimal maintenance of instruments. Previous research has demonstrated the advantages of hyphenating CE and (portable) NMR[1], which improves the ability to identify components in a complex mixture by first separating the compounds chemically and then providing structural identification. The coupled analytical technique presented in this work is based on a miniaturized, homebuilt CE integrated with a portable microNMR system (see Fig. 1). On-line detection and structure elucidation of weak organic acids and perfluorinated compounds is presented. Our results demonstrate that the use of homemade 'bubble' cell capillaries, which increase the observable sample volume in the NMR coil, the integration of shim coils and temperature control devices enhance the NMR spectral sensitivity and resolution to 0.02-0.2 ppm. Furthermore, the influence of the CE current on the NMR performance showed the NMR peak linewidth broadening during high CE current runs can be corrected via shimming. This is a fundamentally important result, allowing continuous current-flow CE-NMR measurements in the portable device without applying any further hardware developments. Additionally, the data shows that useful CE performance can be achieved with the CE-NMR instrument using NMR as the information-rich detector.[2]

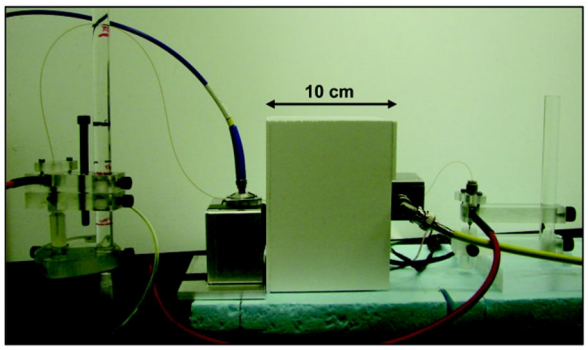

Fig. 1: Miniaturized CE-NMR System with magnet, UV/VIS detector, separation capillary, CE buffer and sample vials, and the high voltage supply.

This project is supported by the DFG under Grant VO597/19-1 and it was partly performed under the auspices of the U.S. Department of Energy by Lawrence Livermore National Laboratory under Contract DE-AC52-07NA27344.

References:

1. Diekmann, J.; Adams, K.L.; Klunder, G.L.; Evans, L.; Steele, P., Vogt, C.; Herberg, J.L. *Anal. Chem.* **2011**, 83, 1328-1335.
2. Diekmann, J.; Adams, K.L.; Klunder, G.L.; Vogt, C.; McDowell, A.F. *Anal. Chem.* **2011**, *submitted*.

OY2

Magnetic Resonance Velocimetry in a Vortex Flow Reactor

Antoine Vallatos, Melanie M. Britton,

School of Chemistry, University of Birmingham, Birmingham B15 2TT, United Kingdom

Taylor Vortex Flow (TVF) occurs in the annulus of two concentric cylinders, when the inner one is rotated above a critical rotation rate. TVF is characterised by counter-rotating axi-symmetric vortices along the length of the tube. Kose[1] (1994) and Seymour et al[2] (1999) produced NMR velocity maps of this flow. By adding axial flow, a Vortex Flow Reactor (VFR) is produced (Fig. 1a). This type of reactor is used for numerous applications (such as catalytic, electrochemical and enzymatic reactions) due to its plug-like flow and mixing properties. Despite widespread application, many questions concerning this flow remain, including plug-flow properties and inter/intra vortex mixing. It is expected that MR velocity and diffusion maps will provide answers for these questions.

A challenge for imaging flow in this system lies in the periodic motion caused by the moving vortices. This causes imaging artifacts and errors in velocity measurements. However, by adapting the pulse sequence timing to the flow period[3], it is possible to simulate steady state and obtain velocity maps. We used PGSE imaging sequence and timed data acquisition to the Taylor vortices translation period to produce the first high-resolution NMR velocity maps of the VFR flow (Fig.1b).

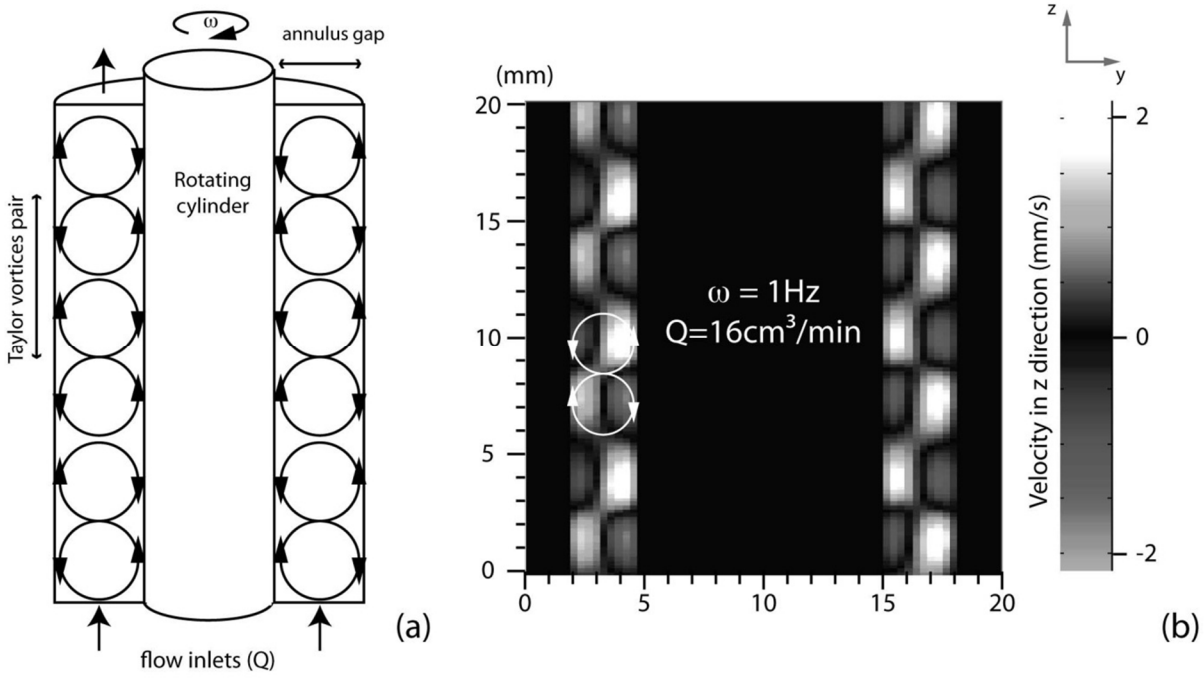

Fig.1: (a) Vortex Flow Reactor (VFR) schema, (b) Magnetic Resonance velocity map of the VFR flow in the z direction at ω=1Hz and Q=16cm3/min

References:
1. Kose, K. Physical Review Letters 1994, 72, 1467.
2. Seymour, J. D.; Manz, B.; Callaghan, P. T. Physics of Fluids 1999, 11, 1104.
3. Han, S. I.; Stapf, S.; Blumich, B. Physical Review Letters 2001, 8714.

OY3

Rotating permanent magnets: Towards MAS NMR/MRI on a static sample

A. Cedric Hugon[a], *B. Guy Aubert*[b], *C. Dimitris Sakellariou*[c],

[a]Departement de Chimie, Ecole Normale Superieure, 24 rue Lhomond, F-75005 Paris
[b]DSM/IRFU CEA Saclay, F-91191 Gif sur Yvette
[c]DSM/IRAMIS/SIS2M/LSDRM CEA Saclay, F-91191 Gif sur Yvette

One important goal for MRI and MRS is to analyze the metabolism in a localized region of a living subject. However, the resolution is limited by the anisotropy of the magnetic susceptibility in living tissues. Such limitations can also be found when studying rock cores, which feature high susceptibility variations. A well-known solution to such issues is Magic Angle Spinning (MAS)[1,2]. While the standard MAS method consists in spinning the sample at several tens of kHz, this option is not available with a living subject. The obvious answer to that objection is to rotate the field instead of the sample, but previous attempts using electromagnets or hybrid permanent-electromagnet designs did not achieve the required field homogeneity for high-resolution studies [3,4,5].

We have recently proposed a pure permanent magnet generating a field of 0.2T at about the magic angle with its axis (± 0.5°) [6]. We have adjusted this magnet so that it now offers a "sweet spot" located exactly on the geometrical axis of the magnet, with a homogeneity of about 45 ppm over about 1.5 mm^3. This demonstration prototype is assembled on a dedicated machine providing rotation of the magnet up to 35Hz with high stability, without balancing. The sweet spot being on the axis of revolution, the spectrum shape is stable during the rotation. We will discuss this experimental setup and present, for the very first time, results of NMR experiments on anisotropic static samples in a rotating magnetic field. Significant line narrowing effects are observed and offer good promises for more advanced magnet systems.

References:

1. Andrew, E. R.; Bradbury, A. and Eades, R. G. Removal of Dipolar Broadening of Nuclear Magnetic Resonance Spectra of Solids by Specimen Rotation. Nature, 1959, 183, 1802-1803.
2. Andrew, E. R. and Eades, R. G. Possibilities for high-resolution nuclear magnetic resonance spectra of crystals. Discuss. Faraday Soc., 1962, 34, 38-42.
3. Sakellariou, D.; Meriles, C. A.; Martin, R. W. & Pines, A. NMR in rotating magnetic fields: Magic angle field spinning. Magn. Reson. Imag., 2005, 23, 295-299
4. Schlueter, R. and Budinger, T. Magic Angle Rotating Field NMR/MRI Magnet for In Vivo Monitoring of Tissues. IEEE Transactions on Applied Superconductivity, 2008, 18, 864-867
5. Meriles, C. A.; Sakellariou, D.; Moulé, A.; Goldman, M.; Budinger, T. F. & Pines, A. High-resolution NMR of static samples by rotation of the magnetic fields. J. Magn. Reson., 2004, 169, 13-18
6. D. Sakellariou, C. Hugon, G. Aubert et al., "Permanent Magnet Assembly producing a Stong Tilted Homogeneous Magnetic Field: Towards Magic Angle Field Spinning NMR and MRI", Magnetic Resonance in Chemistry 2010, 48, 903-908.

OY4

Breaking the sensitivity limit of low-field NMR by using para-hydrogen induced polarization

Qingxia Gong [a], *Stephan Appelt* [b], *Bernhard Blümich* [c]

[a] Fachgebiet Technische Physik II / Polymerphysik, Technische Universität Ilmenau, Germany, [b] Central Institute for Electronics, Research Center Jülich, Germany, [c] Institut für Technische und Makromolekulare Chemie, RWTH Aachen University, Germany

Low-field NMR without cryogens is inexpensive and can be made mobile. Its use promises new applications in well-logging, the analysis of objects of cultural heritage, food quality control, and in the chemical and material sciences which are prohibited by or difficult to perform with high-field machines. Compared to high-field NMR, the obvious disadvantage of low-field NMR is the inherently low sensitivity due to the small differences in the thermodynamic equilibrium populations of the spin states. Two general strategies known as thermal prepolarization and hyperpolarization have been demonstrated to overcome this disadvantage. Thermal prepolarization can be realized via establishing a new thermal equilibrium state of the sample in a strong, but not necessarily homogeneous magnetic field before signal detection at low field.[1] Hyperpolarization is achieved by transferring the high polarization of photons or the high spin order of a second group of spins to the target nuclei.

Parahydrogen induced polarization (PHIP) as a chemical hyperpolarization method has been developed to improve the NMR sensitivity by several orders of magnitude.[2-9] Furthermore, PHIP combined with NMR spectroscopy has very recently become a powerful tool to provide profound insight into the reaction mechanisms and kinetics of the catalytic hydrogenation. As prerequisites for the PHIP effect to occur, the two hydrogen atoms in a para-hydrogen molecule must be transferred as a pair to non-equivalent positions upon their addition to a substrate, and spin-lattice relaxation times of these atoms must be longer than the duration of the catalytic cycle. Recently, an alternative approach to generate PHIP sensitized materials based on reversible interactions with para-hydrogen which is known as NH-PHIP has been developed.

In this contribution, the feasibility of applying PHIP based technique to increase the sensitivity of low-field NMR will be discussed and compared with other hyperpolarization techniques. Efforts in improving the PHIP based technique in NMR will be outlined as well.

References:

[1] S. Appelt, H. Kühn, F. W. Häsing and B. Blümich, Nature Phys. 2006, 2, 105-109.
[2] J. Natterer and J. Bargon, Prog. Nucl. Magn. Reson. Spectrosc. 1997, 31, 293-315.
[3] S. B. Duckett and C. J. Sleigh, Prog. Nucl. Magn. Reson. Spectrosc. 1999, 34, 71-92.
[4] C. R. Bowers, Encyclopedia of Nuclear Magnetic Resonance 2002, 9, 750-770.
[5] I. V. Koptyug, K. V. Kovtunov, S. R. Burt, M. S. Anwar, C. Hilty, S. I. Han, A. Pines and R. Z. Sagdeev, J. Am. Chem. Soc. 2007, 129, 5580-5586.
[6] L. S. Bouchard, S. R. Burt, M. S. Anwar, K. V. Kovtunov, I. V. Koptyug and A. Pines, Science 2008, 319, 442-445.
[7] R. W. Adams, J. A. Aguilar, K. D. Atkinson, M. J. Cowley, P. I. P. Elliott, S. B. Duckett, G. G. R. Green, I. G. Khazal, J. López-Serrano and D. C. Williamson, Science 2009, 323, 1708 - 1711.
[8] K. D. Atkinson, M. J. Cowley, P. I. P. Elliott, S. B. Duckett, G. G. R. Green, J. Lopez-Serrano and A. C. Whitwood, J. Am. Chem. Soc. 2009, 131, 13362-13368.
[9] Q. Gong, A. Gordji-Nejad, B. Blümich and S. Appelt, Anal. Chem. 2010, 82, 7078-7082.

OY5

Bayesian Techniques in Magnetic Resonance

D.J. Holland[a], *A. Blake*[b], *J.G. Ross*[a], *A.J. Sederman*[a], *L.F. Gladden*[a]

[a] Department of Chemical Engineering and Biotechnology, University of Cambridge
[b] Microsoft Research Cambridge

Magnetic Resonance (MR) is widely used in a diverse range of applications including medical diagnosis, well-logging, and chemical processing. A common problem in all of these applications is the long time taken to acquire images. Therefore, significant research has been devoted to developing techniques for reducing the acquisition times of experiments. This is even more critical given the increasing interest in low-field MR technology. One particularly promising route for reducing acquisition times is through the use of sparse sampling techniques in combination with Bayesian analysis.

In a Bayesian analysis experiment, the goal is to go directly from the measured data to the desired information. In a conventional imaging experiment, a measurement is performed and a data point sampled for each pixel required in the final image. The resulting image is then analyzed to extract the desired information. However, this process involves the acquisition of a significant amount of redundant information. For example, we might be interested in determining a bubble size distribution in a multiphase flow which could be described by only two values – a mean and variance – compared with the 4096 pixels that might be required to describe an image. Given the simplicity of the information that we wish to extract, it should be possible to obtain this information from far fewer data points than are required to obtain the image. Bayesian analysis enables us to do this by going directly from a set of data points to the desired information.

In this work we describe a Bayesian approach to MR. The approach is demonstrated on two applications: (1) sizing of gas bubbles in a two-phase flow (see Fig. 1) and (2) grain sizing in rock cores. This approach enables the extraction of the key information from up to two orders of magnitude less data than would conventionally be required. In each case, validation experiments are performed using either optical or x-ray techniques. The Bayesian MR approach can then be used in situations where these conventional techniques cannot be applied, such as high voidage multiphase flows.

A particular strength of the Bayesian approach is that it is robust in poor signal-to-noise applications. In Bayesian analysis the noise is incorporated into the analysis ensuring that as much information is extracted from the signal as is available. This robustness makes the Bayesian approach ideally suited to low-field MR applications. To demonstrate this, grain sizing measurements are presented for bead packs and rock cores using low-field instruments. This can even be extended to measurements using an Earth's field MR system, where an effective spatial resolution of 0.5 mm can be achieved.

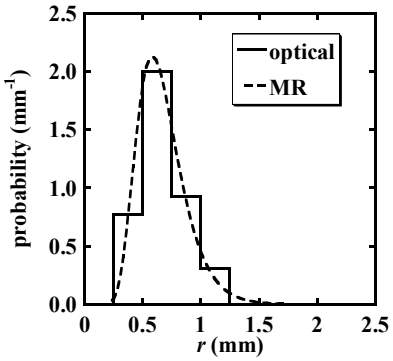

Fig. 1: Comparison of optical and MR measurements of bubble size at low voidage.

OY6

Novel multidimensional rotating frame based techniques for probing low frequency dynamics

Ravinath Kausik, Lukasz Zielinski and Martin Hürlimann

Schlumberger-Doll Research

We present novel multidimensional techniques based on relaxation in the rotating frame, which would provide a unique insight into the low frequency dynamics of various complex fluid systems. By mapping out correlations in the spectral density at selected low frequencies in the 500 Hz to 100 kHz window which is generally difficult to selectively investigate, our techniques are sensitive to the range of correlation times of particular interest in widely studied fields of exchange and aggregation processes in proteins/biological/colloidal systems or fluid-saturated porous media or for core analysis applications.

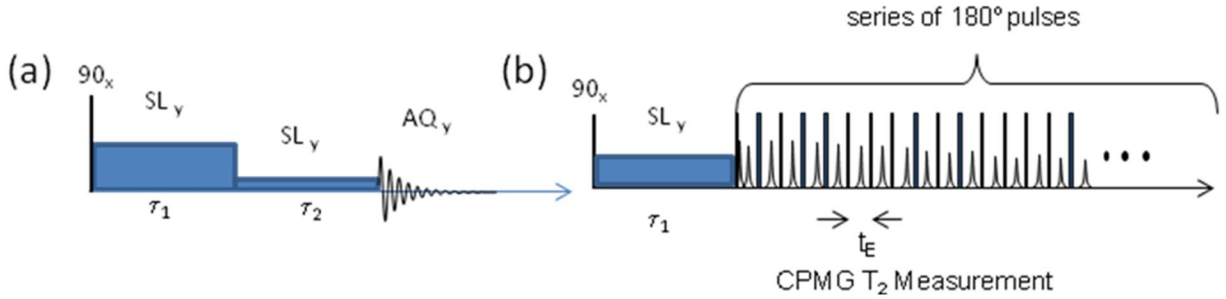

Fig. 1: (a) The RFCORD pulse sequence shown on the left consists of an initial hard 90_x pulse followed by a spin locking pulse of amplitude ω_{1A} for duration τ_1, immediately followed by a second spin-locking pulse of amplitude ω_{1B} of duration τ_2. The intervals τ_1 and τ_2 are varied systematically to cover the whole range of $T_{1\rho}$ values in the system. The correlation distribution between $T_{1\rho}$ corresponding to ω_{1A} and ω_{1B} is obtained by a two-dimensional inverse Laplace transformation with respect to τ_1 and τ_2. (b) The $T_{1\rho}$-T_2 pulse sequence consisting of a spin locking pulse followed by the *CPMG* pulse train is shown on the right.

The standard T_1-T_2 or T_2- T_2 correlation spectroscopy is most sensitive to correlation times near the Larmor frequency and does not have the ability to vary the measurement frequency. While field-cycling has this ability, it is limited to frequencies greater than ~10 kHz other than lacking spectroscopic resolution and requiring expensive specialized hardware. On the other hand, the rotating field relaxation has the potential of universal application on standard superconducting and mobile systems. In this talk we will also discuss how these techniques open up the unique possibility of combination with standard NMR spectroscopy to yield chemical shift resolved correlated relaxation distributions, thus adding a Fourier dimension to the investigation. An application of this technique to the study of aggregation phenomena and dynamics in porous media will be discussed.

O11

High Pressure Magnetic Resonance Imaging with Metallic Vessels

H. Han [a], M. Ouellette [a], B. MacMillan [a], F. Goora [a], K. Adusumilli [a], R. MacGregor [a], D. Green [b], B.J. Balcom [a]

[a]MRI Centre, University of New Brunswick, [b]Green Imaging Technologies, Fredericton, New Brunswick, Canada

During the past half century high pressure NMR spectroscopy has played an indispensable role in diverse areas of physics and chemistry [1]. Magnetic resonance imaging has revolutionized clinical diagnostic imaging and its use exploring and understanding natural science systems is expanding. There is clear merit in combining MRI with high pressure for materials investigation.

A limited number of high pressure MRI studies have been reported. We introduce high pressure magnetic resonance imaging using metallic vessels. A metallic vessel encloses a pressurized MRI RF probe and functions as an RF shield for the RF probe. The metallic pressure vessel, surrounded by temperature control coils, fits inside a standard gradient bore on an MR spectrometer. In previous work [2], we have shown that the implementation of state-of-the-art MRI techniques is possible in the presence of highly conductive metallic structures with appropriate correction of eddy currents.

The metallic pressure vessels envisaged are very general in concept. In this work we choose a core holder for the study of rock core samples as a simple example of a metallic pressure vessel. A core holder fabricated using non-magnetic stainless steel is demonstrated. We show that metallic pressure vessels permit efficient temperature control and optimized sensitivity of the MRI detection compared to conventional practices. Magnetic resonance properties associated with the metallic pressure vessel, such as RF B_1 field, RF shielding, static B_0 field and dynamic B_0 field, have been investigated. The static magnetic field inside metallic pressure vessels is spatially mapped and largely homogeneous.

Eddy currents are dramatically reduced using non-magnetic stainless steel with a relatively low electrical conductivity compared to other metals. Both experiments and simulation show that eddy currents mainly distort gradient waveforms inside the sample space, which can be readily corrected using appropriate eddy current correction schemes such as the MFGM method [3]. Properly designed MRI pulse sequence can also greatly reduce or eliminate the artifacts produced by eddy current field distortions. Imaging of water flooding a rock in the core holder under moderate pressure and temperature shows the great potential of this methodology. This work permits the extension of high pressure NMR studies to MRI. MRI compatible metallic pressure vessels enable macroscopic systems at high pressure and variable temperature to be monitored by MRI.

References:

1. J. Jonas, Nuclear magnetic resonance at high pressure, Science 216 (1982) 1179.
2. H. Han, D. Green, M. Ouellette, R. MacGregor, B.J. Balcom, J. Magn. Reson. 206 (2010) 97.
3. H. Han, R. MacGregor, B.J. Balcom, J. Magn. Reson. 201 (2009) 212.

O12

Advanced Methods for NMR Diffusometry

Marcel Gratz[a], Stefan Hertel[b], Markus Wehring[a], Mario Großmann[a], Stefan Schlayer[a], Frank Stallmach[a], Petrik Galvosas[b],

[a]University of Leipzig, Faculty of Physics and Earth Sciences, Leipzig, Germany
[b]MacDiarmid Institute for Advanced Materials and Nanotechnology, Victoria University of Wellington, SCPS, Wellington, New Zealand

NMR with pairs of pulsed magnetic field gradients [1] allows for the study of molecular diffusion and flow [2]. Necessary NMR hardware (such as gradient amplifiers and probes) is commercially available and able to cover most investigations for instance in porous media, soft matter or medical and biological applications [3]. Moreover, by introducing digital electronics for the gradient subsystem the precision of NMR instruments improved in the last two decades and made them a reliable tool in most cases (without the need of time consuming calibrations). However, special care must be taken, when the molecular mobility is small due to spatial confinement or high molecular mass [3-5]. Here we report on two different strategies for cases where root mean square displacements of the monitored species are well below 100 nm or strong adsorption of adsorbates in porous materials prevents the application of conventional NMR diffusometry.

First, we developed a new NMR probe which allows to generate pulsed magnetic field gradients of up to 93 T/m by design (65 T/m successfully used so far). The constant region of the gradient covers a length of 5 mm and a diameter of 3 mm. This gradient probe was used to measure the diffusion of the triblock copolymer Pluronics P123 (BASF AG, Germany) self-assembled in a hexagonal structure in aqueous solution. Diffusivities measured agree well with previously published values [6] while root mean square displacements perpendicular to the axis of the hexagonal structure are about 10 nm for observation times as short as 30 ms. We consider this results to be an important step towards the values one can obtain with quasi-elastic neutron scattering, thus closing the gap between the two methods.

Second, we followed the concept as proposed by Pampel *et al.* [7] and combined a magic-angle spinning (MAS) probe with a commercial miro-imaging system which allows NMR diffusometry under MAS conditions. We suggest protocols for the alignment of the individual parts of the experimental setup as well as methods which allows to validate obtained diffusivities. Following these procedures we measured the diffusion of mixtures (*n*-hexane and benzene) adsorbed in metal-organic frameworks MOF-5 [8] as an example for the more general case where strong adsorption is reducing both, spectral resolution as well as diffusivity.

References:

1 E. O. Stejskal and J. E. Tanner, J. Chem. Phys. 42 (1965) 288.
2 P. T. Callaghan, *Principles of Nuclear Magnetic Resonance Microscopy* Clarendon Press, (1991)
3 F. Stallmach and P. Galvosas, Annu. Rep. NMR Spectrosc . 61 (2007) 51.
4 W. S. Price, K. Hayamizu, H. Ide and Y. Arata, J. Magn. Reson. 139 (1999) 205.
5 P. T. Callaghan, M. E. Komlosh, and M. Nyden, J. Magn. Reson. 133 (1998) 177.
6 K. Ulrich, P. Galvosas, J. Kärger, F. Grinberg, Phys. Rev. Lett. 102 (2009) 037801.
7 A. Pampel, K. Zick, H. Glauner, F. Engelke, J. Am. Chem. Soc. 126 (2004) 9534 .
8 M. Gratz, S. Hertel, M. Wehring, F. Stallmach and P. Galvosas, New J. Phys. 13 (2011) 045016.

O13

Rotating Microcoils for High-Resolution Magnetic Resonance Microscopy

Alan Wong, Pedro M. Aguiar, Roxane Andurand, Dimitris Sakellariou

CEA Saclay, DSM, IRAMIS, UMR CEA/CNRS no 3299 – SIS2M, Laboratoire Structure et Dynamique par Résonance Magnétique, F-91191, Gif-sur-Yvette Cedex, France

Many microscopic samples cannot be routinely analysed using magnetic resonance spectroscopy or imaging because of their low sensitivity due to the inadequate size of commercial detectors (i.e. poor filling factor). However, sensitivity can be regained by the use of resonant micro-detectors [1], which can be inductively coupled to any standard commercial NMR probe, including magic-angle spinning (MAS), without any probe modifications. This technique is known as Magic-Angle Coil Spinning (MACS). Besides its simplicity, one advantage of MACS over technique with stationary static coils is the fact that it eliminates most of the susceptibility related line-broadening leading to high-resolution spectra.

Here, we present a variety of results, from MACS spectroscopy of biopsies [2], and solid materials [3] to microscopic imaging applications [4-6]. MRI microscopy presented here does not require a standard multi-axes pulsed gradient system, but instead, it uses the stray-field *z*-gradient from a standard NMR magnet and the continuous sample reorientation from a commercial MAS probe. This enables ultra high-resolution multi-dimensional MRI microscopy with *z*-gradient as large as 10 T/m or even higher. The unique spatial encoding and data reconstruction will also be discussed.

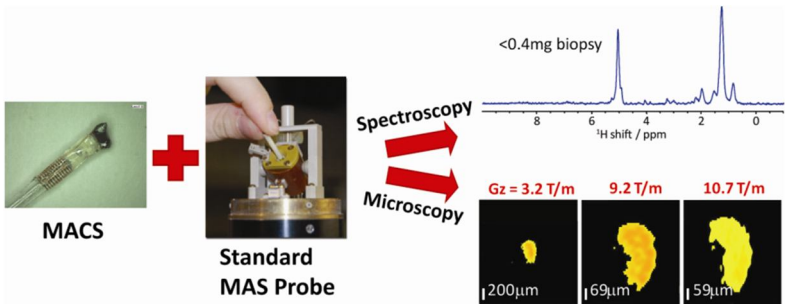

Fig. 1: Illustration of a rotating microcoil application to magnetic resonance spectroscopy and microscopy.

References:

1. D. Sakellariou, G.L. Goff and J-F. Jacquinot, Nature 447 (2007) 694-697.
2. A. Wong, P.M. Aguiar and D. Sakellariou, Magn. Reson. Med. 63 (2010) 269-274.
3. A. Wong, P.M. Aguiar, T. Charpentier and D. Sakellariou, Chem. Sci. 2 (2011) 815-818.
4. J.H. Baltisberger, S. Hediger and L. Emsley, J. Magn. Reson. 172 (2005) 79-84.
5. A. Wong and D. Sakellariou, J. Magn. Reson. 206 (2010) 264-268.
6. A. Wong and D. Sakellariou, J. Magn. Reson. Imaging 32 (2010) 418-423.
7. Acknowledgments: We acknowledge support from the following grant agreements ERC-205119, IIF-237068 and NanoMACS from C'Nano.

O14

Amplitude-modulated CPMG refocusing pulses

S. Mandal[a], *Y.-Q. Song*[a]

[a]Schlumberger-Doll Research, Cambridge, MA

The CPMG spin-echo sequence is widely used for relaxation and diffusion measurements, including cases where the static field is highly inhomogeneous, such as well-logging. In such situations the amplitudes of the first few echoes display a characteristic initial transient before smoothly settling to their asymptotic behavior [1]. This transient is due to magnetization that is not spin-locked to the effective rotation axis of the CPMG refocusing cycle. It complicates the interpretation of relaxation-time distributions, particularly for short values of T_2. We show that it is possible to eliminate the transient by allowing the amplitude and duration of the refocusing pulses to vary as a function of n, the pulse (and echo) number.

We allowed the amplitude of each CPMG refocusing pulse to vary between 0 and 200% of its nominal value, while adjusting its duration to keep the nominal flip angle at resonance constant. We also assumed rectangular RF pulses, a uniform distribution of resonance offsets, and no RF inhomogeneity. However, our work can be easily generalized to arbitrary pulses and (ω_0, ω_1) distributions. Echo amplitudes were found by matched filtering with the asymptotic echo shape. Numerical optimization was then used to minimize the L_2 norm between the actual and ideal echo amplitude functions.

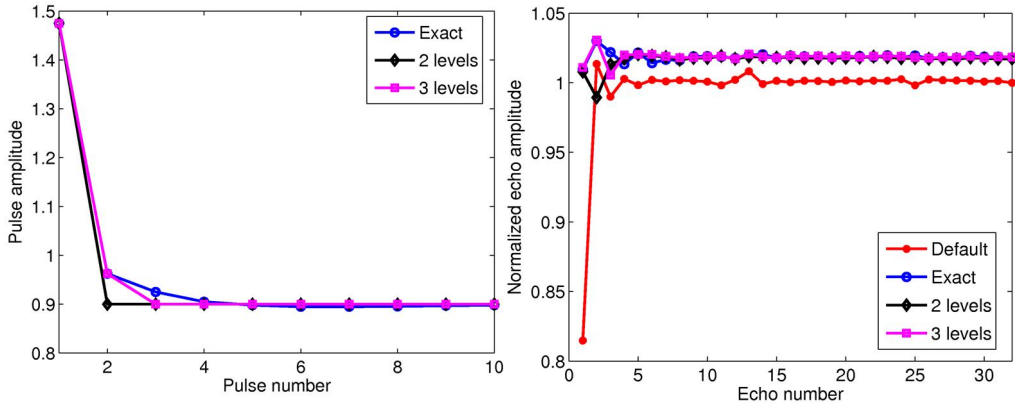

Fig. 1: (a) Optimized CPMG refocusing pulse amplitudes as a function of pulse number, and (b) measured echo amplitudes as a function of echo number.

Figure 1(a) shows the optimal pulse amplitudes found in three cases: exact, 2 levels, and 3 levels, where we allowed all amplitudes, the first 2, and the first 3, to vary, respectively. In each case the amplitude of the first pulse increases by approximately 50%, while the asymptotic value decreases by 10%. Simulations also suggest that these sequences are as robust to systematic errors in the pulse amplitudes as the default sequence, i.e., with no amplitude modulation. We verified our results by performing experiments in a 1 T imaging magnet. Figure 1(b) shows experimentally measured echo amplitudes as a function of echo number for the three situations described earlier, as well as the default case. We see that the optimized sequences eliminate the initial transient, and also increase asymptotic SNR by 2%. Interestingly, this improved performance is obtained in spite of reduced peak power (20%) and energy (10%) in the asymptotic refocusing pulses.

References:

1. M. D. Hürlimann and D. D. Griffin, JMR 143:1 (2000), 120-135.

O15

PGSE NMR measurement of permeability by the short-time effective dispersion coefficient

Tyler R. Brosten[a], *Robert S. Maier*[a], *Sarah L. Codd*[b] *and Joseph D. Seymour*[c]

[a] Engineer Research & Development Center, U.S. Department of Defense, Vicksburg MS
[b] Department of Mechanical & Industrial Engineering, Montana State Univ., Bozeman MT
[c] Department of Chemical & Biological Engineering, Montana State Univ., Bozeman MT

The generalized short-time expansion of hydrodynamic dispersion is derived using non-linear response theory. The result is in accordance with the well-known reduced cases of shear flow in ducts and pipes. In terms of viscous flow in porous media, the generalized expansion facilitates the measurement of permeability, an important parameter governing a porous media's resistance to flow by PGSE-NMR measurement of time dependent molecular displacement dynamics. To be more precise, for porous media characterized by a homogeneous permeability coefficient K, fluid volume fraction ε, and negligible surface relaxivity, the effective dispersion coefficient $D(t) = \langle|\mathbf{R}|^2\rangle/6t$ of molecular displacements $\mathbf{R}$ due to flow and diffusion for a saturating fluid of molecular diffusivity κ in viscous dominated (low Reynolds number) flow is shown to be:

$$D(t) = D_o(t) + \frac{1}{6}\langle \mathbf{u}' \cdot \mathbf{u}' \rangle t - \frac{\langle \mathbf{u} \rangle \cdot \langle \mathbf{u} \rangle}{18} \kappa \varepsilon K^{-1} t^2 + O\left(t^{5/2}\right)$$

as $t \to 0^+$. Here $\mathbf{u}'$ is the fluctuating advective velocity $\mathbf{u}' = \mathbf{u} - \langle \mathbf{u} \rangle$, and $D_o(t)$ is the hydrodynamic dispersion coefficient in the absence of advection. The short-time expansion is shown to be in agreement with PGSE NMR measurement of $D(t)$ in a sphere pack media and analogous random-walk particle tracking transport simulation data using lattice Boltzmann methods.

References:

1. V. Volterra, Theory of functionals and of integral and integro-differential equations, Dover Publications Mineola N.Y. (2005).
2. N. Wiener, Nonlinear problems in random theory, The MIT Press, Cambridge M.A. (1966).
3. M. J. Lighthill, IMA J. of Applied Mathematics 2 (1966) 97.
4. R. T. Foister and T. G. M. Van De Ven, J. of Fluid Mechanics 96 (1980) 105.
5. V. D. Broeck, Physica A: Statistical and Theoretical Physics 112 (1982) 343
6. P. C. Chatwin, J. of Fluid Mechanics 43 (1970) 321.
7. R. Camassa, Z. Lin and R. M. McLaughlin, Commun. Math. Sci 8 (2010) 601.
8. S. L. Codd, B. Manz, J. D. Seymour and P. T. Callaghan Phys. Rev. E 60 (1999) R3491.
9. W. R. Young and S. Jones, Phys. of Fluids A Fluid Dynamics 3 (1991) 1087.
10. J. Bear, Dynamics of fluids in porous media, Dover Publications New York N.Y. (1972).
11. P. P. Mitra, P. N. Sen, L. M. Schwartz and P. Le Doussal, Diffusion propagator as a probe of the structure of porous media, Phys. Rev. 68 (1992) 3555.
12. P. P. Mitra, P. N. Sen and L. M. Schwartz, Phys. Rev. B 47 (1993) 8565.

O16

Permeability mapping in heterogeneous sandstone cores by magnetization prepared centric-scan SPRITE

K. Romanenko, B. Balcom,
MRI Centre, Department of Physics, University of New Brunswick

The concept of permeability is central for hydrocarbon recovery from petroleum reservoirs and for studies of groundwater flow in aquifers. Most sedimentary rocks have spatial variations in bedding structure; contain distinct domains of fixed permeability, fault facies and fractures. Significant progress in interpretation of fluid dynamics data and petroleum core analysis, in particular, could be achieved with spatially resolved measurements of permeability. The mean velocity image, $<Vz>(x,y)$, in the plane across the average flow direction is essential to determine two-dimensional distribution of permeability, $k(x,y)$, in a porous media sample [1, *and the references therein*]. The formulation of Darcy's law on a local scale gives:

$$k(x,y) = Ø\,(x,y)\cdot<Vz>(x,y)\cdot \eta \cdot L \cdot \Pi^{-1} \qquad (1)$$

where $Ø(x,y)$ is local porosity, η -dynamic viscosity, L - length of the core, Π - total pressure drop along the core. Quantitative porosity and mean velocity maps would allow reconstruction of a quantitative 2D permeability map for parallel flow systems. These measurements may be particularly useful for discrimination of different bedding planes, fractures and fault facies in petroleum reservoir cores. The pulse sequence used in this study for velocity mapping combined alternating-pulsed-gradient stimulated-echo (APGSTE) sequence (velocity encoding) and centric-scan SPRITE read-out. These PFG methods substantially reduce errors due to internal magnetic field gradients. The measurement time is critically reduced when only a few samples near the q-space origin are collected. An analytical expression for mean velocity [1] is given by:

$$<Vz> = Im\,\{(dS/dq')^{q'=0}\cdot exp(-i\cdot\varphi)]\}\cdot(2\cdot\pi\cdot|S(0)|)^{-1} \qquad (2)$$

where *Im* stands for imaginary part of the stimulated echo signal $S(q)$; φ is the initial echo phase. Porosity maps free of T_2* weighting were reconstructed from centric-scan SPRITE images acquired with different encoding times. The method is illustrated through measurements of 2D permeability maps in naturally heterogeneous sandstone cores and model porous samples, Fig.1(a) and (b). These samples vary in bulk permeability, porosity and degree of local heterogeneity. The low-q approach (2) makes the measurements very time efficient (experiment times: 20 to 150 mins, depending on the number of q-steps, T_1, and number of signal averages). For porous samples with random bulk texture 3D velocity maps could provide detailed information on the heterogeneity of the flow field. A quantitative 3D velocity map of mean axial velocity can be obtained with only 2 q-space points within reasonable acquisition time of 2 to 3 hours, Fig.1(c).

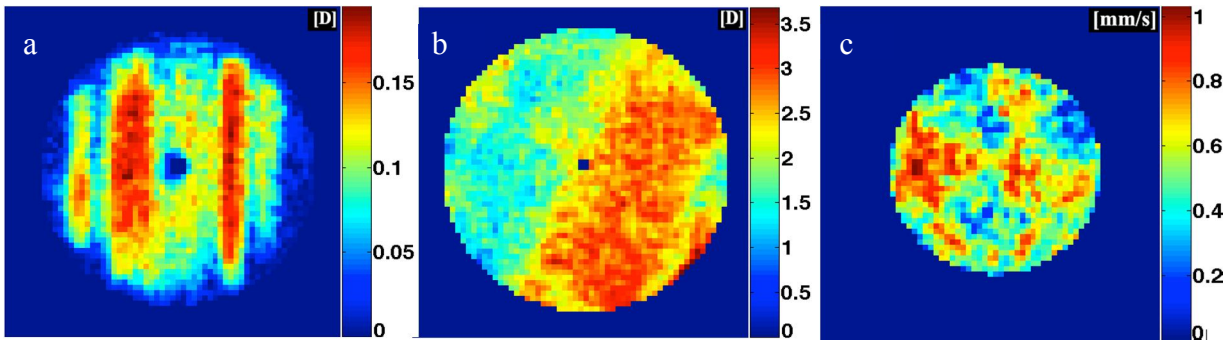

Fig.1 (a) Quantitative permeability map in layered *Corncockle* sandstone core, **2 *q*-space points**; (b) quantitative permeability map in layered *Locharbriggs* sandstone core, **4 *q*-space points**; (c) a 2D slice of the 3D mean axial velocity map in *Spynie* sandstone (random bulk texture); flow rate: 8 ml/min, **2 *q*-space points**.

References:

1. K.V. Romanenko, B.J. Balcom, Permeability mapping in porous media by magnetization prepared centric-scan SPRITE, Exp. in Fluids 50(2) (2011) 301.

O17

Characterization of porous bioresorbable films in physiological conditions by Angular Double-PFG

D. Benjamini, J. Elsner, M. Zilberman and U. Nevo
Department of Biomedical Engineering, the Iby and Aladar Fleischman Faculty of Engineering, Tel-Aviv University, Tel-Aviv, Israel

Introduction

Noninvasive characterization of porous materials is a central task in many scientific fields: Material science, pharmaceutical industry, well logging, tissue characterization, porous polymers and more. A common characteristic of the problem is the lack of accurate *a-priori* knowledge of the pore size distribution. Diffusion NMR is an efficient tool in probing noninvasively the microstructure of water-filled porous media. A common method to extract an average pore size is the single or double Pulsed Field Gradient (d-PFG) **q**-space experiment[1-3]. The goal of this work was to characterize pore sizes in bioresorbable polymers (films) that are developed for the purpose of facilitating slow drug release (tested in solution, as in physiological conditions). These results should validate the expected variability in pore sizes that is caused by changing the synthesis conditions (homogenization rate).

Methods

Different porous poly (DL-lactic – co – glycolic acid) structures polymers were used. These structures were prepared using the freeze drying of inverted emulsion's technique, with different homogenization rates. An increase in the homogenization rate resulted in smaller pore size[4]. The microstructure of the dry polymers was observed using scanning electron microscopy (SEM). Polymers were then soaked in distilled water inside 10 mm MR tubes (New Era Enterprises, NJ) and were left for 1 hr in sub-pressure conditions to remove air bubbles. d-PFG experiments in multiple angles[5] were performed on a Bruker 8.4T NMR spectrometer (Karlsruhe, Germany). The data was fit with our novel analysis (Matlab, The Mathworks, MA) to the theoretical angular-dependence curves, as proposed by Grebenkov[6] and by Ozarslan *et al*[7]**.**

Results

Images of the dried polymers indicate that the pore sizes are indeed in accordance with the expected variance that results from the velocity of rotation during synthesis (Fig. 1, a & b). Based on our analysis we managed to calculate the average pore sizes (Fig. 1, c) and these were in agreement with values found by SEM. These values are the first characterization of such polymers in physiological conditions. Finally, we are also able to characterize the kinetics of dissolution of the polymers over time scales of days, whereby pore walls break, forming bigger pores.

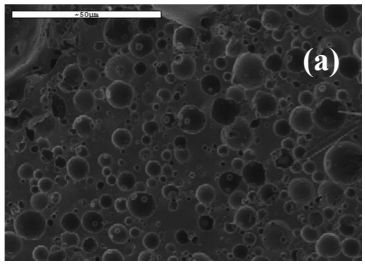

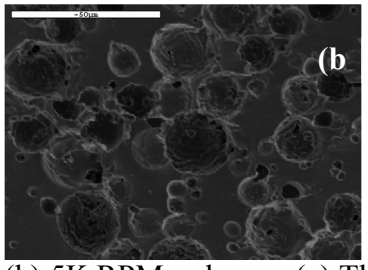

(c)

Homogenization Rate [RPM]	2500	7500	10,000
Average Radius [μm]	15.43	11.39	10.13

Fig. 1: A SEM image of the (a) 10K RPM polymer, (b) 5K RPM polymer. (c) The average radii of the different polymers.

References:

[1] Callaghan, P.T. et al. (1991). Nature, 351
[2] Shemesh, N. et al. (2010). JCP, 132(3)
[3] Komlosh, M. E. et al. (2007). JMR, 189(1)
[4] Zilberman M, (2007). Acta Biomaterialia 3(1).
[5] Koch, M. A. et al. (2005). Proc. ISMRM, 13, 840
[6] Grebenkov, D. S. (2008). Concepts in Mag. Res. (1)
[7] Ozarslan, E. et al. (2009). JCP, 130(10)

O18

Water saturation measurement and visualization research on supercritical two-phase flow in sandstone using MRI under CO_2 storage conditions

Shu Luo[a], Ruina Xu[a], Peixue Jiang[a], Jin Ma[a]

[a]Key Laboratory for Thermal Science and Power Engineering of Ministry of Education,
Beijing Key Laboratory of CO_2 Utilization and Reduction Technology,
Department of Thermal Engineering, Tsinghua University, Beijing 100084, CHINA

Global warming becomes more and more serious to human environment. As a method mitigating global warming, CCS plays a very important role for reducing CO_2 emission. As one of the CO_2 storage sites, geological storage in saline aquifer has the characteristics of large capacity and close to CO_2 emission sources. The injected supercritical CO_2 will displace the brine of the saline aquifer, displacement and flow characteristics during and after the injection process needs further investigations using advanced experimental facilities such as MRI and CT. This article adapts MRI to research the displacement phenomena.

The experimental system consists of five parts, including CO_2 flow part, water flow part, test section part, confining pressure part and outflow part. CO_2 is pumped to supercritical pressure from the CO_2 tank through supercritical CO_2 pump and then been measured mass flow rate by CO_2 flow meter. Water is pumped to the same pressure as CO_2 through water pump. CO_2 and water flow into the thermostatic heater to be heated desired temperature, and then flow into the test section. The systemic pressure is maintained by the backpressure regulator. After flowing through the backpressure regulator, the pressure drops down to atmospheric pressure. Under atmospheric pressure, CO_2 and water can be separated by separator, and then gas and liquid flow rates can be measured by gas flow meter and scale respectively. The confining part is used to simulate the underground conditions as CO_2 geological storage.

The test section is Berea sandstone with a diameter of 24.6 mm and a length of 50 mm. The experimental pressure is 10MPa and the temperature is 25℃. The sandstone is firstly saturated with water and then inserted into the test section. The pure supercritical CO_2 is injected into the test section up to the condition of no water flowing at the outlet. Then CO_2 and water are injected into the test section together with various ratios.

MRI is used to measure the water saturation and achieve online visualization research during the displacement process. Fig. 1 and Fig. 2 show the transient image and T_2 curve achieved by MRI. From the information above, the displacement mechanism can be analyzed and the relative permeability can also be measured. T_2 curve is made up of five peaks showing five kinds of pore structure. For different injection ratios, the number of peaks will not be changed but will migrate. The water saturation in the test section increased with elevated proportion of injected water. T_2 curve will migrate to the bigger T_2 value direction by increasing injected water proportion and the intensity will also increase. The first peak will neither migrate nor increase with different injected ratios displaying the irreducible water. From the T_2 curve, irreducible water saturation will decreased with elevated total injection rate which coincides with the classical principles.

O18

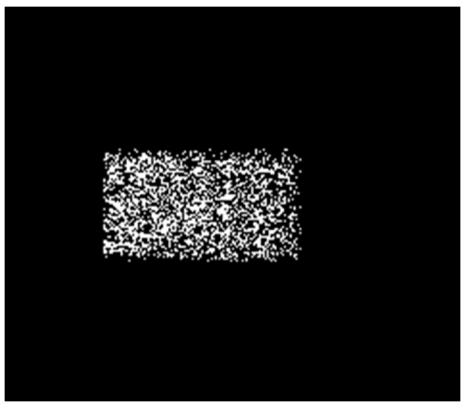

Fig. 1 Saturated water image

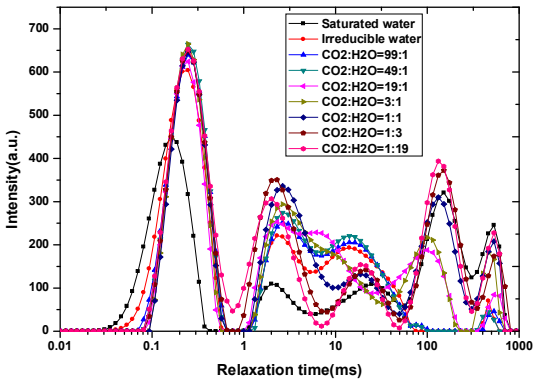

Fig. 2 T_2 curve with various injected ratios

Experimental results show that MRI can be effectively used to measure water saturation and analyze the displacement through transient images and T_2 curves under CO_2 storage conditions. Transient images at different injection ratios display the water and CO_2 distributions. From the T_2 curves, five peaks display five sizes of pore and the first peak stands for the irreducible water whose intensity and T_2 value don't change at different injection ratios. T_2 curve will migrate to the bigger T_2 value direction with elevated injected water proportion and the intensity will also increase. Irreducible water saturation will decreased with the increase of total injection rate.

References:

1. S. E. Buckley and M. C. Leverett: Mechanism of fluid displacement in sands, New York Meeting, 1941.
2. Tomochika Tokunaga, Katsuro Mogi, osamu Matsubara, Hiroyuki Tosaka and Keiji Kojima: Buoyancy and Interfacial Force effects on two-phase displacement patterns: An experimental study, AAPG Bulletin 84(1): 65-74 (2000).
3. Tetsuya Suekane, Shingo Soukawa, Satoshi Iwatani, Shoji Tsushima, Shuichiro Hirai. Behavior of supercritical CO_2 injected into porous media containing water. Energy 2005; 30: 2370–2382.
4. Jean-Christophe Perrin, Michael Krause, Chia-Wei Kuo, Ljuba Miljkovic, Ethan Charoba and Sally M. Benson. Core-scale experimental study of relative permeability properties of CO_2 and brine in reservoir rocks. Energy Procedia 2009; 1:3515-3522.
5. Tetsuya Suekane, Naoto Furukawa, Shoji Tsushima, Shuichiro Hirai and Masanori Kiyota. Application of MRI in the measurement of Two-phase flow of supercritical CO_2 and water in porous rocks. Journal of porous media 2009; 2:143-154.

O19

Nanoparticle Transport Monitored by MRI

J.L. Paulsen[a] Yonggang Wang[b], Huiguang Zhu[c], Vicki L. Colvin[c], Kurt D. Pennell[b], Martin Hurlimann[a], Yi-Qiao Song[a]

[a]Schlumberger-Doll Research, Cambridge, MA 02139, USA

[b]Dept of Civil and Environmental Engineering, Tufts University, Medford, MA, 02155, USA

[c]Dept of Chemistry, Rice University, Houston, TX 77005

The success of nanoparticle probes in medical applications has motivated research into their adaption as geological tracers in order to characterize formation and fluid properties beyond the wellbore into regions invisible to the majority of currently available tools [1]. Such tracers must handle very different environments in the subsurface (e.g., salt concentration > 2% wt), and their development and implementation requires studies of their transport and retention under these harsh conditions. Furthermore, as nanoparticles become more widely used understanding the processes governing their transport in the subsurface will become essential to remediating contamination of these materials [2].

Column flooding experiments were combined with multi-slice multi-echo (MSME) MRI imaging [3] to study nanoparticle transport and retention in unconsolidated sand, examining the behavior of PAA-coated iron-nanoparticles at various salt concentrations. Tracer floods into packed columns yield pseudo one-dimensional flows amenable to standard analyses for transport, while T_2 maps from MSME imaging yield the needed concentration profiles with calibration. The addition of MRI allows us to detect of voxel sized volumes with good sensitivity (ca. 5ppm) over multiple column lengths and at higher time resolution relative to typically analyzing milliliter fractions at the outlet. This additional information greatly improves our ability to identify and fit the appropriate transport models, where parameter differentiation is often an ill-conditioned problem. Furthermore, resolution in the axial plane allows for adjustments to deviations from plug flow improving our ability to accurately determine transport parameters, and to rapidly identify fritting and packing errors that are otherwise difficult to identify based on particle effluent breakthrough data alone.

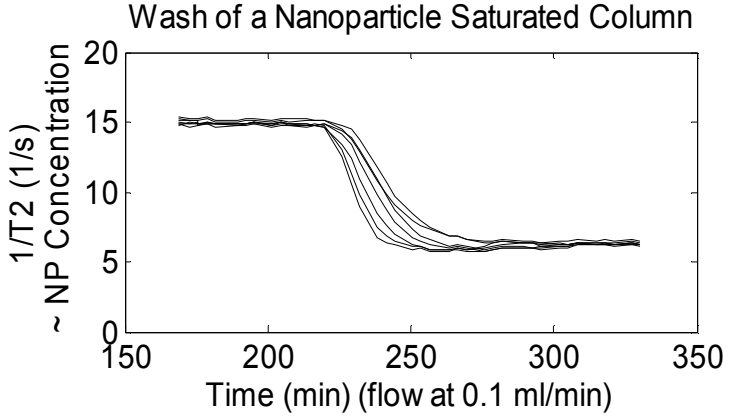

Fig 1: Nanoparticle concentration for a single column length (axial slice) over the course of a wash with deionized water. The flow profile is separated for different radii for the separate curves. Such macroscopic flow inhomogeneities are combined with fraction collection..

The MRI system coupled with packed columns is a valuable tool to characterize nanoparticles transport in porous media greater detail. It could provide detailed reference studies of transport behavior to aid the design and interpreting the large scale conventional column studies over the wide range of conditions needed to develop and fully characterize these probes for eventual geological applications.

References:

1. J. Yu et al. Transport Study of Nanoparticles for Oilfield Application, SPE 121158 (2010).
2. Y. Wang, Y. Li, K.D. Pennell. Env. Tox. & Chem. 29. pp1860. (2008)
3. M.A. Bernstein, et. al, Handbook of MRI Pulse Sequences. Elsevier, 2004.

O20

Fast Flow Velocity Mapping of Hydrodynamic Cavitation

B. Newling, I. Mastikhin, A. Adair

UNB MRI Centre, Dept. of Physics, Univ. of New Brunswick, Fredericton, NB, Canada

A liquid flowing in a pipe will experience pressure variations due to changes in the pipe geometry. In the case of water flowing through a pipe constriction, continuity indicates that the flow speed of the water will increase as the cross-sectional area of the pipe decreases. This increase in flow speed manifests as a decrease in the local pressure of the water. With a sufficiently narrow constriction and high flow speed, the local pressure of the water can drop below the vapour pressure, which results in the formation of bubbles (hydrodynamic cavitation). This effect is a concern in many biological, chemical, and engineering applications as the collapse of these bubbles can erode the pipe wall.

The necessary conditions for hydrodynamic cavitation result in a fast, turbulent, two-phase flow system. MRI measurements of this type of system benefit greatly from pure phase-encode techniques with short measurement time intervals. SPRITE has a measurement time interval on the order of hundreds of microseconds which limits the movement of the water between excitation and acquisition. In addition, as a pure phase-encode technique, SPRITE images have no artifacts due to B_0 inhomogeneity or magnetic susceptibility variations, which result from the air-water interface of the bubbles.

Measurements of the flow effects of hydrodynamic cavitation were acquired using a motion-sensitised PFG version of 3D Conical SPRITE. In addition to the three spatial dimensions of the images, motion-sensitisation was applied individually in the X-, Y-, and Z-directions. From these measurements, velocity maps were created to show the full three-dimensional flow of the water along the constriction. Density maps (and thus void fraction images), were acquired using 3D Conical SPRITE with a very short phase-encoding time. Combined, density and velocity maps are useful to the study of the behaviour of hydrodynamic cavitation.

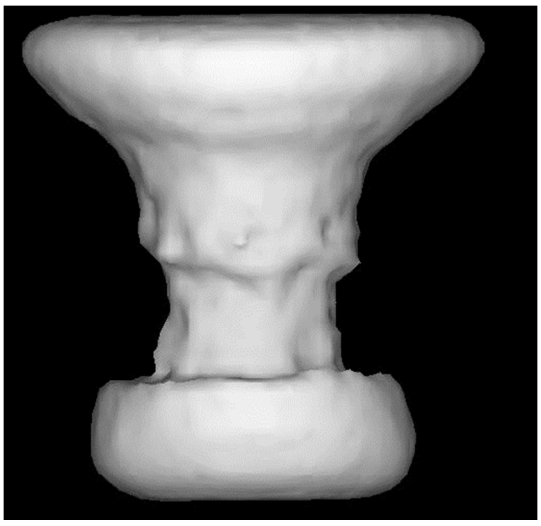

Fig. 1: 3D rendered SPRITE image of water flowing down through a pipe constriction. The bubble cloud resulting from hydrodynamic cavitation is evident as a region of null below the narrowest part of the constriction. At this position, the water is flowing at approximately 25m/s.

References:
1. M. Halse *et al.*, *J. Magn. Reson.* **165** (2003) 219-229.
2. B. Newling *et al.*, *Phys. Rev. Lett.* **93** (2004) 154503.
3. I. Mastikhin and B. Newling, *Phys. Rev. E* **78** (2008) 066316.
4. M. Sankey *et al.*, *J. Magn. Reson.* **199** (2009) 126-135.

O21

Polymers in shear flow at low and high field

U. Böhme, L. Loose, U. Scheler,

Leibniz-Institut für Polymerforschung Dresden e.V.

Polymers under shear flow exhibit shear induced alignment of the polymer chains. A Couette cell has for comparison been placed in 300 MHz imaging system and a 30 MHz Halbach magnet.

The high-field instrument provided spectral resolution and thus permits the separate investigation of the polymer (poly(styrenesulfonate)) and the solvent. The polymer alignment is expected to result in enhanced residual dipolar couplings and thus a shortening of T_2. However, a longer T_2 is found under shear indicating that the enhancement of the polymer chain mobility, originating from the loosening of entanglements under shear is the dominating effect. Because the solvent exhibits opposite behaviour, no significant effect has been found in the low-field experiments, where polymer and solvent are not distinguished. If only the polymer signal is excited via a T_1 filter, a similar behaviour as in the high field experiment is found.

A dedicated probehead for high-temperature rheo NMR operating up to 250 °C sample temperature is described. Extensive temperature monitoring is required to protect the superconducting magnet and the gradients. Melts of poly(propylene) have been studied. At larger molecular weight the effect of the disentanglement of the polymer chains dominates. In the melt no significant alignment-induced residual dipolar coupling are observable.

A strong temperature dependence of T_1 has been found, which is attributed to slowed down spin diffusion as a result of the enhanced mobility. This effect has been applied to investigated the possible temperature increase as a result of shearing the viscous melt. In the present setup where extensive air flow is used to heat the sample and to control the temperature of the probe, no increase of the sample temperature as a result of the shear has been observed, all the changes in the sample are attributed to only the shear.

O22

Early-age cement paste microstructure evolution: a ^{1}H low-field NMR study

Sun Zhenping [a], Yu Yang [a], Pangmin [a], Yang Peiqiang [b], Hu Jingli [b]

[a] Key Laboratory of Advanced Civil Engineering Materials, Ministry of Education, Tongji University, Shanghai 200092, [b] Shanghai Niumag Corporation, Shanghai 200333

Early-age cement paste microstructure evolution is a key to understand fluidity and slump loss of fresh concrete. We present a study on early-age cement paste microstructure evolution using ^{1}H low-field NMR. In this study, early-age cement paste with different fineness at same water-cement ratio of 0.4 was investigated. We found that T2 distribution curve of fresh cement paste with common fineness was bimodal: the peak on the left side corresponded to water in flocculation and the peak on the right side corresponded to water among flocculation. Relative amplitude of left peak decrease with cement hydration and vanished between 4h and 5h loosely corresponding to final setting time. However, T2 distribution curves of cement with fineness of 400m^2/kg, 500m^2/kg and 600m^2/kg had a single peak, T2 of which was almost identical with left peak of cement paste with common fineness. Evolution of T2 manifested itself three stages and had a good relevance to cement hydration. ^{1}H low-field NMR proves to be an effective way to investigate Early-age cement paste microstructure.

[1] J. P. Gorce, N. B. Milstone, Probing the microstructure and water in composite cement blends, Cem. Concr. Res. 37 (2007) 310.
[2] F. F. Paméla, R. Stéphane, Proton NMR relaxation as a probe for setting cement pastes, Magn. Reson. Imaging. 26(2008) 1183.

O23

Magnetic Resonance Microscopy Studies of Polycrystalline Ice

Jennifer R. Brown[a], Timothy I. Brox[b], Sarah J. Vogt[a], Joseph D. Seymour[a], Mark L. Skidmore[c] and Sarah L. Codd[d]

aChemical and Biological Engineering b Department of Physics, c Department of Earth Sciences, dMechanical and Industrial Engineering

In many of Earth's icy environments, such as glaciers, the polar ice sheets, or sea ice, polycrystalline ice is formed which has a dynamic pore structure of liquid-filled intercrystalline veins within a solid ice matrix[1]. The nature of this structure is not fully understood, yet will clearly impact the physical and rheological properties of ice. Recently, metabolically active microorganisms that excrete extracellular ice binding proteins (IBPs), believed to inhibit ice recrystallization, have been found in glaciated environments[2], but the impact of their activity on the vein network structure is largely unknown. Here Nuclear Magnetic Resonance (NMR) techniques are used to study the effect of chemical and biological impurities on vein structure, in particular the presence of salts and an extracellular protein extract, likely including an IBP, from an organism isolated from the accretion ice of subglacial Lake Vostok, Antarctica [3]. NMR has in recent years become a powerful method for probing pore structure and transport dynamics in porous media systems via measurement of relaxation rates, molecular diffusion and dispersion[4]. However, its ability to characterize ice as a porous media has not yet been fully exploited. In this work, the liquid vein structure was characterized with T2 relaxation distributions and time dependent diffusion measurements to obtain information on pore sizes, surface to volume ratios and tortuosity as a measure of vein interconnectivity. Since the ice undergoes recrystallization over time, measurements were repeated at various time intervals in order to monitor the evolution of the microstructure with and without the presence of the extracellular protein extract.

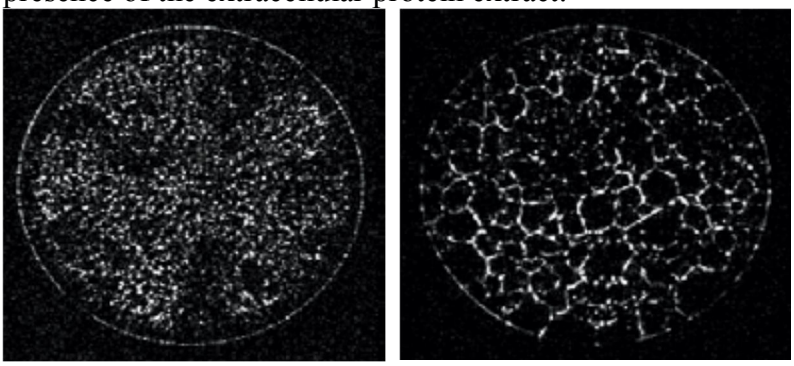

Fig. 1: Images of ice after 500 hours of freezing at -150C.

The spatial resolution is 55x55 m over a 5 mm slice. Salt concentrations are 7 g/l NaCl, similar to that measured in basal (debris-rich) glacial ice. (a) with ~10 g/ml extracellular protein extract (b) without protein present. Note the visible differences in pore structure between the samples.

This work is a novel approach to characterization of the liquid vein structure in ice as it relates to the habitat of microorganisms at sub-zero temperatures, but also is a demonstration of the potential for NMR techniques to model frozen geophysical systems in general ranging from sea ice to permafrost and glacial ice, of interest in a broad range of fields from climatology, biology, and earth sciences to engineering and environmental science.

References:

1. Nye, J.F., *The Geometry Of Water Veins And Nodes In Polycrystalline Ice.* J. of Glaciology, 1989. **35**(119): p. 17-22.
2. Christner, B.C., *Bioprospecting for microbial products that affect ice crystal formation and growth.* App. Microbio. and Biotech. **85**(3): p. 481-489.
3. Raymond, J.A., et al, *A bacterial ice-binding protein from the Vostok ice core.* Extremophiles, 2008. **12**(5): p. 713-717.
4. Song, Y.Q., et al., *Magnetic resonance in porous media: Recent progress.* J. of Chem. Phys, 2008. **128**(5).

O24

NMR imaging studies of wood moisture interaction

S. V. Dvinskikh[a], *I. Furó*[a], *M. Henriksson*[b],

[a]Department of Chemistry and Industrial NMR Centre
[b]Department of Fibre and Polymer Technology and Wallenberg Wood Science Centre, Royal Institute of Technology, SE-10044 Stockholm, Sweden

Wood has potential as a renewable material for a large variety of applications that often call for improved properties such as dimensional stability, moisture insensitivity, and durability. Moisture migration in wood is a particularly important factor in determining the cost-effective service life of wooden constructions. The primary processes for moisture migration in wood include water diffusion in the cell wall, adsorption to and exchange with hydroxyl groups, and vapor diffusion in the lumen [1]. Capillary flow plays a significant role in the uptake of liquid water. Within the present research, high and low field NMR spectroscopy and imaging was applied for studying the spatial distribution and migration of moisture in a number of wood specimens and under varying environmental conditions.

In contrast to green or water-soaked wood, processed construction wood at ambient condition is much less suitable for standard MRI because of the short relaxation times of adsorbed water. Hence, a solid state MRI method - single point imaging (SPI) [2], was applied to assess the spatial variation of the moisture content in wood.

Moisture kinetics in wood was studied upon changing on a controlled manner the relative humidity of the surrounding air [3,4]. By varying the wood sample orientation with respect to the magnetic field gradient the moisture movement along the three principal directions in wood was monitored by SPI MRI. Data were compared to multi-Fickian numerical simulations of transient moisture transport [3].

Wood conditioned in atmosphere with heavy water (D_2O) can be studied by MRI in order to separate images due to water (^{2}H MRI) and macromolecular wood tissue (^{1}H MRI). By comparing the proton and deuterium images a linear correlation between water and macromolecular contents in wood is clearly demonstrated [5].

We have evaluated the potential of NMR technology based on small portable magnets for *in situ* studies of the local moisture content in wood. Low field and low resolution ^{1}H NMR with a unilateral permanent magnet was used to monitor the spatially resolved moisture content of wood claddings [6] and for assessment of moisture protective properties of wood coatings [7]. The method is quick, noninvasive, simple to perform, and does not require removing wooden parts from the structure.

References:

1. Skaar, C. Wood-Water Relations. Springer, Berlin, 1988.
2. S. Emid, J. H. N. Creyghton. Physica B **128**, 81 (1985).
3. S. V. Dvinskikh, M. Henriksson, A. L. Mendicino, S. Fortino, T. Toratti. *Eng. Struct.* (2011). Accepted.
4. J. Eitelberger, K. Hofstetter, S. V. Dvinskikh. *Composites Sci. Technol.* Submitted.
5. S. V. Dvinskikh, M. Henriksson, L. A. Berglund, I. Furó. *Holzforschung* **65**, 103 (2011).
6. S. V. Dvinskikh, I. Furó, D. Sandberg, O. Söderström. *Wood Mat. Sci. Eng.* (2011). In press.
7. P. Pourmand, L. Wang, S. V. Dvinskikh. *J. Coat. Technol. Res.* (2011). Submitted.

O25

Sensitivity in Small-scale Spectroscopy

Andrew F. McDowell

ABQMR, Inc, Albuquerque, NM USA

For small-scale spectroscopic NMR systems (1,2,3) to reach their full potential and find significant application in industrial or laboratory settings, it will be important for them to achieve enough sensitivity to study samples at low concentration. To date, typical published data are from pure liquids or roughly equi-molar mixtures (10-50M). On the other hand, samples for chemical analysis are often at 1 M concentration or below, and molecules of biomedical interest occur at substantially lower concentrations.

We report on the instrumental and software improvements that have allowed us to study samples at concentrations below 1 M. By determining the trade-offs between sensitivity and resolution for various sample sizes in our ultra-compact 1.7 T permanent magnet, we are able to select the optimal coil size for particular applications. Our magnets are equipped with a full set of first and second order shim coils to improve their resolution over larger volumes. Improved thermal management and signal averaging techniques have helped to overcome the field drifts due to temperature variations.

As an example, we have employed a sample size of 400 μm ID, 1 mm length (125nL), to acquire the spectra on low-concentration sodium citrate solutions shown in Figure 1. Concentrations down to 10 mM have been detected, a sensitivity improvement of more than 1000-fold over our previous results using pure water.

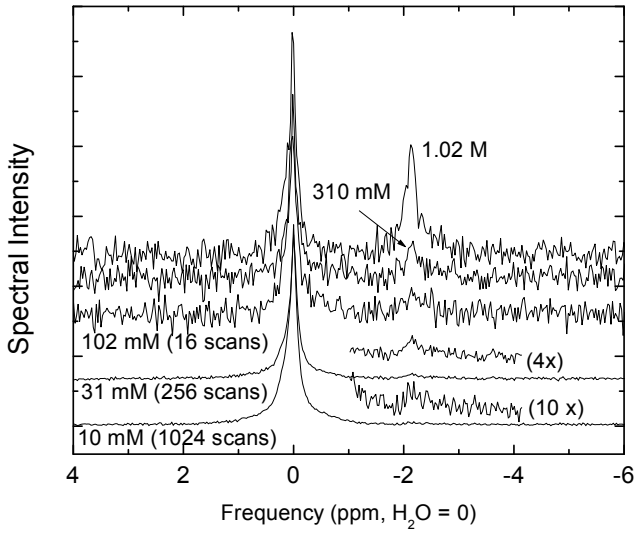

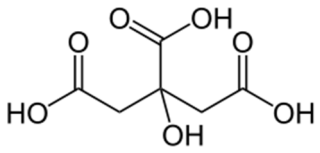

Fig. 1: Sodium Citrate (citric acid) in D_20 with added H_20. The frequencies are referenced to H_20. The peak near -2.2 ppm is due to the 4 methylene hydrogens. Except for the 1M case, each sample contains 1 M H_20 to provide a reference signal. 512 data points were acquired at 1kHz sweep width; TR = 2s, single scans unless indicated. No zero filling or exponential filtering was applied. The spectra each have different vertical scales chosen to show the small peaks at -2.2 ppm.

This level of sensitivity has also allowed us to detect ^{13}C sidebands in the ^{1}H spectra of simple hydrocarbons, as well as ^{19}F spectra of fluorinated organic acids of environmental interest at moderate concentrations. Using a larger 1.0mm sample size, NMR signals from ^{31}P, ^{11}B, and ^{23}Na have also been detected, the latter at 110 mM.

References:
1. McDowell and Fukushima, Appl. Magn. Reson., **35** (2008) 185-195.
2. Danielli, et al., Angew. Chem. Int. Ed. **49** (2009) 1-4.
3. picoSpin, Boulder, Colorado, USA

O26

Polymers under uniaxial stress

U. Böhme, U. Scheler,

Leibniz-Institut für Polymerforschung Dresden e.V.

Local order and dynamics in polymers under mechanical stress is studied by low-field NMR. Permanent magnets in a Halbach arrangement permit NMR investigation without the limits present in high-field NMR. In particular the confined stray field permit the application of NMR in a stretching apparatus and a rheometer. The major drawback of low-field NMR, the lack of chemical shift resolution, is not a problem, because in the study of known materials properties other than their chemical composition are of interest.

Mechanical stress on elastomers results in partial chain ordering and consequently reduced chain mobility. The resulting stronger residual dipolar couplings are manifested in the stronger buildup of double quantum coherences and in a shortening of the slower component of the transverse relaxation time. After releasing the load the return to the dipolar couplings and the relaxation times of the unextended sample is followed on a time constant of tens of minutes

The crystalline and amorphous fractions of semicrystalline polymers are distinguished by their transverse relaxation times. To localise the stress effect in the rf coil, the diameter of the rod under study is reduced in the portion located in the rf coil. Under mechanical load there is a significant shortening of the transverse relaxation time as well as an increase in the residual dipolar coupling which are determined from the build up of double quantum intensities. The shortened relaxation times return to values close to those found in unloaded samples, when the load is kept constant. The time constant of this relaxation appears to be longer than that found in mechanical stress relaxation experiments.

The interaction with paramagnetic moieties in the fillers in polymer nanocomposites has a strong impact on the longitudinal relaxation time. Delaminating filler particles under mechanical stress results in a shorter T_1 of the protons in the polymer, because the contact area between the filler and the polymer increases.

O27

A comparative study on the film formation of bio- and synthetic polymers using single-sided NMR

S. Ghoshal, C. Mattea, P. Denner, S. Stapf

Department of Technical Physics II / Polymer Physics, Institute of Physics, Faculty of Mathematics and Natural Science, Ilmenau University of Technology, PO Box 10 05 65, D-98684 Ilmenau, Germany.

Biodegradable polymer films have received attention from researchers and industry in recent years. In this contribution, the film formation from gelatin, a biopolymer, and Poly(vinyl alcohol) (PVOH), a synthetic but biodegradable polymer, have been followed using a single-sided NMR scanner. Solutions of the polymer samples were prepared and cast on the Petri dish substrates. During its film formation, occurring by evaporation of the solvent, each of the samples was continuously scanned in different layers at a resolution of 50 µm. The Carr-Purcell-Meiboom-Gill (CPMG) pulse sequence was applied to obtain the vertical profiles and to accumulate T_2-weighted echo trains by moving the scanner relative to the sample. The echo decays were fitted and spin-spin relaxation times (T_2) were obtained for each layer (Figure 1). For gelatin film formation, it was found that close to the final drying stage, the T_2 values of the film near the substrate decreases faster than in the vicinity of the sample/air interface. This is explained by the renaturation of gelatin, a known phenomenon in this kind of system resulting precipitation. Moreover, T_2 is found to be shorter in the vicinity of the sample/air interface when compared to the middle part of the sample (Figure 1a). For a dilute gelatin solutions (1%-w/v), the solute is spatially heterogeneously distributed due to the evaporation process; this effect is absent in a more concentrated gelatin sample (10%-w/v). On the other hand, for the PVOH film formation, the NMR relaxation times gradually increase along the direction of the sample/air interface. In the advanced stage of the drying process, the microscopic arrangement of the polymer chains during their solidification is influenced by the referred heterogeneity and determines the final structure of the film. X-ray was used for the study of the gelatin and PVOH films in their final state and the structural heterogeneity suggested by the NMR study was confirmed.

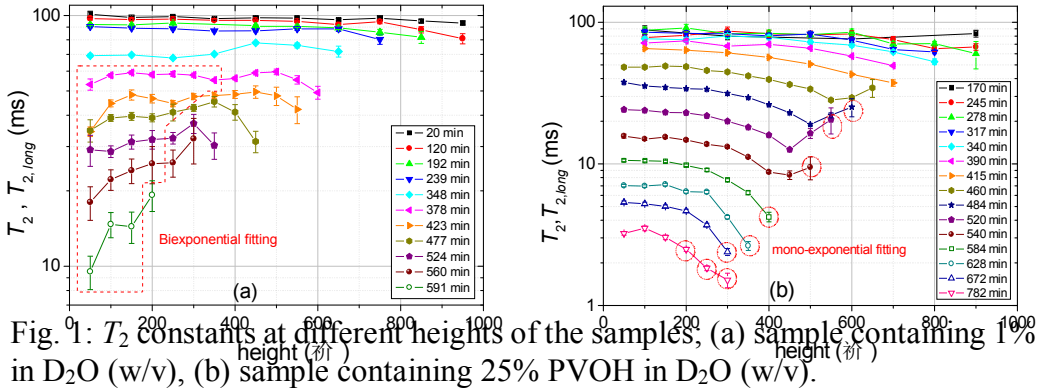

Fig. 1: T_2 constants at different heights of the samples, (a) sample containing 1% gelatin in D_2O (w/v), (b) sample containing 25% PVOH in D_2O (w/v).

References:

1. S. Ghoshal, C. Mattea and S. Stapf, Chem. Phys. Lett. 485 (2010) 343.
2. S. Ghoshal, C. Mattea, P. Denner and S. Stapf, J. Phys. Chem. B 114 (2010) 16356.
3. S. Ghoshal, C. Mattea, P. Denner and S. Stapf, Structural dissimilarities in PVOH films induced by evaporation during the formation process. (Submitted)

O28

Stream function method for a bi-planar single channel shim coil

Daiki Tamada, Yasuhiko Terada, Katsumi Kose
Institute of Applied Physics University of Tsukuba, Tsukuba 305-8573, Japan

In most NMR/MRI study, shim coils are required to accomplish field homogeneity of the order of 1 ppm or less. Since the magnetic field ΔB_0 can be expressed as the superposition of the spherical harmonics [1], a shim coil is typically designed to generate a magnetic field corresponding to one of the spherical harmonics. In most cases, shimming is performed using a number of the shim coil element [1][2] because of complexity of the magnetic field inhomogeneity. Such multi-coil shimming, however, has several problems, namely, decrease of available gap (or bore) space, excessive power consumption, and a complicated power supply system. In order to overcome these problems, our group proposed a single channel shim coil to correct the complex inhomogeneity using the target field approach [3]. Here, we propose an alternative method to design a single channel shim coil to correct the complicated magnetic field inhomogeneity.

Inhomogeneity of yokeless permanent magnet (field strength B_0 = 1.04T at +25 °C, gap width = 40 mm, homogeneity 20 ppm in 20 mm dsv, weight 85 kg) was measured using a 3D lattice phantom [4]. The magnet was installed in a variable temperature thermostatic bath (temperature range = –15 to +50 °C). 3D images of the phantom were measured at –5 °C using 3D SE sequences (matrix = 256^3, FOV = $(38.4\ \text{mm})^3$) with positive and negative readout gradients. We evaluated the inhomogeneity in the central cubic area ($(18\ \text{mm})^3$). ΔB_0 was approximated using 4th order polynomials in the Cartesian coordinate. In this method, the current density of the shim coil ($\mathbf{J}_{\text{shim}}$) was represented as a superposition of current densities $\mathbf{J}_i$ for shim coils corresponding to second order spherical harmonics ($2Z^2–X^2–Y^2$, $X^2–Z^2$, $Y^2–Z^2$, XY). Therefore, $\mathbf{J}_{\text{shim}}$ is expressed as $\mathbf{J}_{\text{shim}} = \sum_i c_i\mathbf{J}_i$, where c_i is the coefficients of $\mathbf{J}_i$. The coefficients were optimized using a genetic algorithm (GA) to minimize the RMS of ($\Delta B_0 + B_{shim}$), where B_{shim} is the magnetic field induced by $\mathbf{J}_{\text{shim}}$. The winding pattern was derived using the stream function method [5][6]. The contour line of the stream function ψ (Fig. 1-(a)) of the optimized $\mathbf{J}_{\text{shim}}$ gave a closed winding pattern (Fig. 1-(b)). The magnetic field calculation shows that the inhomogeneity ΔB_0 (15 ppm (RMS) and 86 ppm (P-P)) was improved to (6.4 ppm (RMS) and 60 ppm (P-P)) using the shim coil. In the experiment, ΔB_0 was improved to the comparable result (5.3 ppm (RMS) and 41 ppm (P-P)). The inhomogeneities corresponding to z^2, y^2 and x^2 were decreased to 0.17%, 18% and 55%, respectively. The image distortion was improved clearly as shown in Fig. 2.

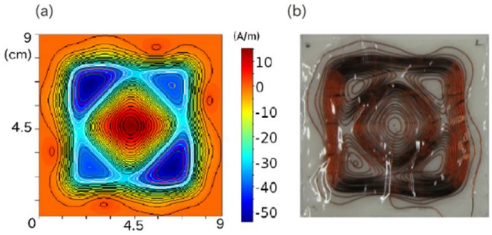

Figure 1: (a) Calculated winding pattern (b) The shim coil built on an FRP plate ($(9\ \text{cm})^2$ in size).

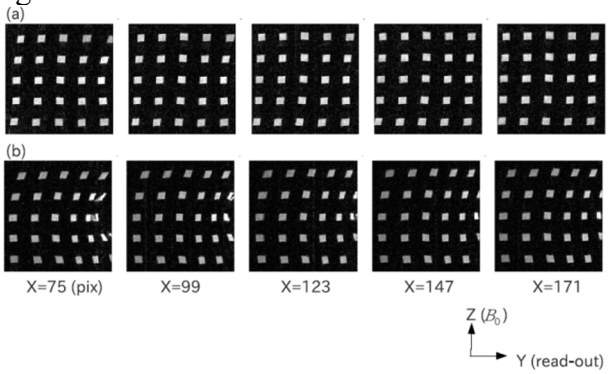

Figure 2: 2D slices selected from 3D image datasets acquired (a) with and (b) without shimming. Measurements were performed using 3D SE sequences (image matrix = 256^3).

This method can be extended to a higher order (3rd, 4th) shim coil design by adding higher order shim coils to element coils, and can be also applied to design for cylindrical shim coils, provided that suitable element coils are given. In conclusion, a single channel shim coil that we designed successfully corrected inhomogeneities corresponding to 2nd order spherical harmonics.

O28

References:
1. F Roméo and D I Hoult. Magnet field profiling: Analysis and correcting coil design. *Magnetic Resonance in Medicine*, 1(1): 44–65, 1984.
2. W A Anderson. Electrical Current Shims for Correcting Magnetic Fields. *Review of Scientific Instruments*, 32(3): 241–250, 1961.
3. R Shigeki and K Kose. A single-channel planar shim coil for a permanent magnet. In *18th Annual Meeting of ISMRM*, page 1542, Stockholm, Sweden, 2010.
4. D Wang, D M Doddrell, and G Cowin. A novel phantom and method for comprehensive 3-dimensional measurement and correction of geometric distortion in magnetic resonance imaging. *Magnetic resonance imaging*, 22(4):529–542, May 2004.
5. R Turner. Gradient coil design: A review of methods. *Magnetic resonance imaging*, 11(7): 903–920, 1993.
6. M A Brideson, L K Forbes, and S Crozier. Determining complicated winding patterns for shim coils using stream functions and the target-field method. *Concepts in Magnetic Resonance*, 14(1): 9–18, 2002.

O29

Optimized Adiabatic and Nonadiabatic Field-Cycling Control Circuit for Prepolarized Earth Field NMR

S. Lother[a], U. Hölscher[a], T. Drießle[a], P. Weber[b], P. Jakob[a,b] and F. Fidler[a]

[a]Research Center Magnetic-Resonance-Bavaria (MRB), Wuerzburg, Germany
[b]Department for Experimental Physics 5 (Biophysics), University of Wuerzburg, Wuerzburg, Germany

Introduction: Prepolarized Earth Field NMR (EFNMR) was the first fast field-cycling experiment which was developed by Packard and Varian [1]. The prepolarization field enhances the magnetization to measureable values which make EFNMR possible. There are two reasonable ways to shut the prepolarization field (B_P) down, in case it is perpendicular to the earth field (B_0). One way is adiabatic (slow in comparison to the Larmor frequency) and the other is nonadiabatic (fast). This has been discussed in literature before [2, 3]. For some application it is beneficial to shut down the prepolarization field adiabatically and for some other the nonadiabatic field-cycling mode is more profitable. We developed a versatile electronic circuit to enable both field ramp behaviors. The circuit uses a new concept of segmenting the shutdown process to avoid high induction voltage and provide the flexibility to choose between adiabatic and nonadiabatic field ramps.

Materials and Methods: For the "nonadiabatic mode" we keep the induction voltage at the prepolarization coil at a constant high level to have a controlled nonadiabatic shutdown slope. This ramp goes almost linear which guarantees a complete shut-off of the magnetic field after the ramp in contrast to exponential convergence (e.g. a LR-circuit). The difference from the "nonadiabatic mode" to the "adiabatic mode" is found in the last moment of slope duration, when the shutdown field $|B_P|$ reaches a critical value of $\sim 10 \cdot |B_0|$. To optimize the "adiabatic mode" we cut the shutdown process into two segments, with two different slopes. In the first segment we use a high induction voltage to reduce the shutdown time and for the second segment we lower the induction voltage to ensure a slope with adiabatic condition. This allows a compromise between sufficient short slope durations and a low level of induction voltage.

Results: A measurement in the "nonadiabatic mode" ($B_P \perp B_0$) eliminates the need of an extra 90° excitation pulse. This was confirmed by a free induction decay (FID) of tap water which we captured directly after the shutdown event.

In the "adiabatic mode" the magnetization has enough time to follow the changes of the effective magnetic field (B_P+B_0) to end parallel to the B_0-field direction after the shutdown duration. We fortify this with a leading excitation pulse of 90° and we record a comparable signal of a FID in contrast to the measurement in the "nonadiabatic mode".

Conclusion: We developed a robust control circuit which is able to ramp a prepolarization field in "nonadiabatic mode" and "adiabatic mode" based on a new concept of a segmentation of the shutdown process. According to that, both modes can be optimized in shutdown duration and induction voltages. The concept is easily expandable to divide the shutdown ramp into further segments with adjustable slopes to optimize the shutdown process for arbitrary coils, prepolarization currents and user wishes.

References:

1. Packard, M. & Varian, R. Phys. Rev., 1954, 93, 941
2. Callaghan, P. T. & Gros Le, M. Am. J. Phys., 1982, 50, 709-713
3. Stepisnik, J., Erzen, V. & Kos, M. Magn Reson Med, 1990, 15, 386-391

O30

Microstructure and rehydration behaviour of freeze-dried fruits and vegetables

A. Voda[a], F. Vergeldt[b], G. van Dalen[a], A. Duijster[c], R. van der Sman[b]
L. van Vliet[c], H. Van As[b], J. van Duynhoven[a,b]

[a] AMDM, Unilever Discover Vlaardingen, The Netherlands
[b] Wageningen University, The Netherlands
[c] Quantitative Imaging Group, Delft University of Technology, The Netherlands

Consumers have a high appreciation of healthy meals rich in fruits and vegetables. Lack of convenience in preparing such foods is impeding consumers to reach their recommended daily intake of fibers and nutrients. Food industry has addressed this by developing food products consisting of dried fruits and vegetables that are rehydrated shortly before consumption. The main challenge in this field is to develop products which deliver health benefits and authentic sensory properties without compromising the convenience of fast cooking. So far most developments in this area have been engineering-driven[1].

We have adopted a microstructure-driven research strategy to investigate the structural impact upon freeze-drying of vegetables and to model their rehydration behaviour. Dried and rehydrated microstructures were assessed in a multi-scale manner (nm-mm) by means of complementary imaging techniques like SEM, µCT and MRI, as it is intuitively shown in Fig. 1A. Quantitative image analysis revealed the pore space topology in the dry state and NMR diffusometry and imaging allowed us to determine the cell walls behaviour upon wetting. Water kinetics during rehydration was studied in real-time and in situ by means of RARE imaging[2]. An example of a time series of 2D longitudinal images revealing the rehydration process of a freeze-dried carrot is shown in Fig. 1B.

Microstructural information was used for the development of a novel model for rehydration, which goes deeper than traditionally used ones for mass transport in porous media[3]. The model considers water dynamics via capillary suction in combination with swelling of the cell wall material. Ultimately, the model will be verified by spatially-resolved moisture profiles acquired by MRI.

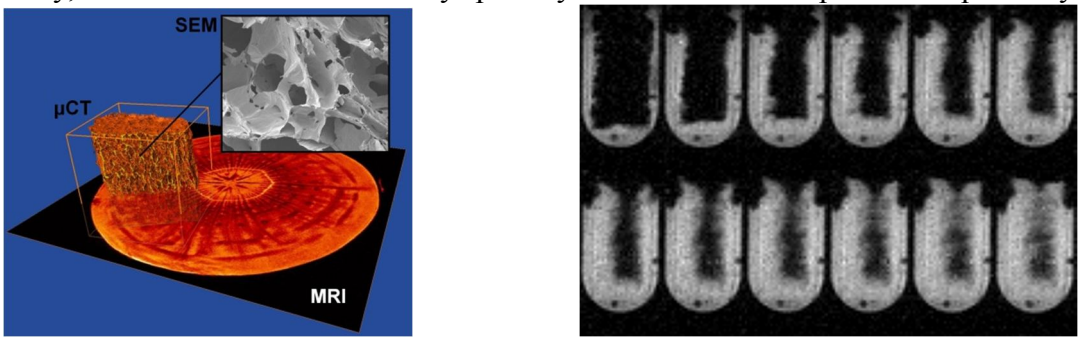

Fig. 1: A) Multi-scale imaging approach employed to assess the microstructure of fruits and vegetables. B) Time series of 2D images (RARE, 1mm slice, 219 µm resolution, 12 s/image time resolution) acquired during rehydration process of a dried carrot piece.

References:

1 K.S. Jayaraman and D.K. Das Gupta, Handbook of Industrial Drying, CRC Taylor & Francis, NY, 2007, 605-633.
2 T.W.J. Scheenen, D.v. Dusschoten, P.A. de Jager, H. Van As, J. Magn Reson., 142, 207-215.
3 A.K. Datta, J. Food Eng. 80(1), 2007, 80-95.

O31

Development of an electrically mobile and remotely operable MRI system for outdoor tree measurements

T. Kimura,[1] Y. Geya,[1] Y. Terada,[1] K. Kose,[1] T. Haishi,[2] H. Gemma,[3] Y. Sekozawa[3]
[1]Institute of Applied Physics, University of Tsukuba, 1-1-1 Tennodai, Tsukuba, 3058573, Japan
[2]MRTechnology Inc, 2-1-6 B5 Sengen, Tsukuba, 3050047, Japan
[3]Agricultural and Forestry Research Center, University of Tsukuba, 1-1-1 Tennodai, Tsukuba, 3058577, Japan

INTRODUCTION

In situ and *in vivo* plant measurements are essential to detect or differentiate plant diseases in natural environments. Although MRI systems are very useful for such studies, only few trials have been reported. In this study, we have developed an *electrically mobile and remotely operable MRI system for trees* to differentiate between diseased and healthy branches of Japanese pear trees in a fruit farm.

MATERIALS AND METODS

Figure 1 shows an overview of our MRI system developed in this study. The system consists of a 0.3 T with an 80 mm gap permanent magnet (~60 kg), gradient coil set, RF probe, and MRI console. The detection units (magnet, gradient, and RF probe) were fixed on a lifting table mounted on an electrically mobile cart (CB-02, Yamaichi-Seikou, Suzaka, Japan). This system can be remotely operated using the *Remote Desktop Protocol for Windows* through a public mobile network.

The whole system (~400 kg) including the MRI console was carried using the cart from our laboratory to the pear fruit-farm to detect a Japanese pear disease (dwarf disease). The distance between our laboratory and the fruit-farm was about 1.5 km and it took about 20 minutes to carry the whole system using the cart. We measured two branches (healthy and diseased) of the same pear tree (*Pyrus pyrifolia* Nakai, Kosui, about 35 years old) using 2D spin echo sequences with motion probing gradients along the branches.

RESULTS AND DISCUSSION

Figure 2 shows diffusion weighted and ADC images of healthy and diseased branches measured on a sunny day in July 2010. Relative *b* values are 0 s/mm^2 for (a) and (d), and 314 s/mm^2 for (b) and (e), respectively. The slice thickness, field of view, image matrix, pixel size, TR, TE, NEX, and total image acquisition time were 10 mm, 25.6 mm × 25.6 mm,128 × 128, 0.2 mm × 0.2 mm, 800 ms, 22 ms, 4 times, and about 12 minutes, respectively. As shown in Fig.2, while the ADC image (Fig.2(c)) of the healthy branch clearly shows an active water transport area, that of the diseased one shows no such area.

Because outdoor plant measurements often require a periodical image acquisition for a long time (whole day to several months) in natural environments, remote operation and portability of the MRI system are highly desired. We think our MRI system meets most of these requirements. From these results, we have concluded that our system is a useful tool for *in situ*, *in vivo, and real-time* tree measurements in outdoors.

Overview of the electrically mobile and remotely operable MRI system. April,

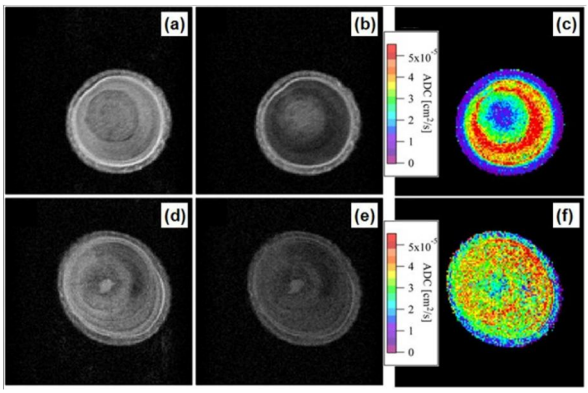

Diffusion weighted and ADC images of healthy (upper) and diseased (lower) branches.

Reference: 1. T. Kimura, Y. Geya, Y. Terada, K. Kose, T. Haishi, H. Gemma, Y. Sekozawa, Development of a mobile magnetic resonance imaging system for outdoor tree measurements. Rev. Sci. Instrum. 2011, in press.

O32

3D Micro-Imaging Study of the Metamorphosis of the Caterpillar and Pupa of the Large Cabbage White Butterfly at 17.6T

Volker C. Behr[a], *Simone C. Müller*[b], *Dieter Mahsberg*[b]

[a]Department of Experimental Physics 5 (Biophysics), University of Würzburg, Germany
[b]Department of Animal Ecology and Tropical Biology, University of Würzburg, Germany

Butterflies are one of the most species rich insect orders. One distinct characteristic of all butterflies is the complete metamorphosis they undergo from the larva, the caterpillar, to the adult butterfly. At the end of the larval period, a pupa develops, which experiences a large-scale re-building of internal organs as well as a complete change in outer appearance. We present an in-vitro study of the metamorphosis of the large cabbage white butterfly (*Pieris brassicae*) using NMR-microscopy.

In order to examine the different stages of growth and metamorphosis, caterpillars and pupas were fixed at different stages in a 4% formalin solution. Afterwards they were positioned in 20mm-NMR-tubes and the surrounding formalin was thickened using hydroxyethyl-cellulose to avoid motion artifacts due to vibrations caused by the gradient unit.

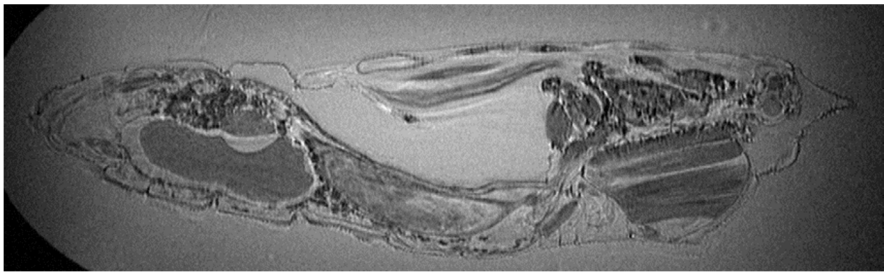

Fig. 1: Central slice of 3D-dataset of an 8-days-old pupa with a total length of 23mm. RARE imaging sequence with TR=1240ms, TE=14.8ms, isotropic resolution of $(47\mu m)^3$, rare factor of 4, and 12 averages.

Imaging experiments were performed using a 20mm homebuilt linear birdcage resonator on a Bruker Avance 750 WB spectrometer equipped with a 1T/m gradient unit. All high-resolution datasets (Fig. 1) were acquired using FLASH and RARE imaging methods, were the latter one showed better contrast in the fixed samples at the expense of longer measurement times.

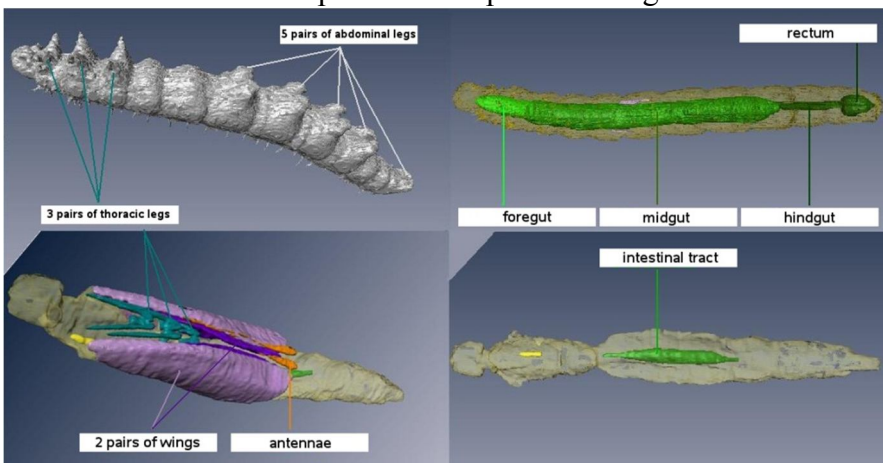

Fig. 2: Segmented datasets of a 19-days-old caterpillar (top) and a 9-days-old pupa (bottom). While the caterpillar's body is mostly comprised of alimentary organs, the pupa shows larger distinct organs such as the two wing-pairs of a butterfly, the antennae, and a greatly reduced intestinal tract. Also, the abdominal legs entirely disappear in the pupa.

The acquired datasets were segmented by hand using Amira (Visage Imaging, Berlin, Germany) and full 3D reconstructions were obtained (Fig. 2). These reconstructions allowed following the metamorphosis in the development of organs and body of the specimen.

Using NMR-imaging provided a means to perform this in-vitro study without dissecting the specimen and risking altering it by the procedure. Furthermore, NMR offers a way to repeat those studies in-vivo without hurting the insect using fast imaging methods.

Acknowledgements: The authors thank IS Insect Services, Berlin, Germany for providing the caterpillars.

O33

Simulation of Magnetic Field Gradient Waveforms in Metallic Vessels

Frédéric G. Goora[a,b], *Hui Han*[a], *Bruce G. Colpitts*[b], *Bruce J. Balcom*[a]

[a]MRI Centre, Department of Physics, University of New Brunswick, Fredericton, New Brunswick, Canada E3B 5A3, [b]Department of Electrical and Computer Engineering, University of New Brunswick, Fredericton, New Brunswick, Canada E3B 5A3

MRI of a sample enclosed within a non-ferromagnetic metal vessel has been reported in [1]–[3]. Metal vessels are natural choices for use in high pressure studies of materials due to their high tensile strength and high thermal conductivity. Such vessels are now the subject of intense investigation in our laboratory.

The use of switched magnetic field gradients in MRI results in the generation of eddy currents within the metal vessel which corrupts the applied magnetic field gradient. Simulations using CST EM Studio™, which uses the finite integration technique, have been completed which permits the investigation of putative vessel designs MR / MRI measurements. A two-dimensional representation of the spatial distribution of eddy currents on a metal vessel resulting from a switched magnetic field gradient is shown in Fig. 1. Simulations reveal the spatial distribution and temporal dependence of eddy currents, the resulting magnetic fields, and their dependence on: the vessel material, vessel geometry, and the orientation of the switched magnetic field gradient. Switched longitudinal and transverse magnetic field gradients have been simulated and observed to result in eddy currents that circulate on the metallic vessel such that essentially linear magnetic field gradients within the sample space result. Asymmetric metal vessels supported a spatially uniform circulating current which produces a $B_0(t)$ field shift. Simulation results have been verified experimentally through direct magnetic field gradient monitor (MFGM) measurement using the MFGM technique [1]–[2] and are in excellent agreement.

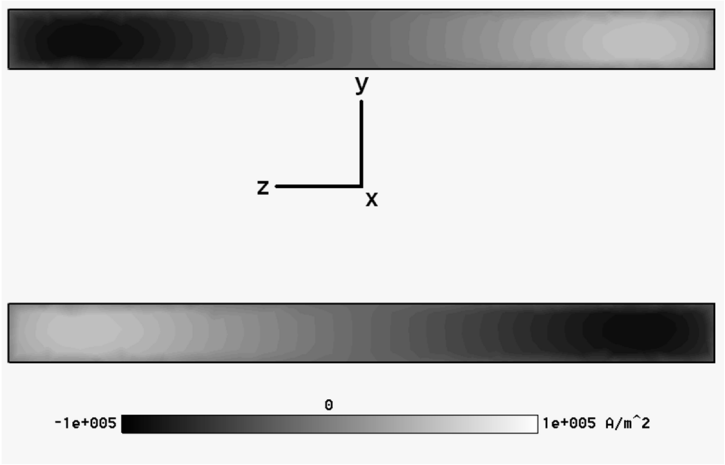

Fig. 1 Eddy current distribution on a metallic vessel due to a switched magnetic field gradient pulse directed along the longitudinal axis.

Although the techniques discussed have been applied specifically to metallic pressure vessels, the use of simulation and direct MFGM measurements can be used to identify and correct the root cause of magnetic field gradient corruption due to eddy currents in virtually any MRI scanner / experiment.

References:

1. H. Han, R. MacGregor, B. Balcom, J. Magn. Resn., 201 (2009) 212-217.
2. H. Han, A. Ouriadov, E. Fordham, B. Balcom, Concept Magn. Resn. A, Vol 36A (6) (2010) 349-360.
3. H. Han, D. Green, M. Ouellette, R. MacGregor, B. Balcom, J. Magn. Resn. **206** (2010), 97-104.

O34

MR Microscopy in Prognosis of Thrombolysis Outcome

I. Serša[a], J. Vidmar[b], F. Bajd[a], N. Bizjak[a], E. Kralj[b], A. Blinc[c]

[a]Jozef Stefan Institute, Ljubljana, Slovenia
[b]Medical Faculty, University of Ljubljana, Ljubljana, Slovenia
[c]Department of Vascular Diseases, University Medical Centre Ljubljana, Ljubljana, Slovenia

Despite enormous improvements in treatment of acute cardiovascular events by mechanical removal of blood clots, biochemical removal of blood clots (thrombolysis) still remains the mainstay of treatment in certain pathologies such as ischemic cerebrovascular stroke and massive pulmonary embolism. Thrombolytic treatment may be hazardous, because administration of thrombolytic agents may result in hemorrhages. Therefore, noninvasive assessment of blood clot structure and anticipated thrombolytic response may be important in deciding between mechanical vs. biochemical removal of blood clots. MR microscopy of blood clots prior to treatment is an efficient tool in assessment of thrombolytic treatment outcome. MR microscopy provides good spatial resolution and exceptional contrast that allows an efficient discrimination between red (RBC-rich) and white (platelet-rich) parts of the clot [1]. In addition, it enables an assessment of clot retraction and with it associated susceptibility of blood clots to thrombolytic treatment [2].

In this study thrombolysis of artificial retracted and non-retracted whole-blood clots was studied by sequential MRI. The clots were inserted into an RF coil inside a 2.35 T MR magnet and connected to a perfusion system containing thermoregulated plasma with the rt-PA thrombolytic agent. Each experiment consisted of eight imaging blocks of 17 min diffusion-weighted imaging (b = 0, 132, 317 and 635 s/mm^2), 8 min multi-spin echo imaging (eight echoes at TE = 18 ms) and 15 min clot perfusion. From DWI and multi spin echo images corresponding ADC and T_2 maps were calculated. In addition, to the thrombolytic experiments another set of experiments was done on parallel samples in which ADC and T_2 relaxation times were measured as a function of the clot retraction level.

Results of the study showed that both, ADC and T_2 decrease with an increase of the retraction level so that clot retraction can be estimated from corresponding ADC and T_2 values. In addition, the expected proportion of lysed clot correlates with its initial ADC or T_2 value (Fig .1). Clot regions with high ADC and T_2 values (ADC > 0.8 10^{-9}m^2/s or T_2 > 130 ms) lysed efficiently, while those with low ADC and T_2 values (ADC < 0.8 10^{-9}m^2/s or T_2 < 130 ms) were resistant to thrombolysis.

With progress of clinical MR systems in a direction of higher resolution, better image contrast and shorter image acquisition times, assessment of blood clot lysabiliyt *in vivo* may soon become reality.

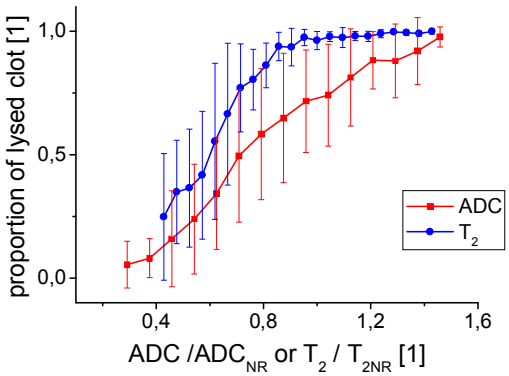

Fig. 1 Proportion of lysed clot as a function of the initial ADC or T_2 value in units of ADC$_{NR}$ = 1.2 10^{-9}m^2/s and T_{2NR} = 210 ms.

References:

1. J. Vidmar, I. Serša, E. Kralj, G. Tratar, A. Blinc, Eur. Biophys. J. 37 (2008) 1235.
2. J. Vidmar, A. Blinc, I. Serša, NMR Biomed., 23 (2010) 34.

O35

Estimation of Irreducible Water Saturation (S_{wirr}) from NMR Logs without Requiring $T_{2cutoff}$ in Tight Gas Sands

Liang Xiao[a], *Zhi-qiang Mao*[a], *Yan Jin*[b]

[a] China University of Petroleum, Beijing, P. R. China;
[b] Southwest Oil and Gas Field Branch Company, PetroChina, Sichuan, P. R. China

It a challenge of estimating irreducible water saturation (S_{wirr}) from NMR logs at present because of the influence of diffusion relaxation to NMR T_2 spectrum. The statistical analysis of experimental $T_{2cutoff}$ from 36 core samples show that it is difficult in defining a fixed value to obtain S_{wirr} in tight gas sands. The experimental results of 11 core samples with four different kinds of saturated conditions, they are fully saturated with water, irreducible water saturation, hydrocarbon-bearing condition and residual oil saturation from the drainage of the samples at hydrocarbon bearing conditions with brine, show that $T_{2cutoff}$ can be usable for S_{wirr} estimation in conventional reservoirs, but lost its role in tight gas reservoirs (figure 1a and figure 1b). To solve this problem, the best method is estimating S_{wirr} from NMR logs without requiring $T_{2cutoff}$.

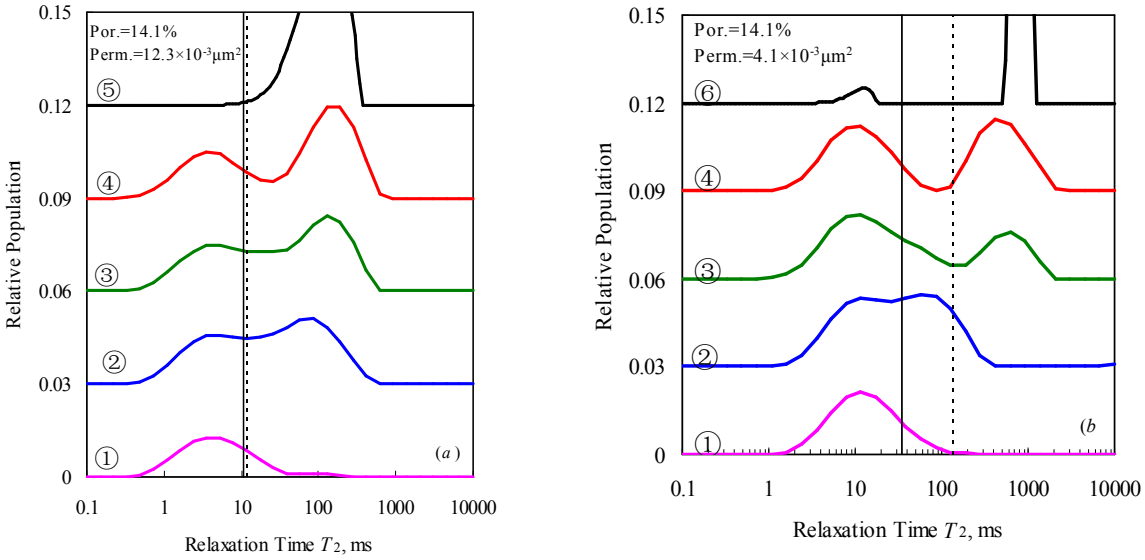

Fig. 1 Comparison of the shape of T_2 spectrum for four different kinds of conditions. ① Irreducible water saturation; ② fully brine saturated; ③ Residual oil saturation; ④ Oil-bearing condition; ⑤ Bulk relaxation of transformer oil; ⑥ Bulk relaxation of kerosene.

With the analysis of classical Timur and SDR models, a novel derived formula of estimating S_{wirr} without requiring $T_{2cutoff}$ is presented, and all the need parameters in it can be acquired from NMR logs directly. With the calibration of 36 core samples from Xujiahe group in Baojie district of Triassic, Sichuan basin, southwest China, the values of these parameters are obtained. A field example shows that the proposed model is reliable, the calculated S_{wirr} with it match well with that of derived from core samples both in tight gas intervals and water-bearing layers, but the calculated results by using $T_{2cutoff}$ are accurate only in water saturated layers, but are higher than the true value in gas-bearing intervals.

References:

1. Coates, G. R., Xiao, L. Z. and Primmer, M. G., Gulf Publishing Company (2000) 78.
2. Kenyon, W. E., The Log Analysis, 38(1997) 21.
3. Staley, C., Applied Physics Letter, 51(1987) 1146.

O36

Advanced Investigation of Low-Power NMR by Frank Excitation

N. Amor[a], J. Kowalski[a], F. Casanova[a], M. Greferath[b], B. Blümich[a]

[a] ITMC of RWTH Aachen University
[b] School of Mathematical Sciences, University College Dublin

Recently, a new NMR method employing an rf excitation scheme with strongly reduced power has been introduced, which is based on modulating rf pulses according to Frank sequences [1]. For many applications, a reduction of rf power is essential, e.g. to eliminate bulky rf pre-amplifiers or in medical high-field MRI to preserve patient safety. Another benefit of the new scheme are very short dead times allowing for measurements of samples with short relaxation times. While Frank excitation has been shown to be feasible for low-power MRI [2], the details of the effect of the sequence on a spin system have not been discussed in detail yet. Therefore, simulations and according experiments have been performed to quantitatively investigate the dependencies of important characteristics such as excitation profile, steady state, nutation behavior, and sensitivity on rf power, pulse length, and relaxation times. The results of these investigations are reported, including for example quantification of required excitation power limits, derived from simulated profiles (Fig.1), and the effects and interactions of individual Frank wave packages.

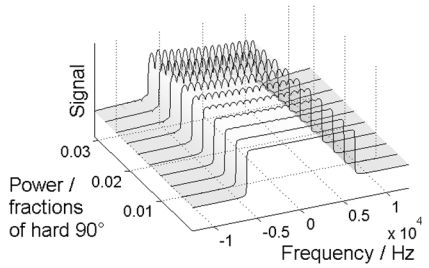

Fig. 1: With increasing rf peak power, non-linear effects lead to distortions of the simulated profile and individual Frank wave packages become visible.

References:
1. B. Blümich et al. J. Magn. Reson. 199 (2009) 18.
2. N. Amor et al. submitted. (2011).

O37

Nonlocal dispersion tensor measurements: Mass transport and medium structure

M. W. Hunter[a], *P.T. Callaghan*[a],

[a] MacDiarmid Institute for Advanced Materials and Nanotechnology, Victoria University of Wellington, Wellington, New Zealand

Dispersion describes the phenomenon whereby particles on the same streamline separate during flow. The physics of dispersion is governed by stochastic processes arising from the interplay between advective velocity gradients, molecular diffusion and boundary layer effects[1]. The dispersion tensor, $\mathbf{D}^*$, is a local measurement in the sense that it does not depend on positional relationships and is measured as time asymptotes[2]. For situations where the length- and time-scales on which transport occurs are not much larger than the scale of the fluctuations in the velocity field, a non-local description is required[3]. The study of fluid dispersion in porous media is important to a wide range of applications including chromatography, filtration, oil recovery, groundwater flows and catalysis.

Pulsed Gradient Spin Echo (PGSE)-NMR provides a wealth of information about the separation of particles and velocity correlations in porous media. Presented here is a set of NMR pulse sequences and a superposition designed to extract the velocity correlations necessary to calculate the dispersion as a function of displacement and hence the non-local dispersion[6]. The experimental method will be tested against the calculable non-local dispersion in a Couette cell[4]. Experiments performed on porous media will be discussed including other tensors and non-local measurements with higher dimensionality[5]. Measurements on rock cores will also be discussed.

The non-local dispersion tensor, $\mathbf{D}^{NL}$, provides a fundamental description of velocity correlations and displacement information in a dispersive system. For such a measurement, a quantitative description of the nature of correlations can be obtained. These correlations, and hence dispersion, are time dependent, therefore giving a detailed picture of the approach to asymptotic conditions. The non-local dispersion tensor enables the description of the mass-transport in new ways and also has the potential to probe grain size information, providing a new link between structure and dispersion.

The Lattice-Boltzmann algorithm has been shown to successfully predict the flow field in porous media[7], and has been used to model the flow field through our model porous medium. This flow field is used to simulate a large ensemble of virtual tracer particles, from which numerical estimates for both the local and non-local dispersion can be determined. Our implementation of this approach is presented here along with a comparison between the experimental and computational results. Numerical simulation will also be used to investigate dimensionalities difficult to obtain in experiment.

References:
1. A. A. Khrapitchev and P.T. Callaghan, Phys. Fluids 15 (2003) 2649
2. J.D. Seymour and P.T. Callaghan, AIChE J. 43 (1997) 2096
3. D.L. Koch and J.F. Brady J. Fluid Mech. 180 (1987) 387
4. M.W. Hunter and P.T. Callaghan PRL 99 (2007) 210602
5. M.W. Hunter *et. al.* Phys. Fluids. 22 (2010) 027101
6. M.W. Hunter *et. al.* JMR 204 (2010) 11
7. B. Manz *et. al.* AIChE J 45 (1999) 1845

O38

NMR measurements of dynamic clogging of porous systems applied to constructed wetlands monitoring

Fahad Shamim, Martin Bencsik, Mike Newton, Robert Morris
School of Science and Technology, Nottingham Trent University, Nottingham, U.K.

Constructed wetlands are used in various stages of wastewater treatment throughout the world. They are an important element in sustainable development both for their role in wastewater treatment and as support for biodiversity and conservation[1]. Constructed wetlands often comprise a gravel matrix in which common reeds are grown through which wastewater flows under gravity. The gravel matrix becomes clogged over time as a result of particulates accumulation and biofilm growth. Remedial action against this clogging is both time consuming and costly once the system has become clogged. By monitoring the clogging online, it might be possible to take more cost-effective action to prevent complete clogging.

The aim of this work is to quantitate the extent to which embedded NMR devices can provide useful assessment of the wetland condition by measuring local NMR parameters, as demonstrated by pilot studies[2].

We performed NMR experiments with mock models of (i) wetlands, and of (ii) waste water. Mock models of wetland were prepared using packed glass beads of sizes 3mm, 8mm and 14mm residing in 3 different 1 meter long acrylic tubes (o.d. = 38mm, i.d. = 32 mm). Three different models of wastewater were made with (i) fine sand (average grain diameter =1/8 -1/4 mm) in water, and (ii) soil in water, and (iii) a mixture of the two previous systems. In separate experiments these were then driven in the tubing which was originally filled with pure water. This way the packed beds undergo accelerated artificial (particulate) clogging with flow rate of 130 ml/min, until complete clogging occur (~half a day). Measurements of the NMR relaxation times were taken at six different locations of the tube, and different stages of clogging, using a 0.5 T Halbach scanner (20MHz Desktop MRI Tomography System, ACT GmbH Germany) to measure T_1 (using a saturation recovery sequence) and T_2^{eff} (using Carr-Purcell-Meiboom-Gill sequence at different echo times) values after every five minutes of accelerated clogging. The overall hydraulic conductivity of the system was assessed by measuring the flow rate at the outlet as well as the inlet and outlet pressures using take off tube manometers.

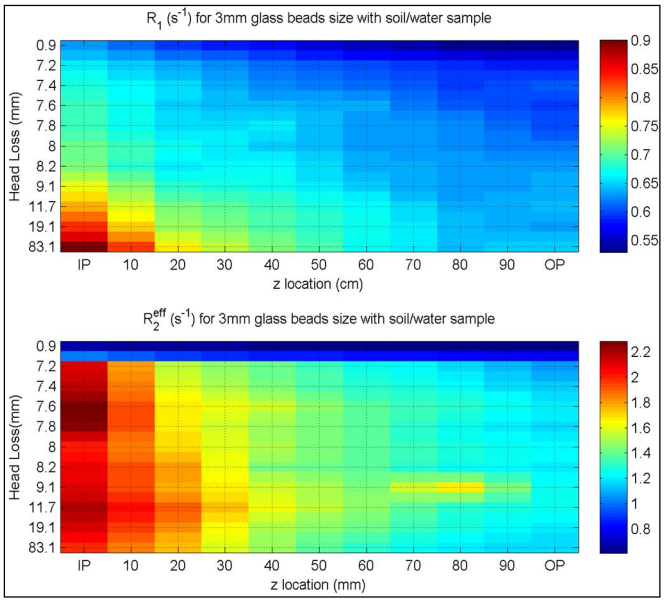

We found that R_1 (= $1/T_1$) and R_2^{eff} (=$1/T_2^{eff}$) are both highly sensitive to clogging (see figure). In all the experiments biggest changes in R_1 and R_2^{eff} are at the inlet which is the main site of clogging. In the figure the dynamic spatial distribution of R_1 and R_2^{eff} are shown for the experiment with 3mm glass bead and soil wastewater. This shows that as hydraulic conductivity decreases (i.e. from top to bottom) R_1 and R_2^{eff} values increase with different sensitivities to clogging. We will discuss the effect of bead size and waste water model on our ability to relate NMR relaxation times to hydraulic conductivity. We hope that in the future NMR can prove to be a useful tool for the cost-effective maintenance of constructed wetlands.

References:

1 R. H. Kadlec & S. Wallace, *Treatment wetlands*, Taylor & Francis (2008);
2 R.H. Morris et al., Analysis of clogging in constructed wetlands using magnetic resonance, *Analyst*, accepted for publication March 2011.

O39

Sands with NMR Logging data

O.A. ElMahdy [a] *and G.M. Hamada* [b]

[a] King Saud University, Riyadh , Saudi Arabia, **omahdy@ksu.edu.sa**
[b] UAE University, AlAin, United Arab Emirates, **ghamada@uaeu.ac.ae**

Petrophysical properties evaluation of heterogeneous gas shaly sands reservoirs is one of the most difficult problems. These reservoirs usually produce from multiple layers with different permeability and complex formation, which is often enhanced by natural fracturing. Therefore, using new well logging techniques like NMR or a combination of NMR and conventional openhole logs, as well as developing new interpretation methodologies are essential for improved reservoir characterization. Nuclear magnetic resonance (NMR) logs differ from other conventional logs. Integration of NMR logs, density logs and core data shall minimize uncertainties in the determination of formation porosity, permeability and capillary pressure curve.

This paper concentrates on determination of three petrophysical parameters of heterogeneous gas sand reservoirs; 1) Determination of DMR porosity, Φ_{DMR}, it is deduced from NMR porosity and density porosity, 2) NMR permeability, K_{BGMR}, it is based on the dynamic concept of gas movement and bulk gas volume in the invaded zone and 3) Capillary pressure, it is derived from relaxation time T_2 distribution.

O40

Time Domain Analysis Numerical Simulation and Influence Factors of NMR Logging

Ranhong Xie, Lizhi Xiao, Jiajun Liu

State Key Laboratory of Petroleum Resource and Prospecting
China University of Petroleum , Beijing 102249, China
Key Laboratory of Earth Prospecting and Information Technology,Beijing

Time Domain Analysis (TDA) of NMR logging data has been successfully used to identify and evaluate quantitatively the oil and gas layers. The successfulness of TDA method, however, can be affected by the complex pore structure of rock and the changing properties of reservoir fluids. This paper uses numerical simulation to study the performance of TDA method in the identification and quantitative evaluation of fluids from different kinds of reservoirs. A number of factors are analyzed, including the type of fluids, different pore sizes, signal-to-noise ratios (SNR) and NMR logging acquisition parameters. The results show that TDA method can accurately identify light oil layer (viscosity < 5mPa.s). In oil-bearing water layer with small-pore movable water, TDA method can accurately determine the oil porosity of formation; in oil-bearing water layer with big-pore movable water, however, TDA method could over-estimate the actual oil porosity of formation. In a macroporous water layer, a short waiting time of 1s is not sufficient for the water to fully recover in the measurement; consequently, the presence of strong water signal in the differential spectrum of TDA could produce a result that is the opposite of the test result. In gas layer, TDA method can accurately determine the gas porosity of formation. However, in gas-bearing water layer with small-pore movable water, NMR results are usually inconsistent with test results. Differential spectra of TDA between gas layer bearing water with big-pore movable water and small-pore oil gas layer can have similar features, which is often difficult to differentiate. It is suggested to combine the dual-echo-spacing logging data to distinguish the gas layer bearing water with big-pore movable water. When the SNR is lower than a certain threshold, the right hand of the differential spectrum signal diverges, which reduces the accuracy in the determination of the hydrocarbon porosity of formation. It is also found that high hydrogen index of gas is useful to distinguish the gas layer. A well-designed pre-logging plan can ensure that all logging parameters are optimized, which will improve the results of TDA method for the identification of hydrocarbon fluids.

References:

1. Coates G R, Xiao L Z, Prammer M G. NMR Logging Principles and Applications. Texas: Gulf Publishing Company, 1999
2. Dunn K J, Bergman D J, Latorraca G A. Nuclear Magnetic Resonance: Petrophysical and Logging Applications. Pergamon: Elsevier Science, 2002
3. Akkurt R, Vinegar H J, Tutunjian P N, et al. NMR Logging of Natural Gas Reservoirs. 36th Annual Logging Symposium Transactions: The Society of Professional Well Log Analysts, Paper: N, 1995
4. Prammer M G, Mardon D, Coates G R, et al. Lithology-independent Gas Detection by Gradient-NMR Logging, SPE30562, 1995, SPE Annual Technical Conference and Exhibition Proceedings, v. Ω(Formation evaluation and reservoir geology), 325-336
5. Xiao L Z, Lu D W, Chai X Y, et al. NMR Logging Interpretation and China Case Studies. Beijing: Petroleum Industry Press, 2001

O41

Nuclear Magnetic Resonance Logging While Drilling Tool：Concept and Design

Xin Li, Lizhi Xiao

China University of Petroleum, Beijing, China
State Key Laboratory of Petroleum Resource and Prospecting
Key Laboratory of Earth Prospecting and Information Technology,Beijing

Pulsed NMR logging is one of the most important methods to perform downhole measurements of petrophysical parameters and fluid properties in geologic formations. NMR logging whiling drilling (LWD) has advantages in terms of saving time and costs, providing real-time information of the un-invaded formation, and pay zone steering. Compared with wireline, NMR LWD faces more rigorous challenges of drilling environment, such as: rigorous room size for magnets, measurement in motion and no electrical power supply from surface ground.

Firstly, key issues in NMR LWD sensor design were discussed. Magnet structures of typical NMR LWD tools were simulated and analyzed systematically. Finite element method (FEM) was employed to calculate their magnetic field distributions. Based on the simulation results, key features for NMR LWD tool were proposed, which can suppress or eliminate the effects of sensitive volume motion during drilling. A NMR LWD sensor prototype was designed and constructed based on these concepts in the laboratory. This tool has following characteristics: (1) capability to be mounted on an API drilling sting; (2) single and low frequency; (3) thick and annular sensitive volume adaptive for tool's rotation and radial vibration; (4) low gradient to detect the intrinsic T2; and (5) a moderate depth of investigation (DOI). The static magnetic field (B_0) distribution measured in the mid-plane of the sensor is showed as Fig.1.

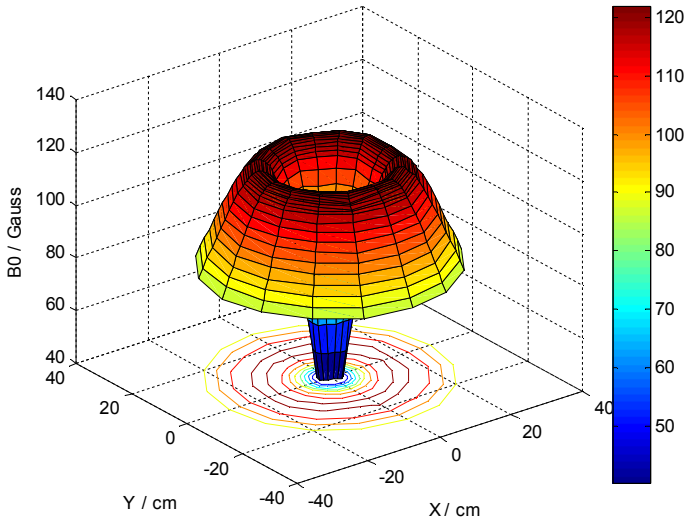

Fig. 1: B_0 distribution (measured) in mid-plane of the sensor.

References:

1 X. Li, L. Z. Xiao, H. T. Hu. Investigation characteristics of NMR logging while drilling tools. Chinese Journal of Magnetic Resonance, 28 (2011) 1.

2 R. J. Alvarado, A. P. Damgaard, P. M. Hansen, et al. Nuclear magnetic resonance logging while drilling, Oilfield Review, 15 (2003) 2.

O42

Characterization of microporosity in reservoir rocks by Nuclear magnetic resonance (NMR) spectroscopy

Xiangmin Zhang, Scott Campell, Albert Hebing & Mike Burns

Panterra Geoconsultants, The Netherlands

Characterization of microporosity in reservoir rocks is of importance for hydrocarbon exploration and development, especially in unconventional gas/oil, and carbonate reservoirs. We present an integrated investigation on micropore characterizations by NMR spectroscopy, high pressure mercury injection and petrography on several typical reservoir rocks, namely glauconitic sandstone, clay rich bio-turbidite and chalk. NMR tests were first carried out on one half inch plug samples at Sw=100% saturation. After desaturating to irreducible water saturation (Swir) by centrifuge, samples were measured again. High pressure mercury injection tests and petrographic observations were conducted on the trims of the corresponding plug samples. NMR T2 relaxation distribution reveals very similar patterns compared to pore throat size distribution obtained from the high pressure mercury injection tests. The chalk samples show mono-modal, while the glauconitic sandstone and bio-tubidites show distinct bi-modal distributions. Thin section and SEM observations show that the intragranular porosity of glauconite correspond the micro-pores seen in NMR T2 relaxation and high pressure mercury injection data. The abundance of glauconite correlates to the amplitudes of the micropore peaks of NMR T2 relaxation and pore throat size distribution. Intergranular pores of clay minerals contribute to the shorter T2 relaxation peaks in the bio-turbidite. Uniform intergranular pores result from fine grain calcite of broken coccolith grains explain the narrow mono-modal T2 relaxation and pore throat distributions. Using the surface/volume ratios derived from high pressure mercury injection, the relaxtivities of glauconite, calcite and clay were derived.

O43

Applications of NMR Logging in A Clastic Reservoir of Low Porosity and Low Permeability

Yuqin Chen

CNPC Chuanqing Drilling Engineering Company Limited

Logging Company, 400021. E-mail cyq_570915@163.com

Owning to some technical difficulties encountered in conventional logging data interpretations in highly heterogeneous, low porosity and permeability clastic reservoir, there are non-unique solutions for reservoir parameters and difficulties in distinguishing the reservoir fluid types. By using the new type of NMR Logging, we have obtained much better results for those cases. The calculations of reservoir parameters like lithology-independent porosity and the bulk volumes of bounded and movable fluids lead to a more realistic in-situ permeability. These parameters helped us to successfully identify the reservoir fluid and producibility. In this real field case study of Sichuan gas field, which is a typical low porosity and low permeability clastic reservoir, the real example of combining the data of NMR Logging, imaging logging, core analysis data and well test analysis is to present the unique advantages of NMR Logging technology for the development of such unconventional reservoirs.

O44

Digital Core Analysis in 3D: Non-Destructive Imaging and Multi-length Scale Flow Modeling

J. Gelb[a], H. Dong[b], M. Blundt[c], A. Gu[a], T. Fong[a], L. Hunter[a], S. H. Lau[a], and W. Yun[a]

[a] Xradia, Inc. Pleasanton, CA, USA
[b] iRock Technologies, Beijing, China
[c] Imperial College, London, UK

As traditional oil supplies become scarce and consumer demands continue to rise, oil companies are beginning to look elsewhere for supplies of fossil fuels. While many different types of oil reserves exist, there remains a largely untapped potential in stored reserves inside of geological structures. From limestone to shale, tar sands to tight gas sandstones, there are enormous oil reserves still awaiting discovery.

Cost-effective utilization of these reserves requires sophisticated and precise exploration methods involving strategic drilling approaches. While these feasibility studies have traditionally been performed on generalized models using direct flow measurements, such methods are cumbersome and often very time consuming. Smaller pore sizes may take several weeks for enough statistics in order to make a conclusion, slowing down the speed at which decisions for exploration may be made and increasing development costs.

Recent trends in geological exploration are now growing toward numerical simulation approaches, utilizing modern high-power computing technologies and high-resolution imaging methods. X-Ray computed micro- and nanotomography have now become routine characterization tools in these digital core analysis labs, uncovering a wealth of valuable information, such as porosity and permeability, used as input into flow simulations. The non-destructive nature of x-rays enables these experiments to be carried out through many different length scales, enabling one single sample to be analyzed all the way from a 25 mm core to its 50 nm pore throats, with results in as short as a few hours.

Here, we will present the results of performing x-ray CT analysis on a variety of different core types, from carbonates to silicates. The results will be shown to offer new insight at the smaller length scales and a unique bridge between existing length scales that increases efficiency of typical oil exploration & feasibility studies.

O45

Lattice Boltzmann Simulations on the Flow Mechanisms of Micro-Fractures in Low Permeability Gas Reservoirs

Yihua Zhu[1,2], Guo Tao[1] , Junxiao Li[1] , Hui Zou[3]

State Key Laboratory of Petroleum Resource and Prospecting
China University of Petroleum, Beijing 102249,China
Technology Center, China Petroleum Logging CO.LTD., Xi'an, Shanxi 710021, China
CNPC Technical Service Company, Beijing, China, 100007

Studies on the gas flow behaviors in very low permeability reservoirs have attracted increasing attention. Among the detected gas reservoirs in recent years, nearly over 80% of which is low permeability gas reservoir. It has been predicted the low permeability gas reservoir will play a dominant role in the untapped gas reservoirs. Therefore, exploration in low permeability gas reservoir is paid increasing attention. However, micro-fractures of different degrees are always developed in the low permeability gas reservoir, where the change of permeability is of great complicated and the flow event is way too peculiar.

In fluid mechanics, the fluid flow can be divided into molecular flow and particle flow, the latter of which can be subdivided into laminar flow and turbulent flow. And transition flow is found between each status. Generally, the flow between molecular flow and laminar flow is called gliding flow. When the pore size in porous media is grater than the gas molecular mean free path, the flow is called viscose flow. When in experimental research, it's better to control the flow in the laminar flow. For under this status, the rate of flow and differential pressure presents a linear relation and satisfies the Darcy law. If the pressure and flow velocity are both very low, gliding flow is generated when the pore size in porous media and the gas molecular mean free path have the same order of magnitude. Abundance of experimental research results[1-6] indicate that gliding flow happens frequently in the low porosity and low permeability core experiments in rocks with low porosity and low permeability because the size of micro-pore and micro-fracture have reached to the micro-scale domain. This paper mainly discussed the gliding flow in micro-fractures. The rebounded coefficient was introduced in order to microscopically apply the Lattice Boltzmann method (LBM) into the research on the gas flow mechanism of micro-fractures based on the slide boundary condition. Therefore, a micro-fracture model with the opening of 2μm was simulated. The results showed the feasibility of applying this method into gas flow mechanism of micro-fractures and thus laid foundation of research on the micro-scale permeable mechanism of low porosity and low permeability gas reservoir.

This paper, for the first time, introduced the Micro-channel concept used in the micro-electro-mechanical system into the research on the micro-fractures in low permeability gas reservoir.. Lattice Boltzmann method was applied with a new algorithm of the flow boundary treatment to study the flow mechanism of gas flowing in the micro- fracture in low permeability reservoir at the micro scale. And it has been verified by the analytic solution. It may lay the foundation for the researches on the gas flow mechanisms at micro scale in unconventional low porosity and low permeability reservoirs. Finally, the Klinkenberg effect of gas flow in low permeability reservoir rock is simulated to interpret and verify the macroscopic experiment result in laboratory with the observed microscopic mechanisms.

O46

Digital Core Approach to the Effects of Clay on the Electrical Properties of Saturated Rocks Using Lattice Gas Automata

Wenzheng Yue[1], Guo Tao[1], Xiyuan Chai[2], Bing Xie[3] , Hui Zou[4]

State Key Laboratory of Petroleum Resource and Prospecting
Key Laboratory of Earth Prospecting and Information Technology, China University of Petroleum
Bohai Drilling Engineering Company LTD Logging Company
PetroChina Southwest Oil & Gasfield Company
CNPC Technical Service Company, Beijing, China, 100007.

Clay has a significant influence on the relationship between resistivity index I and water saturation S_w of reservoir rocks as it complicates the current paths of these rocks. In this paper, we present a digital rock approach to effectively study these clay effects on the electrical transport properties of reservoir rocks at pore scale using lattice gas automata (LGA) method. The digital rock samples are constructed with the information from rocks. The LGA is then applied on these digital rocks fully saturated with fluids to simulate the electrical transport properties for revealing the effects of volume and distribution patterns of clay on the non-Archie behaviors of the I-S_w relationship. The very good agreement between the simulated results and the laboratory measurements clearly demonstrates the validity of the LGA in numerical research of rock physics. Based on these studies, a new model has been developed for quantitatively describing the relationship between the saturation exponent and the volume of clay (V_{sh}). This development may improve the evaluation for the fluid saturations in reservoir rocks.

O47

Visualisation of Supercritical CO_2 Miscible Displacement in Porous Media Using MRI

Yuechao Zhao, Yongchen Song, Yu Liu, Min Hao, Ningjun Zhu and Tonglei Wang

Key Laboratory of Ocean Energy Utilization and Energy Conservation of Ministry of Education
Dalian University of Technology, Dalian, Liaoning, 116024, P.R. China

CO_2 flooding has proven to be an efficient Enhanced Oil Recovery (EOR) method. This article addresses the use of a 400MHz MRI system to visualize the performance of CO_2 miscible displacement at high pressure condition. In this study, supercritical CO_2 flooding in an artificial consolidated sandstone core plug, water flooding and subsequent supercritical CO_2 flooding in an artificial consolidated sandstone core plug and supercritical CO_2 miscible displacement in a stack of three artificial consolidated sandstone core plugs were investigated in an-Decane/$MnCl_2$ aqueous solution system, respectively. The fronts and interfaces between displaced and displacing fluids and fluid flow characteristics are dynamics monitored in situ during displacement process. The development of the miscible regions and the piston-like CO_2 displacement front was directly observed. The viscous fingering and gravity override caused by the low viscosity and density of the CO_2 was restrained effectively. MRI demonstrates to be a useful imaging tool for the evaluation of the efficiency of CO_2 miscible displacement.

Keywords: MRI, Porous media, CO_2 miscible displacement, Enhanced Oil Recovery (EOR).

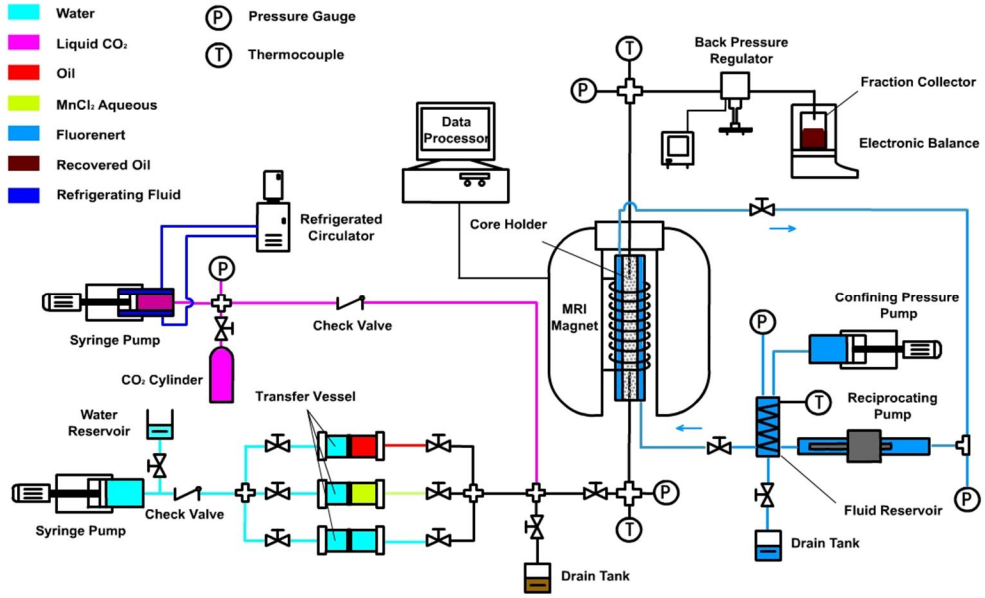

Fig. 1: Simplified schematic of the experimental setup.

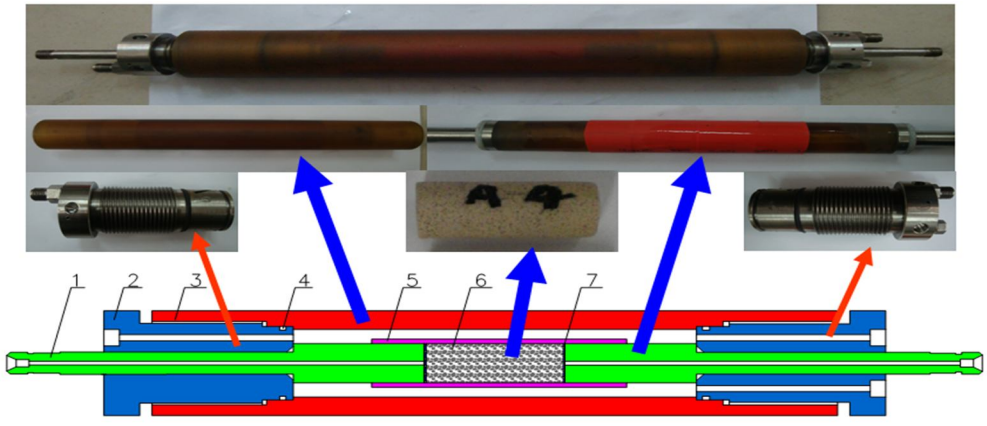

Fig. 2: Simplified schematic and photo of core holder.

O47

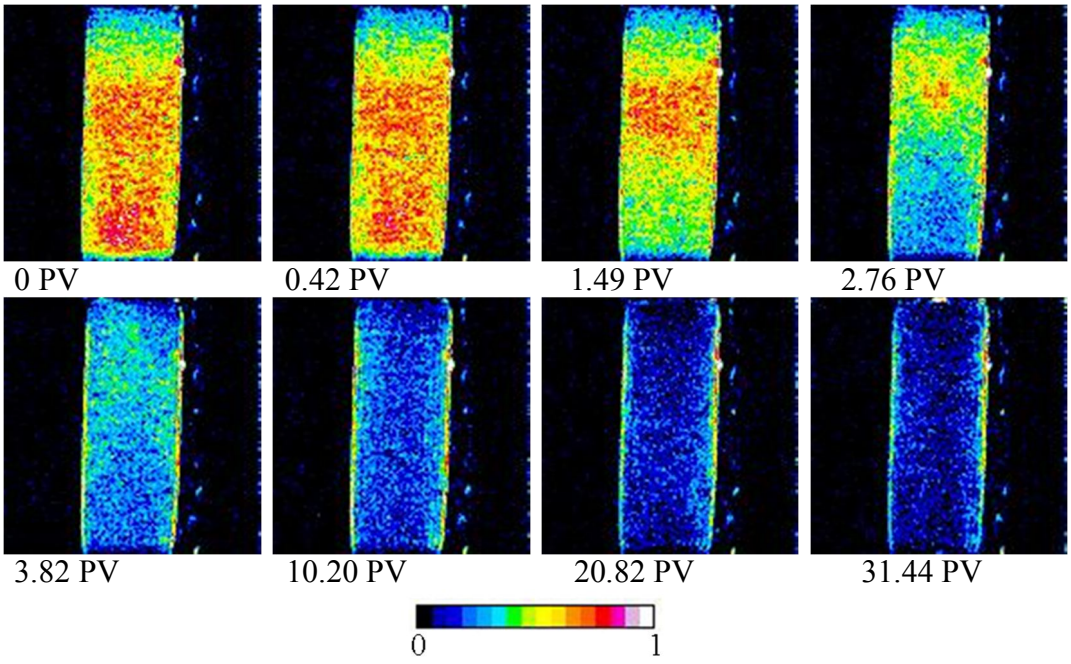

Fig. 3: Distribution of NMR signal intensity in the artificial consolidated sandstone core plug at 8.5MPa, 40℃ during CO_2 flooding.

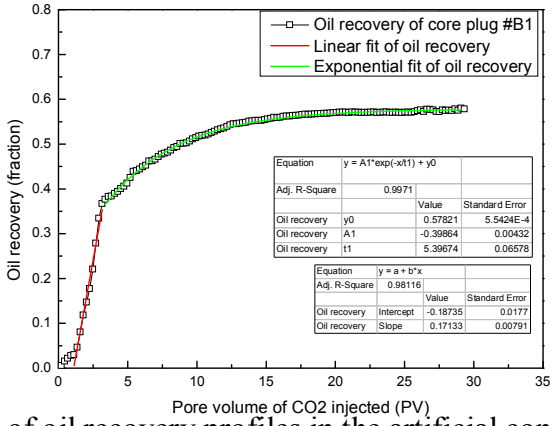

Fig. 4: Evolution of oil recovery profiles in the artificial consolidated sandstone core plug at 8.5MPa, 40℃ during CO_2 flooding.

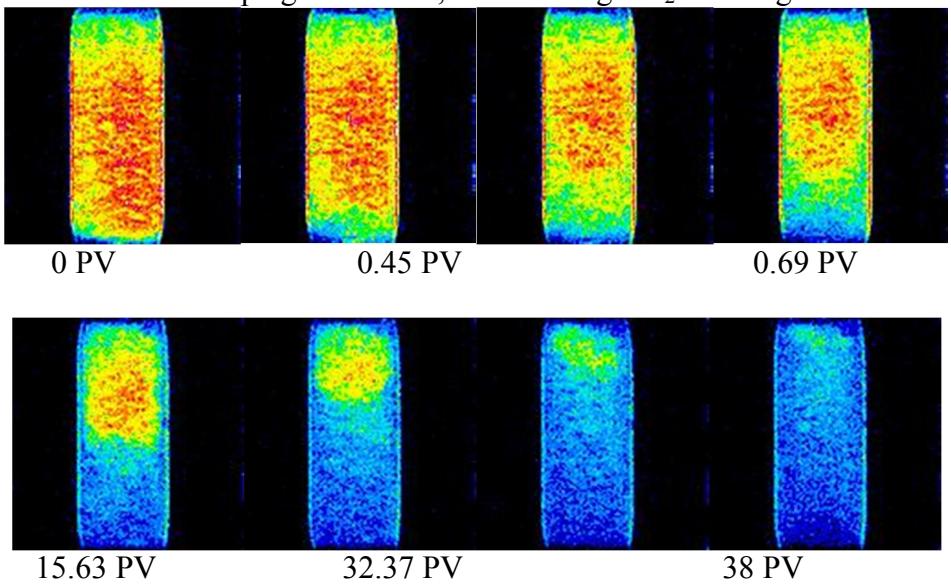

Fig. 5: Distribution of NMR signal intensity in the artificial consolidated sandstone core plug at 8.5MPa, 40℃ during water flooding.

O47

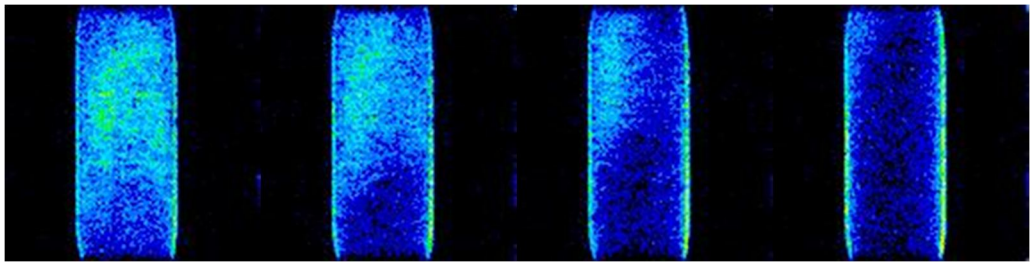

Fig. 6: Distribution of NMR signal intensity in the artificial consolidated sandstone core plug at 8.5MPa, 40℃ during subsequent supercritical CO_2 flooding.

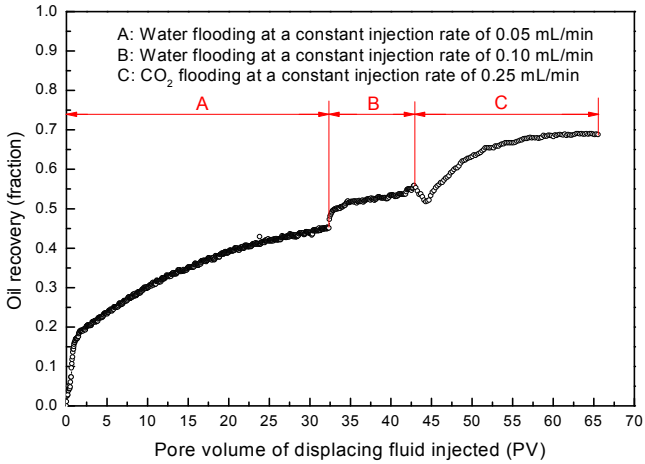

Fig. 7: Evolution of oil recovery profiles in artificial consolidated sandstone core plug at 8.5MPa, 40℃ during water flooding and subsequent supercritical CO_2 flooding.

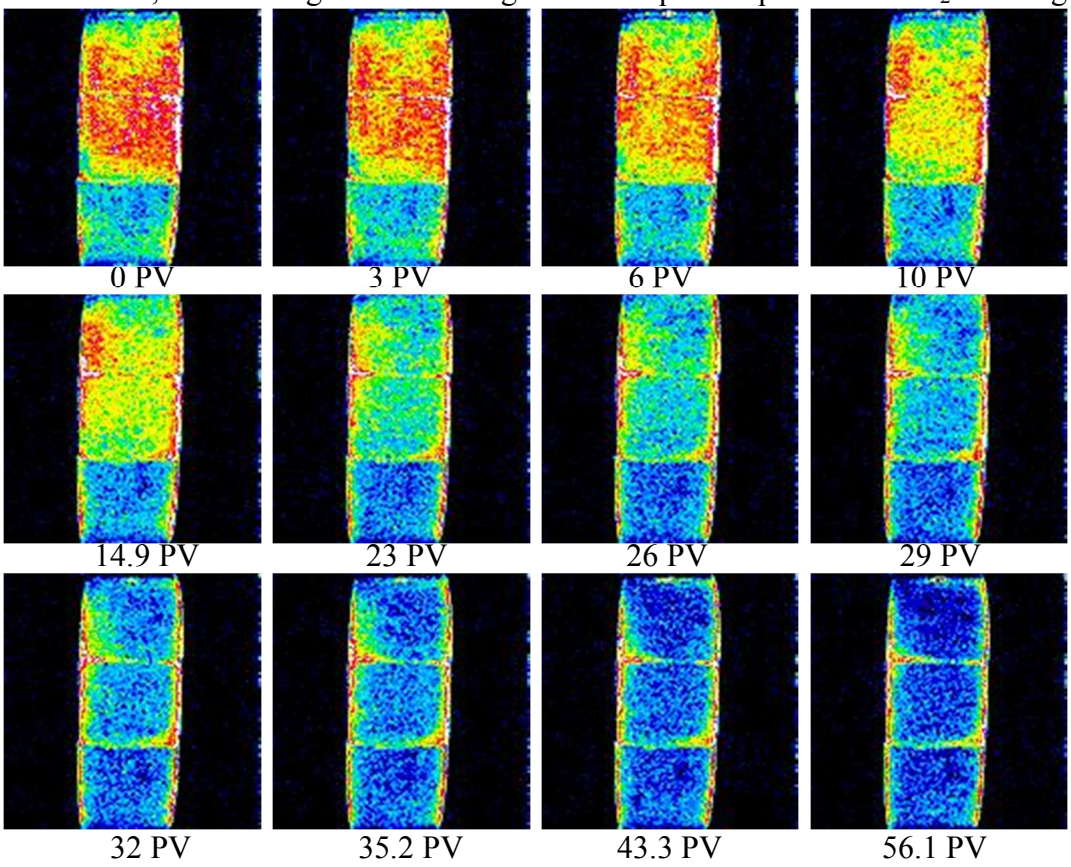

NMR signal intensity/arbitrary unit.

Fig. 8: Distribution of NMR signal intensity in the three stacked core plugs at 8.5MPa, 40℃during CO_2 flooding.

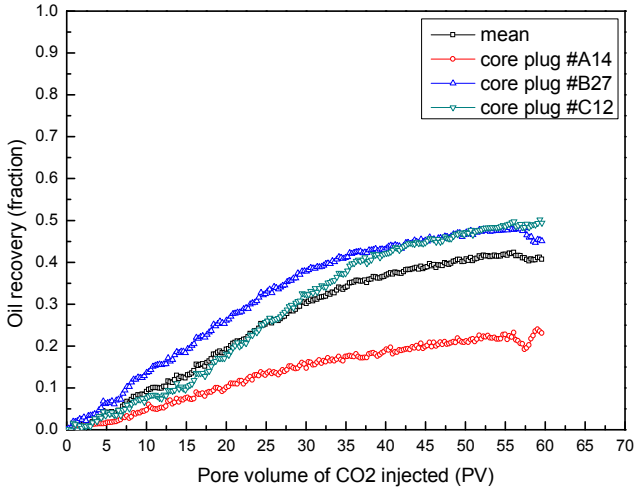

Fig. 6: Evolution of oil recovery profiles in the stacked core plugs at 8.5MPa, 40℃during CO_2 flooding.

References:

1 L. Romero-Zeron, S. Ongsurakul, L. Li, B. J. Balcom, Visualization of waterflooding through unconsolidated porous media using magnetic resonance imaging. Pet. Sci. Technol. 27(2009) 1532.

2 L. Romero-Zeron, S. Ongsurakul, L. Li, B. J. Balcom, Visualization of the effect of porous media wettability on polymer flooding performance through unconsolidated porous media using magnetic resonance imaging. Pet. Sci. Technol. 28(2010) 52.

3 R. D. Hazlett, J. W. Gleeson, H. Laali, R. Navarro, NMR imaging application to carbon dioxide miscible flooding in west texas carbonates. SCA 9311 in annual technical conference proceedings: Society of Professional Well Log Analysts, Society of Core Analysts Chapter-at-Large, 1993.

4 A. Brautaset, G. Ersland, A. Graue, J. Stevens, Howard, J. Using MRI to study in situ oil recovery during co_2 injection in carbonates. SCA2008-41 in the International Symposium of the Society of Core Analysts, Abu Dhabi, UAE, Oct 29-Nov 2, 2008.

5 T. Suekane, N. Furukawa, S. Tsushima, S. Hirai, M. Kiyota, Application of MRI in the measurement of two-phase flow of supercritical co_2 and water in porous rocks. J. Porous Media. 12(2009) 143.

O48

Determining Klinkenberg Permeability of Tight Gas Reservoir by Lattice Boltzmann Simulation

Junxiao Li[1], Yihua Zhu[1,2], Guo Tao[1], Hui Zou[3]

State Key Laboratory of Petroleum Resource and Prospecting
China University of Petroleum, Beijing, China, 102249
Technology Center, China Petroleum Logging CO.LTD., Xian, Shanxi, China, 710021
CNPC Technical Service Company, Beijing, China, 100007

Understanding the percolation rules of the non-Darcy gas flow in porous media is very important to the development of a low permeability gas reservoir. Many laboratory studies have shown that, due to the Klinkenberg effect, the permeability determination in low permeability rock samples can be very time consuming and costly. Though various correlations between gases and Klinkenberg permeability have been developed to allow prediction of Klinkenberg permeability from just one gas flowing measurement, there have been no any analytical model and method to describe the dynamic process of gas flow in low permeability reservoir accurately. Numerical methods have seldom been applied because of the complex pore geometry of reservoir rocks. In this paper, we employed lattice Boltzmann method (LBM) to simulate natural gases penetrating in artificial digital rock samples of variable structure parameters and the digital representatives of real reservoir cores, as LBM has the unique advantages to deal with complex geometry in modeling fluid flow through porous media. Our simulations have clearly demonstrated the mechanisms and the controlling factors of Klinkenberg effect. We subsequently studied the influences of rock and gas properties, temperature and pressure to the procedure of gas flowing through the low permeability rocks systematically. A new factor *b* for slippage correction for permeability measurements is proposed based on our studies. A numerical simulator based on the LBM for the two-phase gas slippage phenomenon and its effect on gas relative permeability in tight gas reservoirs were further studied and compared with the physical laboratory data. These results have demonstrated that LBM is an effective numerical model for non-linear fluid flow in low permeability gas reservoir. It can be used in conjunction with lab core experiments to measure permeability of very low permeability samples more accurately with much higher efficiency. The Klinkenberg coefficient and the numerical model for non-Darcy gas flow in low permeability gas reservoir obtained in this study can be the bases for further study the liquid-gas two phase transport phenomena in low permeability gas reservoirs.

O49

Non-destructive 3D Pore Modeling using X-ray Computed Microtomography and Nanotomography

Jeff Gelb, Allen Gu, Tiffany Fong, Luke Hunter, S H Lau, and Wenbing Yun

Xradia, Inc. Pleasanton, CA, USA

Modeling of fluid transport properties in geological samples is of increasing importance in recent years. The pore networks inside these samples are very complex, often spanning many different length scales, and few tools exist that are capable of visualizing such features. Among the currently available techniques, x-ray computed microtomography (micro-CT) is increasingly popular, due, in part, to its ability to capture many of these length scales in 3D. Many commercially-available instruments, however, require very small sample sizes for high-resolution imaging, which makes it impossible to simply enlarge a region with single-micron pores for precise analysis without cutting into the sample.

Here, we demonstrate the application of a novel laboratory-based micro-CT system for non-destructive, full length-scale characterization from 100 mm volumes down to 1 μm features. The unique "zoom in" geometry is shown to provide 3D microstructure information down to 1 μm without physically sectioning the sample. Resulting data is analyzed for both porosity and tortuosity, along with other key microstructure parameters (such as pore connectivity), providing unique information for fluid flow models and simulations.

With the introduction of laboratory-based x-ray nanotomography (nano-CT) instruments, new frontiers are being explored in tight sand, shale, and carbonate rocks. We will demonstrate the application of a novel laboratory-based nano-CT instrument for 3D quantitative analysis of these samples with resolution down to 150 nm and beyond. This technology is enabling new developments to be made in studies of samples with very small feature sizes, opening the door to full quantifications of carbonates and shale.

O50

A virtual material studio to study rock petrophysical properties

S. Zhang[a] *& M. Gingras*[b]

[a]Visualization Sciences Group, MA, USA
[b]Department of Earth and atmospheric Sciences, University of Alberta, Canada

A more detailed understanding on the 3D microstructure of rock samples is of growing importance in many technological fields. Using the 3D imaging technologies that are increasingly available to geophysics — at better resolution and lower cost — this study introduces an image-to-simulation framework[1] that supports the full workflow of rock microstructure analysis acquired with MRI [2].

MRI scans of a Tyndall limestone sample, with macroscopic heterogeneities, are reconstructed, visualized, quantified, and simulated with a virtual material studio software framework. Figure 1 shows a preliminary test scan reconstructed by the virtual material studio. Upon automatic and interactive segmentation, quantitative measures such as material composition and porosity distributions can be computed.

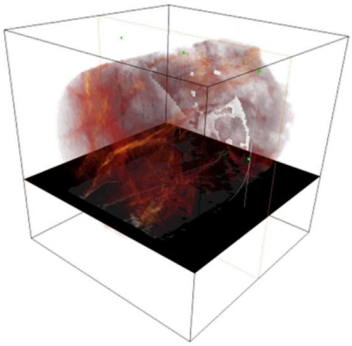

Figure 1. Volume reconstruction from MRI scan

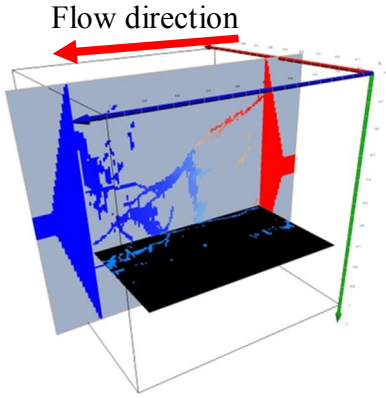

Figure 2. Pressure distribution after simulating a flow through the core

Core Size	R=0.37cm, Z=0.86cm
Scan Resolution	0.0078cm/pixel Isotropic in X, Y, Z
Fracture volume fraction	9.49%
Perm	0.00135cm^2
Flow rate	0.357cm/s

Table 1. Petrophysical properties.

The virtual material studio framework supports the prediction of petrophysical properties, which are otherwise difficult or presently impossible to obtain with a physical materials lab. Figure 2 shows the pressure distribution resolved numerically. Table 1 summarized the most important petrophysical parameters computed from the preliminary test sample. Numerical analyses, such as proposed herein, stand to improve our understanding of several properties in tortuous and complex porous media. For example, anisotropy, spatial heterogeneity and matrix / flow-unit interactions can be better predicted. Such knowledge is especially useful in the analysis of oil and gas reservoirs and for the remediation of contaminated ground-water aquifers.

References:

1. S. Zhang, F.D. Maestra, N. Combaret, R. Klimentidis, P. Barthelemy, R. Albou, D. Lichau & D. Bernard. The Analysis and Simulation of Rock Properties Using FIB-SEM and Virtual Material Studio. NAFEMS World Congress 2011, Boston, USA, May 22-26, 2011.
2. M. Gingras, B. MacMillan & B. Balcom. Visualizing the internal physical characteristics of carbonate sediments with magnetic resonance imaging and petrography. Bulletin of Canadian Petroleum Geology, 50:3, pp363-369, September 2002.

Poster presentations

P01

Dependence of the MR lineshape for white-matter on the orientation of the B_0 field: Insights from a three-phase model

E. Özarslan[a,b], *P.J. Basser*[a],
[a] Section on Tissue Biophysics and Biomimetics, PPITS, NICHD, NIH
[b] Center for Neuroscience and Regenerative Medicine, USUHS

The phase maps obtained via gradient echo imaging exhibit exquisite contrast in the brain due to a frequency shift of the MR signal [1]. This observation has prompted interest in its biophysical mechanisms. An interesting finding is the dependence of the frequency shift on the direction of the main magnetic field [2-4]. We consider a simple, three-phase geometry to represent the myelinated neural cells. We obtained exact expressions for the component of the induced magnetic field along the direction of B_0 for an arbitrary orientation of the axon with respect to B_0. We use this formulation to study the entire MR spectrum.

Figure 1 shows the unit cell (assuming hexagonal packing) in which the axon resides. To have realistic volume fractions, we used a_0:b_0:d_0=0.7:1:1.25. The magnetic susceptibility values were chosen to be 2, 0.33 and 10 ppm relative to that of water for intracellular space, extracellular matrix, and myelin, respectively. The relatively high susceptibility of the myelin assumes that iron–rich oligodendrocytes can be taken to be a part of the myelin sheath [2]. The T_2 values were taken to be 60, 20, and 200 ms, respectively. Figure 2 shows the component of the magnetic field parallel to the main field when the axon makes 0, 30, 60 and 90 degrees with B_0. In Figure 3, we show the proton MR spectrum (in a logarithmic scale) for different values of the angle. Note that there is a significant broadening of the myelin and extracellular space peaks as the angle is increased while the peak due to the intracellular space remains sharp owing to the field being constant inside, independent of the orientation. Note that the frequency at which this peak is observed shifts slightly when angle is increased.

The findings of the paper suggest that valuable information could be obtained if the full MR spectrum is acquired, e.g., using localized spectroscopy or spectroscopic imaging methods. The developed model can be employed in many different contexts, e.g., in and around blood vessels and in numerous material science applications.

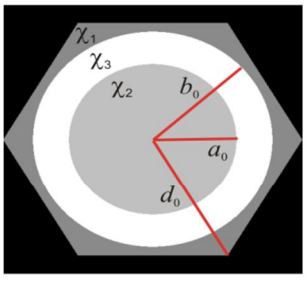

Fig. 1: The geometry considered in this study.

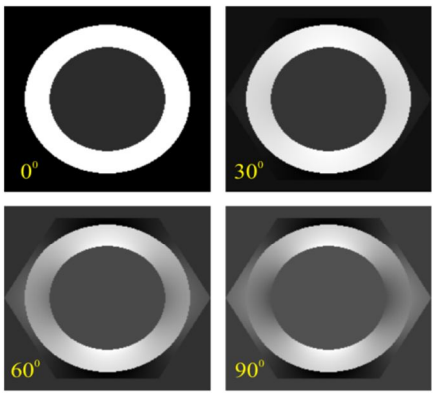

Fig. 2: The z-component of the magnetic field for different angles between the axon and B_0.

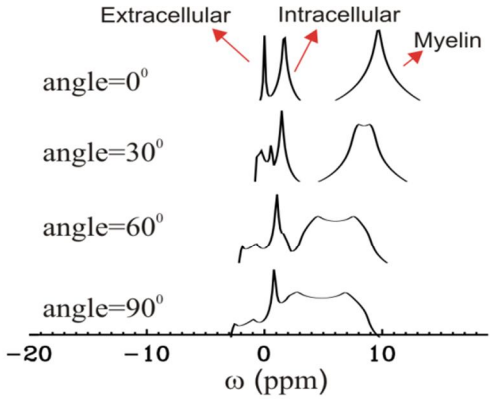

Fig. 3: Predicted proton MR spectra for different values of the angle the axon makes with the main field.

Acknowledgments: Support was provided by the Intramural Research Program of the NICHD and the Department of Defense in the Center for Neuroscience and Regenerative Medicine.

References:

[1] Duyn et al., Proc. Natl. Acad. Sci. USA, 104:11796-11801, 2007.
[2] He and Yablonskiy, Proc. Natl. Acad. Sci. USA, 106:13558-13563, 2009.
[3] Liu, Magn. Reson. Med., 63:1471-1477.
[4] Lee, Proc Natl. Acad. Sci. USA, 107:5130-5135, 2007.

P02

T_2 and $T_{1\rho}$ relaxation are sensitive to the degradation by trypsin and the presence of Gd-DTPA^{2-} ions in bovine nasal cartilage

Nian Wang, Yang Xia
Department of Physics and Center for Biomedical Research,
Oakland University, Rochester, MI 48309, USA (**xia@oakland.edu**)

NMR imaging (MRI) is the most sensitive diagnostic technique for the noninvasive assessment of soft tissue such articular cartilage, where the tissue degradation can be monitored by a number of NMR parameters including diffusion and relaxation (1,2,3). An important factor related to the measurement of relaxation times in clinics is the presence of Gd-DTPA^{2-} ions in the tissues (due to the use of gadolinium (Gd) contrast agent in some clinical MRI protocols such as dGEMRIC) (4). In this project, the sensitivities of both T_2 and $T_{1\rho}$ relaxation times were studied in native and trypsin-degraded specimens of bovine nasal cartilage (BNC), without and with the presence of Gd-DTPA^{2-} ions in the tissues.

Materials and Methods: Quantitative T_2 and $T_{1\rho}$ imaging experiments were carried out on BNC before/after the tissue was immersed in a 1mM solution of Gd-DTPA^{2-} contrast agent *and* when the tissue was degraded by trypsin. A Bruker AVANCE II 7T/9 cm system was used in this investigation. The slice thickness was 1mm; the spatial resolution was 100 μm.

Results: Native BNC exhibits significant $T_{1\rho}$ dispersion in the 500-6000 Hz range (Left). At any given B_1, the $T_{1\rho}$ of degraded specimens is greater than that of native specimen. The largest difference between the native tissue and degraded tissue occur when the tissue contains no Gd ions. With the immersion of tissue in Gd solution, the sensitivity of $T_{1\rho}$ dispersion towards the strength of spin-lock filed reduces markedly. The sensitivities become higher (Right) when the strength of spin-lock filed increases. The immersion of tissue in Gd solution completely eliminates the sensitivity of T_2 and $T_{1\rho}$ towards tissue degradation.

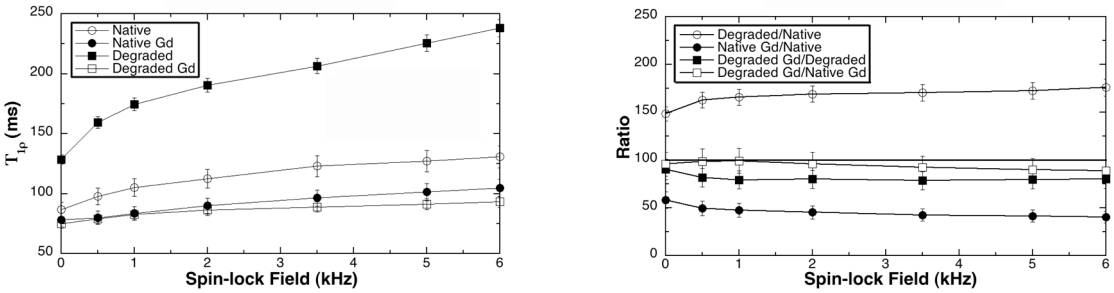

Discussions and Conclusions: Native specimens demonstrate significant $T_{1\rho}$ dispersion. Trypsin degradation can cause a maximum 80% increase in $T_{1\rho}$. With the presence of Gd ions, trypsin degradation causes significantly more reduction in $T_{1\rho}$ values (up to 60%). T_2 values are also sensitive to PG loss, but less than the sensitivity of $T_{1\rho}$ values. When Gd ions are present in the tissue, both T_2 and $T_{1\rho}$ values become insensitive to PG content. However, a compound parameter based on two $T_{1\rho}$ measurements (without and with the presence of Gd ions) could potentially become a new imaging marker for tissue degradation.

ACKNOWLEDGEMENT: Y Xia is grateful for the R01 Grants from the National Institutes of Health (AR045172 and AR052353) and an instrument endorsement from R and J Bennett.

References:

1. Y. Xia, **Magn Reson Med** 1998; 39: 941-949.
2. H. Alhadlaq, et al, **Ann Rheum Dis** 2004; 63: 709-717.
3. Y. Xia, **Osteoarthritis Cartilage** 2007; 15: 363-365.
4. A. Bashir, et al, **Magn Reson Med** 1996; 36: 665-673.

P03

Computer simulation of FSE sequences for bone density measurements of the calcaneus in a 0.2 T compact MRI system

S. Kono, H. Kondo, Y. Terada, K. Kose
Institute of Applied Physics, University of Tsukuba, Tsukuba 305-8573, Japan

INTRODUCTION

Fast spin echo (FSE) sequences are several times faster than conventional spin echo sequences. However, because FSE causes blurring along the phase encoding direction, inhomogeneous image intensity sensitive to the RF field distribution, and ghosting artifacts due to its inappropriate implementation, such effects should be quantitatively evaluated if FSE images are used for quantitative measurements.

Since the year 2000, our group has been developing a compact MRI system for measurements of trabecular bone volume fraction (TBVF) of the calcaneus using a 0.2 T permanent magnet [1]. Our recent studies have clarified that 3D TBVF measurements of the whole calcaneus is indispensable to improvement of its reproducibility, because TBVF is sensitive to the position of the sagittal slice [2]. Because the time for the 3D measurement is limited, a fast imaging sequence such as FSE sequence is required. However, as mentioned above, a careful evaluation is required for quantitative measurements using the FSE images. In this study, we performed a computer simulation of 3D FSE sequences for the TBVF measurements of the whole calcaneus.

MATERIALS AND METHODS

The computer simulation of 3D FSE sequences was performed in 2D because no signal variation was present along the second phase encoding direction. Parameters for the computer simulation are as follows: FOV = $(128\ \text{mm})^2$, image matrix = 128^2, echo train length = 16, and echo spacing = 16 ms. A circular numerical phantom (diameter = 100 mm) with 19 capillaries was used for the calculation. T_1 and T_2 of the protons were assumed to be 170 and 115 ms, corresponding to those of bone marrow protons of the calcaneus. The spatial distribution of B_1 (Fig.1) measured for the solenoid RF coil (aperture: 175 mm × 85 mm, length: 120 mm) was used for both excitation and refocusing of the nuclear spins. The NMR signal in the FSE sequence was calculated from 32 magnetization vectors in the voxel.

RESULTS AND DISCUSSION

Figure 2 shows phantom images calculated for excitation flip angles (FA) and echo numbers from which the data collection starts. The refocusing pulse was assumed to be twice of the excitation pulse. As clearly shown, these images are affected both by the blurring effect along the phase encoding direction (about four times resolution degradation compared with that for the readout direction) and by the RF magnetic field distribution. Figure 3(a) shows image intensities averaged over the phantom and Fig. 3(b) shows image intensity ratios of the inner and outer areas of the phantom which correspond to intensities of ghosting artifacts. These graphs show that the 1st or 3rd echo is better than the 2nd echo for the start of the data collection. In conclusion, we have clarified quantitative aspects of the 3D FSE images of bone marrow protons for TBVF measurements of the calcaneus.

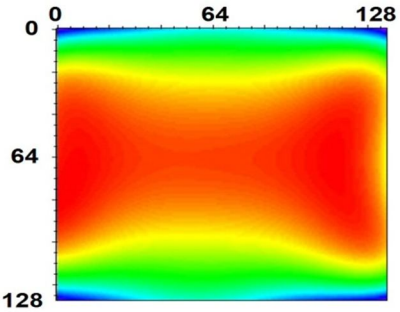

Fig.1 B_1 map for the RF coil.

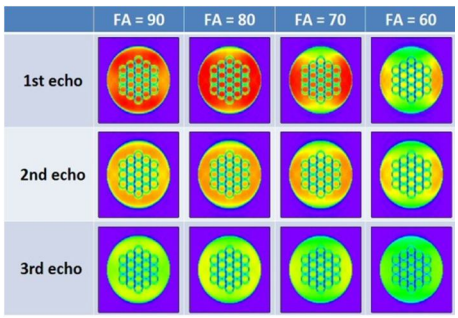

Fig.2 Calculated phantom images.

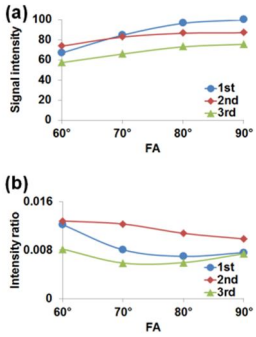

Fig.3 (a) Image intensity vs FA. (b) Intensity ratio vs FA.

References:
[1] K. Kose, et al. Magn Reson Med **52**, 440 (2004).
[2] T. Nakayama, Master thesis, Univrsity of Tsukuba, 2011.

P04

Spectroscopic imaging of metabolite dynamics in plant seeds using Interleaved Variable Density (IVD) acquisition

J. Fuchs[a,b], *G. Melkus*[a,b,c], *L. Borisjuk*[b], *P.M. Jakob*[a,d]

[a]Department of Experimental Physics 5, University of Würzburg, Würzburg, Germany
[b]Insitute of Plant Genetics and Crop Plant Research, Gatersleben, Germany
[c]Department of Radiology and Biomedical Imaging, University of California, San Francisco, California, USA
[d]Research Center for Magnetic Resonance Bavaria e.V. (MRB), Würzburg, Germany

Due to the low natural ^{13}C abundance, ^{13}C-labeled sucrose is an excellent marker and ^{13}C-measurements have proven to be a useful tool in tracking the uptake of sugar in plant seeds (Ref. 1). Because the spatial resolution is limited in these experiments an optimized PSF is desirable and acquisition weighted chemical shift imaging is practicable.

The low sensitivity of direct measurements requires several averages to yield sufficient SNR. This number of averages can easily be traded for an equal number of repetitions to achieve a higher temporal resolution when a sliding window reconstruction is used (Fig. 1).

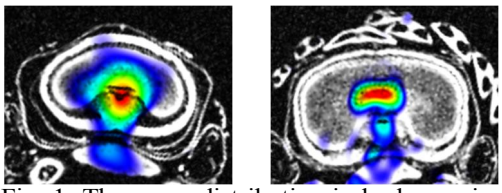

Fig. 1: The sugar distribution in barley grains measured during sucrose feeding using direct ^{13}C-CSI (left) and indirect ^{13}C-geHMQC (right).
^{13}C-CSI: TE/TR = 2.7/1500ms, Res. = 0.5 x 0.5 mm^2, Time for one scan: 30 min, Image reconstructed from 6 repetitions (=3h)
^{13}C-geHMQC: TR=1500ms, Res. = 0.25 x 0.25 mm^2, Time for one frame = 18 min, Image reconstructed from 10 frames (=3h)

Indirect measurements offer higher sensitivities and thus permit higher resolutions without an increase in total measurement time (see Fig. 1). However the number of averages cannot be traded for a number of repetitions in this case as fewer averages are required and it would diminish the advantages of acquisition weighting. Interleaved Variable Density (IVD – Ref. 2) imaging allows splitting a single acquisition weighted image into several undersampled frames (Fig. 2). Again, using a sliding window these frames can be combined to yield a fully sampled weighted k-space, but the resulting images are just shifted by the time it takes to record a single undersampled frame.

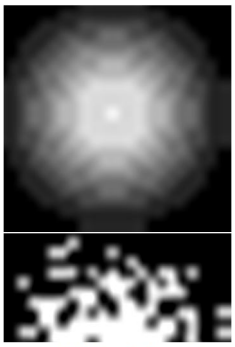

In conclusion the IVD approach is a valuable addition to our indirect ^{13}C-studies of plant seed metabolism, as it effectively improves the temporal resolution from 3 hours down to 18 minutes.

References:

1 G. Melkus et al, Dynamic 13C/1H NMR imaging uncovers sugar allocation in the living seed, Plant Biotechnology Journal (2011), in press
2 K. Wang et al, Interleaved variable density sampling with a constrained parallel imaging reconstruction for dynamic contrast-enhanced MR angiography, Magn Reson Med. (2011), early view

P05

NMR Diffusion studies using super-high gradient pulses

Marcel Gratz[a], Mario Großmann[a], Stefan Schlayer[a], Petrik Galvosas[b],

[a]University of Leipzig, Faculty of Physics and Earth Sciences, Leipzig, Germany
[b]MacDiarmid Institute for Advanced Materials and Nanotechnology, Victoria University of Wellington, SCPS, Wellington, New Zealand

Nuclear magnetic resonance with pulsed magnetic field gradients (PFG NMR) has gained great importance for the non-invasive investigation of self-diffusion [1]. Current approaches are able to detect molecular displacements in the order of 100 nm. With the aim to extent the accessible length scale towards smaller displacements we developed a new probe (see Fig. 1), which is designed to generate bipolar gradients of up to 93 T/m. An adapted Maxwell coil arrangement was used in combination with commercially available gradient amplifiers providing currents as high as 100 A. Finite element simulations were conducted using COMSOL® yielding sufficient high linearity of the pulsed magnetic field within a cylindrical volume of 3 mm times 5 mm.

Initial calibration procedures [2] for the characterization of the new setup confirm the correct interplay between gradient amplifiers and gradient coil for gradients of up to 70 T/m. First PFG NMR experiments were conducted using samples with well-known properties while employing pulsed field gradients of up to 65 T/m. In particular we used the triblock copolymer P123 (BASF AG, Germany) being dissolved in 50 wt% D_2O, thus forming a hexagonal structure. We found diffusion coefficients as well as the expected diffusion anisotropy in agreement with previously published values [3].

Furthermore, the use of such super-high gradients allows to significantly shorten the observation time during the PFG NMR experiment, while still maintaining a reasonable spin echo attenuation. Thus, we were able to find root mean square displacements for short observation times (<120 ms) that are in the order of a few 10 nm, which confirms the potentials of the presented setup for the extension of the accessible length scales towards smaller values.

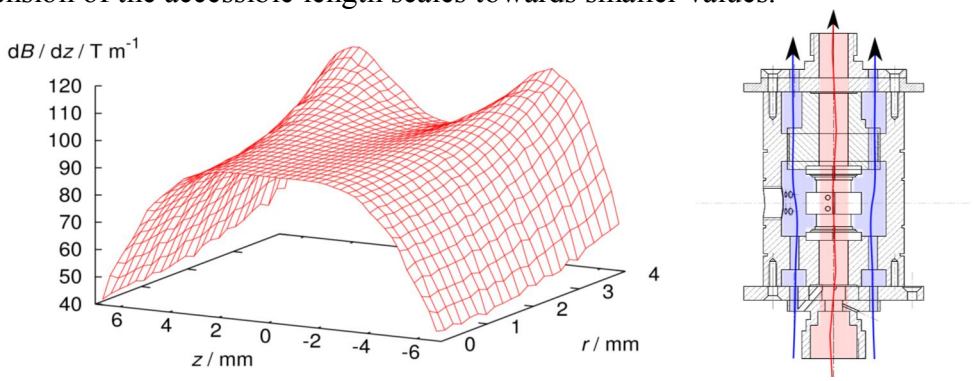

Fig. 1: New probe design. The gradient profile at the sample region deviates only by 0.4% (left). The scheme of the hardware (right) outlines gradient cooling (blue) and temperature control of the sample (red) by separated air streams.

References:
1. F. Stallmach and P. Galvosas, Annu. Rep. NMR Spectrosc . 61 (2007) 51.
2. A. C. Wright *et al.,* J. Magn. Reson. 186(2007) 17.
3. K. Ulrich et al., Phys. Rev. Lett. 102 (2009) 037801.

P06

Diffusion and advection probed by relaxation exchange NMR

A. M. Olaru, J. Kowalski, V. Sethi, and B. Blümich

Institute of Technical and Macromolecular Chemistry, RWTH Aachen University, Germany

The characterization of fluid flow in porous media represents a matter of high interest in fields like the construction industry, oil exploitation, and soil science. Low flow rates, such as those which occur in soil during rain or in oil recovery (1-5 ml/h), are difficult to characterize by classical high-field NMR velocimetry due to the high gradient values and elaborate methods required for adequate signal encoding. The necessity of field studies raises additional technical problems, which can be solved only by the use of light, portable, low-field instruments that can be easily operated in situ [1].

In this work we extend the use of low-field relaxation exchange experiments from the study of diffusive transport to that of advection. We show that velocity-related information can be obtained with a simple low-field device. In order to establish a correlation between the flow rate and the NMR relaxation of the fluid in the pores, T_2-T_2 relaxation exchange experiments were performed using a home-built Halbach magnet (9.6 MHz for ^{1}H) on model porous systems with controlled pore-size distributions exposed to unidirectional flow of Newtonian and non-Newtonian fluids (water and xantane gum solution). The results show that different flow rates leave distinctive marks on the exchange maps obtained by inverse Laplace transformation of the time domain data, due to the superposition of exchange, diffusion and inflow/outflow in multiple relaxation sites of the liquids in the porous media.

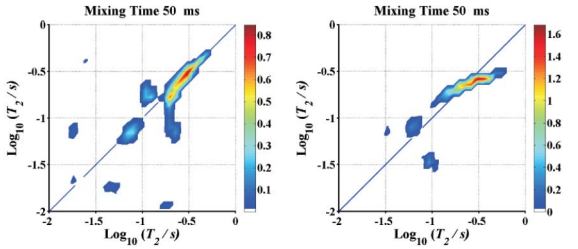

Figure 1. Enhanced exchange and tilt of the main diagonal peak for slow flow rates: 1 ml/h (left) and 2.6 ml/h (right).

At low velocities the exchange maps exhibit strong asymmetries. In the case of slow velocities there is no loss of signal due to outflow, and the relaxation-exchange effects prevail, leading to a tilt of the diagonal distribution around a pivot point with increasing mixing time and enhanced exchange (Fig. 1). For high velocities the inflow-outflow effects dominate, and the relaxation-time distribution collapses towards lower values of the average spin-spin relaxation time.

Shifts and tilts in the exchange maps can be simulated by solving the relaxation site-averaged Bloch-Torrey system forward in time and assuming an asymmetric closure for the transport. This might be realistic for preferential flow phenomena or for pore size distributions with two or more clearly distinct pore size classes. The derived model also suggests a way of extracting the average velocity information from the data, however further work is needed to perform a rigorous quantitative flow-field analysis. Nonetheless, the results obtained reveal the possibility of characterizing flow induced effects and fluid velocities in porous systems by simple correlation experiments performed with inexpensive and mobile hardware.

References:

1. B. Blümich et al., Small-Scale Instrumentation for NMR of Porous Media**,** special issue on Physics of Magnetic Resonance of Porous Media, New Journal of Physics 13 (2011) 0150031.

P07

In situ longitudinal relaxation-time measurements of pear fruits during the growing process using a mobile MRI system: the first year trial

Y. Geya,[1] T. Kimura,[1] Y. Terada,[1] K. Kose,[1] T. Haishi,[2] H. Gemma,[3] Y. Sekozawa[3]

[1]Institute of Applied Physics, University of Tsukuba, 1-1-1 Tennodai, Tsukuba, 3058573, Japan

[2]MRTechnology Inc, 2-1-6 B5 Sengen, Tsukuba, 3050047, Japan

[3]Agricultural and Forestry Research Center, University of Tsukuba, 1-1-1 Tennodai, Tsukuba, 3058577, Japan

INTRODUCTION

MRI is a powerful tool for *in situ and in vivo* plant studies. However, it is not easy to set up MRI systems in outdoor environments. To solve this problem, we have developed an electrically mobile MRI system using a permanent magnet, a compact MRI console, and an electric cart (1). In this study, we have measured relaxation times of pear fruits for about two months to clarify the water property in their growing process.

MATERIALS AND METHODS

The MRI system consists of a permanent magnet (field strength = 0.2 T, gap width = 16 cm, homogeneous area = 10 cm dsv, weight = 200 kg, Neomax Engineering, Japan), a gradient coil set, an RF probe, and a compact and mobile MRI console (Fig.1). The magnet was fixed on the fork of a mobile lift (GL-4, Genie Industries, USA) and mounted on an electrically motorized cart (CB-02, Yamaichi-Seikou, Japan). Because the MRI console was connected to the cart, the whole MRI system was carried using the cart. It took about 20 minutes from our laboratory to the pear fruit-farm in our university.

We measured T_1 and T_2 of six Japanese pears (*Pyrus pyrifolia* Nakai, Kosui) using inversion recovery and CPMG sequences for about two months. The measurements started from June 25, 2010, and the pears were harvested on August 19, when the relaxation times were measured before and after the harvest. After that day, relaxation times were measured in our laboratory using the same magnetic field (0.2 T).

RESULTS AND DISCUSSION

Figures 2 and 3 show T_1 and T_2 plotted against time. These graphs clearly show that the relaxation times monotonously increased with time, which is probably due to the increase of free water proportion in the pear fruit cells accompanied by the growth of the pear fruits. The graphs show a discontinuous change in T_1 but not in T_2. We think that this is caused by the fact that T_1 measurement is more sensitive to the inhomogeneity of the RF coil than T_2 measurement; it was difficult to place the pear fruits at the center of the RF coil before the harvest, and large error in positioning would lead to an increase in the inhomogeneity in the measured volume and to large error in T_1 values. In conclusion, we have successfully measured relaxation times of *in situ* pear fruits for about two months and observed their monotonous increase. In 2011, we are planning to start the measurements from May, when the number of cell is still increasing.

Fig.1

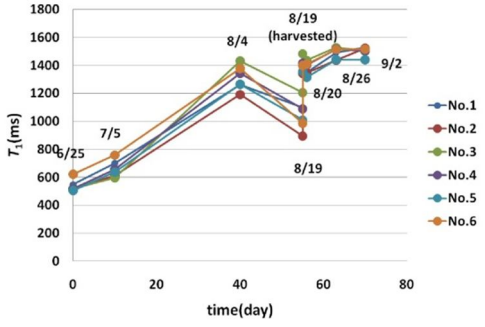

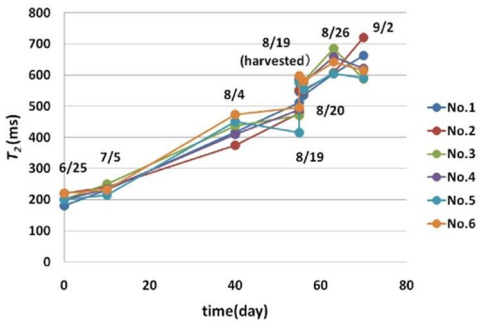

Fig.2

Fig.3

Reference: 1. T. Kimura, Y. Geya, Y. Terada, K. Kose, T. Haishi, H. Gemma, Y. Sekozawa, Development of a mobile magnetic resonance imaging system for outdoor tree measurements. Rev. Sci. Instrum. 2011, in press.

P08

Trabecular bone volume fraction measurements of the calcaneus using a 3D FSE sequence in a 0.2 T compact MRI system

H. Kondo, T. Nakayama, D. Tamada, S. Kono, Y. Terada, K. Kose

Institute of Applied Physics, University of Tsukuba, Tsukuba 305-8573, Japan

INTRODUCTION

Osteoporosis is a chronic disease that frequently causes hip fractures. Bone density measurements are indispensable for diagnosis and precaution of osteoporosis. MRI is a unique bone density measurement method that can measure trabecular bone volume fraction (TBVF) both safely and exactly. However, TBVF measurement using a whole body MRI system is not cost effective. Therefore, since the year 2000, we have been developing compact MRI systems for measuring TBVF of the calcaneus using low field (0.2 T) permanent magnets [1]. Our recent studies have suggested that reproducibility of the TBVF can be improved by the 3D measurements, because TBVF is sensitive to the position of the sagittal slice [2]. In this study, we optimized a 3D fast spin echo (FSE) sequence for bone marrow protons of the calcaneus and evaluated reproducibility of the TBVF measurements.

MATERIALS AND METHODS

The compact MRI system consists of a 0.2 T permanent magnet (160 mm vertical gap, 35 ppm homogeneity in 20 cm × 20 cm × 12 cm DEV), a gradient coil set, an RF probe, a local RF shield, and a compact MRI console. The RF coil is an oval solenoid (aperture: 175 mm × 85 mm, length: 120 mm) whose aperture is optimized for the calcaneus. Parameters for a 3D FSE sequence were optimized for 3D image measurements of the calcaneus as follows: FOV = $(128\ \text{mm})^2 \times 64$ mm, image matrix = 128 × 128 × 32, ETL = 16, echo spacing = 16 ms, TR = 1200 ms, measurement time = 5.12 min. A cylindrical plant oil phantom (diameter = 85 mm, thickness = 70 mm) and a calcaneus of a female volunteer were repeatedly measured ten times using the 3D FSE sequence with an external reference oil phantom.

RESULTS AND DISCUSSION

Figures 1 and 2 show vertical slices selected from 3D image datasets of the cylindrical phantom and the calcaneus. The triangles in the images are ROIs for external reference. The domain bounded by the broken curve in the cylindrical phantom corresponds to the location of the calcaneus, of which segmented 3D volume is shown in Fig.3. The image intensity ratio between the curved ROI and the triangular ROI was calculated for the cylindrical phantom and the calcaneus. The coefficient of variance (CV: standard deviation divided by the mean) for the ten times sequential measurements of the image-intensity ratio was 0.0066 and 0.026 for the cylindrical phantom and the calcaneus as shown in Fig.4. The relatively large CV for the calcaneus may be caused by errors produced in the image segmentation process. In conclusion, we have successfully implemented a 3D FSE sequence to measure TBVF in the calcaneus. Improvements in the image segmentation process and developments of T_2 decay correction technique will be future problems.

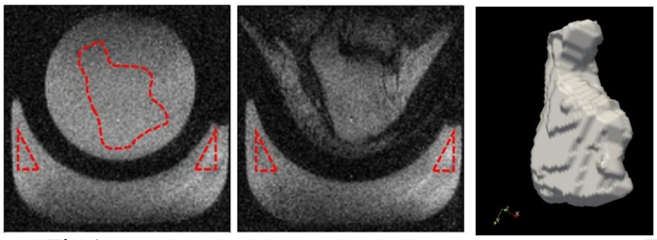

Fig.1

Fig.2

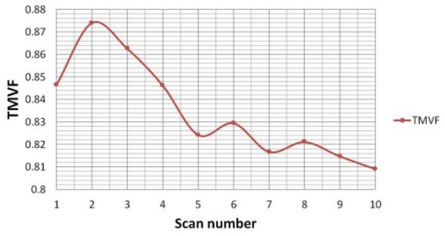

Fig.3

Fig.4

References:

[1] K. Kose, et al. Magn Reson Med **52**, 440 (2004).
[2] T. Nakayama, Master thesis, Univrsity of Tsukuba, 2011.

P09

Slow MAS, a Non-, or Minimally Invasive Method for High Resolution ^{1}H NMR Profiling of Small Molecules

Jian Zhi Hu, Ju Feng, Hardeep S. Mehta, Mary Hu
Pacific Northwest National Laboratory, Richland, WA 99352, USA; E-mail: Jianzhi.Hu@pnl.gov

NMR, a potentially quantitative, non-destructive method that requires no or minimal sample preparation, is one of the leading analytical tools for profiling small molecules in biological samples, including food and other fluid or semi-solid materials. ^{1}H NMR is widely used for these studies because of its high sensitivity and its ability of detecting a large range of small molecules. However, ^{1}H NMR spectrum obtained in vivo (biological samples) or in situ (fluid or semi-solid samples) often suffers from poor resolution due to variations in the bulk magnetic susceptibility present, e.g., in biological specimens near boundaries of inter- and intra-cellular structures, which makes spectral analysis difficult and sometimes impossible. Traditionally, the technique of magic angle spinning (MAS) using a sample spinning rate of several kHz or more, i.e., the so-called hr-MAS, is used to obtain high resolution ^{1}H NMR spectrum in these samples. Despite its remarkable success, there are two shortcomings associated with hr-MAS. The first is that hr-MAS is an invasive method due to the large centrifugal force arising from the high spinning rate used. The second is that the size of the samples is limited to a few tenth of mg due to the combined difficulties of sealing an intact fluid sample inside a MAS rotor without fluid leakage and simultaneously reaching a high sample spinning rate.

We found (1) that the line broadening can be effectively suppressed using a combination of slow magic angle sample spinning and special rotor position synchronized RF pulses. Two classes of methodologies have been developed in our laboratory. With ^{1}H PHORMAT applied at a sample spinning rate of 1 to 4 Hz, in vivo and localized high resolution ^{1}H NMR on a live mouse are possible. With ^{1}H-PASS method applied at a sample spinning rate between 30 and 300 Hz, high resolution and high sensitivity ^{1}H NMR spectra of small sized intact biological objects are obtained. Because of the slow, or ultra-slow sample spinning used, slow-MAS offers a non, or minimally invasive method for high resolution ^{1}H NMR profiling of small molecules. In this presentation, applications of these slow-MAS methods will be given. In particular, we will report a novel slow MAS probe for the ^{1}H-PASS experiment. The combination of the slow-MAS probe and the ^{1}H-PASS makes it possible to perform high resolution and high sensitivity metabolic profiling on biological samples, including fluid containing or semi-solid samples, with volume as small as a few hundred nanoliters to sample volume as large as a few milliliters. The nanoliter capability has the potential to follow the metabolic changes through a continued investigation on a single small laboratory animal over a long period of time using minimally invasive blood and tissue biopsy samples. While the milliliter capability would allow minimally destructive studies of intact biological object with size as large as a few cm. Preliminary results are illustrated in Figure 1. The latest development on the probe and its applications on a wide range of sample sizes ranged from about 200 nl to larger than 1.0 cm^3 will be presented.

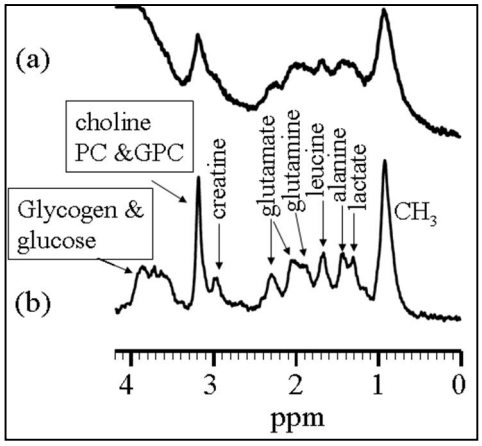

Figure 1. *The water suppressed 300MHz ^{1}H NMR spectra of **0.8 mg** (800nl) excised mouse spleen. (a) The static spectrum. (b) The 80 Hz ^{1}H PASS spectrum acquired using a total data acquisition time of 8.5 minutes. The S/N of the CH_3 peak at about 0.93 ppm was ~85.*

Reference

1. Wind RA, Hu JZ, *In vivo* and *ex vivo* high-resolution ^{1}H NMR in biological systems using low-speed magic angle spinning, *Progress in Nuclear Magnetic Resonance Spectroscopy* **49**, 207-259 (2006).

P10

Evaluation and correction of B_0 inhomogeneity in a temperature-variable MRI system with a 1.0 T yokeless permanent magnet

Y.Terada, D. Tamada, K. Kose
Institute of Applied Physics, University of Tsukuba, Tsukuba 305-8573, Japan

INTROTUCTION

MRI has the potential to map out temperature-dependent phenomena in three dimensions. In a conventional MRI system, to measure a specimen at various temperatures, the specimen should be stored in most cases in a temperature-regulated cell in an RF coil. However, this scheme has several drawbacks (e.g., poorness of the RF coil filling factor and size limitation of the specimen to fit in the small cell). To overcome these, we have proposed temperature regulation of the whole signal detection system including a specimen, RF coil, gradient set, and magnet [1, 2]. Here, we measured the spatial mapping of the B_0 inhomogeneity as a function of temperature and designed a single-channel shim coil to correct the inhomogeneity.

EXPERIMENTAL

The MRI system consists of a small yokeless permanent magnet (field strength = 1.04 T at +25 °C, gap width = 40 mm, homogeneity about 20 ppm in 20 mm dsv, weight = 85 kg), a planar gradient coil set, a solenoid RF coil (diameter = 30 mm, length = 35 mm), and an MRI console (Fig. 1 (left)). The permanent magnet was installed in a variable temperature thermostatic bath (temperature range = -15 °C to +50 °C, inner size = 620 mm (W) × 340 mm (D) × 1154 mm (H); FMU-263I, Fukushima Industries, Osaka, Japan).

RESULTS AND DISCUSSION

We first evaluated the B_0 inhomogeneity at temperatures from –5 °C to 45 °C (Fig. 1 (right)). The series expansion analysis revealed that the inhomogeneity had the specific spatial characteristics; the second-order terms z^2, x^2, and y^2 were dominant in this order and they scaled linearly with temperature. The simple scaling law ensures that the magnet field inhomogeneity can be corrected over a wide temperature range by using a single-channel shim coil that is properly designed to correct the inhomogeneity at a certain temperature. Accordingly we designed and fabricated the single-channel shim coil (Fig. 1 (left)). With shimming, the B_0 inhomogeneity reduced drastically over the wide temperature range.

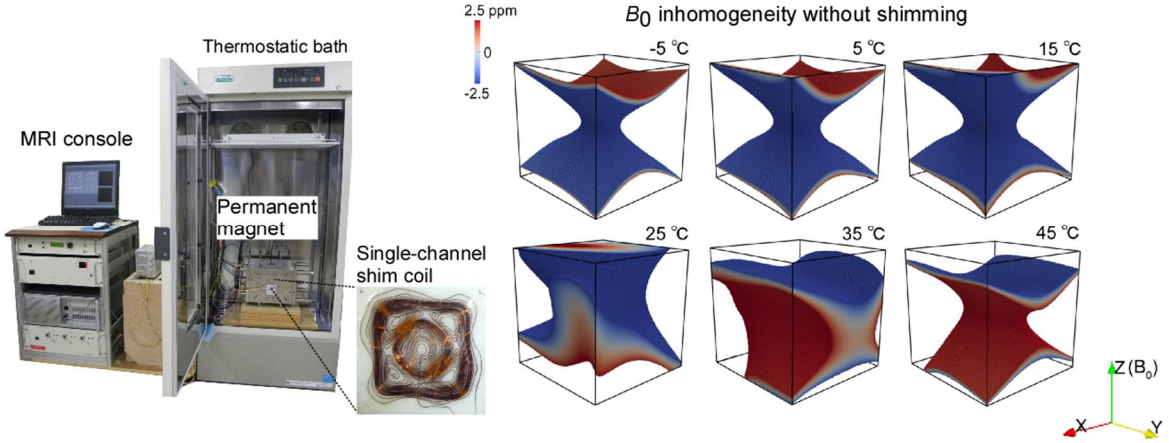

Fig. 1: (Left) Overview of temperature-variable MRI system. (Right) Spatial distribution of B_0 inhomogeneity without shimming.

References:

1. S. Adachi et al. Rev. Sci. Instrum. **80** (2009) 054701.
2. Y. Terada et al. Proc. ISMRM (2011) 1802.

P11

A method to choose the optimal number of singular values in the fast inverse Laplace transform for the two-dimensional NMR distribution function

A. Shi JingSheng[a], B. Jiang ZhiMin[a], C. Zhu TaoTao[a], D. Wang WeiMin[a]

[a] Institute of Quantum Electronics, School of Electronic Engineering and Computer Science, Peking University, Beijing 100871, China;

Two-dimensional (2D) NMR distribution functions are powerful tools in the study of porous media. In this paper we propose a practical method to make proper truncation of singular value decomposition (TSVD) in the inverse Laplace transform for extracting the 2D NMR distribution function from the observed NMR data. By analyzing basic algorithms for inverse Laplace transform (inversion), we find that proper TSVD doesn't affect the inversion result for an ill-conditioned problem with zeroth-order Tikhonov regularization. A new method is proposed to choose the optimal number of singular values for data compression achieved by TSVD in each dimension. The method makes full use of the redundancy nature of data with a finite signal to noise ratio (SNR) in ill-conditioned problem and well balances the tradeoff between speed and bias. The method does not require the stochastic information of the estimated parameters, which makes it possible to choose the optimal number of singular values in advance in most applications of 2D inverse Laplace transform.

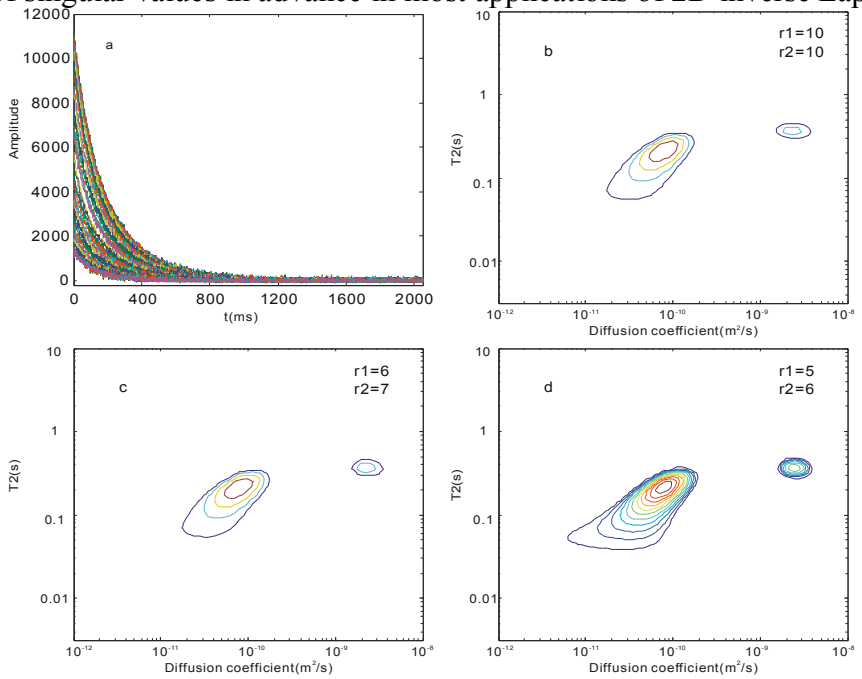

Fig. 1:D-T2 distribution inversion result of a reservoir core. (a) The experimental data for the reservoir core (b) The distribution function obtained with r1=6, r2=7 (c) The distribution function obtained with r1=10, r2=10 (d) The distribution function obtained with r1=5, r2=6.

References:

1. K. R. Brownstein and C. E. Tarr, Phys. Rev. A 19 (1979) 2446.
2. P. C. Hansen, SIAM Rev. 34 (1992) 561.
3. L. Gabriela, J. Edmund and T. Fordham, Magn. Reson Imag. 23 (2005) 305.
4. L. Venkataramanan , Y. Q. Song and M. D. Hürlimann, IEEE Trans. Signal Process, 50 (2002) 1017.

P12

An efficient Design for a Quadrature Birdcage at 750 MHz

G. Lykowsky[a,b], M.A. Lopez Terrones[c], and V.C. Behr[a],

[a]Department of Experimental Physics 5, University of Würzburg, Würzburg, Germany
[b]MRB Research Center, Würzburg, Germany
[c]Department of Electronics and Electromagnetism, University of Seville, Seville, Spain

Achieving quadrature polarization for ultra-high-field birdcage coils is known to be troublesome due to high frequency phenomena. A feasible and efficient design to address this problem is presented.

A standard eight rung high pass birdcage (Ref. 1) with 28 mm diameter and inner rung length of 29 mm was built. The outer copper shield fits the 57 mm diameter of the Mini 0.5 gradient system of a 17.6 Telsa Bruker Avance 750WB. The coils quadrature channels are inductively coupled and fed with bazooka-baluns to suppress shield currents. The cable grounds are soldered together over the full length to avoid ground potential differences. Inductive coupling was favored over capacitive coupling since its influence on the electrical symmetry of the birdcage is lower. To minimize the disturbance introduced by the tuning network, a variable capacitor and an inductance are connected between a rung and an additional tuning ring (Fig 1). Thus the resonator frequency may be raised or lowered around the center frequency without severely breaking the birdcage symmetry. These steps result in an adequate isolation of the two quadrature channels of -22 dB without further measures.

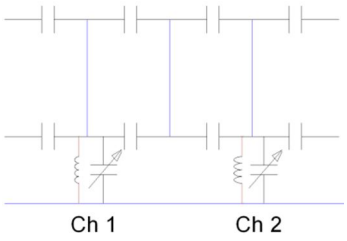

Fig. 1: Tuning networks

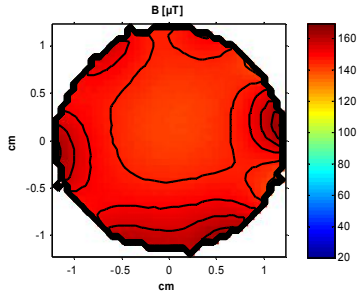

Fig. 2: The central axial slice of the B1-map shows the good homogeneity of the quadrature birdcage. The isolines indicate changes of 4 % in relation to the central value.

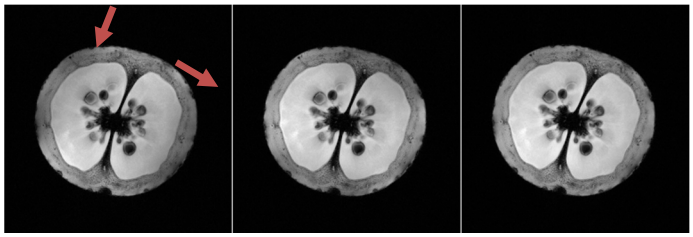

Fig. 3: FLASH images of a tomato (TE: 5.37 ms, TR: 500 ms, FA: 30°, matrix: 256^2, FOV: 3.0^2 cm^2, TA: 2 min 8 s). From left to right: channel 1, channel 2, and both channels in quadrature. The arrows indicate the direction of the linear modes.

To map the birdcage's B1-field an oil phantom (23 mm diameter) and a FLASH sequence with variable pre-pulse (Ref. 2) were used. Fig. 2 shows the good homogeneity of the final coil. A tomato was imaged to illustrate the imaging quality of the coil (Fig. 3). Both channels independently show good homogeneity. In quadrature mode the expected improvement in SNR (about 30 %) and homogeneity is achieved.

References:

8. C.E. Hayes et al.: An Efficient, Highly Homogeneous Radiofrequency Coil for Whole-Body NMR Imaging at 1.5 T. J. Magn. Reson. 63: 622-628, 1985.
9. J. Murphy-Boesch et al.: Precision mapping of the B1 field using the rotating-frame experiment. J. Magn. Reson. 73(2): 293–303, 1987.

P13

Magnetic Resonance Studies of Chemical Reactions under Flow

Jan Novak and Melanie M Britton

Department of Chemistry, University of Birmingham, Birmingham, UK

Due to the ability of MRI to quantify both chemical patterns and flow processes it has become a valuable tool in the field of non-linear chemistry. The Belousov-Zhabotinsky (BZ) reaction is an autocatalytic, oscillatory reaction which produces a wide range of chemical patterns, including waves, spirals and stationary structures, all of which have been compared to similar structures found in nature[1] Patterns are formed via a coupling between autocatalytic reaction and diffusion. With the introduction of flow (advection), novel pattern formation can be observed. These reaction-diffusion-advection processes have enabled the formation of structures including stationary flow-distributed oscillations (FDOs), flamelets and distributed reaction fronts. Uniquely, MRI techniques are able to, almost simultaneously probe both the chemistry and flow allowing the processes in the coupling between non-linear chemistry and flow to be better understood. For example, FDO patterns in optically opaque packed bed reactors have been shown to have a conical shape which was linked to the inhomogeneous flow within a packed bed[2].

In our work we have produced chemical patterns in stationary Taylor vortices[3], travelling Taylor vortices (vortex flow reactors) and in pipe flow for the first time. An MR image of a distributed reaction front propagating through a series of stationary Taylor vortices is shown in Figure 2 (a). Wave propagation velocities (Figure 2 (c)) were enhanced by increased flow, as shown in Figure 2 (b). A discrepancy can be seen at 2.3 Hz in Figure 2 (b) where a significantly lower wave velocity was observed. This is induced by transient vortex flow where a rich variety of patterns were observed.

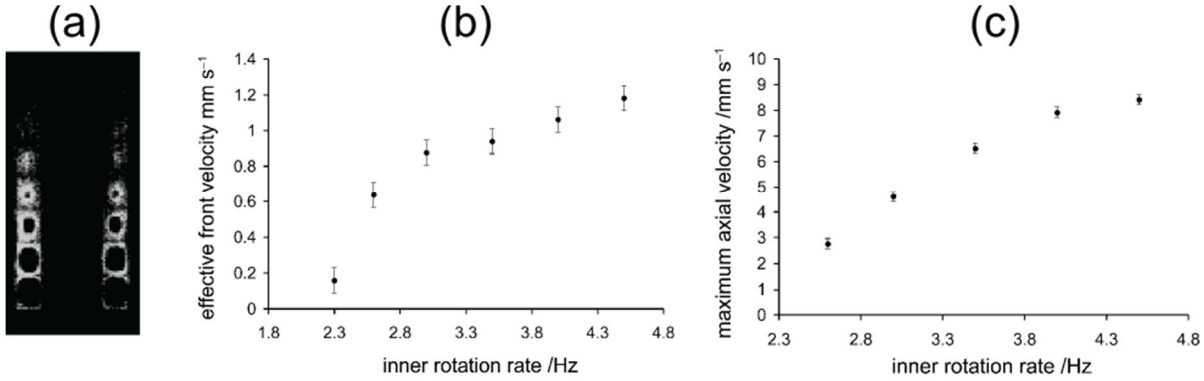

Figure 2 (a) A vertical slice MR image of a distributed reaction front propagating through Taylor vortices. (b) Effective velocities of the distributed reaction fronts as a function of rotation rate. (c) Flow velocities within the Taylor vortices as a function of rotation rate.

References:

1. P. Ball, *The self-made tapestry: pattern formation in nature*, Oxford University Press, Oxford [England]; New York, **1999**.
2. M. M. Britton, A. J. Sederman, A. F. Taylor, S. K. Scott, L. F. Gladden, *J.Phys. Chem. A* **2005**, *109*, 8306.
3. B. W. Thompson, J. Novak, M. C. T. Wilson, M. M. Britton, A. F. Taylor, *Phys. Rev. E* **2010**, *81*.

P14

Shimming Coil Design for Magnet Field based on Spherical Harmonics Analysis

Xiaonan Li[a], Cédric Hugon [a], Dimitris SAKELLARIOU[a]

[a]Laboratoire de Structure et Dynamique par Résonance Magnétique DSM/IRAMIS/SIS2M/LSDRM, CEA Saclay

A complete design for active shimming for permanent magnets is presented and is based on the original paper by Romeo and Hoult [1]. Based on Gauss and Ampere theory for the production of static magnetic field, the field is developed in Spherical Harmonics. When the static field produced by magnet aligns along the z axis in a Cartesian coordinate frame, the field correcting system can be divided into zonal and tesseral subsystems, as a function of the symmetry properties of the coils. In a practical shimming procedure for an new magnet, after plotting real distribution of the field inside magnet, by letting the coefficient of a certain harmonic be equal in amplitude and opposite in sign to that of corresponding measurement, it is easy to reach expected performance of homogeneity.

In this paper, circular coils for Zonal harmonics and arcs for Tesseral Harmonics are employed. For either Zonal or Tesseral harmonics, the properties involving symmetry and anti-symmetry structure, which give great convenience in harmonic design, are presented in detail and formulas are derived. Compared to Finite Element Analysis, this analytic method is irreplaceable and under Fourier synthesis in spherical coordinates, confusions encountered when using Cartesian coordinates can be avoided. High order shim coils are presented together with numerical simulations demonstrating their theoretical performance.

References:

1. Francoise Romeo and D. I. Hoult, Magnet field profiling: Analysis and correcting coil design, Magnetic Resonance In Medicine 1 (1984) 44.
2. M. J. E. Golay, Rev. Sci. Instrum. 29 (1958) 313.
3. I.N. Sneddon, Special Functions of Mathematical Physics and Chemistry, Oliver & Boyd, Edinburgh(1961).
4. D. Sakellariou, C. Hugon, A. Guiga, G. Aubert, S. Cazaux and P. Hardy, Permanent magnet assembly producing a strong tilted homogeneous magnetic field: towards magic angle field spinning NMR and MRI, Magn. Reson. Chem. 48 (2010) 903.

P15

The relation between stretch exponential function characteristics and the width and median of its Inverse Laplace Transform (ILT): Application of PFG NMR to diffusion of pore confined fluids

Xiaoliang Gong [a], Zhenshu Zhu [b], E.W. Hansen [c] and Qun Chen[a]

[a] Department of Physics and Shanghai Key Laboratory of Magnetic Resonance of East China Normal University
[b] Department of Polymer Science of Nanjing University
[c] Department of Chemistry of University of Oslo

It is well known that the PFG NMR response function R(x) of the diffusivity D of a pore confined fluid can be approximated by a stretch exponential function $R(x) = \exp[-(D_S x)^{\beta}]$. And its ILT-function F_{ILT} can be characterized by a width $_{ILT}$ and a median D_{ILT} (analogous to the definition of the width and the median of a molecular weight distribution):

$$\sigma_{ILT} = \sqrt{\ln\left(\frac{\int_0^{\infty} D \cdot F_S(D)dD \Big/ \int_0^{\infty} F_S(D)dD}{\int_0^{\infty} F_S(D)dD \Big/ \int_0^{\infty} (1/D) \cdot F_S(D)dD}\right)} \quad \text{and} \quad \int_0^{D_{ILT}} D \cdot F_{ILT}(D)dD = 1/2 \int_0^{\infty} D \cdot F_{ILT}(D)dD$$

The objective of this project is to correlate the two set of parameters (D_{ILT}, $_{ILT}$) and (D_S,) in order to determine more efficiently the two former parameters from a PFG NMR measurement, without resorting to any ILT. Figure 1A shows the ILT of a SEF for a fixed D_S (= 10^{-10}) and various and reveals an approximately linear relation between $_{ILT}$ and (Figure 1B). Importantly, $_S$ was found to be independent of D_S.

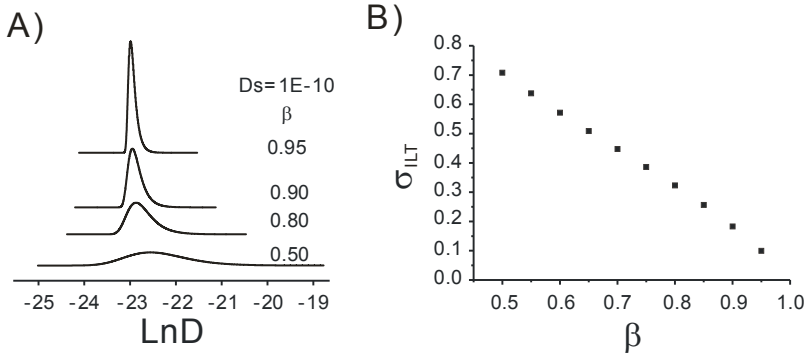

Fig 1: A) The Inverse Laplace transform of a SEF ($D = 10^{-10}$) for various The width parameter $_{ILT}$ versus

In contrast, preliminary work suggests that D_{ILT} depends on both D_S and However, this work is in progress and will be reported elsewhere.

References:

[1]. Rubinstein, M.; Colby, R. H. *Polymer Physics*: Oxford university press, **2004**

P16

Mobility, miscibility, and microdomain structure in nanostructured thermoset blends of exopy resin and amphiphilic poly (ε-caprolactone)-block-polybutadiene-block-poly (ε-caprolactone) triblock copolymers characterized by solid-state NMR

Zhang Rongchun[a], *He Xin*[b], *Chen Tiehong*[b], *Li Baohui*[a], *Sun Pingchuan**[b], *Jin Qinghua*[a], *and Ding Datong*[a]

[a] School of Physics, Nankai University
[b] Key Laboratory of Functional Polymer Materials, Ministry of Education, Institute of Polymer Chemistry, College of Chemistry, Nankai University, Tianjin, 300071, China

Abstract: Various solid-state NMR methods were used to characterize the heterogeneous dynamics, miscibility, and microdomain structure in nanostructured thermoset blends of epoxy resin (ER) and amphiphilic PCL-PB-PCL triblock copolymers. ^{1}H wideline spectra and WISE experiments proved the existence of the heterogeneous dynamics in the blends as well as phase separation between the block copolymers and cured-ER matrix. At the same time, an improved method based on 12-pulses dipolar filter spin-diffusion experiments made it possible for us to determine the domain size. Combined with the results of DSC and SAXS, it was concluded that the PCL blocks were only partially miscible with the rigid cured-ER network, and some PCL blocks were locally expelled out of the network, which formed another mobile microphase with PB. The residual immobilized PCL blocks were intimately mixed with some partially cured-ER matrix and formed interphase region.

References:

1. Hillmyer, M. A.; Lipic, P. M.; Hajduk, D. A.; Almdal, K.; *et al. J. Am. Chem. Soc.*, 1997, 119, 2749
2. Li, X. J.; Fu, W. G.; Wang, Y. N.*et al*. *Polymer* 2008, 49, 2886.
3. Sun, P. C.; Dang, Q. Q.; Li, B. H.*et al*. *Macromolecules* 2005, 38, 5654
4. Meng, F. L.; Zheng, S. X.; Zhang, W. *et al. Macromolecules* 2006, 39, 711

P17

Continuously Dissolved Hyperpolarized ^{129}Xe for Analysis and Biomedical Applications of Hollow Fibers

N. Amor[a], K. Hamilton[b], L.Utiu[a], U. Steinseifer[b], S. Appelt[c] , B. Blümich[a] , T. Schmitz-Rode[b]

[a] ITMC of RWTH Aachen University
[b] AME of RWTH Aachen University and Hospital
[c] Research Center Juelich

NMR of hyperpolarized (HP) ^{129}Xe is of great interest because of the good solubility of the inert gas and its very sensitive chemical shift. The main obstacle for many applications is the efficient and continuous dissolution into carrier agents without formation of foams or bubbles. This challenge has successfully been met by so-called "xenonizer" setups [1,2]. They mainly consist of commercially available hollow fiber membranes typically used in clinical oxygenators (Fig. 1).

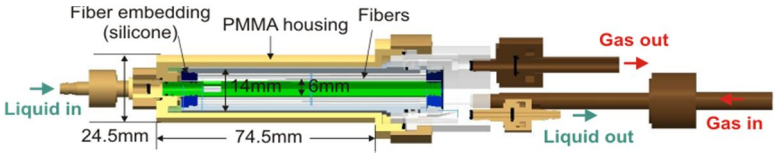

Fig. 1: Xenonizer module with embedded hollow-fiber membranes.

A purpose-built xenonizer setup has been developed and analyzed in detail by NMR spectroscopy (Fig. 2) and MRI for varying fiber materials as well as for different fluids, including porcine blood and its individual constituents [3]. Furthermore, blood with pre-dissolved HP ^{129}Xe has been employed in various biomedical studies. For example, capillary blood flow was investigated by MR imaging, and blood de-oxygenation could be monitored online. As a result, the xenonizer technology could be further understood and improved, and new applications of HP ^{129}Xe for biomedical NMR were explored.

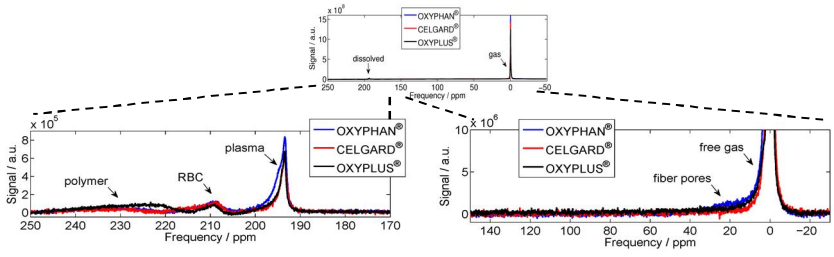

Fig. 2: Example HP ^{129}Xe NMR spectra acquired in whole porcine blood using three different hollow fibers.

References:

1. D. Baumer et al, Angew. Chem. Int. Ed. 45 (2006) 7282.
2. N. Amor et al, J. Magn. Res. 201 (2009) 93.
3. N. Amor et al, submitted (2011).

P18

Oscillatory flow phenomena in simple and complex fluids

Loribeth Q. Evertz[a], *Erik M. Rassi*[a], *Sarah L. Codd*[a], *and Joseph D. Seymour*[b]

[a] Dept. of Mechanical and Industrial Engineering, Montana State Univ., Bozeman, MT, USA
[b] Dept. of Chemical and Biological Engineering, Montana State Univ., Bozeman, MT, USA

The human body depends on the heart to circulate blood and it does so as a pulsatile flow. Gaining a better understanding of oscillatory flow in complex fluids similar to blood and the particle migration that can occur could help in the prevention and diagnosis of disease and enhance drug delivery. Oscillatory flows are also prevalent in many other industrial and natural systems. Nuclear Magnetic Resonance (NMR) is a non-invasive method for evaluating fluid mechanics and can be used to obtain spatially resolved velocity maps in complex fluids. A system has been constructed to provide a controllable and predictable oscillatory flow in order to gain a better understanding of the impact of oscillatory flow on colloid suspensions (fig. 1). A core shell particle colloidal suspension is used as a model system since measurements can be obtained separately from the suspending fluid (water) and the liquid particle core (hexadecane oil) using NMR[1, 2]. The oscillatory flow is generated by using a motor with an adapted arm to drive a piston cylinder. An inductive sensor is used to detect when the arm passes a specific point in the cycle. The sensor then triggers the MR spectrometer which measures the velocity distributions and dynamics of the fluid undergoing oscillatory flow at specific points in the oscillation cycle.

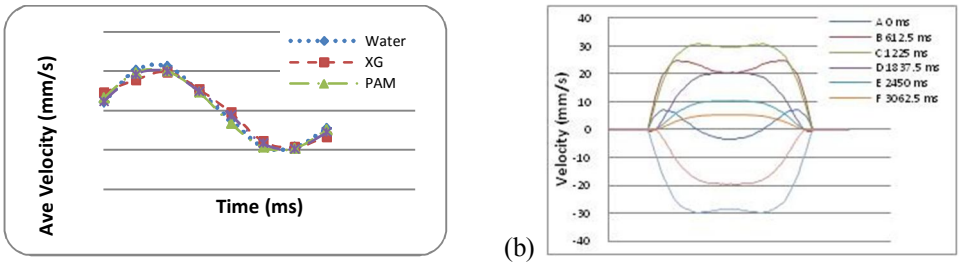

(a) (b)

Fig. 1: (a) Oscillatory flow obtained from water system for a 5s period. (b) Corresponding velocity profiles.

For oscillatory pipe flow, velocity profiles are characterized by the Womersley number, α, which is the ratio of the unsteady forces to the viscous forces[3]:

$$\alpha = R\sqrt{\frac{\omega}{\upsilon}}$$

where R is the tube radius, ω is the oscillatory flow frequency, and υ is the kinematic viscosity of the fluid[3]. In most fluids, a low α will result in a parabolic shaped velocity profile. Whereas, for a high α the velocity profile is flat and sometimes split as the unsteady forces begin to dominate[4]. In addition to characterization of flow and transport in oscillatory flows this apparatus could potentially be used in Rheo-NMR[5] applications to generate oscillatory flows for characterization of the shear modulus of complex fluids.

References:

1. Brown, J.R. et al. Phys. Rev. Lett. 99 (2007) 240602.
2. Wassenius, H. and Callaghan, P.T. J Magn Reson 169 (2004) 250–256.
3. Ku, D.N. Blood Flow in Arteries. Ann. Rev. of Fluid Mechanics. 29 (1997) 399-434.
4. Womersley, J.R. J. Physiol, 127 (1955) 553-563.
5. Callaghan, P.T. Rep. Prog. Phys., 62(4) (1999) 599-670.

P19

Magnetic Resonance Microscopy (MRM) of the development of the Zebrafish using a standard bore 850 MHz system

Thomas Neuberger[a,b], *Tatjana Neuberger, Keith Cheng*[c]

[a]Huck Institutes of the Life Sciences, [b]Department of Bioengineering, [c]Department of Pathology, Penn State College of Medicine; Pennsylvania State University

The experimental features of the zebrafish, which include transparency, fecundity, and strong genomic tools, have made it a powerful model system for basic biology to disease. Imaging of the zebrafish is frequently needed to assess morphological changes associated with experimental variables. Light microscopy can be used in the more transparent early developmental stages, but decreasing transparency, pigmentation, and size necessitate other imaging modalities in older fish. In this work, a standard bore 20 tesla MRI system (Bruker, Germany), usually used for NMR spectroscopy, was utilized to create high resolution MRM images of groups of zebrafish embryos, with isotropic voxels as small as 8 micrometers.

After fixation, animals of different age groups were immersed into a 2% Magnevist (Bayer, Germany) solution for 1 week to reduce the imaging time. Three dimensional gradient echo images were acquired using a commercial 5 mm ID saddle coil for the smaller animals, and a 10 mm ID saddle coil for the larger animals, respectively. The achieved images and reconstructions (AVIZO, VSG3D, USA) are shown below. Anatomic detail in the brain of older animals reveal an unusual level of detail due to the high contrast to noise ratio. Simple segmentation allowed us to plot eye volume over a period of 2 years, which ranged from 0.002 to 4.8 mm^3. Multiple fish can be scanned at early ages, but further development will be needed to image whole adult zebrafish at this resolution within a single scan.

This study adds images of the developing zebrafish to similar work (1,2) conducted by other groups. Despite the small bore size, the high magnetic field of 20 tesla and the extremely high magnetic field gradients (3000 mT/m) allowed a throughput of more than 60 animals (1dpf and 2dpf) with up to 8 micron resolution. The results suggest that 20T MRM can potentially be used to image the full life-span of the zebrafish.

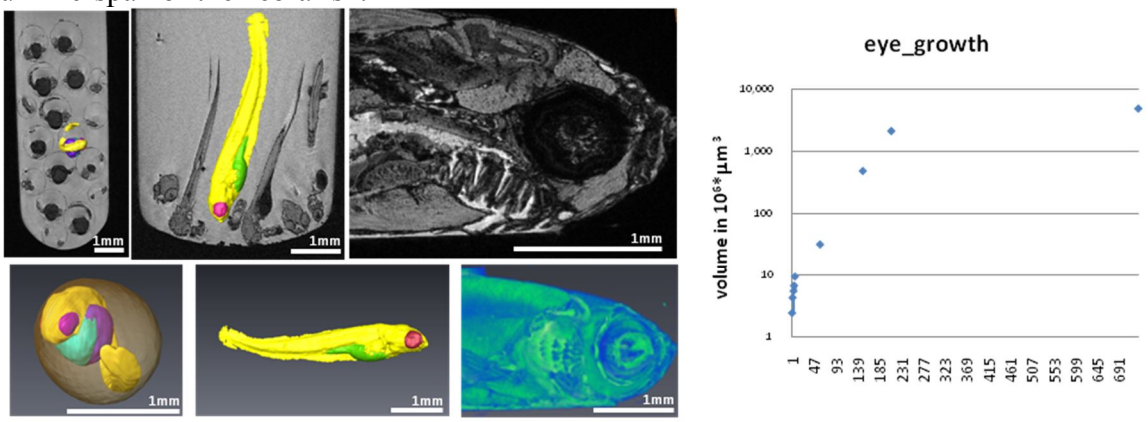

Figure1: Images and reconstruction (Avizo, VSG3D) of the developing Zebrafish 1, 5, and 150 days past fertilization (dpf) are shown on the left. Resolution varies between 12 and 20 microns isotropic, imaging time between 6 and 18.5 h. The right graph shows the growth of the eye over a period of 2 years.

References:

1. Kabli et al, Zebrafish, 9 (2006) 4.
2. Ullmann et al, Neuroimage, 51 (2010) 76.

P20

High-Resolution $T_{1\rho}$ and T_2 Maps of Articular Cartilage at 11.7 T

Ziying Yin[a], *Mrignayani Kotecha*[a], *Richard L. Magin*[a]

[a]Department of Bioengineering, University of Illinois at Chicago, Chicago, Illinois

Introduction: Articular cartilage is a heterogeneous connective tissue composed of three distinct layers: superficial zone (SZ), transitional zone (TZ) and radial zone (RZ), each with a unique framework of chondrocytes, tissue fluid (water) and structural macromolecules (collagens, proteoglycans and other proteins) [1]. Differences in the macromolecular composition of each layer provide the basis for $T_{1\rho}$ and T_2 contrasts. Previous studies at 4 T reported that $T_{1\rho}$ relaxation time depended on the changes of proteoglycans (PGs) in PG-depleted cartilage, compared with T_2 [2]. However, its in-plane resolution of 137 μm may not provide sufficient details to detect early stage of PG loss resulting from aging or degenerative joint diseases. In this preliminary study, we acquired high resolution $T_{1\rho}$ and T_2 maps ($39\times39\times50$ μm^3) from healthy bovine knee cartilage at 11.7 T and observed the $T_{1\rho}$ and T_2 heterogeneity as a function of cartilage depth.

Materials and methods: Cartilage plugs (n = 7, diameter = 4 mm) with subchondral bone were harvested from medial femoral condyle of 6-month-old bovine knees. Experiments were conducted on a Bruker DRX-500MHz Avance Spectrometer/56-mm vertical bore magnet/5-mm RF saddle coil system. Cartilage surface was perpendicular to B_0 field. T_2 was mapped using a modified Bruker MSME sequence to eliminate the diffusion losses by placing the bipolar read-refocusing gradient pair after the 180° pulse (TR = 3 s, TE = 7 – 224 ms, 36 echoes) [3]. $T_{1\rho}$ map was acquired using a preparatory pulse cluster with self compensation (90_x-(spin-lock)$_y$-(spin-lock)$_{-y}$-90_{-x}) followed by a readout FSE sequence to minimize B_1 and B_0 field imperfections (TE = 8 ms, TR = 3 s, TSL = 10, 20, 40, 80, 120 ms, spin-lock frequency = 500 Hz) [4].

Results and discussion: The high resolution maps of T_2 and $T_{1\rho}$ are shown in Fig. 1a and 1c respectively. The depth-wise profile of T_2 (Fig 1b) reveals the laminar structure of cartilage by short T_2 in SZ and RZ and long T_2 in TZ, which could be used to distinguish histologic zones of cartilage. The depth-wise profile of $T_{1\rho}$ (Fig. 1d) shows a decreasing tread with highest $T_{1\rho}$ values in the SZ, which indicates weak interactions between water molecules and PGs on the surface. This result agrees with the observation that matrix in SZ has a lower PG concentration than the other zones. A little peak observed in RZ may be due in part to the high chondrocyte density, which could lead to the decrease in PG concentration. The results suggested a role of high-resolution $T_{1\rho}$ map in early PG loss detection.

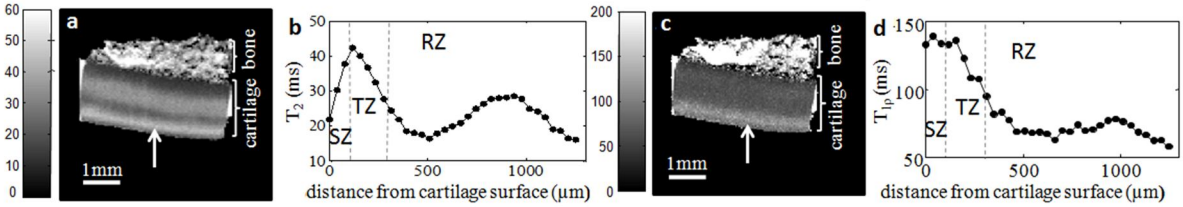

Fig.1 T2 map (a) and T1ρ map (c) and corresponding profiles (b and d) across the cartilage. The profiles were computed by averaging the columns across the cartilage (marked by arrow) over 7 samples.

References:

1. **Buckwalter JA** et al, **Instr Course Lect.** 2005; 54:465-80.
2. Regatte RR et al, **Academic Radiology**. 2002; 9(12):1388-1394.
3. **Hsu EW** et al, **J Magn Reson B.** 1995; 109(1):66-9.
4. Witschey II WR et al, J Magn Reson. 2007; 186(1):75–85.

P21

A Thermally Variable Setup for the Study of Moisture Transport in Silica during Drying under Temperature Gradients at 17.6T

Anna Vilter[a], *Matthias Wiener*[b], *Gudrun Reichenauer*[b], *Volker C. Behr*[a]

[a]Department of Experimental Physics 5 (Biophysics), University of Würzburg, Germany
[b]ZAE Bayern, Bavarian Center for Applied Energy Research, Würzburg, Germany

Highly porous silica is an often applied material in thermal insulation systems. For the understanding of moisture transport in this material it is important to know the redistribution of water under a temperature gradient. A thermally variable setup for a Bruker Avance 17.6T WB system with a 300mT/m gradient unit was designed. The measurement setup consists of a linearly polarized 8-rung high-pass birdcage coil and a temperature cell which serves as sample container and allows to generate a temperature gradient inside the silica (Fig. 1).

A challenge in NMR measurements on silica samples is that most of the included water is adsorbed which leads to very short T_2^* times and a weak NMR signal. For this reason it is necessary that there are no signal-creating materials used for components next to the coil.

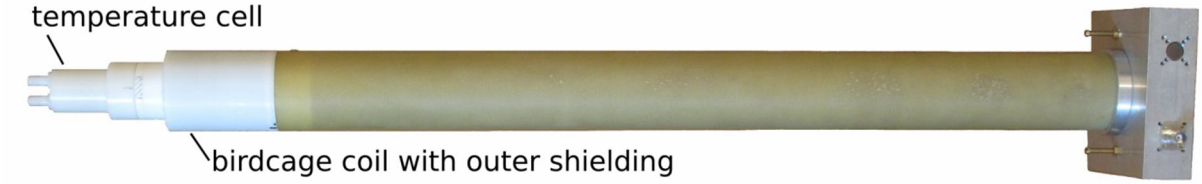

Fig. 1: Thermally variable measurement setup consisting of a probe head with a 8-rung high-pass birdcage coil and a temperature cell. The upper part of the probe base and the body of the temperature cell are made by polytetrafluoroethylene (PTFE) instead of the previously used material polyoxymethylene (POM) because of POM creates a signal as strong as the silica sample. An outer shielding on electrical ground level covers the coil and the tuning and matching network to avoid a coupling of resonator and gradient unit.

The birdcage resonator was fabricated with discrete capacitors soldered on etched copper laminate which was applied on a PTFE tube of 30mm inner diameter. The tuning and matching unit was realized by two variable capacitors. A triaxial balun is used for balancing the voltage in the system and preventing in combination with cable traps sheath currents on the signal cable.

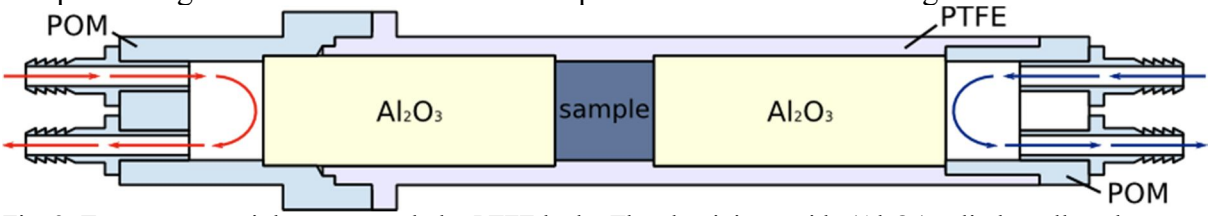

Fig. 2: Temperature unit bases on a tubular PTFE body. The aluminium oxide (Al_2O_3) cylinders allow thermostatting the ends of the sample via two separate thermostats that transport water of defined temperatures.

The temperature unit bases on a tubular PTFE body. Inside the tube a cylindrical sample volume is arranged. The end planes of the probe volume are contacted with two aluminium oxide (Al_2O_3) cylinders. This ceramic material with high thermal conductivity allows controlling the temperature at both ends of the sample using a water circuit (Fig. 2). The high permittivity of Al_2O_3 leads to a frequency shift of 13MHz in the resonator which has to be taken into consideration for the birdcage design.

Preliminary studies have shown the functionality of the temperature cell for temperature ranges from 10 to 60°C. Images of the adsorbed water in silica with the desired resolution of $(0.5mm)^2$ in-plane could be obtained in NMR measurements of a few minutes.

Acknowledgements: We acknowledge Friatec AG Mannheim for the Al_2O_3 samples and our department's machine shop for manufacturing the probe base and temperature cell.

P22

Low-field one-dimensional contrast agent relaxation imaging of bovine articular cartilage

E. Rössler, C. Mattea, S. Stapf

Dep. of Technical Physics II, TU Ilmenau, Germany

The structure of articular cartilage is separated into three layers of differently oriented collagen fibers, described as the arcade model in literature [1]. Furthermore, this kind of tissue exhibits gradients of increasing glycosaminoglycane and decreasing water concentration from the top layer towards the bone interface. The combined effect of these structural variations results in a change of the longitudinal and transverse NMR relaxation times as a function of tissue depth. In this contribution both relaxation times measured in different joints (hip and stifle) of bovine femur bones, using the stray field of a single sided NMR spectrometer (NMR-MOUSE) at a low-field of 0.27T are presented. In order to enhance the relaxation properties in the cartilage, different contrast agents were used. Whereas non-charged contrast agents like Gd(HPDO3A) seem to distribute uniformly through the tissue, charged contrast agents like Gd-(DTPA)2- do not show this behaviour. Due to the negatively charged glycosaminoglycane molecules the Gd-DTPA2- spreads within the cartilage in a spatially inverse relationship to the concentration of the glycosaminoglycanes. Knowing this fact, it is possible to estimate the glycosaminoglycane concentration [2]. In addition, evidence for an orientational dependence of relaxation times with respect to an axis normal to the surface plane could be found. Similar observations have recently been reported in literature using high-field MRI and were explained by preferential orientations of collagen bundles in each of the three cartilage zones [3].

References:

1. Y. Xia, Relaxation anisotropy in cartilage by NMR microscopy (μMRI) at 14-μm resolution. Magn. Reson. Med. 39 (6), 941-949 (1998).
2. A. Bashir, M.L. Gray, D. Burstein, Gd-DTPA2- as a measure of cartilage degradation. Magn. Reson. Med. 36 (5), 665-673 (1996).
3. S. Zheng, Y. Xia, The collagen fibril structure in the superficial zone of articular cartilage by μMRI. Osteoarthritis Cartilage 17 (11), 1519-1528 (2009).

P23

MAS PFG NMR diffusion measurements: handling and application

M. Gratz[a], S. Hertel[a,b], M. Wehring[a], F. Stallmach[a], P. Galvosas[b]

[a]University of Leipzig, Faculty of Physics and Earth Science, Leipzig, Germany
[b]MacDiarmid Institute for Advanced Materials and Nanotechnology, SCPS, Victoria University of Wellington, Wellington, New Zealand

Pulsed Field Gradient (PFG) NMR proved to be a powerful tool for the study of self-diffusion of molecules inside the framework of porous materials without disturbing the system [1,2] For many applications like chemical separation and catalysis it is desirable to know the diffusion behaviour especially of mixtures adsorbed in porous materials. One way to obtain self-diffusivities of mixtures is to analyse the PFG NMR signal under the influence of the pulsed magnetic field gradients separately for corresponding peaks in the spectra. In the case of static NMR experiments this is often impossible because ^{1}H NMR resonance lines of adsorbed species are usually broad and thus impede the separation of individual peaks in the spectra due to likely overlaps, see Fig. 1 (left).

In solid state NMR spectroscopy rapid sample spinning at the magic-angle (θ = 54.7°) is routinely used to reduce line broadening [3]. Following the approach of Pampel et. al [4] we combined a commercial Bruker Micro 2.5 imaging gradient probe with a narrow bore MAS probe to perform NMR diffusometry under MAS conditions.

The aim of this work is to introduce and describe routines that are necessary for the combination of PFG and MAS techniques. We report on protocols for the indispensable sample alignment along the MAS rotational axis and gradient direction by means of an adapted 1D imaging procedure. Gradient mismatches were excluded by time domain measurements incorporating read gradients in standard diffusion pulse sequences. Thus, we were able to reliably obtain the individual self-diffusion coefficients of *n*-hexane and benzene molecules being co-adsorbed in the metal-organic framework MOF-5 [5, 6] as outlined in Fig.1 (right).

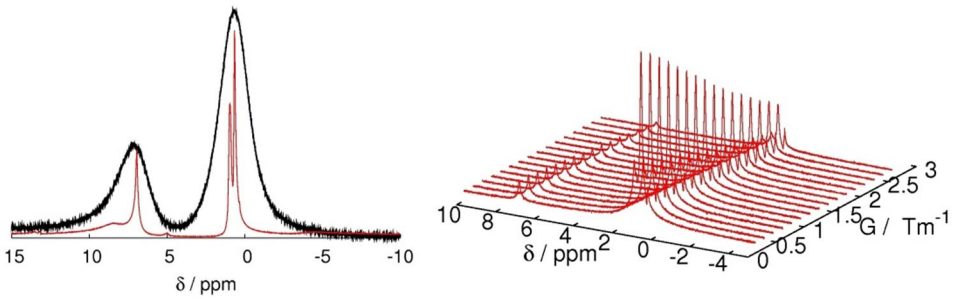

Fig. 1: Left: Comparison of the Fourier transform NMR spectra of n-hexane (δ_{hex} = 1.3 ppm) and benzene (δ_{benz} = 7.2 ppm) absorbed at MOF-5 as obtained with static NMR (black) and MAS NMR (red) measurements. The signal intensities are scaled for better comparability. Right: Fourier transform MAS PFG NMR spectra of *n*-hexane and benzene adsorbed at MOF-5 for increasing gradient strength G.

References:

1. E. O. Stejskal and J. E. Tanner, J. Chem. Phys. 42 (1965) 288
2. F. Stallmach and P. Galvosas, Annu. Rep. NMR Spectrosc . 61 (2007) 51
3. E. R. Andrew, A. Bradbury , and R. G. Eades, Nature 183 (1959) 1802–1803
4. A. Pampel, K. Zick, H. Glauner, F. Engelke, J. Am. Chem. Soc. 126 (2004) 9534
5. H. Li, M. Eddaoudi, M. O'Keeffe, O. M. Yaghi, Nature 402 (1999) 276–279
6. M. Gratz, S. Hertel, M. Wehring, F. Stallmach and P. Galvosas, New J. Phys. 13 (2011) 045016

P24

Microstructure and rehydration behaviour of freeze-dried fruits and vegetables

A. Voda[a], F. Vergeldt[b], G. van Dalen[a], A. Duijster[c], R. van der Sman[b]
L. van Vliet[c], H. Van As[b], J. van Duynhoven[a,b]

[a] AMDM, Unilever Discover Vlaardingen, The Netherlands
[b] Wageningen University, The Netherlands
[c] Quantitative Imaging Group, Delft University of Technology, The Netherlands

Consumers have a high appreciation of healthy meals rich in fruits and vegetables. Lack of convenience in preparing such foods is impeding consumers to reach their recommended daily intake of fibers and nutrients. Food industry has addressed this by developing food products consisting of dried fruits and vegetables that are rehydrated shortly before consumption. The main challenge in this field is to develop products which deliver health benefits and authentic sensory properties without compromising the convenience of fast cooking. So far most developments in this area have been engineering-driven[1].

We have adopted a microstructure-driven research strategy to investigate the structural impact upon freeze-drying of vegetables and to model their rehydration behaviour. Dried and rehydrated microstructures were assessed in a multi-scale manner (nm-mm) by means of complementary imaging techniques like SEM, µCT and MRI, as it is intuitively shown in Fig. 1A. Quantitative image analysis revealed the pore space topology in the dry state and NMR diffusometry and imaging allowed us to determine the cell walls behaviour upon wetting. Water kinetics during rehydration was studied in real-time and in situ by means of RARE imaging[2]. An example of a time series of 2D longitudinal images revealing the rehydration process of a freeze-dried carrot is shown in Fig. 1B.

Microstructural information was used for the development of a novel model for rehydration, which goes deeper than traditionally used ones for mass transport in porous media[3]. The model considers water dynamics via capillary suction in combination with swelling of the cell wall material. Ultimately, the model will be verified by spatially-resolved moisture profiles acquired by MRI.

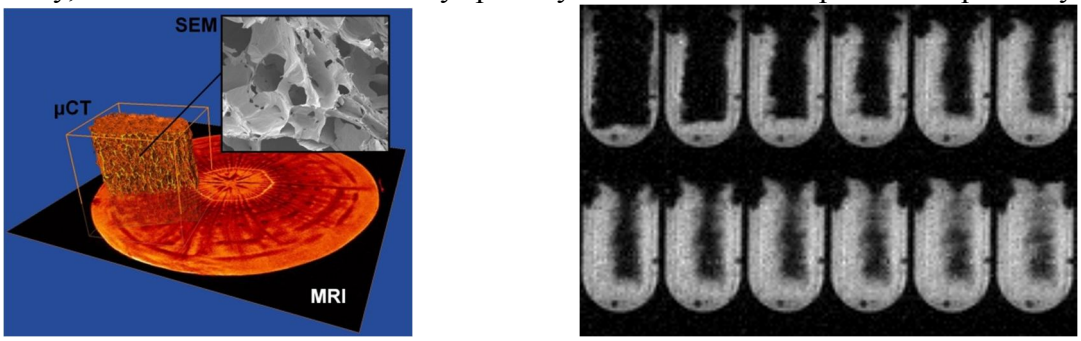

Fig. 1: A) Multi-scale imaging approach employed to assess the microstructure of fruits and vegetables. B) Time series of 2D images (RARE, 1mm slice, 219 µm resolution, 12 s/image time resolution) acquired during rehydration process of a dried carrot piece.

References:

4 K.S. Jayaraman and D.K. Das Gupta, Handbook of Industrial Drying, CRC Taylor & Francis, NY, 2007, 605-633.
5 T.W.J. Scheenen, D.v. Dusschoten, P.A. de Jager, H. Van As, J. Magn Reson., 142, 207-215.
6 A.K. Datta, J. Food Eng. 80(1), 2007, 80-95.

P25

Natural porous media investigated with low-field NMR

A. Haber[a], S. Haber-Pohlmeier[a] and B. Blümich[a],

[a] Institute of Technical and Macromolecular Chemistry, RWTH Aachen University, Worringerweg 1, 52074 Aachen, Germany;

Mobile NMR has its origin in well-logging. By now there are numerous applications of mobile NMR in materials analysis and chemical engineering where, for example, unique information about the structure, morphology and dynamics of matter is obtained, and new opportunities are provided for geo-physical investigations.[1] In particular, dynamic information can be retrieved by two-dimensional Laplace exchange NMR, where the initial NMR relaxation environment is correlated with the final relaxation environment of molecules migrating from one environment to the other within a so-called NMR mixing time t_m.[2]

Relaxation-relaxation exchange experiments were performed with saturated [3] and un-saturated soil samples at low field with a simple, homemade, portable Halbach-Magnet. By executing such exchange experiments for several mixing times and inverting the results to 2D T_2 distributions (reminiscent of joint probability densities of transverse relaxation times T_2) with the help of the inverse 2D Laplace Transformation (ILT), we observed characteristic exchange processes: Soils consisting mainly of silt and clay components show predominantly exchange between the smaller pores at mixing times of some milliseconds. There exists also weaker exchange with the larger pores observable for longer mixing time. In contrast to that fine sand exhibits 2D T_2 distributions with no exchange processes which can be interpreted that water molecules move within pores of the same size class. The results from fully saturated samples are compared to exchange at different saturation levels.

References:

1. B. Blümich, J. Mauler, A. Haber, J. Perlo, E. Danieli, F Casanova, Petroleum Science 6 (2009) 1-7.
2. K. Washburn, P.T. Callaghan, Physical Review Letters 97 (2006) 175502.
3. A. Haber, S. Haber-Pohlmeier, F. Casanova, B. Blümich, Vandose Zone Journal 9 (2010) 1-5.

P26

^{27}Al NMR thermometry of an operating catalytic reactor

A.A. Lysova[a,b], I.V. Koptyug[a], A.V. Kulikov[b]

[a]International Tomography Center SB RAS, Novosibirsk, Russia
[b]Boreskov Institute of Catalysis SB RAS, Novosibirsk, Russia

The occurrence of an exothermic reaction in a fixed catalyst bed can result in a hot spot formation, reactor overheating and even reactor runway. The number of *in situ* techniques capable of providing the data on the temperature distribution and heat transfer processes in the catalyst bed in the course of the reaction is limited [1-3]. In the current work, we propose a new *in situ* NMR imaging method based on the detection of the ^{27}Al NMR signal of a solid phase to map the temperature distribution in the catalyst bed during the exothermic gas phase reaction.

Recently it has been shown that the NMR signal of the solid phase can be detected on a common liquid phase NMR imaging instrument, without application special NMR solid state hardware and techniques [4]. It has been also demonstrated that the NMR signal intensity and the T_1 relaxation time of ^{27}Al of alumina exhibit a pronounced temperature dependence [5]. Based on this, a 1D NMR thermometry of an operating catalytic reactor has been performed [3]. The spatially resolved axial 1D profiles of the ^{27}Al NMR signal intensity of Al_2O_3 in the course of a propylene hydrogenation have been detected and a clear correlation between the signal intensity and the catalyst temperature have been obtained.

The work has been continued in the current investigation. A special reactor allowing one to perform a highly exothermic reaction (hydrogen oxidation) inside the NMR imaging instrument has been designed. The 2D ^{27}Al NMR images of a catalyst pellet (4%Pt/γ-Al_2O_3) have been detected in some stationary regimes characterized by a different rate of a hydrogen supply under conditions of a constant air supply rate. These 2D images were then recalculated into the temperature maps by the use of a special calibration curve. The obtained in such a way 2D maps show a significant temperature gradient inside the catalyst pellet in a radial direction bound with a non-symmetrical placement of the catalyst pellet in the reactor.

The obtained results show the perceptivity of the application of the NMR thermometry based on the detection of the ^{27}Al NMR signal of the solid phase for the *in situ* investigations of the heat transfer in the functioning catalytic reactors.

Acknowledgement. A.A.L. and I.V.K. thank the RAS (grant 5.1.1), the SB RAS (integration grants 67 and 88), the RFBR (11-03-93995-CSIC_a) and the Ministry of Education and Science (contract # 02.740.11.0262) for financial support of this work. A.A.L. acknowledges the SB RAS (Lavrentiev grant for young scientists) and the Council on Grants of the President of the Russian Federation (MK-2492.2011.3).

References:

[1] M. T. Reetz, M.H. Becker, K.M. Kuehling, A. Holzwartz, Angew. Chem. Int. Ed. 37 (1998) 2647.
[2] L.F. Gladden, F.J.R. Abegão, C.P. Dunckley, D.J. Holland, M.H. Sankey, A.J. Sederman, Catal. Today 155 (2010) 157.
[3] I.V. Koptyug, A.V. Khomichev, A.A. Lysova, R.Z. Sagdeev, JACS 130 (2008) 10452.
[4] I.V. Koptyug, A.A. Lysova, R.Z. Sagdeev, V.A. Kirillov, A.V. Kulikov, V.N. Parmon, Catal. Today 105 (2005) 464.
[5] I.V. Koptyug, D.R. Sagdeev, E. Gerkema, H. van As, R.S. Sagdeev, J. Magn. Reson. 175 (2005) 21.

P27

Designing Halbach magnets for the unilateral NMR based on genetic algorithm

Pan Guo, Zheng Xu, Wei He

College of Electrical Engineering, Chongqing University

This paper proposes an inverse method of designing magnets for unilateral NMR. Basic on the analytic expression[1] of the magnetic field distribution of the rectangle magnet, the magnetic field of five Halbach magnets[2] of the same size whose centers are in a straight line could be calculated by the affine coordinate transformation[3], and the magnetizations directions of magnets are shown in Fig. 1. In order to make the uniformity of the total magnetic field along z axis to be minimum, the genetic algorithm is used to attain the optimal combination of magnetization directions.

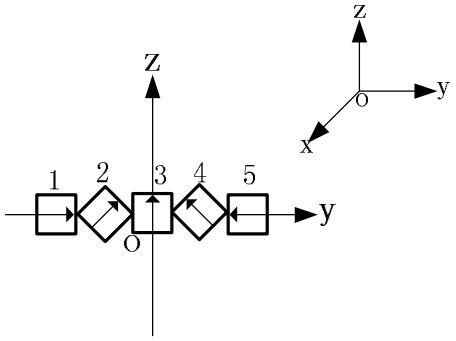

Fig. 1: the magnetization directions of magnets

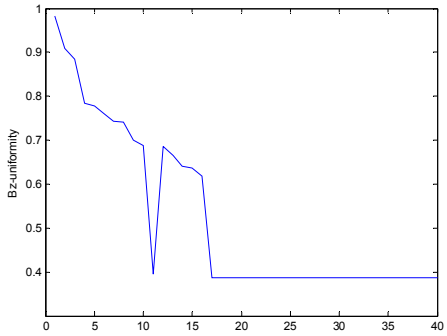

Fig. 2: the search result of genetic algorithm

The variable range of 2,3,4 magnets' magnetization directions are [-15°,15°], the 1 magnet is [-15°,0°], and the 5 is [0°,15°]. The search result of genetic algorithm is shown in Fig. 2. The comparison of uniformity is in table 1, and the calculation equation of uniformity is as following:

$$B_Z\_uniformity = \frac{\max(B_Z) - \min(B_Z)}{B_Z\_center} \quad (1)$$

Table 1: the comparison of uniformity

	α1	α2	α3	α4	α5	Bz_uniformity
before optimizing	90	45	0	-45	-90	0.8042
after optimizing	89	50	15	-54	-81	0.3875

This method has just provided a rough approach for designing magnets of unilateral NMR. In the future work, we intend to take the size, position and magnetization directions of magnets as the optimum parameters. Meanwhile, the active shim could be used to reduce the uniformity of the magnetic field.

References:

1 Gou Xiaofan, Yang Yong, Zheng Xiaojing. Analytic expression of magnetic field distribution of rectangular permanent magnets. Applied mechanics and mathematics. Vol.25, no.3, Mar.2004

2 Chen JH.Raich,P.Blumler. Design and construction of a Dipolar Halbach array with a homogeneous field from identical bar magnets:NMR mandhalas[J]. Magnetic Resonance Engineering, Vol.23B(1)16-25(2004)

3 You Chengye. analytic geometry. Peking University Press

P28

A high pressure setup to examine wood drying at 7T using ^{1}H and ^{13}C NMR in a supercritical CO_2 atmosphere at 20 MPa

Martin W. Schmid[a], *Robert A. Franich*[b], *Hank Kroese*[b], *Roger Meder*[c], *Volker C. Behr*[a]

[a]Department of Experimental Physics 5 (Biophysics), University of Würzburg, Germany;
[b]Scion, Rotorua, New Zealand; [c]CSIRO Plant Industry, Brisbane, Australia

Fresh green wood can contain large moisture content (mc) compared to its dry weight, so it requires drying before technical or industrial use. E.g. the mc of sapwood of radiata pine (*Pinus radiata* D. Don), a commonly used lumber, is often in the range 150-200% [1].

The Franich-process™[1], a new method of wood-drying using supercritical CO_2, was investigated by $^{1}H/^{13}C$-NMR. For this purpose, a dedicated double-resonant birdcage-coil for ^{1}H and ^{13}C was built. Furthermore, a new NMR-suitable, non-ferromagnetic pressure-cell was developed based on the experiences of [2] for examining wood-samples at a maximum pres-sure of 20 MPa. It consists of a PEEK cylinder with accessories of brass (Fig. 1).

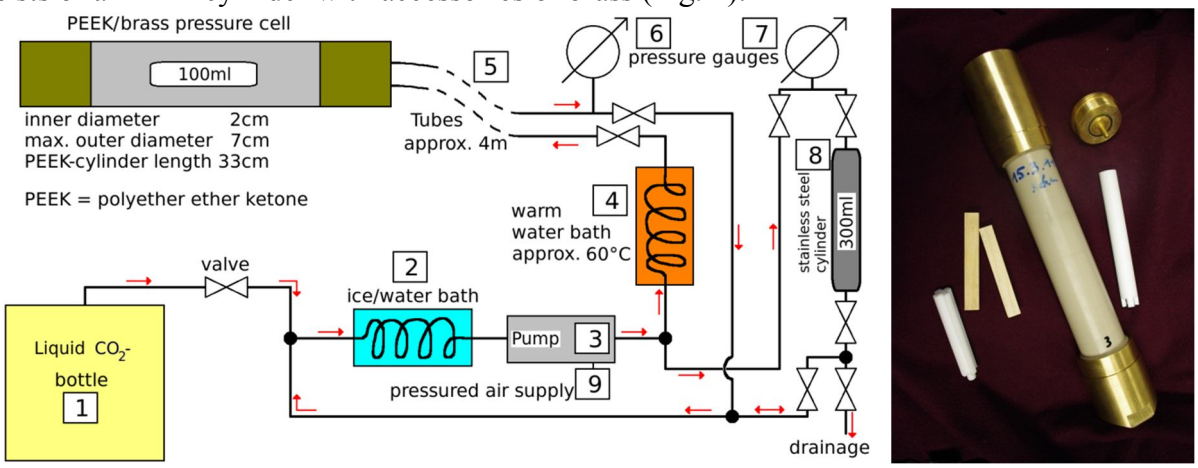

Fig. 1: Left: schematic view of the high pressure setup. Liquid CO_2 is taken from the bottle (1) and kept liquid through the ice/water bath (2) at 0°C and ca. 5 MPa to pump (3) (air-driven by supply (9)), which compresses the liquid into the preheated warm water bath (4), such that the CO_2 reaches the NMR-cell in the supercritical phase, at a maximum pressure of 20 MPa and temperatures above 31°C. The braided pressure tubes (5) are long enough to have all the numbered parts in a sufficient distance to the NMR-scanner (not shown). The pressure gauges (6) and (7) are used to measure the pressures of the CO_2-bottle and the NMR-cell independently. Enriched $^{13}CO_2$ can be stored for re-use in the stainless steel cylinder (8) if necessary. Right: photo of the NMR-cell with two samples of *P. radiata* wood and two teflon-spacers. A sample can be centered inside the container by the spacers to suppress motion artifacts due to gas flow or gradient induced vibration. The cell is hermetically sealed by its end piece that includes a receptacle for a sensor for monitoring temperature during the experiment.

The setup yielded high-resolution ^{1}H-images of the water distribution inside the samples, ^{13}C-spectra as well as ^{13}C-CSI-images using natural abundance CO_2. The use of enriched $^{13}CO_2$ will increase SNR and shorten acquisition times in the ^{13}C-studies.

Acknowledgements: We acknowledge our machine shop's support in manufacturing the pressure-cell.

References:

1. R. A. Franich, S. S. Gallagher, H. W. Kroese: "Improvements relating to wood drying" International application published under the patent cooperation treaty (PCT), International Publication Number: WO 2008/091163 A1, International Publication Date: 31 July 2008
2. W. Behr, A. Haase, G. Reichenauer and J. Fricke: "High-pressure autoclave for multipurpose nuclear magnetic resonance measurements up to 10 MPa" Rev. Sci. Instrum. **70**, 2448 (1999); doi:10.1063/1.1149775

P29

A Novel DWI Sequence and a Controllable MRI Phantom for Obtaining and Validating DWI Data in Moving Media

R.Z. Freidlin[a], J.W. Kakareka[a], T.J. Pohida[a], M.E. Komlosh[b], and P.J. Basser[b]

[a]Division of Computational Bioscience, Center for Information Technology
[b]Section on Tissue Biophysics and Biomimetics, Eunice Kennedy Shriver National Institute of Child Health and Human Development, National Institutes of Health, United States

Motion artifacts are a serious confound for phase and amplitude MRM studies. In phase MRM, motion causes phase offsets and phase wrap-around, distorting measured displacement and velocity maps. In amplitude MRM, velocity distributions and intravoxel shear lead to signal loss, e.g., in diffusion MRM, velocity shear within a voxel causes signal attenuation that appears like diffusion ("pseudo-diffusion"). To reduce sensitivity to bulk and shear velocity distributions, we propose a DWI sequence that utilizes a single bipolar PFG pulse within a spin echo sequence, rather than a pair of PFGs, thus shortening the diffusion time. We demonstrate the improvement of this sequence with a novel MRI moving phantom.

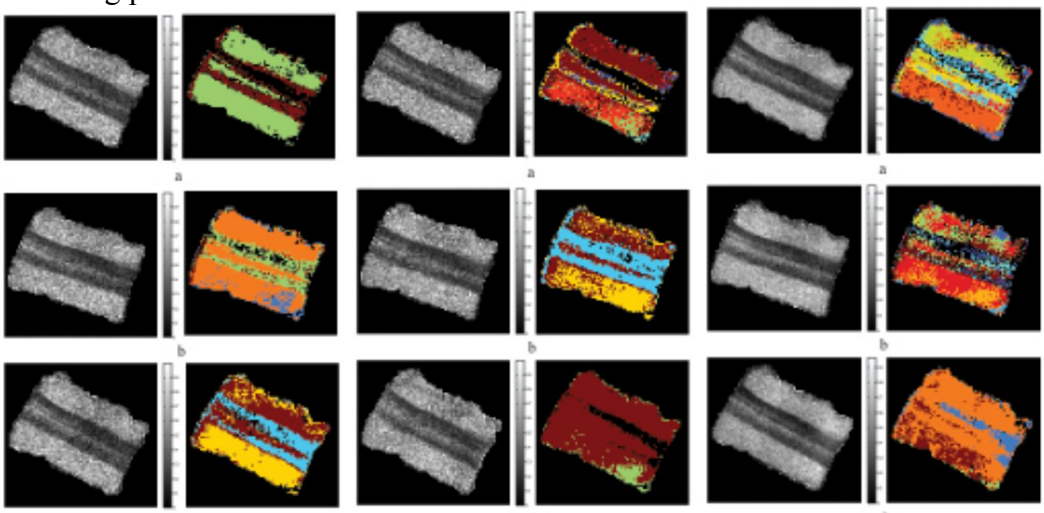

Fig. 3 SS-BP: a) no rotation; b) rotation w/o delay; c) rotation w/ delay

Fig. 2 BP: a) no rotation; b) rotation w/o delay; c) rotation w/ delay

Fig. 1 ST: a) no rotation; b) rotation w/o delay; c) rotation w/ delay

We modified the Bruker Rheo-NMR[1], so that its shaft and fixture can exhibit arbitrarily complex, jerky motions. A custom module to prescribe shaft rotation waveforms uses a trigger input, with "motion-less" periods. Excised pig spinal cord was scanned in a modified cell. Stejskal-Tanner [2] (ST), bipolar [3] (BP) and single-sided bipolar (SS-BP) DWI SE sequences were used. DWIs were acquired: 1) without rotation; 2) with rotation at 1Hz and with diffusion gradients synched with the pause in motion (no delay); and 3) with rotation at 1Hz and with diffusion gradients delayed by 2ms with respect to the pause.

Although, the Fractional Anisotropy (FA) maps for all three sequences (gray scale) do not show significant differences, the average FA in white matter was biased, underestimated by approximately 0.1 for ST DWIs acquired with motion and a 2ms delay. The number of tissue clusters with similar DTI properties, identified by a multivariate hypothesis testing clustering algorithm, was reduced from 8 to 4 (color maps) for ST DWIs in presence of motion and a 2ms delay. A BP DWI sequence had a similar response to jerky motions with the reduction of identified clusters from 7 to 2. The newly proposed SS-BP DWI showed consistent results for motion and no-motion experiments.

References:

1. P. T. Callaghan, Rep. Prog. Phys. 62 (1999)
2. E. O. Stejskal, JE Tanner, J Chem. Phys. 42(1)(1966)
3. X Hong, WT Dixon, J Mag. Res. 99 (3) (1992)

P30

Compact magnet design with significantly reduced eddy currents based on ferrite material

R. Kartäusch[a], T. Drießle[a] , S. Wintzheimer[a] , M. Ledwig[a] , P.M. Jakob[a,b] and F. Fidler [a]

[a]Research Center Magnetic-Resonance-Bavaria (MRB), Wuerzburg, Germany
[b]Department for Experimental Physics 5 (Biophysics), University of Wuerzburg, Wuerzburg, Germany

Introduction: Applications requiring fast and strong gradient switching like flow measurements are in general disturbed by eddy currents. Active shielding of the gradients result in a less compact design with reduced energy efficiency. In this work a compact magnet is presented with significantly reduced eddy currents. It is based on non conductive ferrite material and a compact magnet design.

Materials and methods: The magnet consists of two opposite pole plates made from ferrite material and two blocks of permanent NdFeB magnets as shown in figure 1. Size of the magnet is 10 cm * 10 cm * 6 cm, with a gap of 2 cm and a field of view of 1 cm³ in the center with a field strength of 195 mT. It contains an unshielded gradient system with a maximum gradient strength of 230 mT/m. It contains a solenoid coil with a length of 1 cm and a diameter of 1 cm. Additionally, a mechanical shim system was implemented, consisting of two in two directions(x-z) adjustable iron rods. A design has been chosen to increase the distance between the conducting material, the iron rods and NdFeB magnets, and the gradient system. A spin echo sequence with strong gradients that are full reversed before acquisition is used to estimate the influence of eddy currents. Additionally flow measurements were performed in a 4 mm tube. Signal was received with a homebuilt mobile MR-unit.

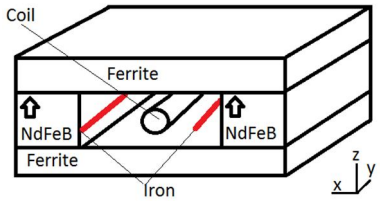

Fig. 1 Schematic of a novel compact magnet. A mechanical shim is implemented by adjusting the two iron rods in x-z direction

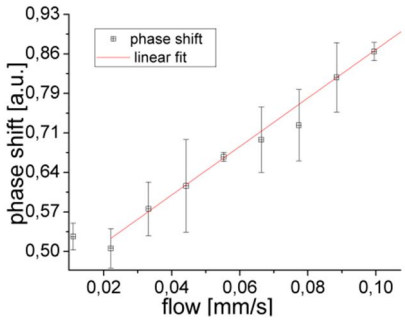

Fig. 2 Correlation of water flow to phase shift. The resolution of 0.03 mm/s is mainly limited by the pump error

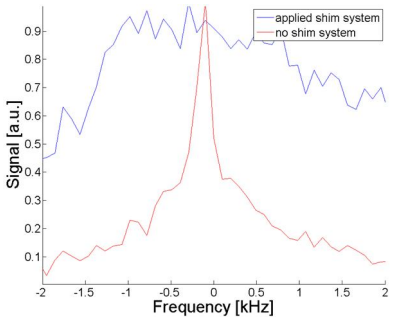

Fig. 3 Spectra of the magnet with/without applied shim system. Field homogeneity can be adjusted to 26 ppm using the shim system.

Results: Field homogeneity in the compact magnet can be adjusted to 26 ppm on 1 cm³ (figure 3). The spin echo sequence with full reversed gradients shows considerably less disturbance by eddy currents, compared to the results of the measurement with a comparable magnet with conventional iron pole shoes. Flow measurements using a flow encoding gradient of 100 mT/m switched in 200 µs show excellent between correlation measured phase shift and given flow. Flow velocities down to 0.025 mm/s can be detected with a mainly pump based error of 0.03 mm/s (figure 2).

Conclusion: The compact magnet allows fast switched gradients at high strength with no disturbance by eddy currents. Active shielding of the gradients is not necessary if the non conductive ferrite material is used. Measurement of water flow with a resolution of 0.03 mm/s was possible.

P31

Two-dimensional DESIRE implementation at ultra high field

I.O. Jelescu, N. Boulant, D. Le Bihan and L. Ciobanu

NeuroSpin, CEA Saclay

Higher field and gradient strengths bring the full implementation of the DESIRE (Diffusion Enhancement of SIgnal and REsolution) technique[1] within reach. Previous achievements include the 1D observation of this effect and the first DESIRE 2D image (i.e. each voxel being the difference between overall sample signal with and without saturation at that location) with a resolution of 100 microns[3]. Here we report on the implementation of DESIRE with higher spatial resolution and enhancement level.

Materials and methods: Spiral-shaped gradient waveforms and RF pulses necessary for the localized saturation were generated using custom-written Matlab (The MathWorks) scripts. MR imaging was performed in a 17.2 T horizontal magnet (Bruker BioSpin) equipped with gradients of up to 1 T/m and using a home-built microcoil as RF transceiver. The phantom was a glass capillary (1 mm ID) filled with silicon oil. The aimed saturation "hole" sizes were 80 μm (pulse length: 8.41 ms for a 1.8 mm FOV) and 40 μm (pulse length: 22.51 ms for a 1.4 mm FOV). The effective saturation holes were imaged with a standard spin-echo sequence following an increasing number of repetitions of the DESIRE pulse.

Results and discussion: Figure 1 shows the resulting 80 μm saturation in 2D, following a train of 1, 2, and 3 DESIRE pulses. The apparent "hole" size increases with the pulse train length due to diffusion in the oil, while signal in the rest of the sample remains unaltered. The full widths at half maximum of the saturation region are 56, 70 and 90 μm respectively.

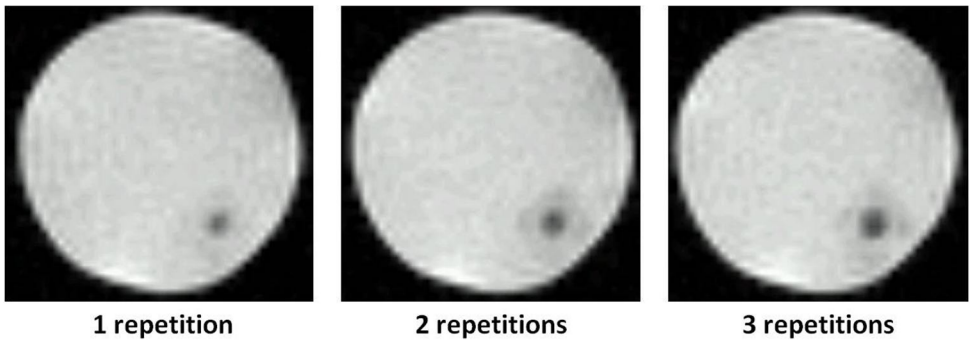

Fig.1: The DESIRE effect is imaged after a 2D saturation over 80μm: the region of no-signal increases due to diffusion.

We have successfully implemented the 2D-DESIRE technique at 17.2 T and observed the expected enhancement from diffusion. Future work will focus on obtaining a DESIRE image with 80 and 40 μm resolution and long pulse trains. Comparing enhancements in oils of various viscosities and at different distances from a barrier should be of great interest.

References:
4. P.C Lauterbur, W.B. Hyslop and H.D. Morris, in XI ISMRC, Vancouver, B.C. (1992).
5. L. Ciobanu, A.G. Webb and C.H. Pennington, J Magn Reson. 170 (2004) 252-6.
6. L. Ciobanu, N. Boulant and D. Le Bihan, EUROMAR 2010, Florence, Italy.

P32

Origin and Applications of Drilling Fluid NMR Technology

Zhizhan Wang, Xinhua Zhang, Wei Zhang and Huangsheng Lu

Sinopec Research Institute of Petroleum Engineering, Room 918, North Star Times Tower, No.8 Beichendong Road, Chaoyang District, Beijing 100101, China, phone +86 10-84988382, pjes@163.com

Magnetic Resonance–Mud Logging (MR-ML) technology analyzing rock sample breaks the ice that mud logging can't quantificationally and rapidly evaluate petrophysics for a long term, breaks through the bottleneck that mud logging technology in existence can't evaluate the distribution of pore fluid, so it gets wide applications in oil fields, and improves the coincidence rate of hydrocarbon zone interpretation. But, with the development of drilling technology and complication of exploration and exploitation, Oil-bearing grade of cuttings and value of gas survey got obviously reduced, weak oil and gas showing have been becoming a wide phenomenon and a challenge for logger. Where is the oil in wellbore after oil layer drilled ? Without a doubt, it exists in drilling fluid, and that is a long-term blank for logging. So we need develop a method to detect the oil content in drilling fluid, and the test results proved NMR technology is the best method.

When using drilling fluid NMR technology, we need to solve such three problems: the first one is to separate the signals of drilling fluid and in-place oil, as we know relaxation time of different oil is also different[1], so in some cases the signals of drilling fluid and oil may overlap; the second one is oil content correction for different property oil, because different property oil has different hydrogen index and NMR response; the last one is how to precisely evaluate the oil content coming from formation when drilling fluid was mixed organic additive such as crude oil, sulfonated gilsonite, etc. On the basis of test, we got the way to solve above-mentioned problems, and make this technology getting mature. This technology fills the gap of mud logging, and perfect mud logging technique series. It is benefits to distinguish the origin of drilling fluid fluorescence or oil in drilling fluid, and can substantially improves drilling efficiency, recognition rate of weak oil showing, accuracy rate of oil and gas layer evaluation, and thus improves the benefits of hydrocarbon exploration and exploitation.

Key words: drilling fluid NMR，oil content, weak oil showing, organic additive, mud logging

References:

1. K.Mirotchnik, K.Allsopp, A.Kantzas. Determination of oil and water compositions of oil/water emulsions using low field NMR relaxometry. Petroleum Society's Canadian International Petroleum Conference 2000, paper 2000-95

P33

Relaxation Exchange NMR and T_2 weighted imaging of Porous Ceramics

Y. Zhang, B. Blümich,

Institute of Technical and Macromolecular Chemistry, RWTH Aachen University

NMR is an important technique for characterizing porous materials, for example, in terms of the surface-to-volume ratio and the pore-size. Our work is focused on characterizing the homogeneity of novel porous ceramics by T_2-T_2 exchange correlation NMR and T_2 weighted imaging of water-saturated samples.

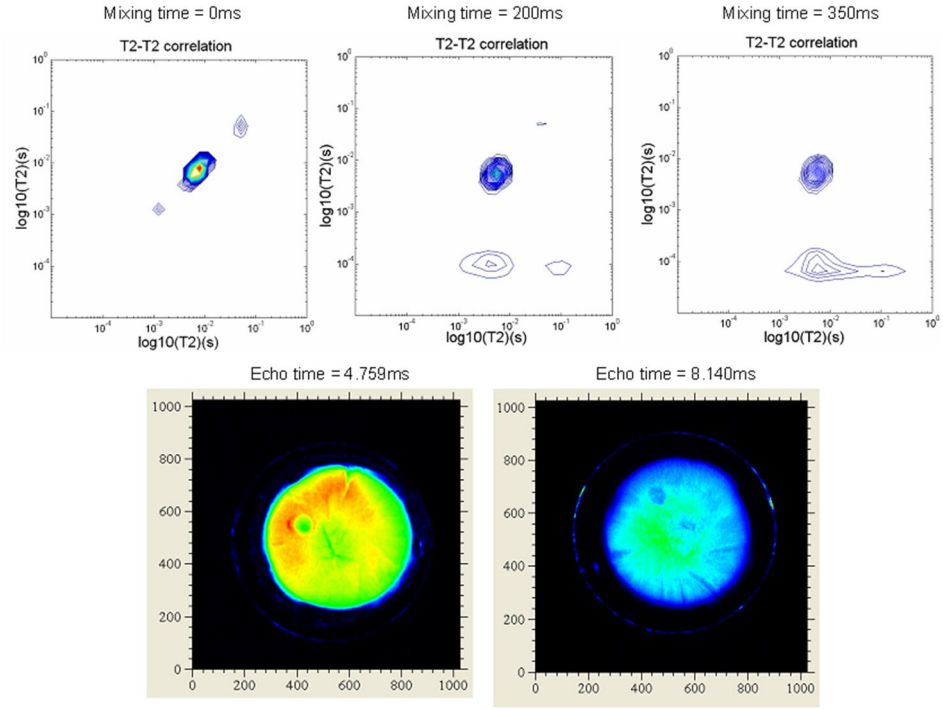

Fig. 1: 2D T_2-T_2 correlation maps for different mixing times and spin-echo images with different echo time of cylinder ceramic sample with diameter of 6.15mm and height of 6.4mm.

In 2D relaxation exchange experiments of the entire sample, asymmetric off-diagonal peaks are observed (Fig. 1), which grow with increasing of mixing time. These peaks indicate the existence of a very weak diagonal peak near 10^{-4} s. NMR imaging reveals that the sample is heterogeneous on the millimeter scale. The center part has longer T_2 than any other part of the sample. From earlier work of Van Landeghem et al [1] it is known that contrary to frequency exchange NMR, diagonal peaks may vanish at short relaxation times due to the combined influence of T_2 and T_1 relaxation during the experiment, and that for more than two exchanging sites the exchange map can become asymmetric. Ongoing work concerns the analysis of the heterogeneity on the mm scale of the pore space mapped by relaxation exchange NMR on the micrometer scale by combining 2D Fourier imaging and Laplace NMR methodologies.

References:

1. Maxime Van Landeghem, Agnes Haber[1], Jean-Baptiste D'espinose De Lacaillerie, Bernhard Blümich, Concepts in Magnetic Resonance Part A 36A(2010) 153.

P34

Estimation of T2-Cutoff Value Based on Relevant CORE Laboratory Data, NMR Spectrometry, Conventional Logs and NMR Logs Data in Malaysian Basin.

W N Safawati W M Zainudin, Masood Akhtar**, M Nizam B M Zain**

* Petronas Research Sdn Bhd, Malaysia
** Orogenic Resources Sdn. Bhd, Malaysia

T2 cut off value plays an important role for the estimation of bulk volume irreducible (BVI) water from NMR logs. The standard T2 cut off value used for clastics (33 ms) is frequently found to be unrealistic for log interpretation due to mineralogy dependent surface relaxivity effects which shift the T2 spectra. Therefore, it is vital to calibrate T2 cut off values with core NMR measurements.

Data Integration of capillary pressure, NMR Spectrometry and the corresponding NMR Logs derived mean values of BFV, Swirr (for each value of T2-Cutoff) have been integrated together and used to generate various graphical plots for the entire NMR logged interval, to estimate the best value of T2 cut off.

Laboratory measurements of T2 cut offs and Swirr based on Sum T2 and Initial Amplitude methods and their comparison with Swirr based on mass considerations. These laboratory T2 cut off values have been used to compute BFV from the NMR Logs data corresponding to each one of these T2 cut off values and then mean values of BFV and Swirr have been computed for the entire logged interval and for reservoir layers. Further to these laboratory measured T2-Cutoff values, three more values of T2-Cutoff, 33, 40 and 50 ms have also been used to compute BFV and Swirr to have a considerable range of variation of T2 cut off values in order to capture the sensitivity of Swirr on the variations in T2 cut off values. The relevant mean value of PHIT_DMR has been used to compute Swirr from the BFV values.

Multiple histograms and cross-plots have also been generated using Swirr computed at various T2 cut off values and compared these different Swirr values with the open hole Swt value to further confirm the new T2 cut off range is more appropriate to be used rather than the industry standard value of 33 ms as used for clastics. The composite display of various water saturation profiles acts as a sensitivity analysis tool for the most appropriate selection of T2 cut off value.

P35

On line NMR monitoring of chemical reactions catalyzed by supported catalysts

Qingxia Gong, Siegfried Stapf

Fachgebiet Technische Physik II / Polymerphysik, Technische Universität Ilmenau, Germany

Heterogeneous catalysts are widely utilized in industrial catalytic processes such as hydrogenation[1], hydroformylation[2] and carbonylation[3] reactions. Heterogeneous catalysis can overcome the drawbacks in homogeneous catalysis which concern the difficulties in separating the reaction products from the soluble catalyst and the solvent, in recovering the catalyst and in applying the reaction system in conventional fixed-bed reactors. These heterogeneous catalytic processes are mostly carried out in fixed-bed reactors under continuous flow conditions, in which the catalysts are packed into a process unit. There are many factors affecting the catalyst activity inside these fixed-bed reactors, including the nature of active metal, support effects, metal-support interactions, active site, the morphology of the catalyst, reaction conditions (temperature, pressure), mass transport properties as well as steric effects[4-6]. Despite the widespread application of heterogeneous catalysts in fixed-bed reactors, our understanding of local variations in molecular transport, flow field and chemical composition in these systems remains limited[7].

In this work PFG NMR methods and NMR relaxometry will be applied to investigate continuous reactions catalyzed by supported metal catalysts in real-time. By the investigation of the catalyst activity and the mass transport properties inside the continuous multiphase reaction, further understanding of the supported metal catalysts in the reaction will be obtained to optimize the catalyst parameters like the metal particle size, distribution and shape. These fundamental studies will promote the design of supported metal catalysts for further industrial applications.

References:

[1] M. Ruta, G. Laurenczy, P. J. Dyson and L. Kiwi-Minsker, *J. Phys. Chem. C* **2008**, *112*, 17814-17819.
[2] M. Haumann, M. Jakuttis, S. Werner and P. Wasserscheid, *J. Catal.* **2009**, *263*, 321-327.
[3] A. Riisager, B. Jorgensen, P. Wasserscheid and R. Fehrmann, *Chem. Commun.* **2006**, 994-996.
[4] J. P. Mikkola, J. Warna, P. Virtanen and T. Salmi, *Ind. Eng. Chem. Res.* **2007**, *46*, 3932-3940.
[5] L. B. Datsevich, *Catal. Today* **2003**, *79-80*, 341-348.
[6] L. B. Datsevich, *Applied Catalysis A: General* **2003**, *250*, 125-141.
[7] D. Weber, D. J. Holland and L. F. Gladden, *Applied Catalysis A: General* **2011**, *392*, 192-198.

P36

Colloid Transport and Biofouling in Model Porous Media

Sarah J. Vogt[a,b], *Hilary T. Fabich*[a,b], *Alexis B. Sanderlin*[a,b], *Sarah L. Codd*[b,c], *Joseph D. Seymour*[a,b]
[a]Department of Chemical and Biological Engineering, [b]Center for Biofilm Engineering, [c]Department of Mechanical and Industrial Engineering

The study of colloid transport and biofouling in porous media is an area of interest across many disciplines, including the modeling of contaminant transport through the subsurface, biomedical filtration and the delivery of drugs through body tissue. Biofouling of porous media begins with deposition of colloidal microbes within the pore structure and the presence of biofilm in turn impacts the transport of colloids such as precipitated uranium and therapeutic proteins or nano particulate drugs. Understanding the mechanisms of deposition and resuspension of colloids during flow through porous structures is an important area of research in the context of understanding the impact of microscale dynamics on macroscale transport. This research focuses on direct measurement of colloid dynamics by NMR in model porous media. Polymer core shell microcapsules with either perfluorodecalin oil or hexadecane oil encased within a poly(methylmethacrylate) shell are used in this study. For the perfluorodecalin oil particles, the fluorine NMR signal from the oil can be obtained separate from the hydrogen NMR signal, allowing the analysis of the dynamics of the suspending fluid and the colloidal particles separately without the issue of resonant frequency overlap which occurs for hexadecane oil as the core fluid. For the hexadecane oil particles, the signal from the particles and the fluid may be separated using the difference in chemical shift or difference in T_2 between the oil within the particles and the suspending water phase. Two dimensional propagator-T_2 correlation experiments[1-3] have been developed and are used to study the separate dynamics of the particles and the suspending fluid. As the particles are deposited in the pore network of a porous media, the change in the pore size distribution impacts the T_2 distribution of suspending fluid within the porous media. The measurement of the translational dynamics from the propagator for each T_2 population quantifies the impact on the pore scale dynamics of colloidal deposition.

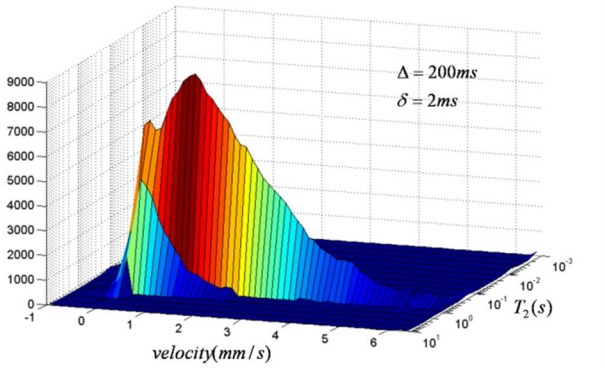

Fig. 1: 2D propagator-T_2 correlation for water flowing through a 240 m diameter polystyrene bead pack with average velocity of 1.77 mm/s.

References:
1. M.M. Britton, R.G. Graham and K.J. Packer, Journal of Magnetic Resonance **169** (2) 203-214 (2004).
2. K.E. Washburn and P.T. Callaghan, Journal of Magnetic Resonance **186** (2) 337-340 (2007).
3. J. Mitchell *et al*., Journal of Magnetic Resonance **193** (2) 218-225 (2008).

P37

Quantitative MRI studies of Controlled Drug Delivery Systems

Chen Chen, Lynn F. Gladden, and Mick D. Mantle

Department of Chemical Engineering and Biotechnology, University of Cambridge, Pembroke Street, Cambridge, CB2 3RA, UK

In recent years, MRI has proven to be a potent tool in pharmaceutical research. In this area, one major challenge is to acquire quantitative data from fast evolving controlled drug release systems[1]. In this study, a state-of-the-art ultrafast preconditioned RARE imaging sequence[2] developed in our laboratory was utilized to study the dissolution process of various formulations of hydroxypropylmethyl cellulose (HPMC) in phosphate buffer solution.

Quantitative maps of absolute water concentration, spin-spin relaxation time and water self-diffusion coefficient are obtained in less than 3 minutes each. A collective analysis of this data gives a thorough overview of tablet dissolution process. For example, figure 1 highlights the need to examine both water concentration and T_2 maps to determine, for example the boundaries of the gel layer which are critical to our understanding of drug mass transfer in such controlled delivery devices.

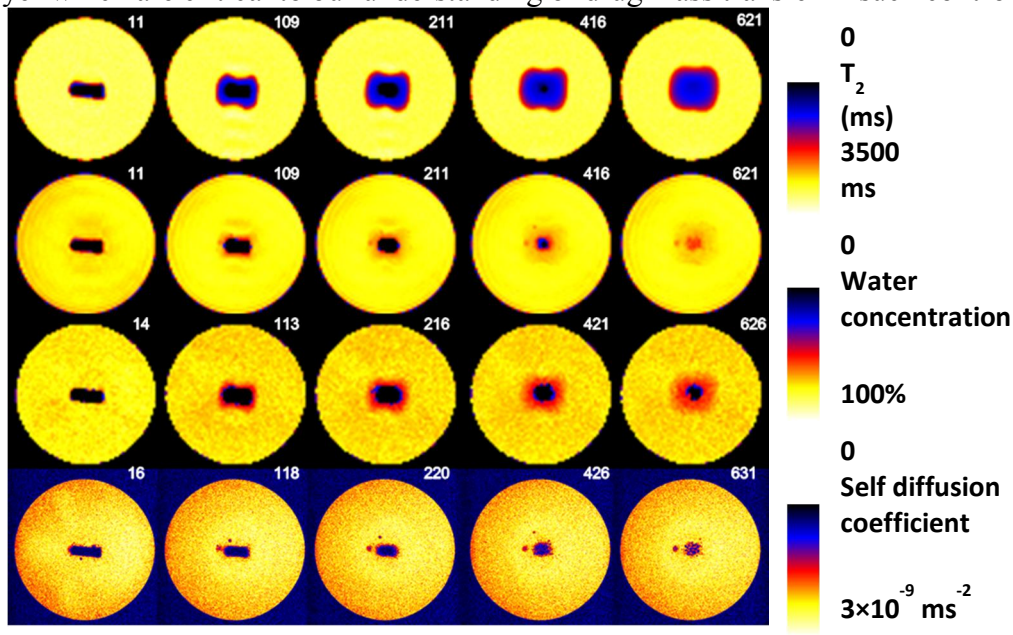

Fig. 1 Quantitative maps of HPMC K4M tablet upon dissolution in PBS pH = 7.4. From top to bottom:(1) T_2 map 2) water concentration map (3) Self diffusion coefficient map (4) Hi-res spatial FLASH image.

MRI experiments were performed for a variety of different HPMC tablets. Our results show that intrinsic polymer properties, such as molecular weight, branching density and particle sizes, greatly affect the swelling and dissolution process of the tablet. Molecular weight regulates the gel layer formation and evolution, which potentially has a great influence on drug release rate. Additionally, we also show that a slight difference in substitution group content contributes to an essential change in gel layer and dry core behaviour. This is attributed to the different polymer particle morphology determined by the strength of molecular interaction.

References:

1. M.D. Mantle, Int. J. Pharm. (2011), doi: 10.1016/j.ijpharm.2010.11.035
2. YY. Chen et al, J. Pharm. Sci. (2010), Vol. 99, 3462-3472

P38

Increased throughput for quantitative high resolution MRI determination of lipid in crop seeds

T. Neuberger[a] *and L. Borisjuk*[b]

[a] Department of Bioengineering, Pennsylvania State Univ., University Park, PA 16802, USA.
[b] Insitute of Plant Genetics and Crop Plant Research, Gatersleben, Germany

The lipid content and its distribution in plants can be characterized in a non destructive way using different techniques including quantitative high resolution magnetic resonance imaging (1). However, the application of the NMR based technologies did not become wide spread. The costs of the high magnetic field strength MRI systems and a very low throughput are the main handicaps of this technique.

We aimed to develop a simple and robust technique with increased throughput and reasonable resolution for the evaluation and the monitoring of oil seed quality. In this study a high magnet field strength (600 MHz, 14,1T) and an original custom designed ceramic resonators (2,3) were used to demonstrate that MRI allows to visualize and quantify the lipid deposition within a number of seeds (>10) in one experiment. As an example, this mid throughput method enables the quantitative 3D mapping of tissue specific lipid distribution within at last 11 rape seeds or more than 30 flax seeds in a single experiment with an isotropic resolution of 20 micrometer (Fig1C). In contrast to already existing NMR/MRI methods, the use of the extended homogenous magnetic field of the dielectric resonator allows a larger number of seeds being imaged in one experiment and hence leads to faster and less expensive non invasive mapping of lipids in seeds. The described approach can be extended to investigation of other varieties of seeds or specimens.

The proposed NMR platform provides an efficient instrument for the investigation of the lipid topology in plant with a high resolution. We suggest that its application for seeds research will facilitate further advances in crops science and biotechnology.

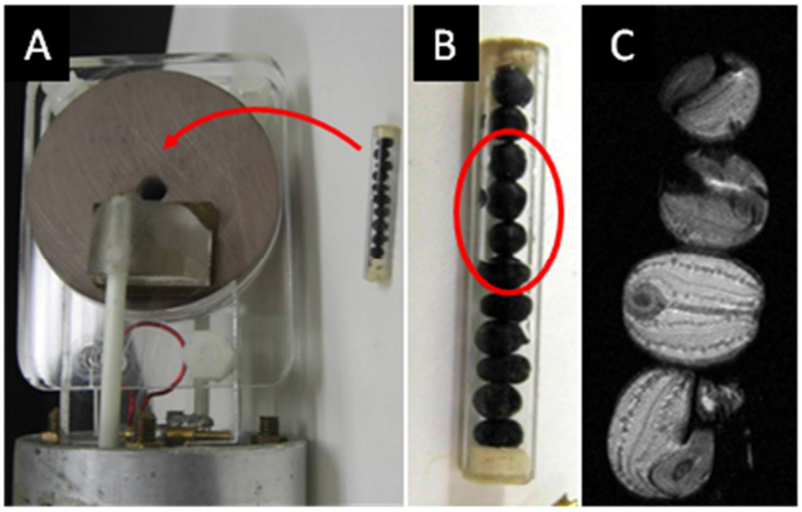

Fig.1: (A) Image of the ceramic resonator with horizontal cylindrical opening for glass tube filled with seeds (arrow). (B) Enlargement from (A) shows 11 seeds within the tube. (C) Fragment of the reconstruction of the 3D dataset of individual seeds demonstrate spatial distribution of oil within the individual seeds.

References:
1. Neuberger T et al: Plant Biotechnology Journal 2008; 6: 31-45.
2. Neuberger T et al: Concepts Magn. Reson. B Magn. Reson. Eng. 33B (2008) 109–114.
3. Haines KT et al: Journal of Magnetic Resonance Volume 200, Issue 2, Pages 349-353.

P39

Local T_2 Measurement Using Spatially Selective Shinnar-Le Roux RF Pulses

S. Vashaee, B. Newling, B.J. Balcom
MRI Research Centre, Dept. of Physics, Univ. of New Brunswick, Fredericton, NB, Canada

Most porous medium are characterized by an inhomogeneous distribution of pore sizes.if the material is fully saturated (filled with fluid) the NMR signal depends on the pore structure, type of the medium and type of the fluid [$1/T_2 \sim (\text{surface/volume})_{\text{pore}}$]. The bulk CPMG sequence measures T_2 based on the signal yielded by the whole sample.

This study uses spatially-selective saturation RF pulses designed by Shinnar-Le Roux algorithm (SLR) [1] followed by the CPMG sequence to measure T_2 for a selected slice of interest. To demonstrate the new technique, two samples with different T_2 were located end to end. In the first step the SLR pulse was applied in the presence of slice select gradients followed by a one dimensional centric-scan SPRITE imaging sequence (known as 1D double half k SPRITE) [2] to check the position of slice of interest. In the second step, the slice selection was repeated, but followed by the CPMG sequence instead of SPRITE to acquire a T_2-signal from the selected slice only. The offset frequency for selective pulse was changed in order to measure T_2 for different slices of interests.

The SLR pulse has the ability to isolate a specific slice through the subject and saturate all the magnetization outside the slice. The spins in the slice of interest are largely untouched (along the +z direction) so the signal will not be distorted due to transverse magnetization decays (T_2 and T_2^* decay). The SLR pulse can easily be designed using the MATPULSE program [3]. This selective saturation approach allows localized assessment of (surface/volume) pore in a variety of porous media without the time cost of a full T_2 mapping measurement.

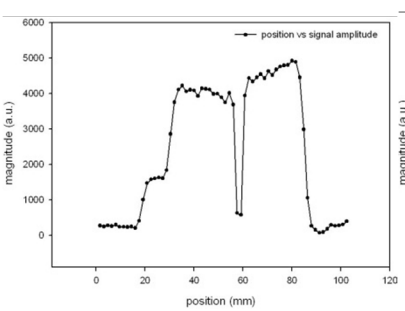

Fig. 1: 1D profile of doped water and doped gel (with $CuSO_4$) end to end, with T_2 s of 870 and 70 ms.

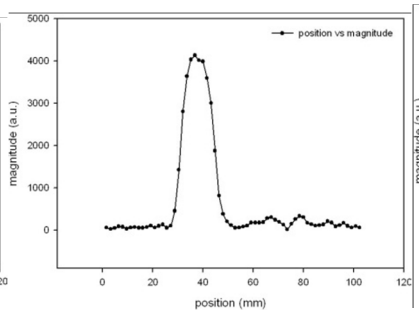

Fig. 2: 1D profile of a selected slice of gel. T_2 for the gel slice was measured to be 84.6±0.3 ms.

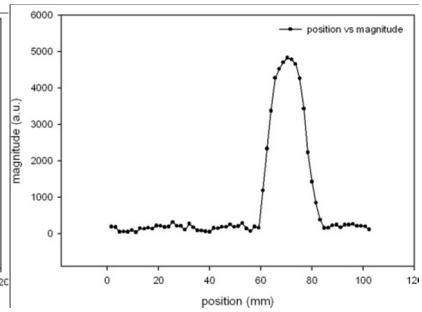

Fig. 3: the 1D profile of a selected slice of liquid. T_2 for the liquid was measured to be 868±1 ms.

References:

1. J. Pauly, P. Le Roux, D. Nishimura, and A. Macovski, IEEE Transactions on Medical Imaging, 10 NO. 1 (1991).
2. M. Halse, J. Rioux, S. Romanzetti, J. Kaffanke, B. MacMillan, I. Mastikhin, N.J. Shah, E. Aubanel, and B.J. Balcom, J. Magn. Reson. 165 (2003) 219.
3. G. B. Matson,, Magn. Reson. Imaging. 12 (1994) 1205.

P40

Comparison of a Solenoid and Scroll Coil Probe at 750 MHz

G. Lykowsky[a,b], *V. Sturm*[a], *and V.C. Behr*[a]

[a]Department of Experimental Physics 5, University of Würzburg, Würzburg, Germany
[b]Research Center for Magnetic Resonance Bavaria e.V. (MRB), Würzburg, Germany

Small RF coils of about 5 mm diameter are commonly used for ultra-high-field microscopy. In this study a classical solenoid coil is compared to a scroll coil (Ref. 1) in matters of field homogeneity, SNR and practical aspects on a 17.6 T Bruker Avance 750WB.

The solenoid coil consists of four turns of heavy silver plated copper wire of 1.5 mm diameter (Fig. 1). The scroll coil is fabricated of two layers of 35 µm copper and about 370 µm Teflon which serves as dielectric (Fig. 1). Both coils have an inner diameter of 5 mm. The solenoid coil has a total length of 8 mm and the scroll coil of 10 mm. The coils are both driven by a capacitive balanced coupling network. B1-maps (Fig. 1) were acquired with an oil phantom to avoid dielectrical resonances. The B1-field strengths are roughly identical at the center of the coils. The B1-maps show the exceptional high homogeneity of the scroll coil compared to the solenoid coil.

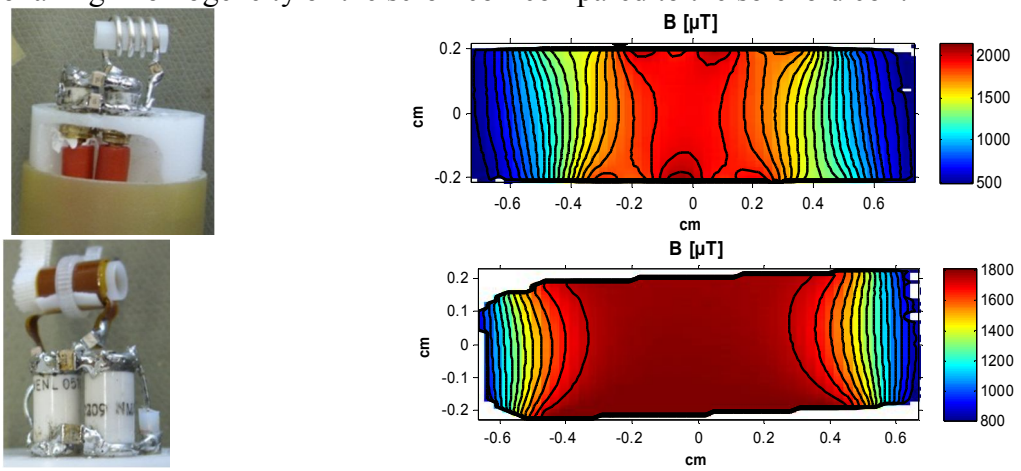

Fig. 1: upper row: The solenoid coil and its sagittal B1-map; lower row: The scroll coil and its sagittal B1-map; The isolines indicate B1-field changes of 4% in relation to the coil center.

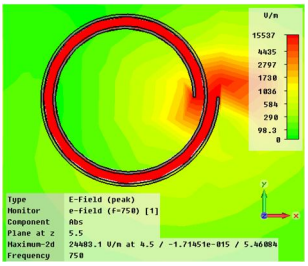

Fig. 2: Simulation of the E-field of a scroll coil

A further drawback of the solenoid coil is its high dielectric losses which result in very high resonance frequency shifts (up to 80 MHz) with different samples. This complicates retuning the coil without changing capacitors. In contrast the scroll coils resonance shifts only a few MHz thanks to its inherent E-field shielding (Fig. 2). The high sample induced losses of the solenoid coil also lead to significant SNR penalties when conductive samples are imaged. For highly ionic saline solutions SNR drops up to a factor of five compared to the scroll coil were observed. In conclusion the scroll coil is a highly efficient and homogenous probe for ultra-high-field hydrogen MRI with distinct advantages over solenoid coils.

References:

1. S.C. Grant et al.: Analysis of multilayer radio frequency microcoils for nuclear magnetic resonance spectroscopy. IEEE Trans. Magn. 37: 2989–2998, 2001.

P41

Non-destructive 3D Pore Modeling using X-ray Computed Microtomography and Nanotomography

Jeff Gelb, Allen Gu, Tiffany Fong, Luke Hunter, S H Lau, and Wenbing Yun

Xradia, Inc. Pleasanton, CA, USA

Modeling of fluid transport properties in geological samples is of increasing importance in recent years. The pore networks inside these samples are very complex, often spanning many different length scales, and few tools exist that are capable of visualizing such features. Among the currently available techniques, x-ray computed microtomography (micro-CT) is increasingly popular, due, in part, to its ability to capture many of these length scales in 3D. Many commercially-available instruments, however, require very small sample sizes for high-resolution imaging, which makes it impossible to simply enlarge a region with single-micron pores for precise analysis without cutting into the sample.

Here, we demonstrate the application of a novel laboratory-based micro-CT system for non-destructive, full length-scale characterization from 100 mm volumes down to 1 μm features. The unique "zoom in" geometry is shown to provide 3D microstructure information down to 1 μm without physically sectioning the sample. Resulting data is analyzed for both porosity and tortuosity, along with other key microstructure parameters (such as pore connectivity), providing unique information for fluid flow models and simulations.

With the introduction of laboratory-based x-ray nanotomography (nano-CT) instruments, new frontiers are being explored in tight sand, shale, and carbonate rocks. We will demonstrate the application of a novel laboratory-based nano-CT instrument for 3D quantitative analysis of these samples with resolution down to 150 nm and beyond. This technology is enabling new developments to be made in studies of samples with very small feature sizes, opening the door to full quantifications of carbonates and shale.

P42

Reduced Field of View Imaging of Long Core Samples Employing Spatially Selective Adiabatic Inversion Pulses

S. Vashaee, B. Newling, B.J. Balcom

MRI Research Centre, Dept. of Physics, Univ. of New Brunswick, Fredericton, NB, Canada

Frequently in MRI one images small samples that fit within the natural field of view and high resolution MRI is possible. In the case of imaging petroleum reservoir core samples and core plugs, the samples of interest may frequently be much longer than the natural field of view defined by the RF probe and region of gradient linearity. Imaging such samples in a typical low field permanent magnet MRI will result in distorted, non-quantitative profiles near the edge of the field of view. In order to solve this problem spatially selective RF pulses are usually used to restrict the FOV to a region of interest (ROI) that is a small portion of the long core sample.

In our measurements, a 22.5 cm Berea core sample was chosen as representative and a spatially selective adiabatic inversion pulse (Hyperbolic Secant pulse) was applied in the presence of a slice select gradient (to invert the spins in the ROI) followed by a one dimensional centric-scan SPRITE imaging sequence (known as double half k SPRITE) [1] to image the inverted slice. The imaging sequence was applied a second time without the ROI selection to image the whole sample. The subtraction of these two image profiles yields an ROI only image and the signals from out of slice parts were completely removed. To design optimum HS inversion pulses, the master equations and numerical analysis were employed as described by Bendall et al. [2]

This approach gives us a uniform and quantitative image of the ROI because spatially selective adiabatic pulses are insensitive to B_1 variation [3]. Spins in the ROI are inverted in a manner that avoids T_2 and T_2^* contrast and minimizes T_1 contrast ($T_1 > T_2$) so as to maintain a density contrast in the final image. Although spatial encoding and excitation are non-ideal near the edges of the FOV, If the non idealities are constant between two scans, excellent ROI profile results. In this measurement, the RF power for the complete inversion of spins in the ROI is only 50% of that required for a hard 90^o pulse.

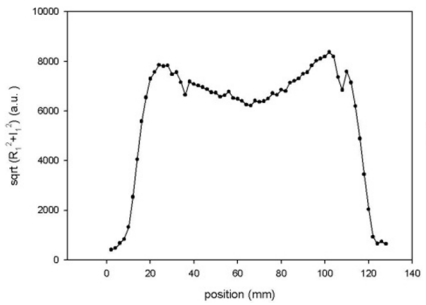

Fig. 1: Berea core 1D magnitude profile

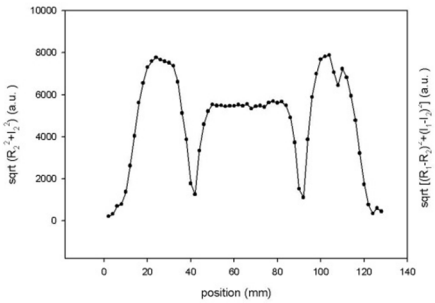

Fig. 2:1D magnitude profile of the Berea core after spatially selective inversion.

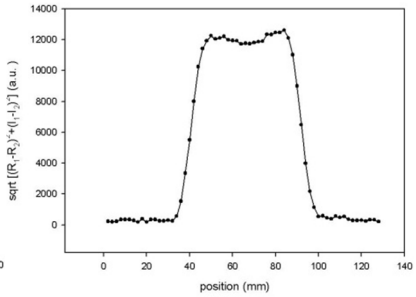

Fig. 3:1D profile of ROI, obtained from subtraction of raw data, in Figures 1 and 2.

References:

1. M. Halse, J. Rioux, S. Romanzetti, J. Kaffanke, B. MacMillan, I. Mastikhin, N.J. Shah, E. Aubanel, and B.J. Balcom, J. Magn. Reson. 165 (2003) 219.
2. Y.A. Tesiram and M.R. Bendall, J. Magn, Reson. 156 (2002) 26.
3. A. Tannus and M. Garwood, MRI in Biomedicine, 10 (1997) 423.

P43

NMR study of complex transport phenomena

Loribeth Q. Evertz[a], *Alexandra Olaru*[b], *Federico Casanova*[b], *and Bernhard Blümich*[b]

[a] Dept. of Mechanical and Industrial Engineering, Montana State Univ., Bozeman, MT, USA
[b] Institute of Technical and Macromolecular Chemistry, RWTH Aachen University, D-542074 Aachen, Germany

NMR is a non-invasive tool that can be used to characterize flows as well as perform relaxation, imaging and spectroscopy measurements. Many of these experiments require the use of high-field magnetic resonance. However, advances in the low magnetic field have led to the development of low field instruments that can carry out many of the required measurements. One benefit of low field NMR is the instruments are portable, making it possible for on-site measurements. In addition, the use of permanent magnets as opposed to super conducting magnets in high-field requires less maintenance and overall is less expensive.

It has already been shown NMR can be used to probe the microstructure of porous media and the associated transport phenomena by means of 2D relaxation and diffusion exchange experiments[1,2,3].

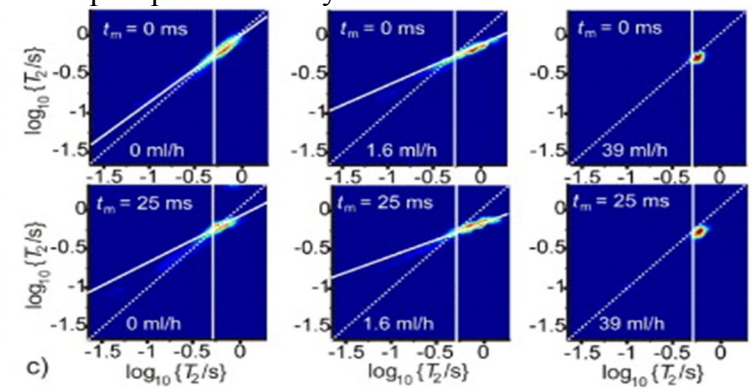

Fig. 1: The distance range probed by relaxation exchange NMR in soil and covered by diffusion is increased by directional flow. The signature of the relaxation exchange of sand maps varies dramatically as the flow rate increases from the equivalent of light rain to heavy rain, reproduced from 4.

Utilizing molecular displacement data obtained in low-field NMR exchange experiments, the main objective of analyzing filtration processes as they occur naturally in soil and biological tissues was achieved. A unidirectional flow of water was applied by means of a pressure gradient through sand columns (using commercially available sands with narrow and broad pore size distributions) to evaluate the water transport.

The 2D T_2-T_2 exchange data processed through ILT showed, with the flow rate increasing, the signature of relaxation exchange from water saturated sand maps varies dramatically. This results in a strong diagonal distribution around a pivot point at slow flow, proportional to the mixing time[4]. The skew of the diagonal distribution was observed previously by Washburn and Callaghan[5] (fig. 1). This appears to be connected to molecular displacements occurring in the inherently long period of signal detection due to diffusion caused by internal field gradients and advection.

At faster rates, the spins were exiting the coil during the detection period. Thus, the diagonal distribution collapses into a single point, located at lower T_2 values compared to previous results. The decrease of the spin-spin relaxation time is directly proportional to the liquid's velocity.

The complexity of the results makes the data difficult to interpret in quantitative terms. However, we believed that by using an adequate mathematical model which takes into account both the diffusive and advection effects the flow-related information can be extracted from such experiments.

References:
1. M. V. Landeghem, et. al. Concepts in Magnetic Resonance Part A Vol 36A (2010) 153-169.
2. L. Monteilhet, et. al. Physical Review E 74 (2006) 061404.
3. Y.-Q. Song, et. al. Journal of Magnetic Resonance 154 (2002) 261-268.
4. B. Blümich, et. al. New Journal of Physics. 13 (2011) 015003.
5. K.E.Washburn, et. al. J.Magn.Reson. 186, (2007) 337-340

P44

Effects of metallic implants on rf and image quality

C. Elschner[a], *U. Scheler*[a],

[a]Leibniz-Institut für Polymerforschung Dresden e.V.

Metal object such as medical implants are known to effect the quality of NMR images. Most attention has been given to the effects of the changes in the magnetic susceptibility and thus the distortion of the magnetic static field and the gradients. Metals give rise to eddy currents, limiting the rise times of gradients.

The present study focuses on the effect of metal objects on the radio frequency field, which influences both the excitation and the detection of the NMR signal. A simple copper plate has been used as a test object, showing the strong dependence of the orientation of the plate with respect to the rf field. Almost no distortion is found when the object is parallel to the linear polarized rf field, while the image is largely distorted by an object perpendicular to the rf field. Strong artefacts and signal amplification is found at the edges.

To overcome such distortions in medical applications, surface patterning has been tested, which drastically reduces the conductivity. A PEEK plate has been coated with a continuous film and a patterned film of almost no surface conductivity. While the complete covered film distorts the image nearly as much as the copper plate, there is negligible distortion from the plate patterned without percolation. The biologic activity of the patterned layer is retained. So an alternative for medical applications has been found as demonstrated in a rat femur. These results are in excellent agreement with simulations.

For larger objects like surgical screws a minimal distance to the region of interest has been determined in our system to be 3 mm.

P45

MAG-PGSTE: a new STE-based PGSE NMR sequence for the determination of diffusion in inhomogeneous samples

G. Zheng, W. S. Price,

Nanoscale Organisation and Dynamics Group, College of Health and Science,
University of Western Sydney, Penrith, Australia

A new stimulated-echo-based pulsed gradient spin-echo sequence, MAG-PGSTE (Fig. 1), has been developed for the determination of self-diffusion in magnetically inhomogeneous samples [1]. The sequence was tested on two glass bead samples (i.e., 212-300 μm and <106 μm glass bead packs). The MAG-PGSTE sequence was compared to the MAGSTE (or MPFG) [2, 3] sequence and Cotts 13-interval [4] sequence using both glass bead samples.

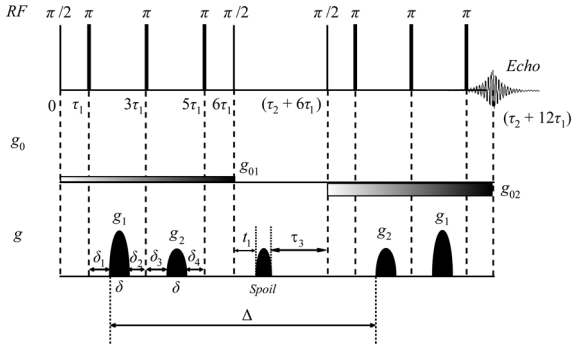

Fig. 1: The MAG-PGSTE sequence with half-sine shaped gradients. The narrow bars represent $\pi/2$ and π *RF* pulses, g_{01} and g_{02} are background gradients, g_1, g_2 and "*Spoil*" are half-sine shaped gradient pulses with different amplitudes.

The MAG-PGSTE and MAGSTE (or MPFG) sequences outperformed the Cotts 13-interval sequence in the measurement of diffusion coefficients; more interestingly, for the sample with higher background gradients (i.e., the <106 μm glass bead sample), the MAG-PGSTE sequence provided higher signal-to-noise ratios (Fig. 2) and thus better diffusion measurements than the MAGSTE and Cotts 13-interval sequences. In addition, the MAG-PGSTE sequence provided good characterization of the surface-to-volume ratio for the glass bead samples.

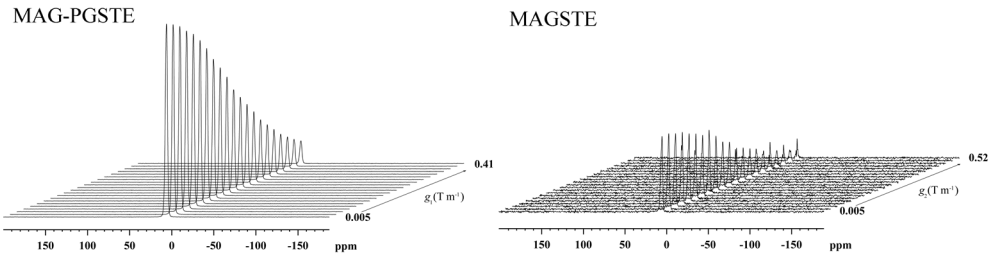

Fig. 2: A series of 500 MHz ^{1}H MAG-PGSTE and MAGSTE spectra on the sample containing $CuSO_4^-$doped water and < 106 μm glass beads.

References:
1. G. Zheng, W. S. Price, J. Magn. Reson. 195 (2008) 40.
2. P. Z. Sun, J. Magn. Reson. 187 (2007) 177.
3. P. Galvosas; F. Stallmach; J. Kärger, J. Magn. Reson. 166 (2004) 164.
4. R. M. Cotts; M. J. R. Hoch; T. Sun; J. T. Marker, J. Magn. Reson. 83 (1989) 252.

P46

Cultural heritage investigated via mobile NMR

A. Haber[a], B. Blümich[a], D. Oligschläger[a], E. Del Federico[b], A. de Vita[c], I. Schaefer[d],

[a] ITMC, RWTH Aachen University, 52074 Aachen, Germany
[b] Pratt Institute, Department of Mathematics and Science, Brooklyn 11205, New York, USA
[c] British School of Rome, 00197 Rome, Italy
[d] Wallraf-Richartz-Museum & Fondation Corboud, Obenmarspforten, 50667 Cologne, Germany

A compact and mobile single-sided ^{1}H NMR sensor, the NMR-MOUSE® [1,2], has been employed to characterize non-invasively the layer structure of historic walls and canvas [3]. Different paint and mortar layers were studied at Villa of the Papyri and Casa di Salone Nero in Herculaneum. Moisture profiles were recorded through the Mosaic of Neptune and Amphitrite, also in Herculaneum, revealing large differences in moisture content of the tesserae and the same moisture content in the supporting mortar [4]. Diffusion measurements were performed in the laboratory on mock up fresco and secco samples with different conservation treatments. A Rembrandt self-portrait was examined to determine the different paint layer structures. These investigations encourage the use of the portable and single-sided NMR technology for non-invasive studies of the layer structure and conservation state of historic objects of art.

References:

1. N. Proietti et al., Journal of Magnetic Resonance 177 (2005). 111-117
2. B. Blümich et al, Journal of Magnetic Resonance 161 (2003) 204-209.
3. B. Blümich er al, Accounts in Chemical Research 43 (2010) 761–770.
4. A. Haber et al, Analytical and Bioanalytical Chemistry, submitted.

P47

Hybrid-SPRITE MRI

Dan Xiao, Bruce Balcom

Physics Department, University of New Brunswick, Canada

In a FID based frequency encoding MRI experiment the central part of *k*-space is not intact due to the probe dead time, which is crucial for image reconstruction. Single point imaging (SPI) gives good quality images as a pure phase encoding technique. SPRITE (single point ramped imaging with T_1 enhancement), SPI with a linearly ramped phase encode gradient, has been used for short relaxation time systems for many years with great success. As it requires high magnetic field gradient strengths, short encoding times, and low flip angle RF pulses to cover the sample bandwidth, the sensitivity (SNR over square root of acquisition time) is sub-optimal. We now propose a new sampling scheme, termed Hybrid-SPRITE, combining phase and frequency encoding to ensure high quality images with reduced acquisition times, reduced gradient duty cycle and increased sensitivity.

The essential idea in Hybrid-SPRITE is to acquire the *k*-space origin data by pure phase encoding and to fill in the *k*-space periphery by frequency encoding. There are intermediate *k*-space points which may be acquired through both methods.

In Hybrid-SPRITE, gradients are ramped in the same fashion as in SPRITE for the first few phase encoding steps, with time domain data collected for the latter *k*-space steps as in FID based frequency encoding. The number of phase encode steps depends on the sample T_2^*. The shorter the T_2^*, the more phase encode steps should be acquired to control T_2^* blurring. 3 to 5 phase encode steps is generally a good choice in a 64 point profile. Because there are much fewer RF pulses than in SPRITE, the relaxation delay between each scan can be shortened accordingly. Larger flip angle RF pulses are possible due to reduced bandwidth and may be employed to increase SNR. Segmenting the nature of *k*-space encoding leads naturally to the idea of differential sampling in other respects, such as increased signal averaging of some portions of *k*-space.

The figure below shows the profile of a saturated Berea core plug from Hybrid-SPRITE experiment.

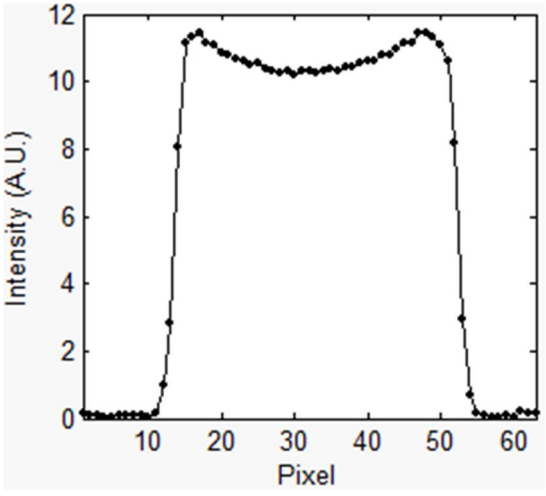

Figure 3: Profile of Berea core plug from Hybrid-SPRITE experiment.

P48

Slice-selective CPMG with DANTE-Z preparation for T_2 mapping in short relaxation time samples

O. V. Petrov[a], *B. J. Balcom*[a],

[a]MRI Research Centre, Physics Department, University of New Brunswick, Canada

A spatially resolved measurement of T_2 (T_2 mapping) is appealing for core analysts due to its ability to probe the occupancy of pores by water and oil phases [1]. It is desirable that a T_2 mapping scheme provides as wide an interval of measurable T_2 as possible for a comprehensive analysis of relaxation data. Ideally, spatially resolved T_2 measurements should yield T_2 distributions of similar quality to bulk CPMG measurements. It is also important to achieve a high SNR, since low field magnets are traditionally used for rock core analysis.

Recently [2], we presented two MRI pulse sequences for T_2 mapping with phase spatial encoding. Although allowing to measure T_2 relaxation at all positions along the sample at a time, these techniques have the drawback of either limiting the measurable T_2 to values greater than 2 ms or being time consuming and giving a poor SNR.

Herein, we present a different technique which is based on slice selective CPMG. To select a slice of interest, we employ a DANTE-Z scheme [3] with a sinc-modulated inverting DANTE selective pulse train. The DANTE-Z scheme leaves only selected frequencies in the resulting signal, even though a regular (non-selective) CPMG sequence is applied after the DANTE pulses. Since the prepared magnetization lies along z axis, it is affected only by T_1 relaxation while waiting for eddy currents to dissipate after applying a slice gradient, which is advantageous for short T_2 samples with $T_1 > T_2$ (typical for water in rocks). For the same reason, DANTE-Z does not introduce any phase problems when combined with another pulse sequence (CPMG) and does not need a refocusing lobe in the slice gradient.

Test measurements conducted on model composite samples and natural water-saturated rocks show it is possible to select a single quasi-rectangular slice of less than 0.8 cm width at an arbitrary position over a 6-cm long sample. The lower limit of measurable T_2 is found to be at least 0.2 ms, which considerably exceeds that accessible with MRI-based T_2 mapping sequences. For homogeneous test samples, T_2 distributions coincide with those by a regular (bulk) CPMG.

The sequence can be, therefore, recommended as a supplement or alternative to MRI-based T_2 mapping techniques for measuring T_2 distributions in samples with $T_2 < 1$ ms (water-saturated reservoir rocks, cement pastes, food products, etc.), especially when T_2 is required to be measured at only few particular positions along the sample and a resolution of ~1 cm is acceptable.

References:

1. G. R. Coates, L. Xiao, and M. G. Prammer, NMR logging: principles and applications Halliburton Energy Services, Houston, 1999.
2. O. V. Petrov, G. Ersland, and B. J. Balcom, J. Magn. Reson. 209 (2011) 39.
3. D. Boudot, D. Canet, J. Brondeau, and J.C. Boubel, J. Magn. Reson. 83 (1989) 428; C. Roumestand, D. Canet, N. Mahieu, and F. Toma, J. Magn. Reson. A 106 (1994) 168.

P49

Dynamic Nuclear Polarization for Studying Coacervate Aggregation

Sandra Garcia,[1] Jeffrey H. Walton,[1] Ravinath Kausik,[2]
Brandon B. Armstrong,[2] Songi Han,[2] Michael J. McCarthy[1]

[1] Food Science & Technology, University of California, Davis, Davis, USA
[2] Department of Chemistry and Biochemistry, University of California, Santa Barbara, Santa Barbara, USA

Overhauser DNP is powerful tool for analyzing water dynamics in samples such as lipids, proteins and coacervate systems. In DNP experiments, the coupling factor between the electron and the nucleus, ρ, dictates the obtainable enhancement. By measuring the coupling factor between water and the electron of a nitroxide spin label placed on the molecule of interest and by invoking the force-free hard-sphere model, a translational correlation time, τ, can be determined. The size of the coupling factor depends on the translational correlation time of the nuclear spin and electron spin; the faster the motion of the two spins the larger the coupling factor. The coupling factor is itself field dependent and can have a maximum value of 0.5 for pure dipolar coupling and -1 for pure scalar coupling.

Overhauser DNP polarizers operating at 0.35 T and 0.04 T have measured coupling factors of 0.22 and 0.39 respectively for 4-oxo-TEMPO dissolved in water [1,2]. A DNP polarizer at a magnetic field of 0.04 T is capable of probing translational correlation times that occur between 0.1–10 ns whereas a polarizer at 0.35 T probes translational correlation times between 0.01–0.5 ns. A coacervate system composed of spin labeled polyaspartic acid or polyvinylimidazole polymers is analyzed at both magnetic fields. At 0.35 T the results in figure 1 show that the coupling factor is ~0.16 above pH 6.5 where polyaspartic acid is negatively charged and polyvinylimidazole is neutrally charged. A similar coupling factor is found below pH 4 where polyaspartic acid is neutrally charged and polyvinylimidazole is positively charged. However, when the pH approaches 5.5 the polymers carry a positive and negative charge and aggregate, causing the coupling factor to go to zero [3]. The same coacervate system gives a coupling factor of 0.06 at pH 4.5 when it is measured at 0.04 T. The coupling factor at 0.04 T shows that a lower magnetic field is beneficial in studying systems whose translational correlation times have slowed past the 0.5 ns.

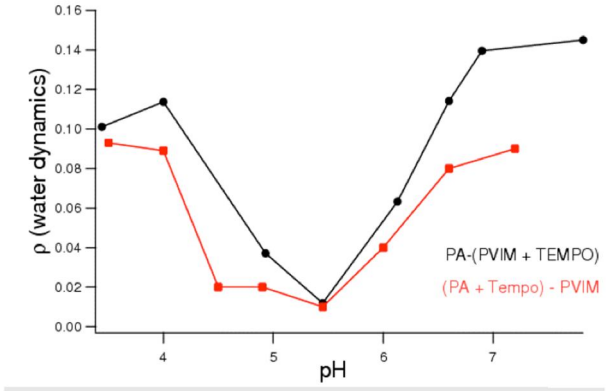

Figure 1: Coupling factor vs. pH at 0.35 T.

References:

1 B.D. Armstrong and S. Han, Overhauser dynamic nuclear polarization to study local water dynamics, *J. Am. Chem. Soc.* **131** (2009), pp. 4641–4647.
2 S. Garcia, J. H. Walton, B. D. Armstrong, B., Han, S-I., McCarthy, M. J., L-Band Overhauser Dynamic Nuclear Polarization, *J. Magn. Reson.* DOI: 10.1016.j.jmr.2009.12.012.
3 R. Kausik, A. Srivastava, P.A. Korevaar, G. Stucky, J.H. Waite and S. Han, Local water dynamics in coacervated polyelectrolytes monitored through dynamic nuclear polarization-enhanced ^{1}H NMR, *Macromolecules* **42** (2009), pp. 7404–7412.

P50

Quantification of internal magnetic field for cylindrical vessel structure

H.S.Jung[a] S.H.Han[a] , Y.K Song[b], G.Cho[b,] Y.-Q.Song[c] and H.Cho[a]

[a] School of Nano-bio Science and Chemical Engineering, UNIST, Ulsan, Korea,
[b] Korea Basic Science Institute, Ochang, Korea,
[c] Schlumberger Doll Research Center, Cambridge, MA,USA.

The orientation and diameter information of micro-vessel is known to provide critical information regarding connectivity and functionality of fibrous tissues. For example, the development of tortuous and dilated micro-vessel is well-known characteristics of tumor angiogenesis.

In this work, we both theoretically and experimentally characterize the nature of internal magnetic field associated cylindrical vessel structure to obtain quantitative information of vessel orientation and diameter.

Figure 1 shows experimental determination of the orientation of randomly packed capillary samples. (A) and (B) show the strength of the experimentally measured internal gradients along the different directions, respectively. (C) overlays both the histogram distribution of the internal gradients. (D) and (E) compared experimentally measured and expected direction of cylindrical axis.

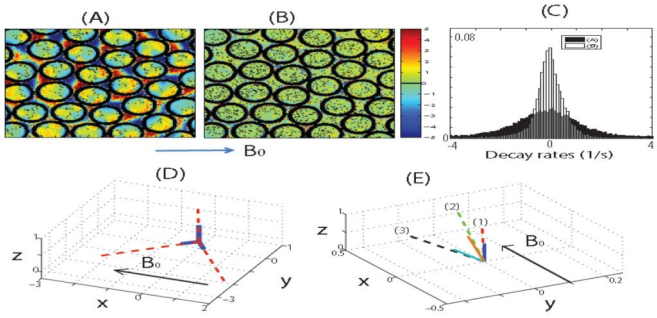

Fig. 1: The determination of long axis for randomly packed cylinders

Figure 2 (A), (B) show calculated 2D internal gradient profiles of two cylinders with different diameter. (C) plots calculated mean and variance of internal gradient distribution as a function of vessel diameter to show strong sensitivity of internal gradient distribution for different vessel sizes.

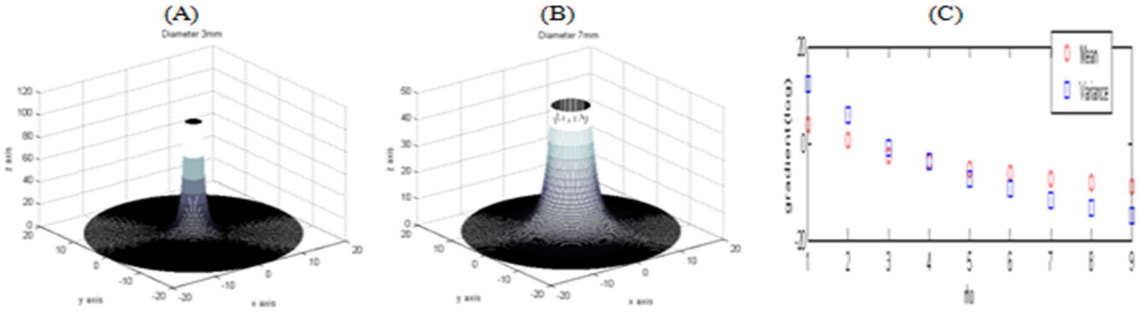

Fig. 2: The sensitivity of internal gradient for different vessel diameter.

References:

1 McDonald, DM, Choyke, PL ***Imaging of angiogenesis: from microscope to clinic***. Nat Med 2003;9, 713-725.

2 H.Cho, S. Ryu, J. L. Ackerman, and Y. Q. Song J. Magn. Reson. 198(1), 88(2009).

P51

2D Relaxation and Diffusion Correlations in Biopolymers

Sarah J. Vogt[a,b], *Hilary T. Fabich*[a,b], *Jennifer R. Brown*[a], *Matthew L. Sherick*[a,b], *Joseph D. Seymour*[a,b] *and Sarah L. Codd*[b,c]

[a]Department of Chemical and Biological Engineering, [b]Center for Biofilm Engineering [c]Department of Mechanical and Industrial Engineering

Two dimensional relaxation and diffusion correlation experiments[1,2] have been performed on biopolymer systems relevant to biomedical and biological materials engineering applications. A primary focus is on alginate biopolymer systems which form physical gels with cations. These gels are candidates for tissue growth constructs[3] due to the ability to spontaneously form structures such as capillaries during diffusive reaction[4] and their role in chronic *P. aeruginosa* infections in cystic fibrosis (CF) patients[5]. The differences in gel structure between algal and microbial produced alginates are investigated. Of particular interest is the difference in gel structure and formation between acetylated alginate formed by a *P. aeruginosa* isolate FRD1 from CF patients and deacetylated alginate from a genetic mutant FRD1153.

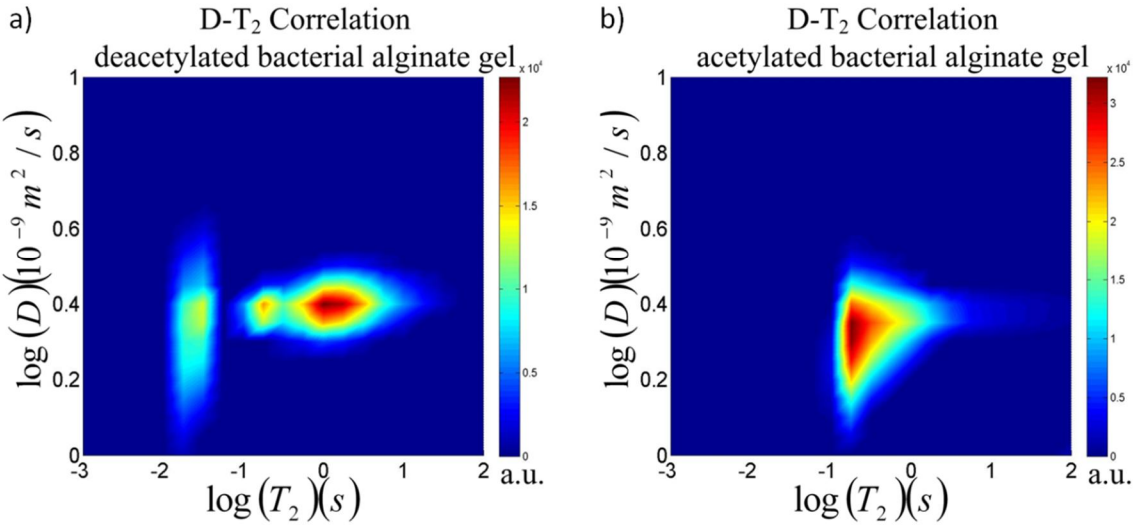

Fig. 1: Diffusion-T_2 spectra of alginate gels formed with 1M $CaCl_2$ from 2%wt. alginate solutions from two different genetic variants of *P. aeruginosa*: a) FRD1153 which produces deacetylated alginate, and b) FRD1 which produces acetylated alginate.

References:

1. P. Galvosas and P.T. Callaghan, Comptes Rendus Physique **11** (2) 172-180 (2010).
2. Y-.Q. Song, Progress in Nuclear Magnetic Resonance Spectroscopy **55** (4) 324-334 (2009).
3. A. Khademhosseini *et al.,* Scientific American, 64-71 (2009).
4. J.E. Maneval, D. Bernin, H.T. Fabich, J.D. Seymour, S.L. Codd, in press Mag. Res. Chem. (2011).
5. S. Sarkisova *et al*., Journal of Bacteriology **187** (13) 4327-4337 (2005).

P52

MRI of Metal Hydrides

Bryce MacMillan[a], Uncharat Setthanan[b], Sean McGrady[b], Bruce Balcom[a],

[a]MRI Centre, Department of Physics, University of New Brunswick, PO Box 4400, Fredericton, NB, Canada, E3B 5A3

[b]Department of Chemistry, University of New Brunswick, PO Box 4400, Fredericton, NB, Canada, E3B 5A3.

With the resurgence of interest in hydrogen and its potential as an energy carrier, much attention has been focused on the challenge of storing significant amounts of hydrogen in a gravimetrically and volumetrically efficient manner. As hydrogen storage media, light metal hydrides are particularly attractive from a safety perspective and because of their high weight- and volume-hydrogen densities.

The technical challenges still to be overcome include the often adverse absorption and desorption kinetics, which are a function of intrinsic reaction rates and practical operating temperatures. Modifying and controlling these kinetics requires a thorough understanding of the hydrogen absorption and desorption processes.

In this study, we have investigated the thermal decomposition of aluminum hydride, AlH_3, and lithium aluminum hydride, $LiAlH_4$, with Magnetic Resonance Imaging. Utilizing Double Half-k SPRITE[1], we acquired time resolved density weighted profiles from which we extracted reactant and product concentrations and determined reaction rates and nucleation factors as a function of position. This allows us to investigate realistic applications where temperature gradients and irregular geometric configurations are encountered.

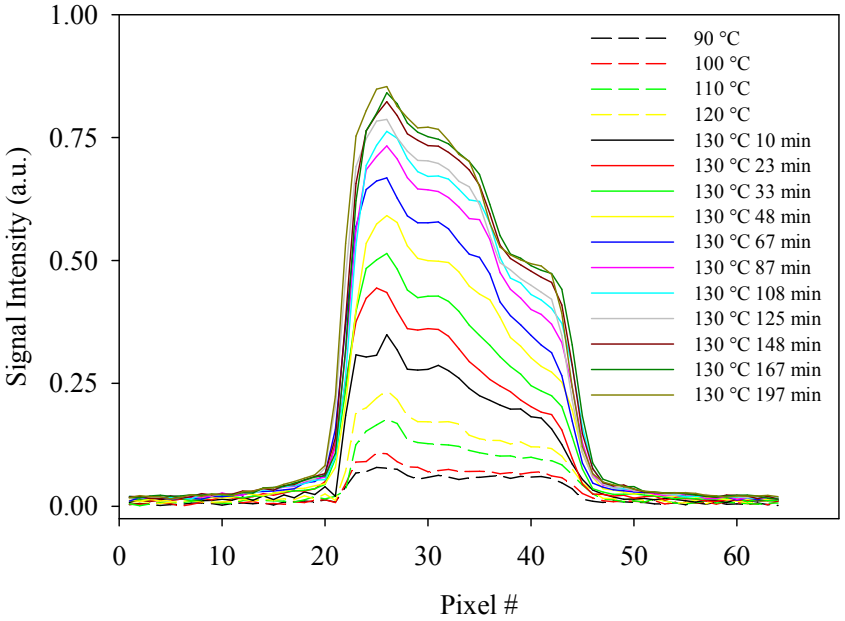

Time resolved one dimensional ^{27}Al images of $LiAlH_4$ during decomposition at 130°C.

References:

1. K. Deka, M.B. MacMillan, A.V. Ouriadov, I. V., Mastikhin, J.J. Young, P.M. Glover, G.R. Ziegler, B.J. Balcom, J. Mag. Res. 178 (2006) 25-32.

P53

Dynamics of liquids confined in porous media studied by relaxation-diffusion and diffusion-diffusion NMR exchange spectroscopy

C. Mattea, O. Neudert, S. Stapf

Dept. of Technical Physics II, Institute of Physics, TU Ilmenau, Germany

Transport properties like molecular exchange and diffusion of fluids embedded in pore structures with characteristic length scales in the order of nano to micrometers, are usually studied by nuclear magnetic resonance (NMR) [1]. When these kinds of studies are performed at high magnetic fields, magnetic susceptibilities could influence the results by the presence of undesirable local gradients in the sample. Diffusion performed at low field NMR can overcome these difficulties. In the presence of high strength gradients, as in the case of the stray field of permanent magnets, the magnetization has contributions from different coherence pathways. In this contribution, a study of the molecular dynamics of n-hexane confined in zeolites is presented with the help of two-dimensional (2D) NMR diffusion correlation experiments together with relaxation–diffusion correlation experiments performed at low magnetic field using a single-sided NMR scanner. In order to select the desired coherence pathways for the experiments, a suitable phase cycling scheme was introduced [2]. The influence of the relaxation time T2 on the diffusion measurements is also discussed. The molecular exchange properties of n-hexane in the bimodal pore structure of the zeolite are determined by this method. The exchange time covers a range from 10−3 to 10−1 s [3]. The influence of the spin–lattice relaxation properties of the fluid molecules inside the zeolite particles on the signal intensity is also discussed.

References:

1. W. Price, NMR Studies of Translational Motion, Cambridge Univ. Press, 2009.
2. O. Neudert, S. Stapf, C. Mattea, J. Magn. Reson. 208 (2011) 256.
3. O. Neudert, S. Stapf, C. Mattea, New J. Phys. 13 (2011) 035018.

P54

Off-resonance Frequency Distributions of Capillary Configurations

M. Rückl[a], *T. Kampf*[a], *C. Ziener*[b], *W. R. Bauer*[b], *P. M. Jakob*[a]

[a] Department of Physics, Julius-Maximilians University, Würzburg, Germany
[b] Department of Medicine, Julius-Maximilians University, Würzburg, Germany

The two dimensional Krogh model has been investigated in great detail to analyse spin dephasing in tissue supplied by a single cylindrical capillary [1, 2]. In this work more sophisticated tissue configurations were investigated concerning their off-resonance distributions. It turns out that there are significant deviations from predictions of the Krogh model for low diffusion rates, when the FID is primarily determined by the static frequency distribution of the off-resonance field.

It has been shown in [3] that the ordering of capillaries in myocardium can be described by a two-dimensional one component plasma (2D1CP) which is characterized by its coupling parameter Γ. Hence several capillary configurations were generated according to the algorithm provided in [3] and the frequency distributions of the off-resonance fields were calculated.

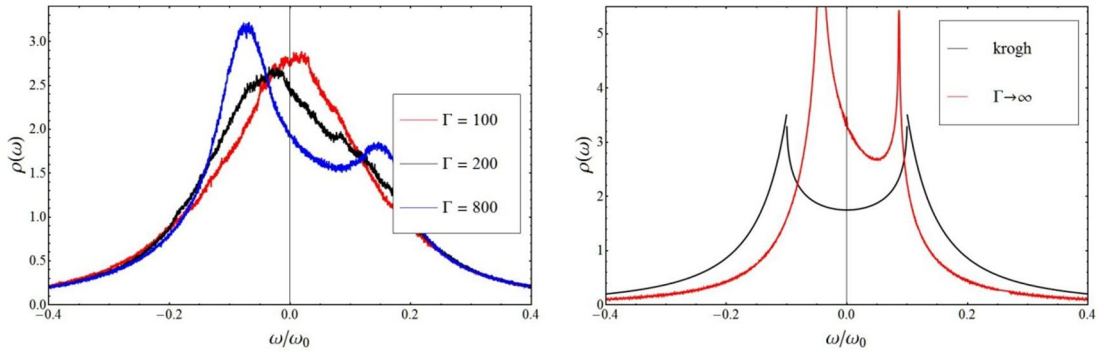

Left: Frequency distributions of 2D1CP simulations. For Γ > 140 the plasma starts to crystalize into a hexagonal lattice and the distribution is losing its symmetry.
Right: Frequency distributions for a regular hexagonal lattice and the Krogh Model.

For Γ ≈ 3 (real tissue) the frequency distributions can be approximated by a lorentzian. Hence in real tissue the FID shows a good mono exponential decay even for slow diffusion, whereas the Krogh models spiked frequency distribution predicts some more complex decay behaviour.

For applications with higher symmetry, and thus a non lorentzian frequency distribution, one could theoretically obtain information about the microscopic order of the fields sources by measuring the frequency distribution. However, this is only possible at sufficiently low diffusion rates or high off-resonances because otherwise the diffusion process, which acts similar to a convolution with a smoothing kernel in frequency domain, would again lead to a mainly mono exponential decay of the FID.

References:

1 C. H. Ziener, T. Kampf, G. Melkus, V. Herold, T. Weber, G. Reents, P. M. Jakob, and W. R. Bauer. Physical Review E 76, 031915 (2007)
2 C. H. Ziener, W. R. Bauer, P. M. Jakob. Magma (2005) 18: 225–230
3 R. Karch, M. Neumann, F. Neumann, R. Ullrich, J. Neumüller, W. Schreiner. Physica A 369 (2006) 599–611

P55

Optimal Parameters for the Estimation of the Local Frequency Distribution with Diffusion in Strong Collision Approximation – A numerical study

T. Kampf[a], M. Rückl[a], C. H. Ziener[a,b], P. M. Jakob[a], W.R.. Bauer[b]

[a]Department of Experimental Physics 5 , University of Würzburg

[b]Medizinische Klinik und Poliklinik I, University hospital Würzburg

Recently Ziener et al. introduced a formalism to calculate the Fourier Transform of the FID signal around magnetic inhomogeneities using the strong collision (SC) approximation [1]. In this approximation it is possible to investigate the full dynamic range from the motional narrowing to the static dephasing regime. Explicit expressions were given for cylindrical and spherical geometries. In a further paper the numerical solution of the Bloch-Torrey equation for these generic geometries was presented and a short comparison with the results of the SC approximation was performed [2]. The presented results for different diffusion coefficients in [2] indicate that the SC approximation systematically overestimate the influence of diffusion suggesting that a larger apparent correlation time should be used.

However, it is not clear whether this effect is due to a smaller apparent diffusion coefficient or whether the geometry parameters should be adapted as well. In this work this issue is investigated by fitting the SC model to the numerical simulations similar as performed [2].

The results suggest that a significant improvement in the accuracy of the local frequency distribution under the influence of diffusion could be achieved if the free parameters in the SC approximation are adjusted accordingly (Fig. 1 left). Furthermore the results indicate that an apparent volume fraction have to be used in addition to an apparent correlation time. The deviations from the original parameters can be significant in some cases (Fig. 1 right).

The simulations show that depending on the product of off-resonance frequency and apparent correlation time either an increase or a decrease of the volume fraction is necessary.

At the moment the scaling is only investigated numerically. Theoretical models of the parameter scaling will increase the understanding and the applicability of the SC approximation and will be part of future work.

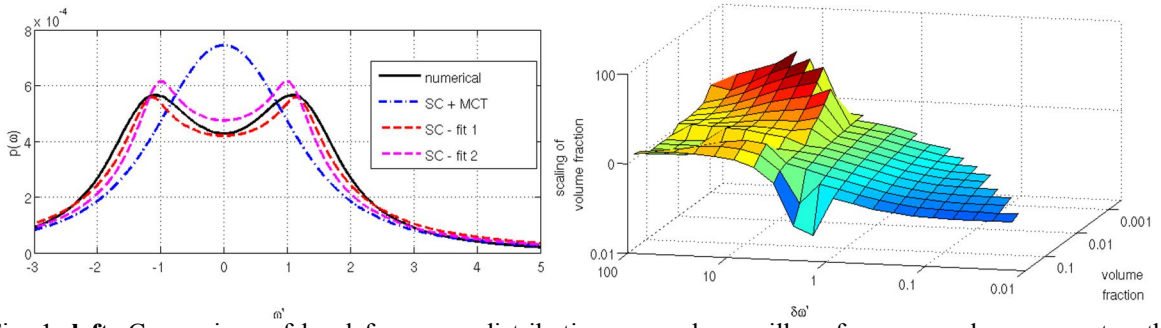

Fig. 1: **left:** Comparison of local frequency distributions around a capillary for a exemplary parameter, the numerical (black), SC approximation with mean correlation time [1] (blue), SC -fitted with variable off-resonance frequency and fixed volume fraction (magenta), SC-fitted with variable off-resonance frequency and volume fraction **right:** scaling factor of the volume fraction for different sets of off-resonance frequencies and volume fractions.

References:

1 C. H. Ziener et al.: Local frequency density of states around field inhomogeneities in magnetic resonance imaging: Effects of diffusion, Phys. Rev. E **75** 031915 (2007)

2 C. H. Ziener et al.: Spin dephasing in the dipole field around capillaries and cells: Numerical solution, Phys. Rev. E **80** 046701 (2009)

P56

Transformer-coupled NMR probe

S.Utsuzawa, S.Mandal, Y-Q. Song
Schlumberger-Doll Research, Cambridge, MA, USA

In this study, we propose a transformer-coupled NMR probe that operates over a wide frequency range (500 kHz ~ 5 MHz in our example) without the need for matching adjustment. Such a circuit could be useful for mobile NMR applications in which the gradient field is used for 1D profiling or diffusion measurement [1]. The transformer-coupled probe can simplify the tuning operation when moving from one frequency to another.

We used a transformer with a ferromagnetic core as a part of the tank circuit, unlike previous usage [2] where a transformer was located outside the tank circuit (i.e. in front of a preamp). The ferromagnetic core provides strong mutual coupling that result in efficient energy transfer between the sample coil and an NMR spectrometer. Also, the confined coupling field does not disturb the B_1 field generated by the sample coil. We found that a transformer with a ferromagnetic core works properly in a modest static magnetic field (~500 G).

In order to demonstrate the performance of the transformer-coupled circuit, NMR signal was measured and compared with that of a conventional capacitor-coupled circuit using the same coil. A transformer with 1:36 impedance ratio (T36-1+, Mini-Circuits) was used to transform the impedance of a series-tuned circuit to a higher value (Fig. 1). Both circuits were adjusted to the same impedance (90 Ω at 2 MHz as seen through a 50 Ω coaxial cable of 2 m length), thus should give the same signal/noise levels if there is no loss introduced by the transformer.

Figure 2 shows the CPMG data obtained with two circuits. The transformer-coupled circuit gave 0.8 dB less SNR, in good agreement with the sensitivity estimate based on RF power (i.e. SNR α $B_1/\sqrt{P}$, where B_1 is fixed for a given pulse length and P is the input power). This result is also consistent with the transformer's characteristics measured separately. When compared with the capacitor-coupled probe matched to 50 Ω, the SNR reduction was ~1 dB.

From these results, we concluded that the losses introduced by the transformer can be made small (≤ 1 dB) when an appropriate transformer and frequency range were chosen. Also, imperfect impedance matching due to the fixed impedance ratio will not degrade the SNR very much as long as the loading condition is consistent from sample to sample.

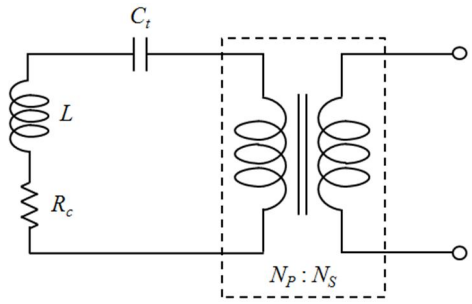

Fig. 1: Series-tuned circuit using a transformer (shown in the dashed lines). Sample coil's inductance L =20 μH and resistance R_c = 2 Ω at 2 MHz. Transformer's turns-ratio N_P:N_S = 1:6.

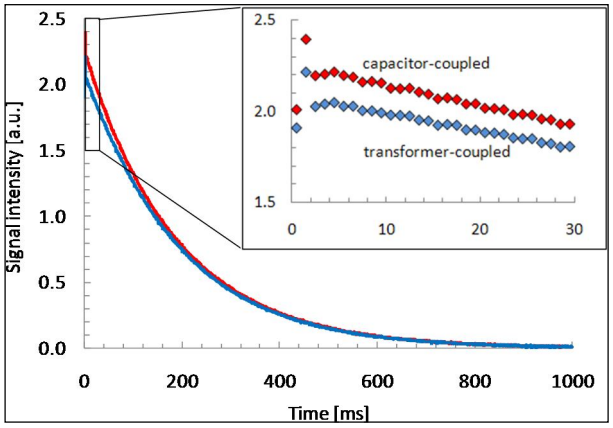

Fig. 2: CPMG data obtained with and without a transformer. SNR was 802 and 879, respectively. The first few data points oscillate due to spin dynamics in an inhomogeneous magnetic field [3].

References:

[1] B. Blümich, J. Perlo, F. Casanova, *Prog. Nuc. Magn. Reson. Spec.* 52: 197-269 (2008).
[2] J.D. Ellett *et al.*, *Adv. Magn. Reson.* 5:117-176 (1971).
[3] M.D. Hürlimann and D.D. Griffin, *J. Magn. Reson.* 143:120-135 (2000).

P57

A Low-frequency Magnetic Resonance Apparatus for NMR Logging Tool Testing

Huijun. Yu, Lizhi. Xiao, V. Anferov, S. Anferova, Xin. Li, Huabing. Liu, Baoxin. Guo

China University of Petroleum, Beijing 102249,China
State Key Laboratory of Petroleum Resource and Prospecting
Key Laboratory of Earth Prospecting and Information Technology,Beijing

We present a construction of a low frequency NMR apparatus for testing and modification of antennas for NMR wire-line and while-drilling logging tools providing one-dimensional or two-dimensional measurements. This apparatus includes Digital part, Power amplifier, De-coupler, Preamplifier and Q-Switch (See Fig.1a). Digital part is a key module of apparatus, consisting of Digital Signal Processor (DSP), Field Programmable Gate Array (FPGA), Direct-digital Synthesizer (DDS) and Analog-to-Digital Converter (ADC). It generates all the timing and control signals required by all modules, converts the analog echo signal to digital signal and processes the digitized echo signal. To acquire the high SNR of echo train data, an oversampling technique is used. Sampling clock is set to sixteen times of the Larmor frequency. The echo signal is sampled directly without mixing.

Power Amplifier with Class-D full-bridge architecture [1] was designed to satisfy the high power requirement of NMR logging tool antenna (high impedance of a few hundred Ohms, low frequency less than 2MHz). The power of power amplifier can be up to 2 kW, and the frequency can be up to 4MHz. An active De-coupler was designed based on high voltage MOSFETs controlled by digital part. Its main function is to isolate preamplifier from antenna during transmission and to assist the dumping of energy stored in antenna using an auxiliary Q-switch. Q-switch based on high power MOSFETs was designed to reduce the recovery time of antenna [2]. Preamplifier was built on low noise principle to guarantee the optimum noise performance.

CPMG echo train envelope acquired by apparatus from doped water with copper sulfate is shown in Fig.1b.

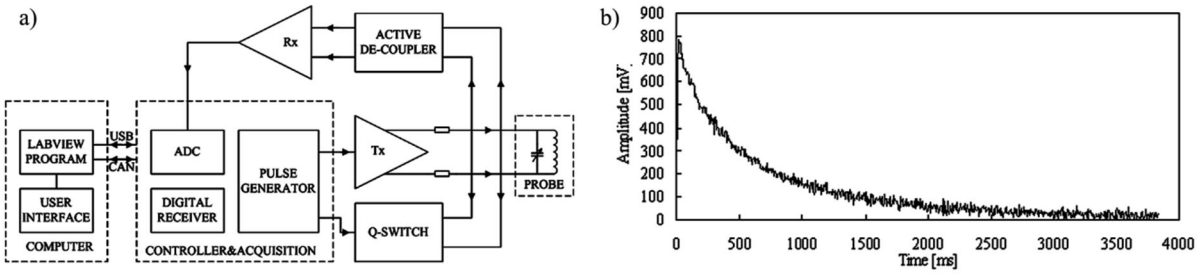

Fig. 1: a) Block diagram of designed apparatus; b) CPMG echo train envelope acquired by designed apparatus

References:

1 T.Hopper, S.Mandal, D.Cory, et al., J. Magn. Reson. 2011, doi: 10.1016/j.jmr. 2011.02.014.

2 A.S.Peshkovsky, J.Forguez, L.Cerioni, et al., J. Magn. Reson. 177(2005):67-73.

P58

Construction of a Mobile Magnetic Resonance Scanner for Geophysical Applications

Huijun. Yu, Lizhi. Xiao, V. Anferov, S. Anferova, Huabing. Liu, Baoxin. Guo

China University of Petroleum, Beijing, China, 102249
State Key Laboratory of Petroleum Resource and Prospecting
Key Laboratory of Earth Prospecting and Information Technology,Beijing

We describe a construction of a mobile benchtop NMR Scanner (MRS) which includes a small and compact spectrometer and a Halbach Probe for geophysical applications (See Fig.1a and Fig.1b). Preamplifier, De-coupler, Power Amplifier, and the NMR Probe have been designed. Digital part of the spectrometer is based on a broadband light-weight LapNMR console manufactured by Tecmag. It produces all the timing and control signals required by all modules of the MRS. The MRS permits analysis on water-saturated full cylindrical cores and plugs either in the laboratory or at the drilling-platform. Cores can be measured in their original water-saturated state directly after recovery without prior preparation. The MRS is suitable for measurements of porosity, pore-size distribution, and estimates of permeability in core plug. Sample probe sizes up to 60 mm diameter. The results of two-dimension experiments on the glass beads of two different diameters saturated with a fluids mixture of pure water and moderate oil are presented in Fig.1c and Fig.1d.

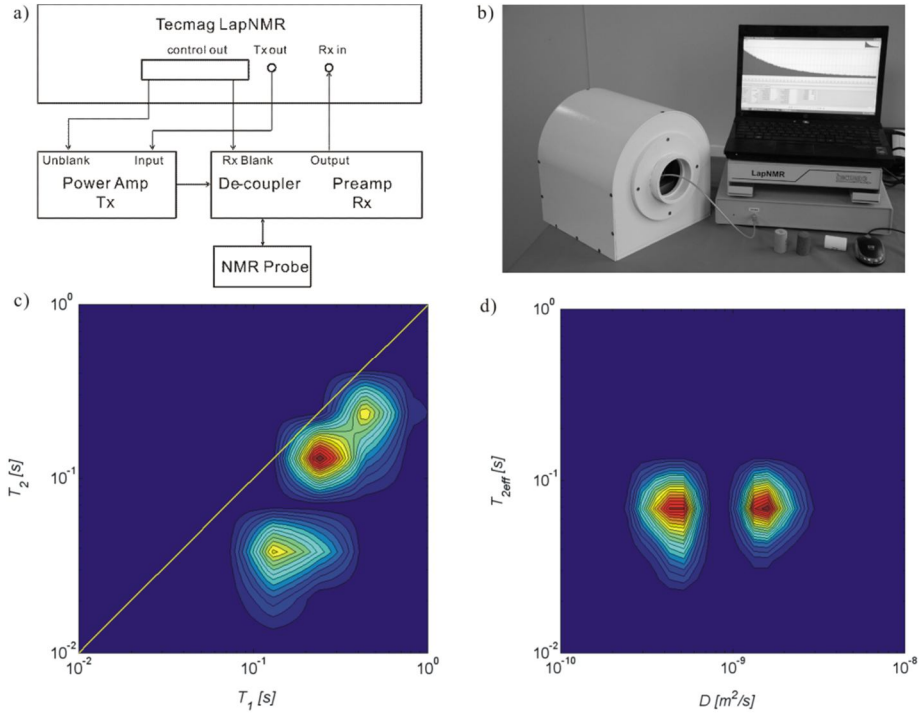

Fig.1: a) Block diagram of the MRS; b) Photo of the designed MRS; c) T_1-T_2 map of glass beads saturated with water and moderate oil; d) T_{2eff}-D map of the same sample

References:

1. S. Anferova, V. Anferov, J. Arnold, et al., Magn. Reson. Imag 25(2007): 474-480.

P59

Design and fabrication for a stripline-type inductor used in NMR detection

Xiaonan. Li, Lizhi. Xiao, Baosong. Wu, Xiaoling. Zhang, Tianlin. An

China University of Petroleum, Beijing 102249, China
State Key Laboratory of Petroleum Resource and Prospecting
Key Laboratory of Earth Prospecting and Information Technology,Beijing

A kind of stripline-type micro inductor is presented and is based on the original paper by J.Bart and Gardeniers. Based on reciprocal theory according to magnetic field, the key figures for a NMR experiment are derived out, for example, Sensitivity and Resolution. It have been proofed that the Signal to Noise Ratio for one reception in NMR is proportional to the characteristic length of receiving inductor. On the other hand, besides lowing cost, there are many other advantages when reducing the volume of sample, such as able to integrate with micro-fluidic chip.

Current problem

The problem currently most encountered is how to increase the resolution present by micro coil used in NMR detection, due to the poor linewidth in spectrum compared to existed commercial probe. In this paper, with the special structure employed here, which originated from Wireless Communication, the copper planes generating the RF magnetic field B_1 will be perpendicular to the magnet's field, i.e., B_0. This intrinsic character would generate less disturbance to B_0 compared to the case with Solenoid.

Method

The micro-stripline inductor features fabrication with Micro Electronic Mechanic System (MEMS) technology and due to the special structure of interlayer, able to excite high homogeneous Radio-Frequency Magnetic Field, which is suitable for excitation in solid as well as rock sample. The primary geometry parameters for a prototype of the device are 60mm×15mm×2mm.

Result and Application (in well-logging)

In our work, we propose an idea to use the micro-stripline inductor for NMR micro-detection in measuring the relaxation behavior and diffusion coefficient of formation fluids. Because of its low power consumption, small volume, and high detection sensitivity, it may be used in the oil field, and especially in logging while drilling.

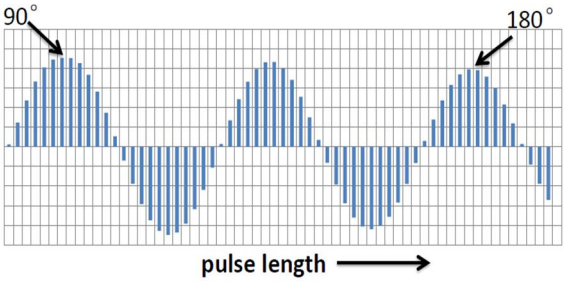

Fig. 1 SEU simulation

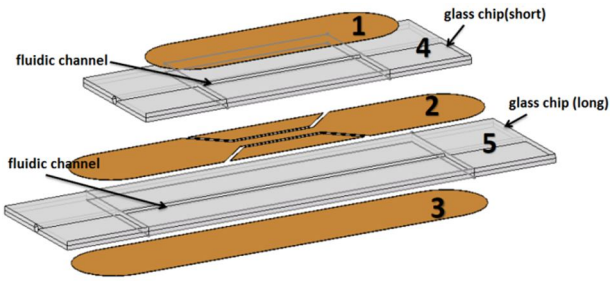

Fig. 2 An exploded view of the device

References:

1. J.Bart, Stripline-based microfluidic devices for high-resolution NMR spectroscopy.2009
2. K. Ehrmann, N. Saillen, F.Vincent, et al. Microfabrication of Helmholtz Coils with Integrated Channels for NMR Spectroscopy, Micro Electro Mechanical Systems. 2006,366 – 369.

P60

Development of a Portable Spectrometer Based on OPENCORE NMR

Xiaoling. Zhang, Lizhi. Xiao, S. Anferova, V. Anferov, Huijun. Yu

China University of Petroleum, Beijing, China 102249
State Key Laboratory of Petroleum Resource and Prospecting
Key Laboratory of Earth Prospecting and Information Technology,Beijing

A flexible and mobile NMR analyzer which can be updated according to different requirements was designed and constructed in our group. NMR analyzer contains Digital Part, Power Amplifier, Preamplifier, De-coupler and NMR Probe. A structure diagram of the mobile analyzer is shown in Fig.1.

The digital part of the analyzer is built on the base of OPENCORE NMR [1]and composed of a Field Programmable Gate Array (FPGA) breadboard and several peripheral modules as shown in Fig.1. The direct digital synthesis (DDS) operates with a 1 GHz clock, and is capable to generate a signal with frequencies up to ~400 MHz. The determined frequency resolution is $1GHz/2^{32}$ = 0.23 Hz according to 32-bit frequency-tuning word. Direct numerical phase modulation with 10-bit resolution is integrated in FPGA. The NMR signal, passed through a low-noise pre-amplifier, is sent to the signal receiver. The signal is demodulated into the intermediate frequency (IF) by a mixer with the reference frequency of the DDS. The IF signal is then fed to an Analog/Digital converter with a sampling rate of 80 MHz and a dynamic range of 14-bit.

The console software is developed in Delphi. Pulse programs are text files which are interpreted by the console software and converted into a hexadecimal code that the pulse programmer built inside FPGA obeys. The console software provides pulse transmission, signal acquisition and some normal data processing. Through editing the pulse program we easily set the frequency, the phase, the amplitude and some other parameters.

The designed digital part could be used with different NMR analog parts and probes. In our group, it is tested with a lab made analog unit and Halbach probe with well defined homogeneous magnetic field. CPMG measurement (100 echoes) result of glycerol is provided in Fig.2.

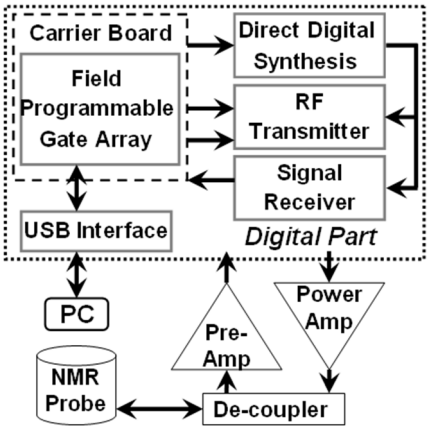

Fig.1: Structure of the NMR analyzer

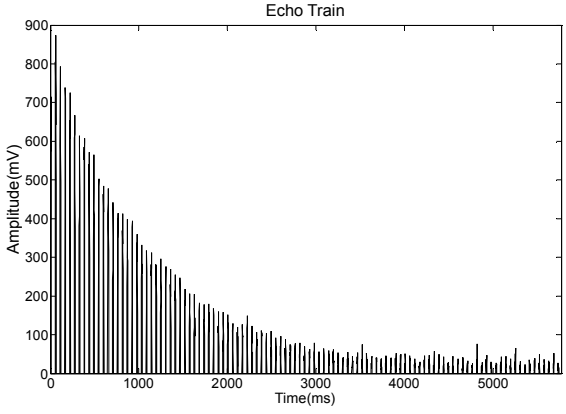

Fig.2: Echo Train measured by the NMR analyzer

References:

1. K. Takeda, OPENCORE NMR: Open-source core modules for implementing an integrated FPGA-based NMR spectrometer. J. Magn. Reson. Rev. 192 (2008) 218-229.

P61

Design of Phase Correction- Adaptive Line Enhancement for Low-Field NMR

Qingming. Xie，*Lizhi. Xiao, Xiaoling. Zhang, Huijun. Yu*

China University of Petroleum, Beijing 102249, China
State Key Laboratory of Petroleum Resource and Prospecting
Key Laboratory of Earth Prospecting and Information Technology,Beijing

Amplitude of low-field NMR is weak, and spin-echo is buried in noise[1]. The reduction of noise is critical to accurately extract echo amplitude. Filter (low-pass, band-pass, high-pass, etc.) is frequently used mainly based on prior knowledge of the spin-echo, the performance is always not sound if the prior knowledge is sufficient; signal to noise ratio (SNR) is improved by accumulation, but it requires abundant acquisitions and time-consuming.

Phase correction-adaptive line enhancement (PC-ALE) is applied to noise suppression based on the principle of adaptive line enhancement and NMR spin-echo characteristics, as shown in figure 1. Normalized least mean square (NLMS) and affine projection (AP) are used to the adaptive algorithm according to the advantage of better SNR, faster convergence and least computation. Step size and tap-weights of NLMS and AP are given as follows[2]

$$\mu_{NLMS}(k) = 1/(2x^T(k)x(k))$$

$$W_{NLMS}(k+1) = W_{NLMS}(k) + [\mu_{NLMS}(k)e(k)x(k)]/[\alpha + x^T(k)x(k)]$$

$$W_{AP}(k+1) = W_{AP}(k) + \mu_{AP}x(k)(x^T(k)x(k))^{-1}e(k)\ ,\ 0< \mu_{AP} <2;\ k = 0,\ 1,\ ...,\ N\text{-}1$$

where N represents the filter order and α is a small constant.

Echo amplitude is calculated after two stage processes. Firstly, narrow-band echo envelope and wideband noise are separated by NLMS algorithm because of its satisfied trace performance on sine wave, and correlation of spin-echo would be enhanced. Secondly, noise can be removed by AP algorithm owing to the improvement of spin-echo correlation. Phase shift from time-delay and filter tap would be compensated in frequency domain.

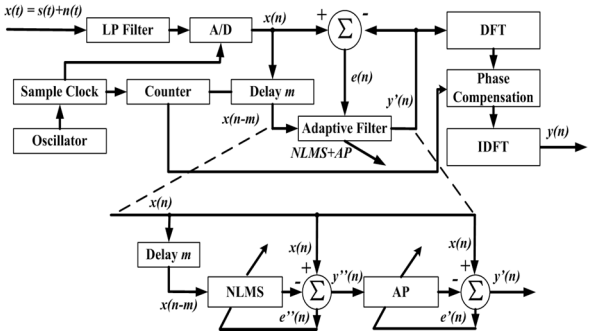

Fig. 1: Principle of Phase Correction-Adaptive Line Enhancement

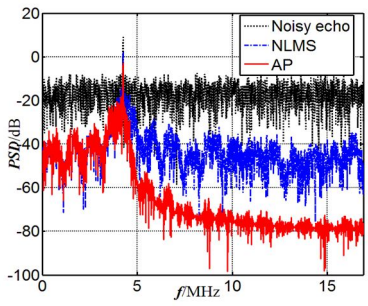

Fig. 2: Power Spectrum Density of PC-ALE, N = 32, a = 1

Spin-echoes with variety SNR are sampled by a low-field NMR spectrometer made by our group in order to verify the effectiveness of PC-ALE. B_0 is 0.100 Tesla, RF frequency is 4.258 MHz, and sample frequency is 34.064 MHz. Power spectral density (PSD) is calculated in the process of noise reduction using PC-ALE, as shown in figure 2. The experiment shows that PC-ALE has prominent performance on noise suppression, envelope recovery, as well as the correction of phase shift.

References:

1 G. R. Coates, L.Z. Xiao and M. G. Prammer, NMR logging: principles and applications. Texas: Gulf Professional Publishing; 2000

2 S. Haykin, Adaptive filter theory. New Jersey: Prentice-Hall; 2002

P62

NMR microscopy of microfluidics

E. Paciok, F. Casanova, and B. Blümich

Institute for Technical and Macromolecular Chemistry, RWTH Aachen University, Germany

NMR has proven to be a powerful tool for the characterization of flow in microfluidic devices[1,2,3]. However, the presence of strong B_0-inhomogeneities caused by the micro-structures, and B_1-inhomogeneities imposed by designated surface rf coils, as well as acceleration-related effects, have hindered the implementation of ultrafast imaging and velocity-mapping methods based on multi-echo generation, such as EPI or RARE. The alternatives, i.e. PGSE or pure phase-encoding methods, suffer from long measurement durations in the range of hours.

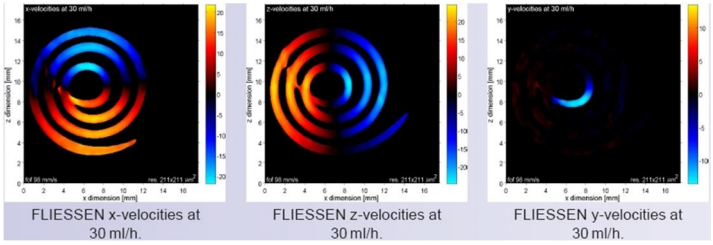

Fig. 1: Velocity-mapping in a microfluidic phantom, resolution (200 μm)^2.

In this work, we exploit the advantages of the FLIESSEN pulse sequence[4], a RARE-based acquisition scheme combined with frequent velocity-encoding updates. The performance of this method is demonstrated on a micro-fluidic phantom equipped with a surface rf coil. Here, high-fidelity 2D velocity maps of acetone flow were acquired within seconds (cf. Fig. 1), proving the resilience of FLIESSEN to the adverse effects of inhomogeneity and acceleration.

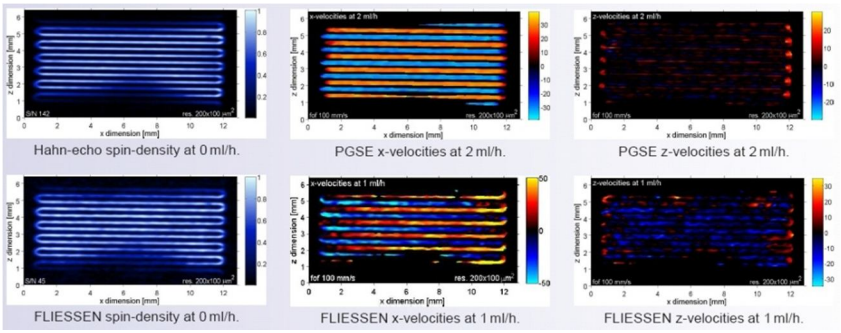

Fig. 2: Imaging and velocity-mapping in an industrial micro-mixer by micronit, Enschede, NL, resolution (200x100 μm)^2.

Stepping to the even smaller dimensions of an industrial micro-mixer, new challenges have to be met. Higher derivatives of motion necessitate an even more elaborate encoding scheme for FLIESSEN. But at this point, small gradient imperfections add up and result in noticeable signal loss and velocity information errors. Thus, the velocity map is compromised and only the general flow pattern is reproduced (cf. Fig. 2). The limits of NMR velocity-mapping are discussed, with respect to both principle limitations of this methodology as well as restrictions set by commercially available NMR imaging equipment.

References:
1 S. Ahola *et al.*, Lab Chip 6, (2006) 90.
2 B.S. Akpa *et al.*, Annal Chem 79 (2007) 6128.
3 V. S. Bajaj *et al.*, Science 330 (2010) 1078.
4 A. Amar, *et al.*, Chem Phys Chem 11 (2010) 2630.

P63

The enhancement of temporal resolution of DCE-MRI with compressive sensing

S.H.Han[a] J.Paulsen[b], G. Zhu[c] , Y.K Song[d], G.Cho[d] and H.Cho[a]

[a] School of Nano-bio Science and Chemical Engineering, UNIST, Ulsan, Korea
[b] Schlumberger Doll Research Center, Cambridge, MA,USA
[c] Bruker Biospin, Billerica, MA, USA
[d] Korea Basic Science Institute, Ochang, Korea.

Dynamic Contrast Enhanced (DCE)-MRI method provides critical information regarding tumor perfusion/permeability by the dynamic measurement of signal increase with the injection of T1-decreasing contrast agent such as Gd-DTPA. Both high temporal and spatial resolution is desired to achieve high sensitivity, however the enhancement of temporal resolution worsens the spatial resolution and vice versa.

In this work, we utilize compressive sensing (CS) algorithm to enhance the temporal resolution of DCE-MRI with optimized CS-FLASH sequence. Bruker FLASH sequence is modified to implement CS-optimized phase encoding scheme and tested on water phantom and animal tumor model. As the number of phase encoding steps is reduced by the application of CS, effective reduction in temporal resolution with same spatial resolution is achieved. Fig.1 compares tumor image obtained with (a) regular (128*128) FLASH sequence (b) CS FLASH sequence. The line comparison is also shown in (c). Fig 2 shows actual reduction of temporal resolution with (a) regular FLASH (b) x4 subsampled CS-FLASH and (c) x8 subsampled CS-FLASH, respectively.

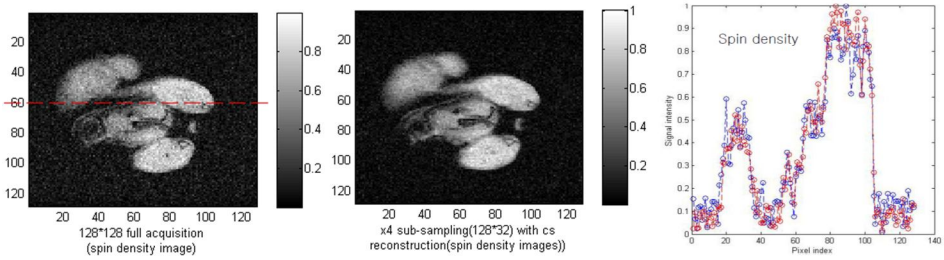

Fig. 1: Tumor image using (a) regular FLASH sequence, (b) x4 subsampled CS reconstruction and (c) the line comparison (a) with (b).

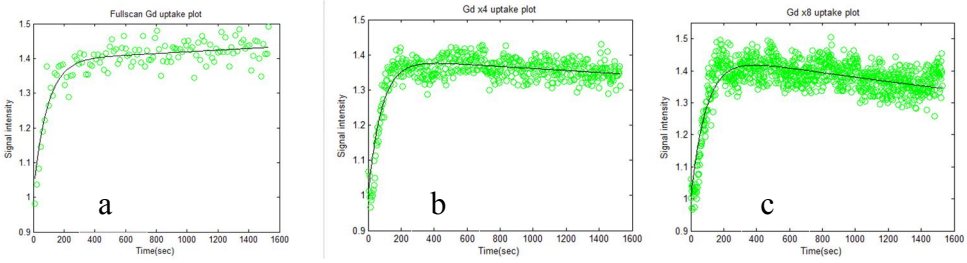

Fig. 2: DCE uptake plot using (a) regular FLASH sequence, (b)x4 subsampled CS-FLASH and (c) x8 subsampled CS-FLASH sequence.

References:

1 Lustig, M., D. Donoho, et al. (2007). "Sparse MRI: The application of compressed sensing for rapid MR imaging." Magnetic Resonance in Medicine 58(6): 1182-1195.

2 Romberg, J. (2008). "Imaging via compressive sampling." Signal Processing Magazine, IEEE 25(2): 14-20.

3 Cho, H., E. Ackerstaff, et al. (2009). "Noninvasive multimodality imaging of the tumor microenvironment: Registered dynamic magnetic resonance imaging and positron emission tomography studies of a preclinical tumor model of tumor hypoxia." Neoplasia (New York, NY) 11(3): 247.

4 Gamper, U., P. Boesiger, et al. (2008). "Compressed sensing in dynamic MRI." Magnetic Resonance in Medicine 59(2): 365-373.

P64

Hyperfine Coupling Bridged Resonant DNP

Richard Y.C. Zhong,

ERICHEN (Shanghai) Ltd., Shanghai, China, 201206

Nitroxide radicals, originally invented as spin labels, have been successfully used as the polarizing agent in dynamic nuclear polarization (DNP) experiments to amplify the NMR signals, both in low and high fields. In nitroxide solution, the DNP enhancement is often described by the Solomon formula [1,2]. In this study, the Solomon formula is modified to predict two new DNP-NMR approaches to obtain resonant Overhauser DNP effects. (1) The proton Larmor frequency can be made to match the nitrogen ENDOR frequencies of nitroxide radicals shown in Fig. 1(a),

$$\gamma_H B = \frac{A}{2} \pm \gamma_N B \pm Q .$$

Under this double-resonance condition, the protons and the nitrogen nucleus can be polarized at the same frequency. Due to the strong hyperfine coupling, the cross-polarization rate between the unpaired electron and the nitrogen nucleus is fast and proportional to A^2 [3]. (2)The proton Larmor frequency can also be made to match the hyperfine coupling constant, being the distance between two hyperfine EPR transition frequencies in nitroxide solution. Besides the two EPR transitions can be simultaneously irradiated by coherent microwave sources.

$$\gamma_H B = A = |\omega_1 - \omega_2| \ ,$$

where ω_1 and ω_1 represent the two microwave frequencies as shown in Fig 1 (b).

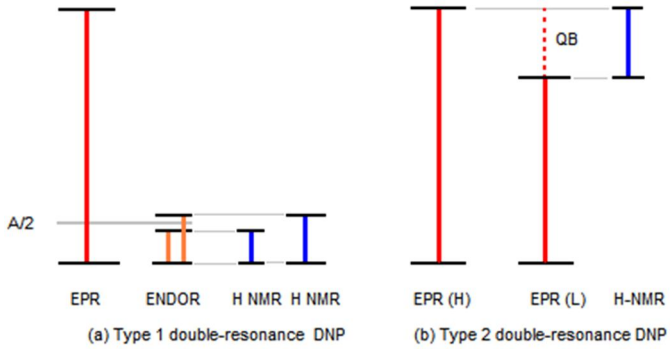

Fig. 1: Proposed double-resonance DNP methods. Type I (a) is applicable for a given polarizing agent with resolved ENDOR transitions. Type II (b) is applicable for a given polarizing agent with resolved EPR transitions. The frequency difference between the two EPR transitions, such as the low-field (L) and the high field (H) EPR transition in ^{15}N nitroxide solution, is denoted as quantum beats (QB).

References:

1. 1. I. Solomon, Relaxation processes in a system of 2 spins, *Phys. Rev.* **99** (1955) 559–565.
2. B.D. Armstrong and S. Han, A new model for Overhauser enhanced nuclear magnetic resonance using nitroxide radicals. J. Chem. Phys. 127 (2007) 10.
3. Y.C. Zhong and J. R. Pilbrow, Electron-spin cross relaxation in electron-nuclear coupled systems: A consistent model for electron-electron double resonance, *J. Magn. Reson.*, **A 112** (1995), 109 – 111.

P65

Higher-Order Spectral Analysis (HOS) Applied to Signal Processing for Multichannel Surface-NMR Instruments

Rafik. Soltani, Lizhi. Xiao

China University of Petroleum, Beijing 102249, China
State Key Laboratory of Petroleum Resource and Prospecting
Key Laboratory of Earth Prospecting and Information Technology, Beijing

The surface-NMR is a modern NMR electronics technology, with proven capabilities for non-invasive, direct and rapid near-surface hydrogeophysical prospecting. Two novel multichannel surface-NMR instruments have been appeared very recently: Numis-Poly [1], and GMR [2]. Fig. 1 shows a field survey at a site in France, which was carried out with the Numis-Poly instrument in Summer 2010. The standard spectral analysis is usually used for signal processing tasks for both instruments. We propose higher-order spectral, aka polyspectral analysis, as a complement to spectral analysis. We also propose a new adaptive signal processing algorithm for such multichannel instruments, using fourth-order cumulants (Fig. 2). Such an algorithm can be viewed as an extension, from second-order statistics to fourth-order statistics, of the actual processing algorithm of the GMR instrument; thus resulting in improved performance. Using field measurements of the Numis-Poly instrument, we demonstrate that higher-order spectral analysis allows to extracting useful information, which is complementary to the conventional spectral analysis. Such a new development is part of our ongoing R&D project on multichannel surface-NMR electronics technology [3, 4, 5].

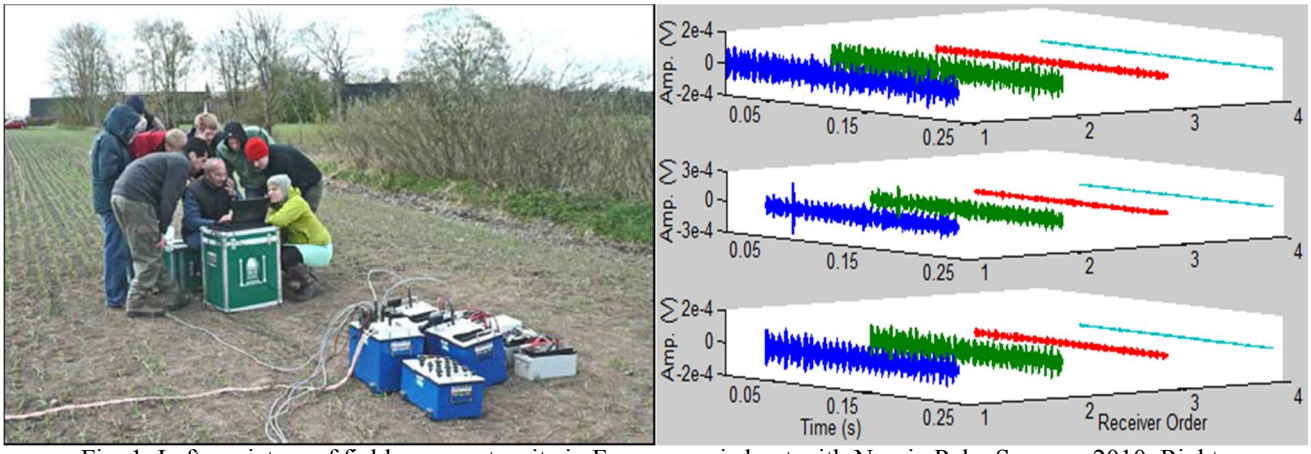

Fig. 1: Left, a picture of field survey at a site in France, carried out with Numis-Poly, Summer 2010. Right, three 4-channel datasets, each recorded by one primary receiver and three reference receivers; top: before first pulse transmission, middle: after first pulse transmission, and bottom: after second pulse transmission.

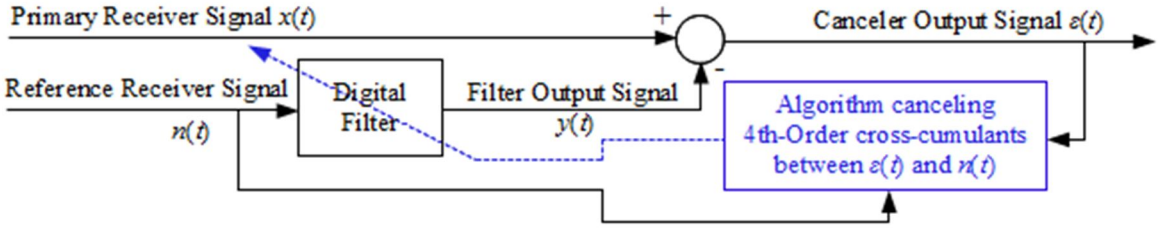

Fig. 2: HOS-based adaptive signal processing algorithm for multichannel surface-NMR instruments.

References:
1. D. O. Walsh, J. App. Geophys. 66 (2008) 140.
2. IRIS-Instruments Website: http://www.iris-instruments.com/index.html.
3. R. Soltani and L. Xiao, MRS'2009, Grenoble, France, October 20-23, 2009.
4. R. Soltani and L. Xiao, IEEExplore, Digital Object Identifier: 10.1109/IIT.2009.5413750.
5. R. Soltani and L. Xiao, ICA Applied to Surface-NMR, ICMRM'11, Beijing, China, 2011.

P66

Study of the sedimentation processes in a colloidal PMMA spheres suspension using NMR microimaging

E.V. Morozov[1,2], O.V. Shabanova[2], V.F. Pavlov[2], O.V. Falaleev[1]

[1]Kirensky Institute of Physics, Krasnoyarsk Scientific Centre SB RAS, Krasnoyarsk, Russia [2]Special designing and technological bureau "Nauka", KSC SB RAS, Krasnoyarsk, Russia

Colloidal PMMA spheres suspension is attractive due to their practical importance (for instance, in photonic crystal preparation technology [1-2]). In addition, the suspension can be used as a model system for many experiments (they involve sedimentation modeling, rheology, fluid mechanics etc.). Nowadays the main results of colloidal PMMA particles suspension investigations have been acquired by means of the optical methods application. On the other hand the NMR microimaging method has some advantages for colloidal system study and it successfully has been employed for different applications in material science and engineering [3].

In this work the results of NMR microimaging experiments for polymethylmethacrylate (PMMA) colloidal particles sedimentation are presented. The water solutions of the PMMA colloidal particles (there are several samples with different particle diameters) prepared according to techniques [4] were examined. Imaging investigations were carried out using microimaging installation based on Bruker AVANCE DPX 200 at field 4.7T, with the probe PH MICRO 2.5 (25mm coil diameter).

In results the dynamic of different phases during sedimentation process was studied. So, the displacement of pure water-colloidal suspension and sediment-suspension interfaces was tracked and the complex structure of these interfaces was shown. Also the strong dependence of phases dynamic and T_1, T_2 spatial distribution from geometry of vessel was observed (see Fig. 1).

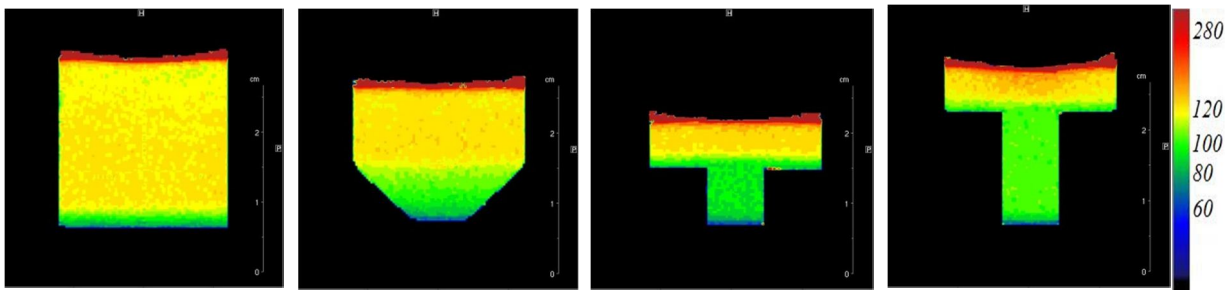

Fig. 1: T_2 maps (ms) of samples with different vessel shapes (PMMA spheres with d=300 nm) after 5 days of sedimentation

Actually it was demonstrated that the phase formation are defined by shape of vessel bottom. Therefore a set of vessels was fabricated for experiment. Theoretical computation of interface displacement rate on base of Stokes equation disagrees with experimental rate. It can be caused by substantial deviation of real system from calculated one. The results of investigation can be interested for both NMR imaging methodology and colloidal system technology.

References:

1. P. D. Garcia, R. Sapienza, A. Blanco, C. Lopez, Adv. Matter. 19 (2007) 2597-2602.
2. N. V. Dziomkina, G.J. Vancso, Soft Matter. 1 (2005) 265-279.
3. S. Stapf, H. S.-I. Han. NMR Imaging in Chemical Engineering. John Wiley & Sons, 2006.
4. R. Schroden, N. Balakrishan. Inverse opal photonic crystals. A laboratory guide. University of Minnesota, p.32, 2001.

P67

Optically Detected NMR Relaxometry

Scott Seltzer, Paul Ganssle, Mark Butler, Thomas Theis, Vikram Bajaj, Alexander Pines
Materials Sciences Division, Lawrence Berkeley National Laboratory
Department of Chemistry, University of California, Berkeley

Alkali-metal atomic magnetometers [1] provide an optical method of detecting and measuring magnetic fields by monitoring the precession of polarized alkali atom spins. Sensitivity better than 1 $fT/Hz^{1/2}$ has been demonstrated to both near-dc and radio-frequency fields, which is comparable to or better than competing sensor technologies, including inductive coils and SQUIDs. In principle, the sensitivity of an atomic magnetometer does not depend on the measurement frequency [2], enabling them to detect proton NMR in the Earth's magnetic field much more efficiently than inductive coils. They operate at or above room temperature and so do not require liquid cryogens, making them eminently portable, low-cost, and low-maintenance. Magnetometers have been demonstrated for a variety of magnetic resonance applications including detection and imaging of bulk fluid samples, detection of hyperpolarized gas, zero-field spectroscopy, and NQR detection.

Left: Basic schematic of alkali-metal magnetometry: A pump laser beam polarizes the atomic spins, while a probe laser beam monitors the precession of the spins. The observed precession frequency of the atomic spin

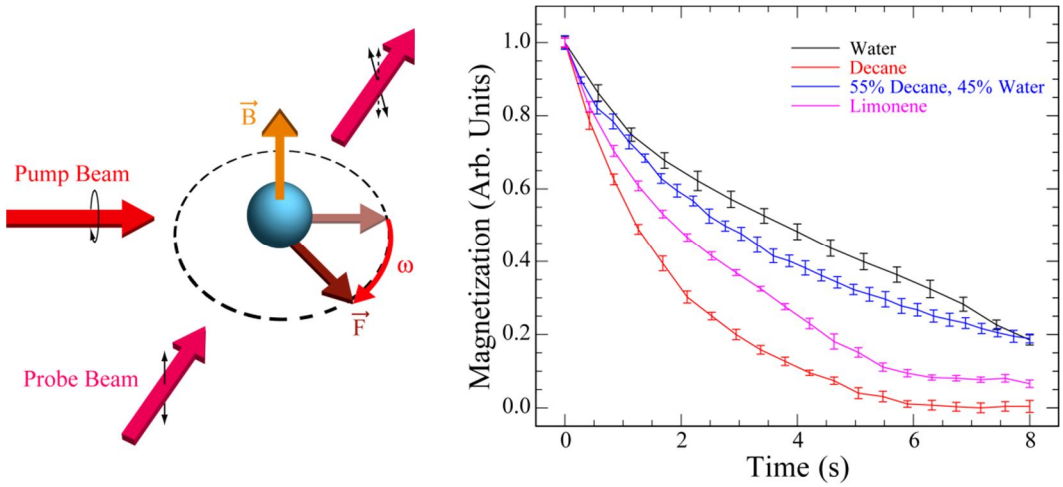

vector **F** provides a direct measurement of the ambient magnetic field strength.
Right: Measurement of longitudinal relaxation of several compounds at the level of the Earth's magnetic field (0.53 G), showing a clear distinction between T_1 relaxation times.

We demonstrate the use of an atomic magnetometer for measuring the relaxation and diffusion properties of protons in various compounds, including water and hydrocarbons. One potential application is well logging, where detection in the Earth's field should enhance relaxation contrast between compounds, compared to the significantly larger magnetic fields traditionally required for detection with inductive coils. The preliminary data displayed in the figure show that water, heavy hydrocarbons, and mixtures can be clearly distinguished at 0.5 Gauss based on their relaxation behavior. We also consider the use of atomic magnetometers for remote measurements of fluid velocimetry, with potential applications in flow monitoring and metering.

This work was supported by the U.S. Department of Energy under Contract No. DE-AC02-05CH11231.

References:

1. D. Budker and M. V. Romalis, Nature Physics **3**, 227 (2007).
2. I. M. Savukov, S. J. Seltzer, and M. V. Romalis, J. Magnetic Resonance **185**, 214 (2007).

P68

Rheo-NMR studies of Ionic Liquids with Silica Additives

Jan Novak and Melanie M Britton

Department of Chemistry, University of Birmingham, Birmingham, B15 2TT, UK

Ionic liquids (ILs) are classified as liquids which are entirely composed of ions at less than 100 °C[1]. Some ILs have shown promise as lubricants which could potentially be used as replacements for more conventional crude oil-derived substances[2]. A number of intrinsic properties make ILs ideal for lubrication applications including negligible vapour pressures, wide electrochemical windows and high thermal stabilities. Despite the increasing number of studies into the lubrication properties of ILs, understanding of the rheology (the study of fluids under shear), is very limited. The rheology of a lubricant could have profound effects on the performance of the ILs as lubricants.

In this study we used Rheo-NMR[3] to study the behaviour of various ionic liquids under shear. Velocity measurements in a Couette cell were used to characterise shear-dependent behaviour over a range of shear rates. The effect of silica nanoparticle additives were investigated in the ionic liquids. In order to understand the interaction between the nanoparticles and the ILs, the surface chemistry of the nanoparticles and the composition of the ILs were varied.

References:

[1] M. Freemantle, *An Introduction to ionic liquids*, RSC Pub., Cambridge, UK, **2010**.
[2] F. Zhou, Y. M. Liang, W. M. Liu, *Chemical Society Reviews* **2009**, *38*, 2590.
[3] P. T. Callaghan, *Current Opinion in Colloid & Interface Science* **2006**, *11*, 13.

P69

An NMR analysis of the effect of multiple degassings on droplet size in an oil-in-water emulsion

Duncan A. MacLean, Benedict Newling, Igor V. Mastikhin

UNB MRI Centre, Department of Physics, University of New Brunswick,
Fredericton, NB, Canada

It has been demonstrated that a stable oil-in-water emulsion can be produced using a freeze-thaw degassing cycle. However the mechanism behind the creation of this stable emulsion is disputed. Two possibilities are that the presence or absence of gas is the deciding factor (as suggested by Pashley[1], 2003) or that it is only the size of oil droplets distributed that decides the stability (as suggested by Burnett et al.[2], 2004). To determine what is the reality a series of 1 in 100 dodecane-in-heavy water emulsions were prepared for a magnetic resonance (MR) experiment. Samples were subjected to a different number of freeze-thaw degassings, ranging from zero to six freeze-thaw cycles. The diffusion coefficient of each sample was measured using a Cotts 13-interval MR pulse sequence with a Cogwheel phase cycle, and the mean oil droplet size within the emulsion is calculated from this. The measurement used ^{1}H as the targeted nucleus, therefore no signal is collected from the heavy water. The results obtained are consistent with the removal of gas causing the stability of the emulsion, and serve as an indicator for future research into the mechanism involved.

References:
1. R.M. Pashley, Effect of degassing on the formation and stability of surfactant-free emulsions and fine Teflon dispersions, *Journal of Physical Chemistry B*, **107** (2003) 1714-1720.
2. G.R. Burnett *et al.,* Surfactant free “emulsions” generated by freeze-thaw, *Langmuir* **20** (2004) 5673-5678.

P70

The Analysis of Error and Geological Reason of Raw Oil Saturation Results Calculated By NMR Data

Haiyan Wu, Liming Qin

Sinopec Research Institute of Petroleum Engineering, Room 918, North Star Times Tower, No.8 Beichendong Road, Chaoyang District, Beijing 100101, China
phone +86 010-84988369, wuhaiyan717@126.com

The oil saturation is one key parameter for the evaluation of the fluid properties and the content of hydrocarbon in the reservoir. In the late 1990s, the NMR core analysis brought a new technical reformation for the experiment techniques. From it, the correlation between NMR property of the rock and the filtration or reservoir capacity of the rock on fluids shows very well[1]. The practices have proved that the NMR technique is one effective method for the core analysis. For the sand reservoir, if the T_2 cut off value is determined, the NMR analysis data can provide the accurate free fluid volume of the rock sample. Moreover, if the hydrocarbon reservoir contains no water through the results of the well testing or other methods, the free fluid volume can be interpreted for the oil volume[2]. For the sealed coring analysis, the loss quantity of the hydrocarbon in sample is less than that of the other methods such as routine drilling or sidewall coring[3]. So, the oil saturation calculated by the sealed coring information is considered closely to the original value at present[3]. From the research in some area of Shengli oil field, the oil saturation by NMR is obviously less than that analyzed by the sealed coring information in the same sample.

This paper shows that the principle on the calculation of the oil saturation by the NMR core analysis and explore the reason of the error between above mentioned two methods from the reservoir formation mechanism. With the thickening of the overlying strata, the structure of the fluids quantity changed in the reservoir. The hydrocarbon in reservoir underwent the overlying strata pressure and buoyancy. For the buoyancy, it was controlled by the oil legs, oil density or other factors, but it had no change and the direction was upward. For the overlying strata pressure, it increased slowly and the direction on hydrocarbon was downward. If the hydrocarbon migrated downward, it needed a dynamic to push, but it did not exist. Therefore, the compaction could not make the accumulated hydrocarbon overflow. But for the water, in virtue of undergoing the overlying strata pressure, it expelled slowly from the reservoirs. Therefore, the changes of the structure of the fluid quantities made the oil saturation at present larger than its original value. The porosity of the core can be divided into two types, the micro pore and the effective flow pore[4]. Generally, the micro pore is occupied by the bound water, but the effective flow pore is filled with the hydrocarbon and free water.

The reason for above mentioned occurrence is that the original porosity in the event of the oil accumulation is larger than that at present and many partial pores in the reservoir are not micro pores during the filling of the hydrocarbons. The micro pores at present are formed by the continuous compaction of the reservoirs. Through the analysis, when we compute the oil saturation by the NMR data, we should recognize the results correctly in the geological condition of reservoir formation, especially the low porosity and low permeability reservoirs, because the results maybe represent the lower limit values of the oil saturation.

References:

1. Ma Dehua, Geng Changxi, Zuo Tieqiu. Method of improving calculation accuracy of oil saturation [J]. Petroleum Geology& Oilfield Development in Daqing, 2005, 24(2): 41-42.
2. Xiao Lizhi. Magnetic Resonance Image Log, Nuclear Magnetic Resonance in Rock and Theirs Application [M]. Beijing: Science Press, 1998, 168.
3. Kong Xiangli, Xuan Zhonghai. A New W ay to Proofread the O il Saturation of the Sealed Coring by Using ordinary Pressure [J]. Fault-Block Oil& Gas Field, 2006, 13(1): 20-28.
4. Guo Gongjian, Gu Changchun. Oil Saturation in Rock Cuttings Measured by Nuclear Magnetic Resonance [J]. Chinese Journal of Magnetic Resonance, 2005, 22(1): 67-72.

P71

Corrections of NMR Logging Response at Downhole Condition

Haitao. Hu, Lizhi. Xiao, X. Wu
China University of Petroleum, Beijing 102249, China
State Key Laboratory of Petroleum Resource and Prospecting
Key Laboratory of Earth Prospecting and Information Technology,Beijing

Nuclear magnetic resonance(NMR) logging is a logging technique for open hole, which can provide effective porosity, free fluid porosity, bound water porosity, pore size distribution and permeability, and contains no contribution from the matrix materials and do not need to be calibrated to formation lithology. However, drilling mud resistivity, formation resistivity and sodium ions have influence on its' radio frequency(RF) field strength and NMR logging signals respectively.

The influences has been simulated numerically in this paper. When drilling mud resistivity *Rm* is 0.02 ohm*m, attenuation index of centric NMR logging tool is 8.9%; When formation resistivity *Rxo* is 0.02 ohm*m, attenuation index of centric NMR logging tool is 9.47%, which is shown in Fig.1. The RF field of eccentric NMR logging tool is affected mainly by formation resistivity, when formation resistivity *Rxo* is 0.1 ohm*m, attenuation index is 17.5%, which is shown in Fig.2. The corresponding correction equation was developed for the first time.

In general, low resistivity drilling mud and formation fluid are due to the high salinity of drilling mud and formation fluid which contain plenty sodium ions. And the sodium ions will produce NMR signal too, on the one hand, sodium ions NMR signals decrease the NMR logging signal to noise ratio(SNR); on the other hand, sodium ions NMR signals add to hydrogen NMR signals, which lead to calculated porosity of NMR logging data is bigger than the real one. The NMR signals come from water and sodium ions respectively are shown in Fig.3. The relevant correction method was developed based on numerical simulation.

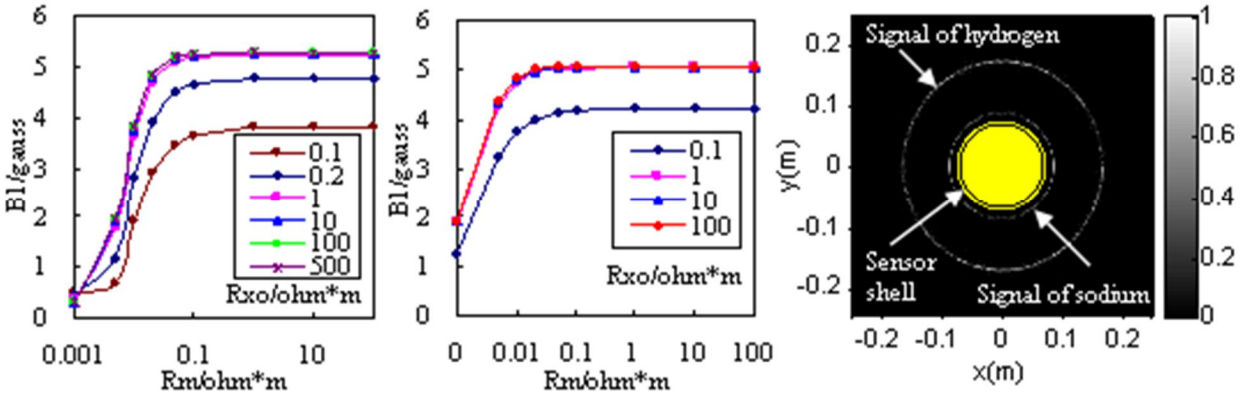

Fig.1 The influence of water base drilling mud – water bearing formation on centric NMR logging tool
Fig.2 The influence of water base drilling mud — water bearing formation on eccentric NMR logging tool
Fig.3 NMR signals come from water and sodium ions respectively

References:

1. G. R. Coates, L. Xiao, M. G. Prammer. NMR logging principles and applications. Halliburton Energy Services, 1999.
2. M. D. Hürlimann, D. D. Griffin. Spin dynamics of Carr-Purcell-Meiboom-Gill-like sequences in grossly inhomogeneous B0 and B1 fields and application to NMR well logging, JMR, 2000(143): 120–135.

P72

Research on stress-sensitivity in the fracture-cave deformation medium of carbonate reservoir

Shang Genhua[1] *Lang Fongjiang*[1] *Li Hongwei*[1] *Guo Dongming*[2]

1-Petroleum exploration and development institute of Sinopec, Haidian，Beijing100083
2 – China French Bohai Geo services Co., LTD.,Tanggu District Tianjin , China , 300452

In this paper, four pore structure types have been determined which is pore and crack, fracture, cave also the combining in the core in Xinjiang Tahe oilfield using nuclear magnetic resonance (NMR) technology with the cores being classified,. The system of CM300 made by Corelab Ltd. was used to measure the permeability and porosity system under the overlying pressure for the different kinds of core stress sensitivity. Then we analyzes the relation of stress sensitivity with coring mineral composition in sandstone and carbonate which main factor in sandstone reservoir of stress sensitivity mineral is the clay content but dolomite in carbonate rocks

At last, relations of the stress sensitivity test results with carbonate reservoir space structure in fracture-cave reservoir had been studied. The stress sensitivity in different types space structure types should be of the difference coorrsponding that help peoples master the know-how in the development the fracture-cave type carbonate reservoir.

Keywords: Stress sensitivity，Carbonate, NMR，Fracture cave reservoir

P73

Application of NMR logging for Identifying Secondary Oil Migration Pathway

Y. Wang, R. Xie, L. Xiao, S. Fu

China University of Petroleum, Beijng 102249, China

A method is presented first time to identify oil migration intervals(OMI) using NMR logging, then assist identifying secondary oil migration pathways(OMP) in exploration boreholes. It can help to discover reservoirs. According to oil migration dynamics, it predicts potential profiles of oil saturation and partial confinement of oil below sealing strata using the displacement pressure(resistant force) from NMR logging and the buoyancy (driving force).

The method performs calculations on NMR logging data and uses pore structure model calibrated by core samples to derive a continuous capillary pressure log for reservoir or carrier bed. A displacement pressure log is calculated from a continuous capillary pressure log by a typical method. Then the displacement pressure is subtracted from the buoyancy to obtain profiles of potential oil migration(lateral) intervals and oil saturation due to partial confinement beneath sealing strata. Here, the highest displacement pressure of a interval is determined the confinement beneath sealing strata. The steps in the calculation of the method have been combined to indentify genuine oil migration intervals from exploration oil wells. Finally, the single well oil migration(lateral) intervals that have been combined with regional faults and unconformities are identified genuine secondary oil migration pathway. An example of the area of Chagan Despression, **oilfield, illustrate the practicality and effectiveness of the proposed method from NMR logging.

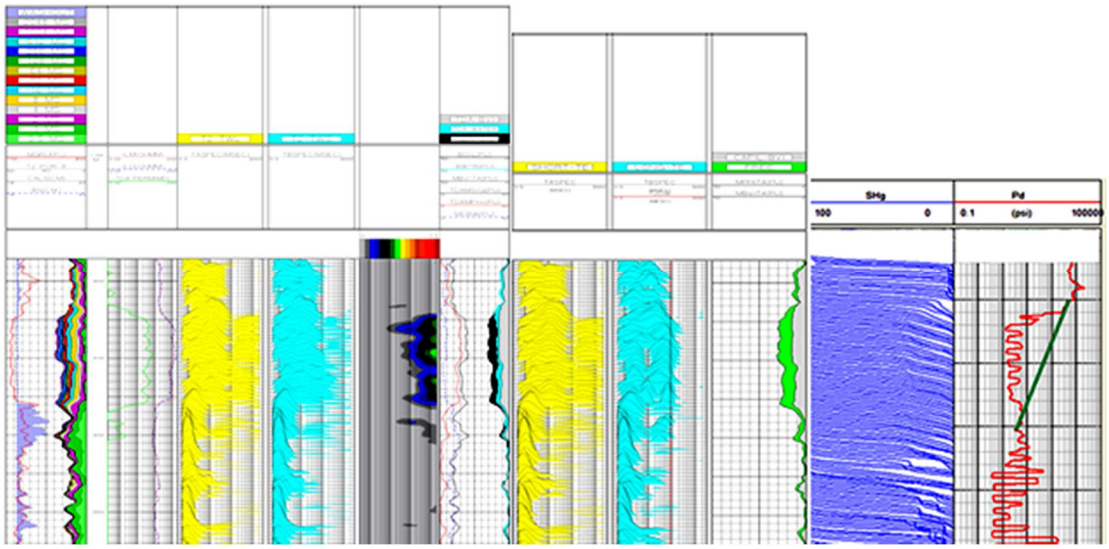

Fig.10 Result map of NMR OMI(Oil Migration Interval) in the A2 well

References:

1 G. R. Coates, L. Z. Xiao, M. G. Prammer. NMR Logging Principles and Applications. Texas: Gulf Publishing Company, 1999.

2 T. T. Schowalter. Mechanics of secondary hydrocarbon migration and entrapment. AAPG Bulletin. 63(1979)723.

3 K. Liu, P. Eadington. A new method for identifying secondary oil migration pathways. Journal of Geochemical Exploration. 78(2003)389.

P74

Relative permeability assessment from the capillary end effect: Low field MRI measurements

Konstantin Romanenko, Bruce J. Balcom

MRI Centre, Department of Physics, University of New Brunswick

A gradient of the wetting phase saturation arising from the discontinuity of the capillarity in the wetting phase at the outlet end of a core is referred to as the capillary end effect. Such end effects are observed in drainage processes, i.e. oil displacing water in water-wet core, or gas -displacing-oil cases. Although these effects are commonly seen as negative factors causing errors in traditional measurements of relative permeability, they can be exploited for estimation of petroleum core properties, particularly, relative permeability curves. Considering a drainage experiment (injecting oil (o) into a water pre-saturated, water wet core) an expression for relative permeability to oil (k_{ro}) can be derived based on a discrete form of Darcy equation and the definition of capillary pressure ($P_c=P_o-P_w$):

$$k_{ro}=-[X(S_w)\cdot Y(S_w)]\cdot q_o\cdot\mu_o\cdot(k\cdot A)^{-1}, \qquad (1)$$

where $X(S_w)=(dx/dS_w)$ and $Y(S_w)=(dP_c/dS_w)^{-1}$ are both functions of water saturation, S_w; x – distance from the inlet edge of the core; q_o - oil flow rate; k - absolute permeability, A - core cross-section area; μ_o - dynamic viscosity of oil. Knowledge of the saturation profile, $S_w(x)$, and capillary pressure curve, $P_c(S_w)$, allows one to calculate the relative permeability curve, $k_{ro}(S_w)$, using equation (1). All constant factors in the equation (1) are known. The proposed approach allows calculation of the relative permeability curve, $k_{ro}(S_w)$, directly without complex models.

An analytic profile equation describing the capillary end effect saturation profile was provided in ref. [1]. It is based on the Brooks-Corey capillary pressure model. If the Brooks-Corey model is valid, the correspondence between $P_c(S_w)$ and $S_w(x)$ curves will allow reconstruction of $k_{ro}(S_w)$ based only on observation of the capillary end effect. Ideally, there is no need for separate capillary pressure curve measurements. Parameters of the Brooks-Corey equation can be determined from the experimental profile $S_w(x)$ using the profile equation. This method is illustrated through the measurements of the capillary end saturation profiles in Berea sandstone.

Experiment: Berea core (5.25cm long; 3.81cm diameter; k = 0.1D); two specially designed end plugs (PEEK) and 3.81cm i.d. Aflas sleeve; D_2O - wetting phase, dodecane - non-wetting phase. MRI setup: an Oxford Maran Ultra DRX system; 2MHz 5 cm i.d. vertical bore permanent magnet; 1D pulsed field gradient. Proton density profiles were measured with the spin-echo SPI method. The use of D_2O allows one to completely separate wetting and non-wetting phases in MRI measurements. The bottom end plug is provided with circular and radial grooves for distributing fluid to the entire injection face and an axial port. The top end plug has a cone-shaped reservoir and provided with inflow and outflow channels. The core placed between the end plugs is put into Aflas sleeve and sealed with Teflon heat shrink. The core holder design is safe in a pressure range of 1 to 4atm with no confinement pressure. Continuous supply of D_2O through the inflow channel of the top plug ensures that at the outlet core end S_w is close to 100%. The vertical holder design implies that dodecane, due to lower density, easily rises to the outflow channel.

Reference:

[1] D.D. Huang, M.M. Honarpour, Capillary end effects in coreflood calculations, Journal of Petroleum Science and Engineering 19 (1998) 103.

P75

Optimized Design and Validation of a NMR Logging Device

L. Xiao, H. Hu, X. Li, H. Yu, V. Anferov, S. Anferova, G. Zhang, W. Zhu

China University of Petroleum, Beijing, 102249, China
State Key Laboratory of Petroleum Resource and Prospecting
Key Laboratory of Earth Prospecting and Information Technology,Beijing

NMR logging is the only measurement that responds solely to formation fluids, which can provide the quantities of the fluids in the rock, the properties of these fluids, the sizes of the pores that contain these fluids, each of which make these tools unique among logging devices. Because of this, NMR logging technique has been developing rapidly in the past 50 years, and various types of NMR logging tools have been developed for commercial application.

A new nuclear magnetic resonance (NMR) logging device has been designed and built for nondestructive investigation of formation. This device has an eccentric probe which can be working in high angle well and salt water well. The permanent magnets of it generate an inhomogeneous field that penetrates into a formation on one side of the logging tool. This tool can be utilized for investigations at multifrequency, multiDOIs, total and effective porosity activation, dual-*TW* activation and dual-*TE* activation. The gradient field design makes this tool can measure diffusion (*D*) of formation fluid, which is used to quantify oil and gas. In addition, we can acquire data at different acquisition parameters with multifrequency and multiDOIs in a single pass, which avoid data quality problems because of ragged hole.

The shape of magnetic fields is optimized and the efficiency of antenna is improved by optimizing sensor configuration. This device has been tested in a calibration tank in order to evaluate its detection performance. NMR echo data are acquired at multifrequency, dual-*TW* activation, dual-*TW* activation.

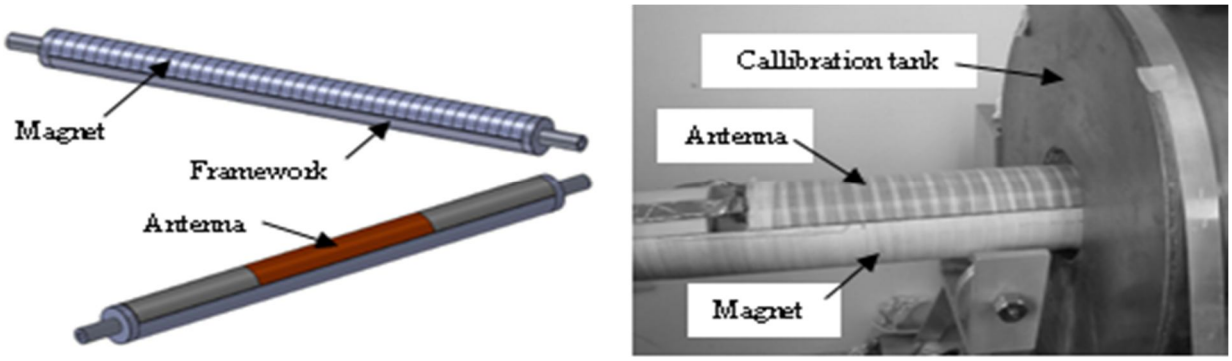

Fig.1.The configuration of NMR logging device permanent magnets and antenna
Fig.2 The calibration tank test of NMR logging device

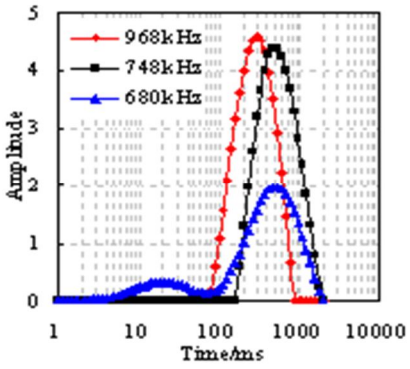

Fig.7 T2 distributions at Multifrequency activatio

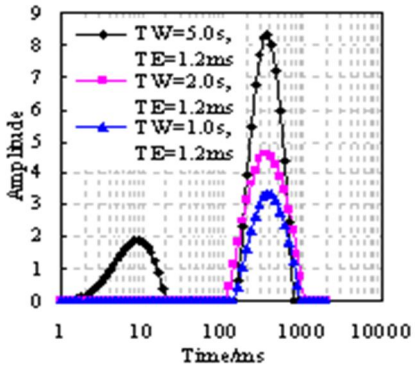

Fig.8 T2 distributions at dual-TW activation

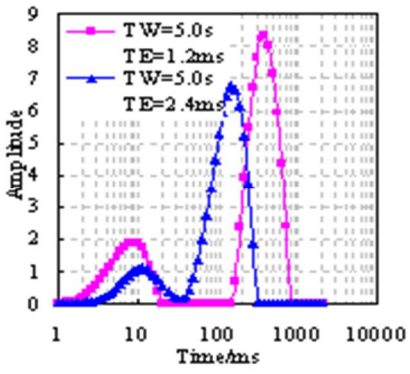

Fig.9 T2 distributions at dual-TE

References:
Coates G R, Xiao L, Prammer M G. NMR logging principles and applications. Halliburton Energy Services, 1999.

P76

The Influence Factors of NMR Logging Permeability

Ranhong Xie, *Lizhi Xiao*, *Ya Tian*

China University of Petroleum, Beijing 102249, China
State Key Laboratory of Petroleum Resource and Prospecting
Key Laboratory of Earth Prospecting and Information Technology,Beijing

Permeability is a basic parameter for reservoir evaluation, and NMR logging has advantage in obtaining the formation permeability. However, because of the complex rock pore structure, various clay minerals and pore fluids in reservoir, the difference between NMR permeability and formation permeability is often existed. In this paper, two commonly permeability estimators i.e. the Coates equation and $T_{2,LM}$ equation are theoretically introduced. The influence factors of NMR logging permeability are discussed based on NMR core measurements. The results show that NMR permeability increases with increasing of the core samples grain diameter. The NMR permeability of core samples with different type and weight percent of clay mineral decays exponentially with increasing of the NMR measurement echo spacing time. The decay rate depends largely on the type, the distribution pattern and the weight percent of clay mineral in core samples. The decay rate is biggest in the samples with rich ferrous chlorite mineral. When there is low viscosity oil in samples, the Coates equation is preferred. When the oil with high viscosity and water T_2 distributions overlap to the extent that they cannot be distinguished, neither the Coates equation nor $T_{2,LM}$ equation will work. This should improve the accuracy of NMR logging permeability in complex reservoirs.

References:

1. Coates G R, Xiao L Z, Prammer M G. NMR Logging Principles and Applications. Texas: Gulf Publishing Company, 1999
2. Richard Sigal., Coates and SDR permeability：Two variations on the same theme, Petrophysics, 2002, 43 (1): 38-47.
3. Gigi Qian Zhang., George J., Hirasaki and Waylon V H., Diffusion in Internal Field Gradients, Rice University SCA-9823.
4. Moss A K., Zacharopoulos A., Freitas M H., Shale Volume Estimates from NMR Core Data, SCA2003-66, 21-24.
5. Ying Zhang., George J H., et.al., Oil and Gas NMR Properties: The Light and Heavy Ends, SPWLA 43th Annual Logging Symposium, June 2-5, 2002.

P77

Probe design for downhole NMR fluid analysis laboratory

Baosong. Wu, Lizhi. Xiao, Huijun. Yu, Tianlin. AN

China University of Petroleum, Beijing 102249, China
State Key Laboratory of Petroleum Resource and Prospecting
Key Laboratory of Earth Prospecting and Information Technology,Beijing

Downhole nuclear magnetic resonance (NMR) fluid analysis laboratory is a multi-functional fluid laboratory that can be used to analyze the reservoir fluids in situ real-time in the well bore. It can monitor contamination and quantitatively evaluate characteristics of formation fluids obtained by formation tester (see Fig.1).

In this paper we describe a probe constructure (as shown in Fig.2). It comprises: magnets in polarization section (part A and part B) for fast polarizing hydrogen nuclei, magnets in resonance section (part C) for resonance measurement, two separate coils, a vessel for providing a passage for fluid, a steel tube with high magnetically permeability.

We propose to make use of Bloch equation to design the magnet length, and determine the optimal length design of each magnet. Two separate coils are designed for measuring T1 parameters of flowing fluids. There is a homogeneous static field (perpendicular to the axial direction) in the central of the probe, and the external is zero stray fields (see Fig.3). The novel design of pre-polarization magnet improves the signal to noise ratio, while reducing the probe length.

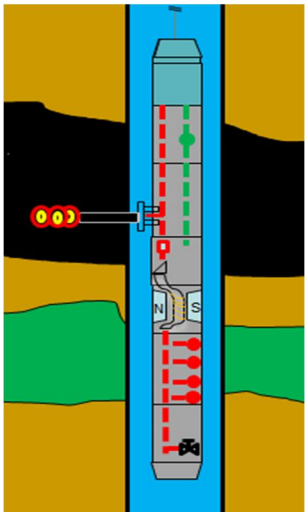

Fig. 1 The schematic diagram of NMR fluid analysis laboratory combined with formation tester

Fig. 2 A probe picture of NMR fluid analysis laboratory

References:

1 M.G.Prammer, J.Bouton, and P.C.Masak. Magnetic resonance fluid analysis apparatus and method. U.S. Patent, US20020140425A1, 2002-10-03

P78

2D T_2 Distribution Mapping in Core Plugs with Optimal *k*-Space Sampling

Dan Xiao, Bruce Balcom

Department of Physics, University of New Brunswick, Canada

Spin-echo single point imaging (SESPI) has been employed for 1D T_2 distribution mapping[1], but a simple extension to 2D is unrealistic since the time increase is *n* fold, where *n* is the number of pixels in the second dimension. Nevertheless 2D T_2 mapping in rock core plugs is highly desirable because the bedding plane structure in rocks often results in different pore properties within the sample. The acquisition time can be improved by under-sampling *k*-space. Commonly employed sampling patterns in pure phase encode include radials, spirals and sectors, which simply zero fill the periphery of *k*-space. In 2D this saves only 20% of the *k*-space data points with resultant minor changes in acquisition time. In our investigation the samples are usually core plugs of cylindrical shape that yields well defined intensity distributions in *k*-space that are efficiently determined by new *k*-space sampling patterns developed in this work. Our typical sampling fractions are 22.2% and 11.7% of *k*-space. Companion density images may be employed in a keyhole imaging sense, following phase and amplitude correction of the data, to improve image quality.

64×64 SESPI experiments were performed on a sandstone with laminar structure. Different patterns of *k*-space were taken for image reconstruction, following which decay curves for each pixel were generated with the local T_2 distribution determined by inverse Laplace transform. The proposed sampling patterns generate good quality images. Zero filling improves SNR but entails blurring, while using SPRITE data for keyhole imaging retains fine image details.

The figures below show the decay curves and T_2 distributions of a common pixel from images reconstructed using the two patterns of 22.2% and 11.7% of *k*-space data. The data are zero-filled, supplemented by SPRITE keyhole data, and compared to full *k*-space data from SESPI experiment. The decays and T_2 distributions are in all cases near identical. T_2 distributions from different bedding plane structures in the sandstone are different, reinforcing the value of a spatially resolved T_2 distribution measurement.

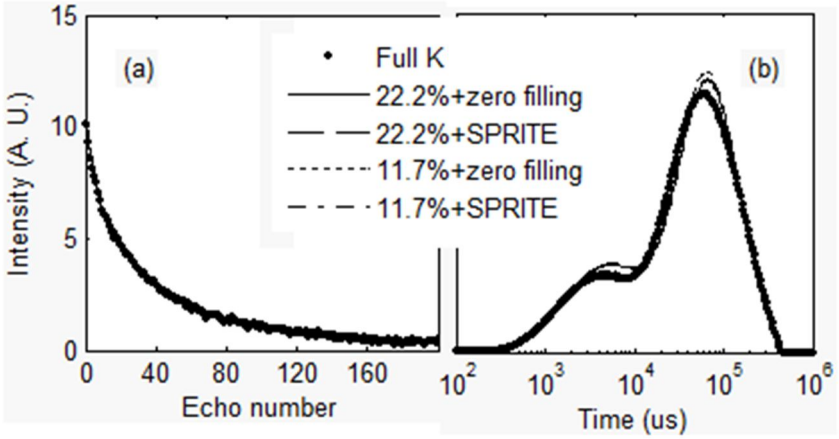

Figure 4: (a) T_2 decay curves, and (b) T_2 distributions of a common pixel from different schemes of image reconstruction.

References:

1. O. V. Petrov, G. Ersland, B. J. Balcom. J. Magn. Reson. 209 (2011) 39-46.

P79

Simulation of NMR response in digital image

Baolei. Zhang, Lizhi. Xiao, Guangzhi. Liao

China University of Petroleum, Beijing 102249, China
State Key Laboratory of Petroleum Resource and Prospecting
Key Laboratory of Earth Prospecting and Information Technology,Beijing

The development of the NMR technology can provide the information of mineralogy-independent porosity, permeability, pore size distribution, hydrocarbon typing, irreducible water saturation etc. The study of the response characteristics of NMR plays an important role in the data interpretation and application. Pore-scale petrophysical models are satisfied to characterize the NMR relaxation mechanisms of fluids in porous medium.

Taking advantage of image processing technology, SEM thin sections are digitalized to obtain the two-dimensional pore-scale petrophysical models; X-ray scanning experiment (Micro-CT) is preformed to obtain three-dimensional pore space of rock to construct three-dimensional pore scale petrophysical model. Based on these models, Monte Carlo random walk method is used to simulate the NMR responses, and T_2 distributions can be inversed from the numerical simulated echo trains. We investigate the characteristics of simulated NMR responses with different lithologies, different pore structures and different fluid components. The influence of magnetic field gradient, the surface relaxivity, molecular diffusion coefficient and other parameters also have been analysised with this micro-scale system.

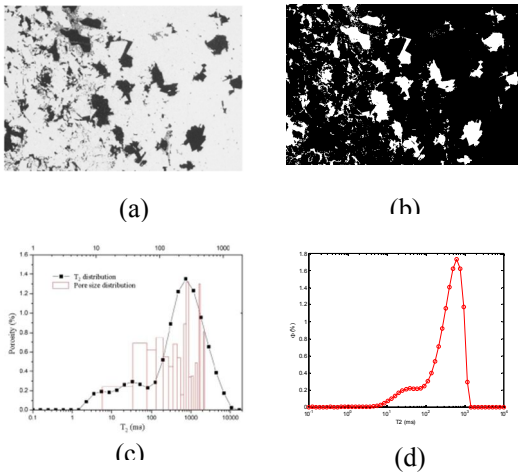

Fig.1: 2D simulation result
(a) SEM image (b) Digitalized image
(c) Experimental result (d) Simulated result

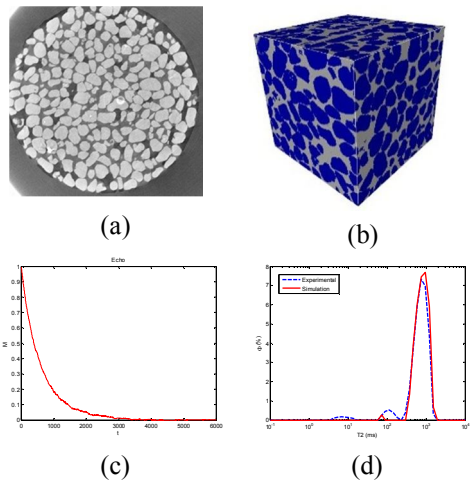

Fig.2: 3D simulation result
(a)-(b) 2D and 3D section of Micro-CT image
(c) Simulated echo train (d) Comparison result

References:

1. E. Toumelin, C. Torres-Verdin and S. Chen, Modeling of multiple echo-time NMR measurements for complex pore geometries and multiphase saturations, SPE 2003.
2. O. Talabi, S. Alsayari etc, Predictive pore-scale modeling: from three-dimensional images to multiphase flow simulations, SPE 2008
3. C.H. Arns and Y.Melean, Accurate simulation of NMR responses of mono-mineralic Carbonate rocks using Xray-CT images, SPWLA 2009.

P80

Corrections of internal gradient for NMR T_2-D map

Shaoqing. Fu, Lizhi. Xiao, Ranhong. Xie

China University of Petroleum, Beijing 102249, China
State Key Laboratory of Petroleum Resource and Prospecting
Key Laboratory of Earth Prospecting and Information Technology,Beijing

In porous media, magnetic susceptibility differences between the solid matrix and fluid filling the pore space lead to internal magnetic field gradient[1]. The diffusion relaxation of fluid can be influenced both by the internal magnetic field gradient and static magnetic field gradient which is produced by NMR well logging tool. When field strength of the internal gradient is bigger than static gradient, the T_2-D map influenced by internal gradient should be considered. However, the internal gradient in multi-fluids saturated porous media is difficult to calculate[2]. When drilled with the water based mud, water exist in the sensitive zone of NMR well logging tool. In this case, the water signal in T_2-D map can be located on the diffusion coefficient of water line which could be calculated with theoretical equations, when internal gradient and static gradient are all appropriate.

In this paper, we propose a new method to calculate the internal gradient in sedimentary formation saturated with water and oil. A more accurate T_2-D map could be get, after adding the internal gradient to inverse the T_2-D map. A T_2-D map which just consider the static gradient is presented in Fig. 1.a. In this figure, the water signal is not located on the water line, and the oil signal is stretched. When adding the internal gradient which was calculated by this new method to inverse the T_2-D map, the new result is presented in Fig. 1.b. In this figure, the water line cross the water signal, and the oil signal is more concentrated. The quantitative analysis of oil and water in porous media based on this new T_2-D map will be more accurate.

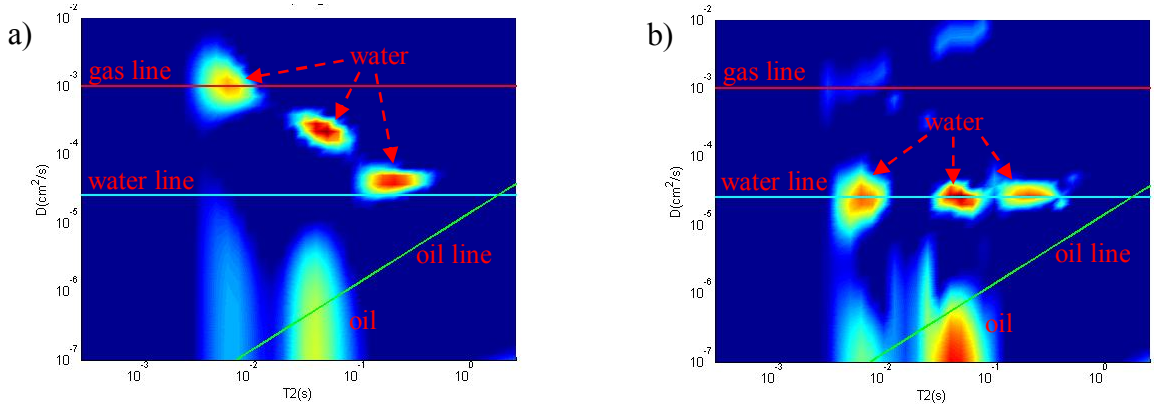

Fig. 1: T_2-D map of sedimentary rock saturated with water and oil. (a)Just using the static magnet field gradient of NMR well logging tool to inverse the T_2-D map; (b) Using both of the static magnet field gradient and internal magnetic field gradient to inverse the T_2-D map.

References:

[1] M.D. Hurlimann. J. of Magn. Reson. 131 (1998) 232-240.
[2] Boqin Sun, and Keh-Jim Dunn. Phys. Rev. E 65 (2002) 051309.

P81

Assessment of Pomegranate Postharvest Quality Using Magnetic Resonance Imaging

Lu Zhang[a], *Michael J. McCarthy*[ab]

[a]Department of Food Science and Technology,
[b]Department of Biological and Agricultural Engineering,
University of California, Davis
Davis, CA 95616

Fruit quality parameters, such as soluble solid content (Brix), total titratible acidity, pH, and Brix/acid ratio, are often used as indicators of fruit maturity and palatability. Measurement of these fruit quality parameters requires a series of destructive methods, which can only be conducted on extracted fruit juice. The aim of this study is to investigate the potential of MRI for quantitative analysis of pomegranate quality attributes. Six MR images with varying proton density, relaxation rate, and diffusion weighing were obtained for each of 229 pomegranate fruits by a permanent magnet MRI system. The pH, Brix, total titrabible acidity, and Brix/acid ratio of pomegranate were also measured by traditional destructive methods. Partial least square (PLS) analysis was applied to the statistical features of the voxel intensities in the MR images and quality parameters to examine the correlation between MR images results and destructive measurements. The result shows that the PLS models based on MR images has a R^2 of 0.59, 0.59, and 0.66 for predicting titratible acidity, pH, and Brix/acid levels, respectively. The correlation between MR image and Brix of pomegranate was poor. In these models, T_2 weighted Fast Spin Echo, Diffusion weighted image, and Spin Echo image with short TE and moderate TR are the most important images in predicting the pomegranate quality attributes. Unlike the traditional destructive methods, MR imaging method is capable of evaluating multiple quality parameters in a single measurement. The performance of PLS model proved that it is possible to use MR imaging as a noninvasive alternative to the traditional methods.

P82

Versatile Halbach sensor for NMR core analysis

Huabing. Liu, Lizhi. Xiao, S. Anferova, V. Anferov, Huijun. Yu, Baoxin. Guo

China University of Petroleum, Beijing 102249, China
State Key Laboratory of Petroleum Resource and Prospecting
Key Laboratory of Earth Prospecting and Information Technology,Beijing

A Halbach sensor for core analysis was employed successfully in 2007 for the first time [1]. In this work, we present a novel version of the Halbach sensor for both relaxation and diffusion measurements on rock plugs (Fig.1a). The magnet system is composed of two identical cylindrical magnet arrays separated by an axial gap of 13 mm. Each array contains 16 magnet blocks (NdFeB), with dimensions of 30×30×100 mm^3. Besides an initial RF coil placed in the center of the magnet with the highest homogeneity (B_0=0.25T, corresponding to a proton (^{1}H) resonance frequency of 10.65 MHz), this RF system contains another solenoidal coil of 0.5 cm length for diffusion measurements. It's positioned in the edge of the magnet system with a nearly constant gradient G=2.3 T/m, the strength of B_0 is 0.17 T, corresponding to a proton (^{1}H) resonance frequency of 7.3 MHz. Both RF coils are supported by a glass tube.

To illustrate the operation of the designed Halbach sensor, T_2 relaxation, T_1-T_2 and T_{2eff}-D correlation experiments were performed on different fluids and saturated rocks (Fig.1b, c). Results are presented and discussed subsequently.

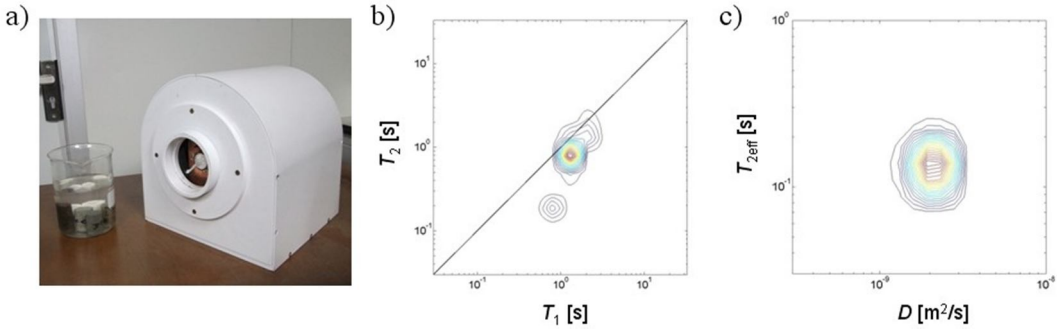

Fig.1: a) photo of versatile Halbach sensor; b) T_1-T_2 map of the rock sample saturated with water; c) D-T_{2eff} map of the rock sample saturated with water.

References:

1. S.Anferova, V.Anferov, J.Arnold, et al. *Magn. Reson. Imag.*, **25** (2007):474-480.

P83

A Compact 4-Channel Digital Spectrometer for Magnetic Resonance Imaging

Liang Xiao

College of Information Science and Technology, Beijing University of Chemical Technology, Beijing 100871, People's Republic of China

In this article, a compact 4-channel spectrometer which is suitable for low-field (0~0.634T) MRI or NMR system is presented. Several leading digital technologies, such as direct digital synthesis (DDS), digital down convert (DDC) and field programmable gate array (FPGA), are adopted to achieve excellent imaging performance and the flexibility of control. On the basis of well-designed architecture, one transmitting channel and four receiving channels are implemented in the device without high expense.

Figure 1(a) describes the block diagram of the spectrometer, and 1(b) shows its photo.

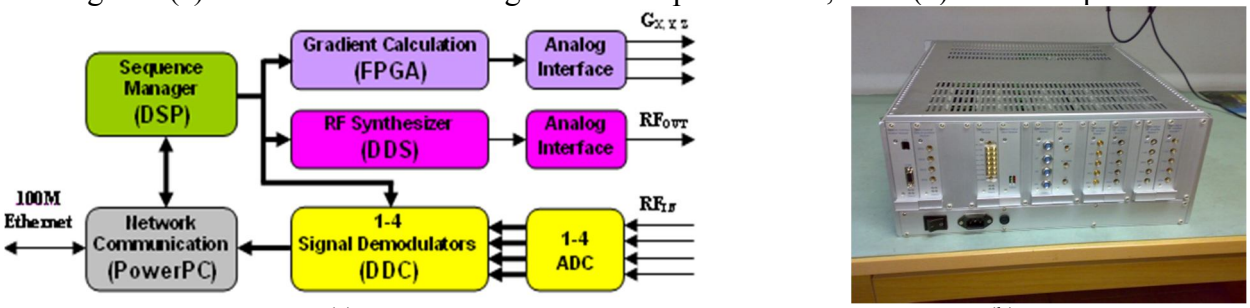

(a) (b)

Fig. 1 (a) the block diagram of the 4-channel spectrometer, (b) photo of the spectrometer.

A digital signal processor (DSP) is used as the sequence manager of the spectrometer. The sequence is written in Visual C++ language, and is translated to machine language of the DSP once sequence running. The system clock of the DSP is 60MHz so as to guarantee the fast and precise execution of the sequence. In addition, spectrometer communicates user's computer through 100Mbps Ethernet.

A highly integrated DDS device, AD9852, is utilized to generate RF pulse under the control of DSP and FPGA. The frequency resolution is about 1 μHz when the system clock of AD9852 is 240MHz, and phase resolution is about 0.02°. Both hard pulse and soft pulse can be generated conveniently.

Signal from the pre-amplifier is directly sampled by the ADC with 60Msps sampling rate and 16Bit resolution, the convert result is fed into AD6620, a digital demodulator, to export I/Q data. The internal data process of AD6620 and AD9852 is synchronized by DSP, consequently the phase of transmit and receive keeps coherent.

Gradient calculation is implemented in a single FPGA chip, including matrix operation for oblique slices and pre-emphasis calculation. For gradient waveform, the amplitude resolution is 20Bit and updating rate can be up to 1MHz.

Imaging experiments of the spectrometer show a satisfied result, figure 2 gives an example.

Fig. 2 T1-weighted image of a phantom

Reference:

1. X. Wu, D. A. Patterson, L. G. Butler, and J. B. Miller, Rev. Sci. Instrum.64(1993), 1235.
2. Etc...

P84

Diffusion Analysis with a Portable Unilateral NMR Sensor

Baoxin. Guo, Lizhi. Xiao, S. Anferova, V. Anferov, Huijun. Yu, Huabing. Liu

China University of Petroleum, Beijing 102249, China
State Key Laboratory of Petroleum Resource and Prospecting
Key Laboratory of Earth Prospecting and Information Technology,Beijing

Diffusion is a phenomenon that is of fundamental interest in liquid analysis. NMR is unique in its capability of measuring the translational self-diffusion. It is important in understanding fluids and fluid mixtures as well as in studying diffusion under confinement in porous media.

The permanent magnets could provide a magnetic field with a constant gradient G in a certain region above their surface. It's easy to construct a single-sided NMR sensor for diffusion measurements. U-shape magnet system was chosen. It consists of two permanent magnet blocks which are separated by a small gap of 17 mm. Distribution of the magnetic field along z axis over the surface is shown in Fig.1. Finding compromise between the strength of the magnetic field and its gradient, a distance of 7 mm over the surface of the magnets was chosen to place a surface solenoidal RF coil. The strength of the static magnetic field in this distance is 0.53 T, which corresponds to a proton (^{1}H) resonance frequency of 22.81 MHz. Distilled water with a known diffusion coefficient D of 2.5 $\times 10^{-9}$ m^2/s at 25 ℃ was used to measure gradient in sensitive volume of the sensor (G= 23.5 T/m).

The pulse sequence used in this study is based on Hahn echo operating in the presence of a steady gradient [1]. In the presence of the strong magnetic field gradient, transverse relaxation is neglected and the diffusion coefficients of samples can be estimated from a series of Hahn echo amplitudes measured with 100 different echo times. The diffusion distributions of distilled water saturated in synthetic core and different oils with variable viscosity have been plotted (Fig.2). T_{2eff}-D correlation experiments have also been studied.

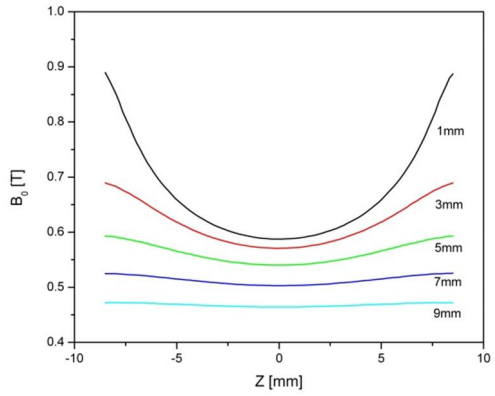

Fig.1: Profiles of magnetic field B_0 along z direction over the magnets.

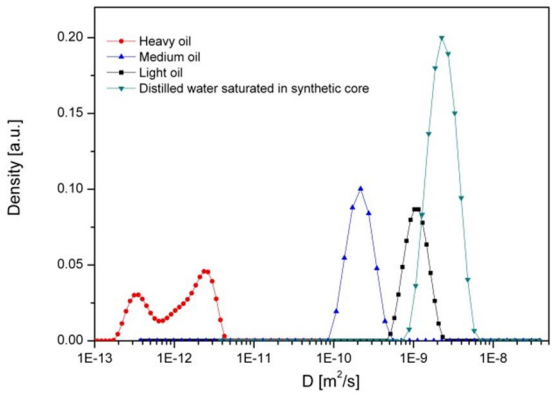

Fig.2: D distributions for different liquids

References:

1. D.G.Rata, F.Casanova, J.Perlo, et al., J. Magn. Reson. , 180 (2006)229.

P85

Withdraw

P86

Three-Dimensional NMR Logging Method for Fluid Typing

Wei. Li, Ranhong. Xie, Lizhi. Xiao, Guangzhi. Liao

China University of Petroleum, Beijing 102249, China
State Key Laboratory of Petroleum Resource and Prospecting
Key Laboratory of Earth Prospecting and Information Technology,Beijing

The development of NMR well-logging technology has been motivated by the unique set of answers that NMR can provide. In particular the benefits include:

1. Lithology-independent porosity measurement.
2. Continuous producibility and permeability estimates.
3. Fluid characterization capability.

It is well known in industry that low resistance oil-bearing layers can be misinterpreted or even missed by conventional resistivity-based interpretation. NMR logging fluid typing method provides a solution to this problem. However, when multiple pore fluids (oil, gas, and water) exist, it also becomes somewhat difficult in one-dimensional (1D) NMR, especially when their T_2 signals overlap. To improve the results, we add diffusion coefficient (D) and longitudinal relaxation time (T_1) information together to generate the three-dimensional (3D) (T_1-T_2-D) distribution by a global inversion.

To obtain the T_1-T_2-D distribution in 3D-space, a suit of CPMG echoes with different waiting times (T_W) and different echo spacing times (T_E) are needed. With the development of NMR logging tool, we can have high SNR 3D data sequence. The relationship between amplitude of echo and T_1, T_2, D can be described as the equations below.

$$b(t,T_W,T_E)=\iiint f(T_1,T_2,D)k_1(T_W,T_1)k_2(t,T_2)k_3(t,T_E,D)dDdT_1dT_2+\varepsilon$$

$$k_1(T_W,T_1)=1-\alpha\cdot\exp(-T_W/T_1)$$

$$k_2(t,T_2)=\exp(-t/T_2)$$

$$k_3(t,T_E,D)=\exp(-\gamma^2G^2T_E^2Dt/12)$$

Numerical simulation results of oil and water in Fig.1 show that 3D-NMR can provide us the fluid signals in (T_1-T_2-D) space. We can obtain more useful information of fluids by 3D-NMR method.

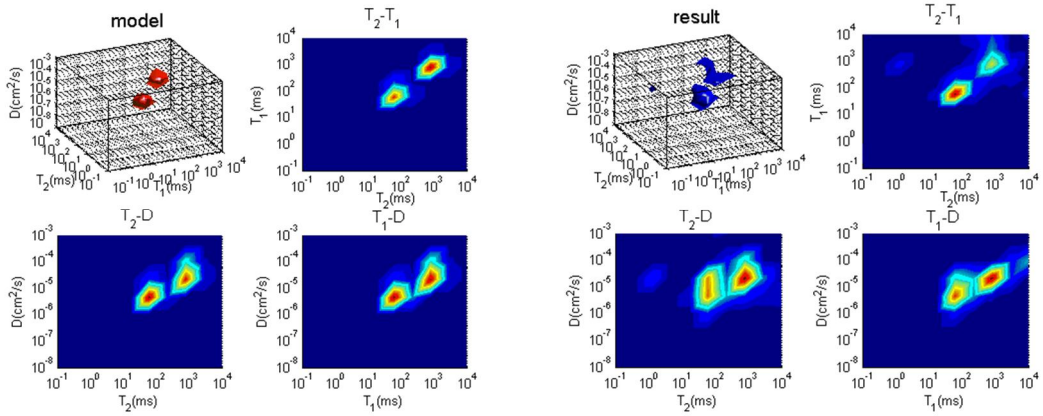

Fig. 1: The left four pictures are the 3D NMR model and its contour maps, the right pictures are the 3D NMR results of numerical simulation and its contour maps.

References:

1. G. R.Coates, Lizhi Xiao, M. G. Prammer. NMR logging principles and applications. Texas: Gulf Publishing Company, 1999
2. B. Sun, K-J Dunn. A global inversion method for multi-dimensional NMR logging. Journal of Magnetic Resonance, 2005

P87

Hybrid Inversion Method of Two Dimension NMR logging In multi-TE activation

Tan Maojin, ZouYoulong
China University of Geosciences, Beijing

One-dimension Nuclear Magnetic Resonance (1D NMR) logging technology is limited for fluid typing in complex reservoirs. Two-dimension Nuclear Magnetic Resonance (2D NMR) logging is being devolved and provides more parameters including diffuse coefficient (D) and transverse relaxation time (T2) in multi-pore media, and the fluid typing is realized according to differences of both parameters. So, 2D NMR logging is more advantageous than 1D NMR logging. Point to the relaxation mechanism of 2D NMR at some gradient field, echo simulation and inversion of 2D NMR is discussed in detail.

For finding appropriate inversion method in 2D-NMR logging, firstly, appoint to an ideal model proposed, a series of spin echoes are simulated with mult-TE activity in gradient field. And LSQR, a damping least squares method based QR decomposing, and SVD, singular value disposed, are applied to inversion test. From the inversion results, LSQR algorithm is better in short relaxation component than in long relaxation component, and improved SVD algorithm is better in long relaxation component than in short relaxation component which is illustrated in Figure 1(a). So, a hybrid method is proposed, namely, LSQR algorithm is first used with the iteration tine of 400, then, as initial values, the primary results are applied into further SVD inversion. In both inversions, the iteration times are both supposed as 400. Figure 1(b) is LSQR-SVD hybrid inversion results, and the bound fluid is more focus than that of SVD inversion results. Furthermore, the inverted T2 distribution agrees well with that of the model. And the diffusion coefficient is also consistent with that of the model. The Slow diffuse coefficient component matches together with model.

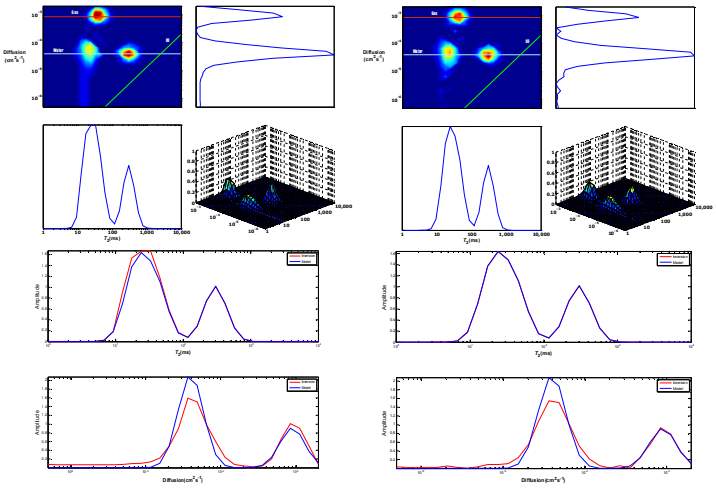

(a) SVD (b) LSQR-SVD

Fig. 1: different inversion method and compare

Inversion efficiency and precision: to improved SVD algorithm, the relative error is 0.2058，and the running time is 59.64s; wherea, the relative error of hybrid inversion method is 0.1499， and the running time is 54.50s, so, LSQR-SVD hybrid inversion method has higher precision and efficiency.

Furthermore, the inversion results of synthesized echo trains from oil and water model indicate that the hybrid method in 2D NMR logging is effect and promise. The research may prepare conditions for fluid typing and multi-dimension NMR logging inversion.

References:

1 1.B Q Sun, K J Dunn, Multi-dimensional NMR logging. J Magnetic Resonance,172(2005)180.
2 2. Xie R H, Xiao L Z, 2009. Two-dimensional NMR logging method for identifying reservoir fluids. Geophysics, 52(9)：2410-2418

P88

Inversion Method for NMR Logging along the Depth Dimension

Ke. Huang, Lizhi. Xiao

China University of Petroleum, Beijing 102249, China
State Key Laboratory of Petroleum Resource and Prospecting
Key Laboratory of Earth Prospecting and Information Technology,Beijing

During NMR logging measurement, the logging result is affected by the surrounding formations due to the tool's vertical motion. However, the conventional inversion method does not consider or correct this phenomenon. Based on the view of T_2 inversion along the depth dimension (B. Sun 2008), we suggest another inversion method for processing a group of NMR logging data simultaneously by replacing the T_2 dimension with a set of B-Splines basis functions and using Walsh function to expanse the response along the depth dimension.

Numerical formation models are built to verify its application to sophisticated stratigraphic combinations. The numerical simulation and results are in Fig.1. (1) Laminated formations models are built (Fig1.a); (2) NMR logging is simulated to get the ideal responses of the tool (Fig1.b); (3) conventional inversion results depth by depth (Fig1.c); (4) inversion results along the depth dimension by the new method (Fig1.d). The result shows improvement of vertical resolution for the logging condition model.

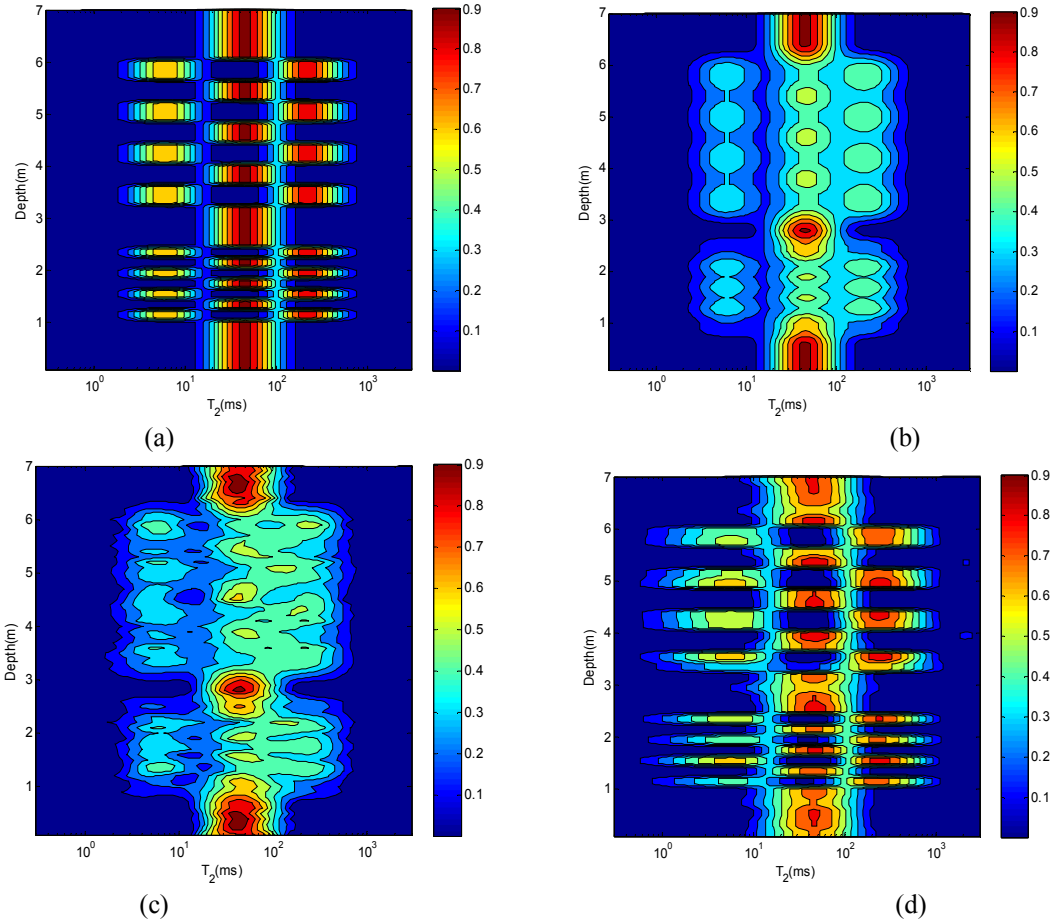

Fig.1 Numerical simulation and comparison of results by conventional and new method

References:

1. B. Sun, M. Skalinski, K. J. Dunn, NMR T_2 inversion along the depth dimension, AIP Conference Proceedings (2008).
2. Y. Qian, Z. Zhong, C. Gao, High resolution inversion of well logs using Walsh functions, ACTA GEOPHYSICA SINICA, 38 (1995) 170.

P89

Characterization of Gas Dynamics in Gas Shale Nanopores by NMR

Ravinath Kausik[a], Chanh Cao Minh[b], Lukasz Zielinski[a], Ridvan Akkurt[a], Yiqiao Song[a] C.B. Liu[c], Sid Jones[c], Erika Blair[c]

[a]Schlumberger-Doll Research, [b]HFE Schlumberger Technology Corporation, [c]Chevron Technology Corporation

Logging in unconventional plays like gas shale is becoming widely practiced because of their potential to help meet the enormous global demand for gas and improved technologies to tap into these reservoirs. The dynamics of fluids in unconventional reservoirs which generally exhibit very low porosity (~5PU) and ultra-low permeability (<100nD) is very different from the conventional reservoirs and thus their understanding poses a major challenge. In this work we study the NMR response of gas in the nanopores of gas shale and show how it is different from bulk gas behavior where the relaxation is dominated by the spin rotation mechanism and the diffusion is generally unrestricted. These changes are due to the manifestation of the additional effects of adsorption, surface relaxation and restricted diffusion. One of the biggest challenges is the quantitative understanding of such effects and coming up with novel methods to determine the quantity of gas associated with the kerogen (the organic matter in gas shale) pores and the kerogen porosity.

The NMR responses of methane gas in Haynesville shale plugs cored from a well in the East Texas field were studied and the effects of adsorption, surface relaxation and restricted diffusion have been characterized. The experiments were done on a 2MHz NMR spectrometer at elevated pressures and temperatures close to reservoir conditions. Mineralogy, elemental analysis and BET experiments have also been carried out on the same plugs for better understanding of the formation characteristics. Faster relaxation modes (few tens of milliseconds) and slower apparent diffusion coefficients (an order of magnitude less than their bulk value) for the confined gas molecules in comparison to their bulk properties have been observed for the first time with the help of 2D NMR D-T2 experiments.

It has been observed that the relaxation spectra for bound fluid and the gas in the small pores overlap, and that the additional diffusion dimension might help in resolving these two fluids. In addition, 2D NMR D-T2 maps have the potential to resolve the gas response in the kerogen nano-pores from the gas in the intergranular pore space. We formulate new relaxation and diffusion models of gas shale and propose that multidimensional NMR logging with pulse sequences optimized for gas shale could open the door for quantifying the gas in kerogen pores as well as the gas in the non-kerogen pores to determine the total gas in place.

P90

Responses of NMR Logging While Drilling at Formation Boundary in Deviated Wells

Xin. Li, Lizhi. Xiao, Ke. Huang

China University of Petroleum, Beijing, China
State Key Laboratory of Petroleum Resource and Prospecting
Key Laboratory of Earth Prospecting and Information Technology,Beijing

Nuclear magnetic resonance logging while drilling can provide real-time petrophysical information for un-invaded formations. Discrimination of formation with different thickness and boundary is critical to NMR geosteering and formation evaluation. NMR logging tools face challenges in HA/HZ wells, because they are designed and calibrated for vertical wells with near-horizontal strata.

Formation response function is proposed based on tool trajectory and a sensitive-volume-unit contribution concept. Forward and inversion numerical modeling are employed to simulate NMR logging response in vertical and deviated wells in stratigraphic combinations.

Comparison of NMR logging response from vertical wells to HA/HZ wells indicates significant differences. In a given formation, a bigger deviated angle results in a thicker apparent thickness of target section and a longer apparent boundary transition along the measured depth. Vertical resolution of NMR logging tool in deviated wells is affected by both the sensitive volume geometry and deviated degree. A short antenna aperture can obtain a distinct boundary, and a deep DOI tool detects the boundary earlier. The geometry relationship between the tool and formations affects the response, porosity characteristics at formation boundaries is less affected by surrounding formations in high-angle wells.

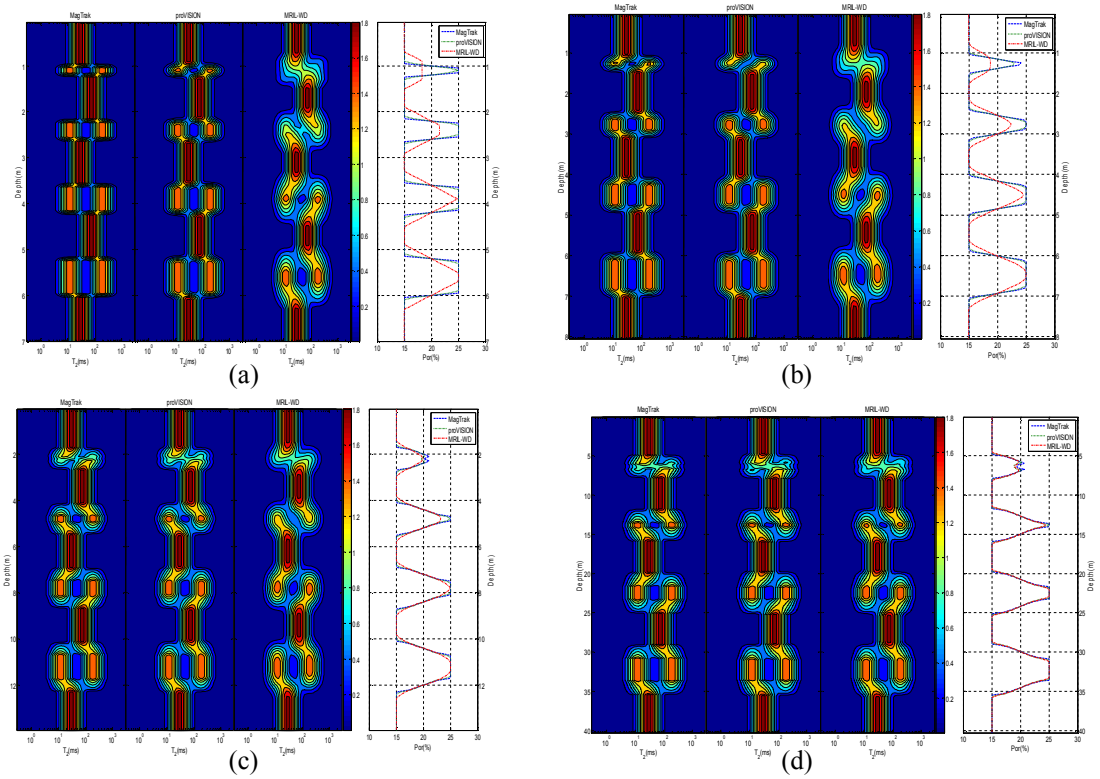

Fig. 1: NMR LWD responses in a deviated well (from a to d : 0º, 30º, 60º and 80º)

References:

1 S. H. Liu, L. Z. Xiao, F. L. Hu, et al. Studies on NMR logging responses at formation boundary. Chinese J. Geophys. (in Chinese), 51 (2008) 4.

P91

The Studies on Formation Evaluation of a Volcanic Rock Reservoir in Song Nan with Core Analysis and Well Logs

Xiuping Wei, Guo Tao

[1]China University of Petroleum, [2] Research Institute of Petroleum Exploration and Development in Sinopec

In view of complicated volcanic lithology, versatile matrix parameter, deeply disturbed reservoir fluid because of lithology and mud invasion, this thesis tentatively researches into a series of work under the aim of guiding gas field development. Combining geology and well logging together, the thesis applies new approaches to the conventional well logging technology in the study of the following work. Firstly, adopting the geologists' advice, the thesis adjusts the naming order for volcanic lithology in Song Nan, and connects volcanic lithology with reservoir types (As shown in figure1). On this basis, the thesis identifies the subclasses of volcanic rock by collecting the drilling core materials and using conventional well logging cross-plots.

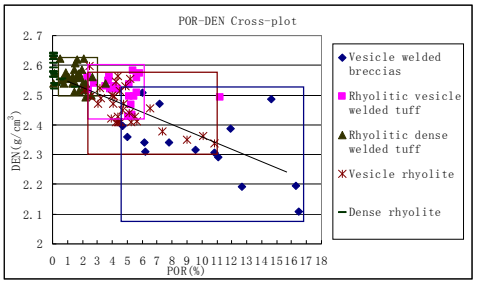

Fig. 1 Cross-plot between DEN and POR

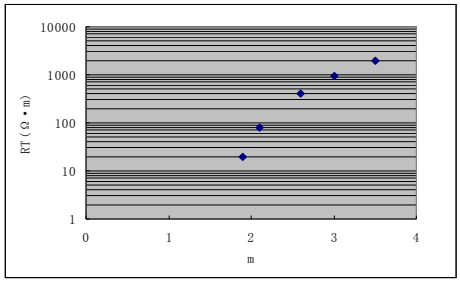

Fig.2 Relationship figure between m value and RT

Secondly, the paper improves the formula to calculate matrix parameters of volcanic rock and works out an approach for the calculation of reservoir porosity based on conventional well logging and CMR; Thirdly, the paper establishes the relationship between m value and deep investigation laterolog resistivity and then calculates gas saturation using versatile m value in Archie formula (As shown in figure2). Fourthly, in view of the body area of volcanic reservoir in Song Nan basin, the paper uses conventional logging method to identify reservoir fluid on the basis of apparent maker bed differential method and works out the cross-plot between gas saturation and porosity. Also, different fluid types are identified in terms of different response characteristics on gas reservoir between nuclear magnetic logging and density logging.

References:

1. A Khatchikian, P Lesta. Log evaluation of Tuffites and Tuffaceous sandstones in southern Argentina. Lafayette, Louisiana: SPWLA 14th Annual Logging Symposium, 1973.
2. L E Wells, S K Sanyal, and M A Mathews. Matrix and response characteristics for sonic, density, and neutron. Tulsa, Oklahoma: SPWLA 20th Annual Logging Symposium, 1979.

P92

Moisture content and diffusion in ancient Roman walls

Wasif Zia[a], *Eleonora Del Federico*[b], *Cindie Kehlet*[b], *Bernhard Blümich*[a]

[a] Institute of Technical and Molecular Chemistry, ITMC RWTH Aachen University, Germany

[b] Department of Mathematics and Science, Pratt Institute, USA

Self diffusion coefficients and depth profiles of ancient Roman walls were measured in Herculaneum, Italy, using a stray field NMR profiler (PM-25). At selected points the correlation of relaxation and diffusion distributions has also been interrogated. The ultimate goal of these studies is to quantify the moisture transport for the benefit of improving conservation treatments to preserve the ancient buildings and wall paintings.

Fig1: Setup of the NMR profiler, illustrating measurements on culture heritage sites. In this particular case self diffusion coefficient is being measured in a mortar layer just below the exterior surface.

P93

High-resolution spectroscopy with a desktop NMR system

Juan Perlo[a], Ernesto Danieli[b], Bernhard Blümich[b], and Federico Casanova[a,b]

[a]ACT GmbH, Pauwelsstr. 19, Aachen, Germany. [b]Institut für Technische Chemie und Makromolekulare Chemie, RWTH Aachen University, Worringerweg 1, Aachen, Germany.

During the last decade several magnet designs based on a Halbach arrays has been proposed for desktop NMR instruments. However, due to variations of the polarization of the magnet pieces used in the assembly, the magnetic field generated by real magnets is strongly inhomogeneous. The field variation is such that only a small fraction of the bore can be excited. To shim this type of magnets we have recently presented a robust method useful to correct strong field inhomogeneities of the order of several thousands of ppm. The first implementation of the method was to generate a spot of highly homogeneous field (fraction of ppm) outside the magnet for single-sided 1H spectroscopy. Later, the method was extended to correct the field inhomogeneities of a Halbach magnet for MRI. In that case, a second Halbach array made of movable pieces was placed in the bore of an existing Halbach to efficiently generate first and second order shim terms. Finally, the method was refined by incorporating the movable pieces into the main magnet design and extending the correcting shim terms to higher orders. Here we present the performance of our last magnet generation working at a field strength of 1 Tesla. To offer the highest performance the magnet is temperature stabilized and furnished with shim coils generating up to second terms. Moreover a lock system is used to correct magnetic field drifts. Figure 1 shows a spectrum of ethyl acetate acquired using 8 scans with this system. The high sensitivity (30000 for a single shot in a water sample) can be appreciated by zooming the spectrum to observe the 13C satellites.

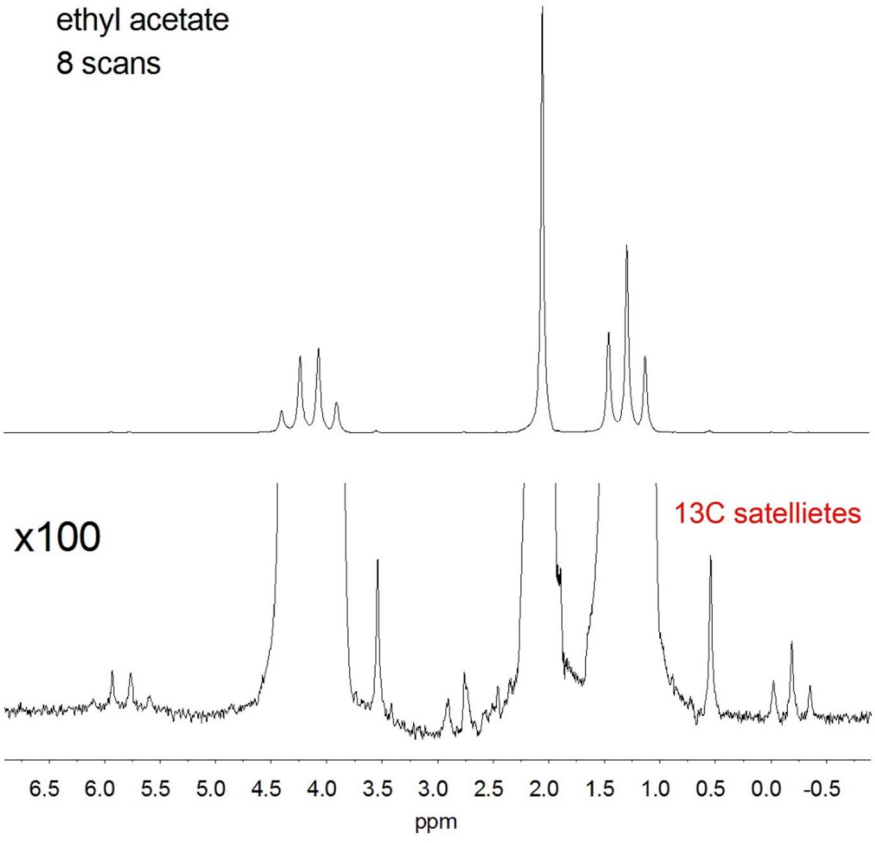

Figure 1. Spectrum of ethyl acetate acquired in 8 scans at 42.57 MHz. The sample was inserted in the magnet using a standard 5 mm od glass tube.

P94

Effect of Block Copolymer Nanoconfinement on the Proton Conductivity Mechanism of Ionic Liquids, Probed by Pulsed-Field Gradient NMR

Megan L. Hoarfrost[a,b], Madhu S. Tyagi[c], Rachel A. Segalman[a,d], and Jeffrey A. Reimer[a]

[a]Department of Chemical and Biomolecular Engineering, University of California, Berkeley, [b]Energy and Environmental Technologies Division, Lawrence Berkeley National Laboratory, [c]NIST Center for Neutron Research, [d]Materials Sciences Division, Lawrence Berkeley National Laboratory

Ionic liquids are of great interest for a wide variety of applications, especially electrochemical applications such as proton exchange membrane fuel cells, due to their high ionic conductivity, high thermal and electrochemical stability, and low vapor pressure. Mechanically durable membranes having high ionic conductivity can be obtained by mixing ionic liquids with block copolymers. In this work, a protic ionic liquid is selectively integrated into one block copolymer phase, resulting in a nanostructured membrane in which one phase is proton-conducting and one phase imparts mechanical durability (Figure 1). It is anticipated that confinement to self-assembled block copolymer nanodomains will affect ionic liquid proton transport properties. Using pulsed-field gradient (PFG) ^{1}H and ^{19}F NMR, this relationship has been investigated for mixtures of poly(styrene-*b*-2-vinylpyridine) (S2VP) block copolymer with the protic ionic liquid imidazolium:bis(trifluoromethylsulfonyl)imide ([Im][TFSI]), where [Im][TFSI] selectively resides in the poly(2-vinylpyridine) (P2VP) domains of the block copolymer.

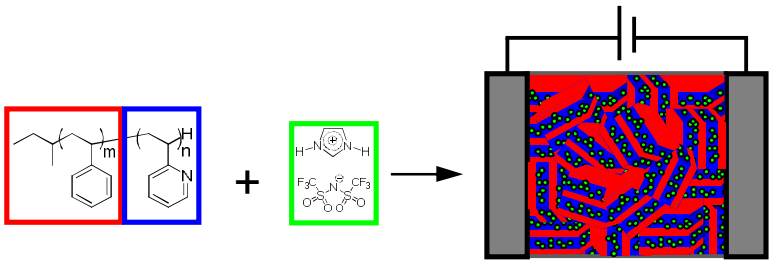

Figure 1: Mixtures of S2VP block copolymers with the protic ionic liquid, [Im][TFSI], result in nanostructured, ion-conducting membranes.

A fast proton "hopping" mechanism is observed when an excess of imidazole is added due to proton transfer from imidazolium cations to imidazole molecules via hydrogen bonds. This is evidenced by the diffusion coefficient of the acidic proton, D_{H+}, being higher than that of the imidazole molecules themselves, D_{Imid}. In the S2VP/[Im][TFSI] mixtures with excess imidazole, nanoconfinement of the ionic liquid alters hydrogen bond networks, resulting in a greatly increased amount of proton hopping compared to non-ordered mixtures of [Im][TFSI] with excess imidazole and P2VP homopolymer. This, in combination with unique ion aggregation behavior, leads to a lower activation energy for ion transport in the nanostructured samples. Therefore, as predicted, proton transport in ionic liquids is greatly affected by confinement to block copolymer nanodomains. Using PFG NMR to probe the relationship between composition, morphology, and the mechanism of proton transport will illuminate important design parameters for new, improved proton-conducting membranes.

P95

Absorption kinetics of human skin monitored in vivo by single-sided NMR

Maxime Van Landeghem[a,b,c], *Ernesto Danieli*[a], *Juan Perlo*[a], *Bernhard Blümich*[a], *and Federico Casanova*[a]

[a] ITMC - RWTH-Aachen Worringer Weg 1, D52056 Aachen, Germany. [b] ESPCI - PPMD, UMR 7615 CNRS UPMC, ESPCI ParisTech, 10 rue Vauquelin, 75005 Paris, France. [c] Saint-Gobain Recherche, 39 quai Lucien Lefranc, BP 135, 93303 Aubervilliers cedex, France.

This work reports in vivo ingress monitoring measurements of water and cosmetic cream into human skin. The experiments were performed with a single-sided NMR sensor generating a reduced but highly uniform static magnetic field gradient. In the magnetic field of this sensor, skin profiles of up to two millimeters depth are measured with a spatial resolution of about 25 mm in experimental times of 30 s. The absorption kinetics of water and cream through the different skin layers was obtained from T_2 relaxation time measurements, which in the presence of a low gradient are not contaminated by molecular self-diffusion. Then, by simply acquiring a CPMG echo train and combining a Fourier Transformation (FT) along the echo acquisition time with an Inverse Laplace Transform (ILT) along the echo decay time, the T_2 distribution was spatially resolved across the human skin (Fig. 1a). Moreover, by using a stimulated-echo sequence in combination with a CPMG detection train, the distribution of diffusion coefficients can be also spatially resolved (Fig. 1b) or correlated with the relaxation times at each position. These powerful methods allowed us to extract the absorption characteristic times as well as changes in the thickness of the different layers during the exposing time to water and cosmetic cream.

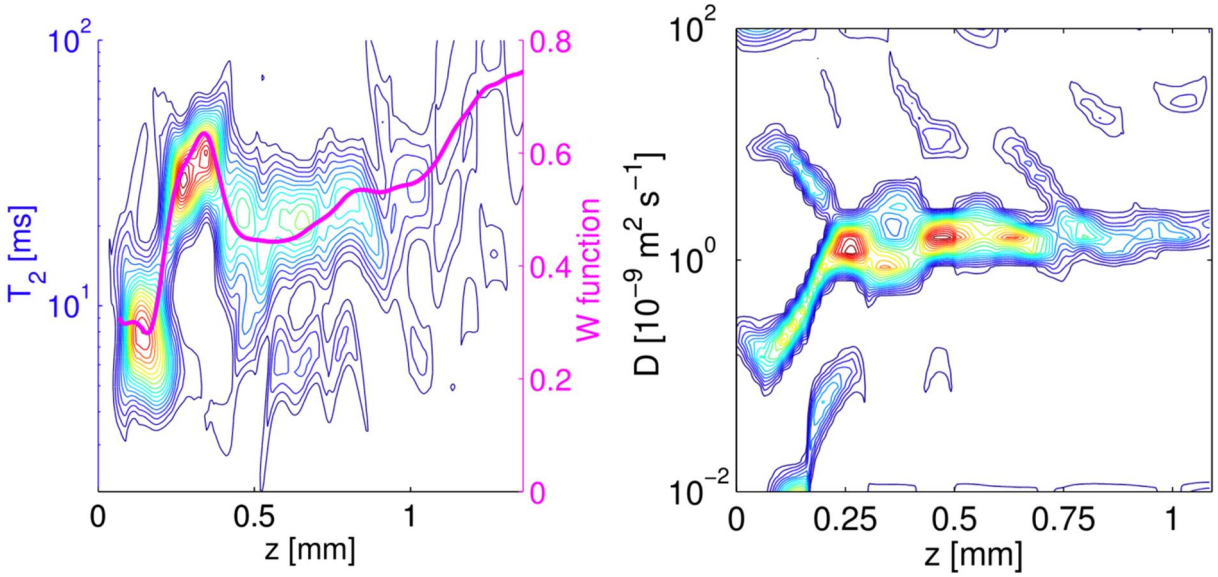

Figure 1. Relaxation time (a) and diffusion coefficient (b) distributions spatially resolved in vivo across the human skin structure.

P96

Quick determination of rock electrical response through Magnetic Resonance Imaging

Bhim. B. Bam[a], *Nicola. Bona*[a], *Marco. Pirrone*[a], *Elio. Rossi*[a]

[a] eni e&p

The amount of hydrocarbons in place in gas and oil bearing reservoir rocks is often estimated by means of down-hole electrical measurements. The equations that relate measured conductivities to unknown water saturations contain both log- and core-derived parameters. The Archie-*n* exponent is one these. It is obtained on partially water saturated core samples and is quite critical. In fact, if *Sw* is unevenly distributed in the sample, the calculated hydrocarbon volumes may significantly differ from the true volumes. 3D MR imaging makes us able to handle any type of *Sw* heterogeneity. Operatively, we acquire two MR images, one under fully water saturated conditions (Fig.1A) and the other after a short centrifuge step in air (Fig.1B), and process the images to generate a 3D conductivity network (Fig1C). The *n* parameter is determined by forcing the numerically-evaluated network conductivity to equal the experimental sample conductivity. The whole process takes one day.

In this poster, particular emphasis is put on the extraction of the 3D *Sw* data, a necessary step for conductivity derivation. We obtain *Sw* from a classic CPMG sequence (voxel size = 2mm cubic; echo time = 2.46 ms), by fitting the T_2-decay curve with a single exponential on a voxel-by-voxel basis. A quality-check is then made, where we use the average sample saturation from weight as a reference. A correction to the MR-derived *Sw*'s is eventually applied where necessary. Generally, these appear to be underestimated, and the lower the water saturation the larger the degree which they are underestimated.

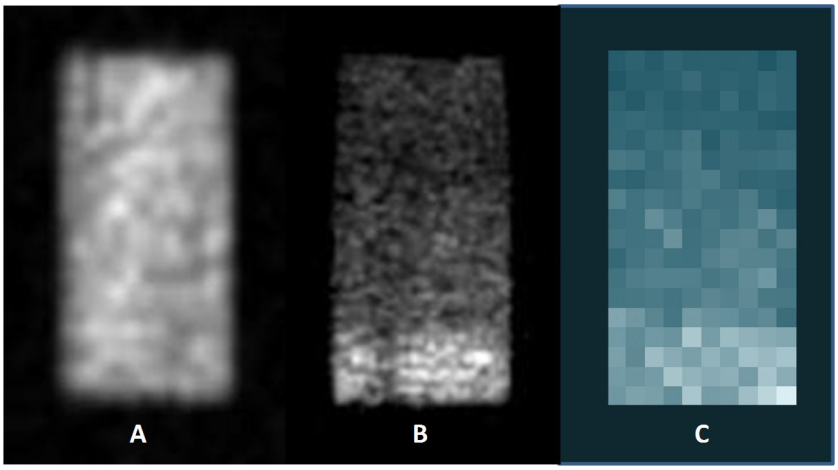

Fig. 1: MR images (A and B) and conductivity network (C) obtained on a sandstone sample. The *n* exponent extracted from the network (1.63) is close to that obtained from the standard procedure (n=1.65).

P97

Characterization of wide size rock cores by means of Field Cycling NMR Relaxometry

V. Bortolotti[a], *S. Bubici*[b], *P. Fantazzini*[c], *M. Polello*[c], *G. Ferrante*[d]

[a]Univ. of Bologna, Dept. DICAM, V.le Risorgimento 2, 40136 Bologna, ITALY
[b]Invento S.r.l., c/o 2I3T Incubator, University of Torino, Via Nizza 52, I-10126, Torino, Italy
[c]Univ. of Bologna, Dept. of Physics, Viale Berti Pichat 6/2, 40127 Bologna, ITALY
[d]Stelar Srl, Via Enrico Fermi 4, 27035 Mede (PV), ITALY

^{1}H-NMR relaxation times of water-saturated rock samples are widely employed to characterize the architecture of pore space and to estimate petrophysical properties, such as permeability and irreducible water saturation. These parameters are used both in laboratory studies and in well logging (NML).

So far, such NMR studies were always carried out at a fixed frequency (typically 10 or 20 MHz in laboratory and 2 MHz in NML). It is well known [1] that NMR relaxation rates are inherently field dependent, a fact which might represent a complicating factor in the above mentioned applications. Mono-exponential analysis of longitudinal relaxation curves so far published [2] indicate that the field dependence does exist, but is quite modest. However, it has been amply shown [3] that the mono-exponential hypothesis is rarely applicable to natural rocks, where one usually observes wide distributions of relaxation rates, due to the wide distributions of pore sizes and their physical and chemical properties.

For this reason, we have investigated the relaxation rate distributions in two sandstones with different porosity:

a) *feldspathic quartz Sandstone* with porosity 22.1
b) *quartzarenite Sandstone* with porosity 17.5

Cylindrical rock samples (1') were saturated by water under vacuum. Their relaxation curves were measured on a Fast Field Cycling NMR Relaxometer equipped with wide bore probe, by of a number of relaxation field values, ranging from 20 kHz to 10 MHz.. Continuous distribution analysis of the curves was performed by UPEN [3].

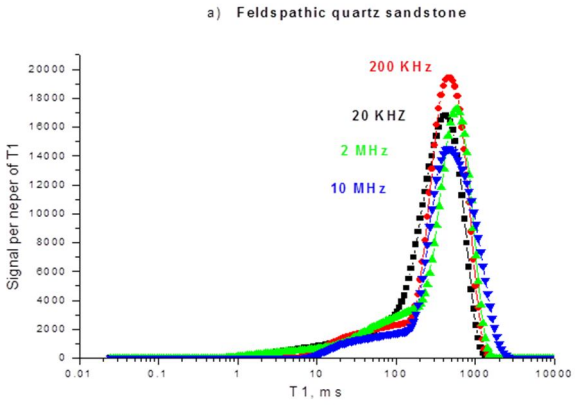

The field dependence of the distribution curves was to be expected. The extent of the variations, however, exceeds intuitive expectations and is subject to further study. We believe that, in principle, analysis of a set of T_1 distribution curves obtained at a number of relaxation field values can allow one to better separate different sample components and associate a distinct field-dependence profile with each of them. Work aimed at achieving this goal is at present in progress.

[1] N. Bloembergen, E.M. Purcell, R.V Pound, *Phys. Rev*. 73, 679 (1948).
[2] S. Godefroy, J.-P. Korb, M. Fleury, R.G. Bryant, *Phys. Rev. E*, 64, 21605 (2001).
[3] G.C.Borgia, R.J.S Brown, P.Fantazzini, *J. Magn. Reson*. 132, 65 (1998); ibidem 147, 273 (2000).